Magnetic Properties of Mexican Soils and Lake Sediments

John David James Braisby BSc. (Hons.)

Thesis submitted in fulfilment of
the requirements for the degree of
Doctor of Philosophy
to the
University of Edinburgh

I declare that this thesis has been composed by myself and it has not been submitted in any previous application for a degree. The work reported within was executed by myself, except where contributions have been stated and duly acknowledged.

Abstract

This study addresses two topics in environmental magnetism, i) the magnetic unmixing of lake sediments in terms of catchment samples and, ii) a connection between soil magnetic properties and annual rainfall. Soil and lake sediment cores from Mexico provided the material used.

Palaeolimnology facilitates the understanding of past environments by the analysis of lake sediments. Many palaeolimnological techniques are both time consuming and destructive. Analysis of pollen and diatoms require an expert to identify and count hundreds of pollen grains or diatoms for each core horizon to be characterised. In contrast, magnetic remanence and susceptibility measurements can be obtained rapidly and without changing the physical properties of the sample that is being measured. The problem with magnetic measurements on lake sediments is the interpretation of the results. Previous workers have analysed trends in the magnetic properties of sediments. Linking high susceptibility to soil erosion, and low susceptibility to reduced sedimentation through, for example, the accumulation of organic material, low in magnetic content.

In order to analyse environmental magnetic results I have developed a new magnetic unmixing technique. It uses non-negative least squares to unmix the magnetic properties of a target sample in terms of the magnetic properties of potential end-member samples. A stepwise technique is used to select appropriate end-members and estimate the errors involved.

The newly developed magnetic unmixing procedure has been applied to the sediments of two lakes in Mexico, Lake Pátzcuaro, in the central Mexican plateau, and Lake Babicora in the northern Mexican highlands. The results for Lake Pátzcuaro indicate changes in the lake sediments' magnetic properties that can be ascribed to climate changes and land use. The main climatic change is a reduction in lake level at approximately 11,000 ^{14}C yr B.P. Human arrival, at approximately 3,500 ^{14}C yr B.P. coincides with a dramatic increase in topsoil erosion. At Lake Babicora the results indicate that two reductions in rainfall led to reductions in the amount of catchment material delivered to the core site. These changes in depositional regime occurred at approximately 29,000 and 11,000 ^{14}C yr B.P.

In this study, the magnetic properties of soil profiles across steep rainfall gradients in Mexico have been analysed. I have generated linear models relating the magnetic properties of soils to annual rainfall. These linear models indicate that soils from regions with high rainfall tend to contain greater concentrations of viscous grain size magnetite. They also show, in comparison to soils from drier regions, magnetic properties similar to those of intact bacterial magnetosome chains.

Acknowledgements

First of all I wish to thank my supervisors Roy Thompson and Sarah Metcalfe, for coming up with the idea for the project and being there to answer questions. The fieldwork element of this project would have been far harder if not for the guidance of Sarah Metcalfe, the camaraderie of Anthony Newton, Beatriz Ortega Guerrero and Nicola Terrett, and a friendly place to stay in Mexico city provided by Liliana and Armando. Also thank you to the geophysics department at UNAM for use of computers and floorspace. Thank you to Barbara Maher, Mark Hounslow and Tom Mutch for help with extraction work at the University of Lancaster. Also thanks to John Walden, at the University of St Andrews for use of laboratory equipment, and advice.

It was during my six month transfer report, when an innocent question from Kathy Whaler, changed the direction of this study, so thanks for asking if I had thought of using non-negative least squares.

This research has been funded by the Natural Environment Research Council, although the carbon dates on the Pátzcuaro core were paid for by the Leverhume Trust (F/158/BL). The Babicora cores were retrieved during fieldwork paid for by the Gilchrist Expedition award. I have also received a Shell postgraduate bursary, which has helped immeasurably during the course of my study. To each of these groups, thank you for your funding.

During My time as a Ph.D. student at Edinburgh University I have come to respect a geology and geophysics department tradition, so I would like to say thank you to all the attendees of the coffee club. Your advice, laughter, smiles and extremes of pedantry (all in the best possible taste) have added to my experiences of this institution. "Nice one Shane". At this point, it also seems fitting to say a special thank you to our computer officers, Justin and Shane, to say that my life would have been harder without your help would be a huge understatement.

I would like to thank my friends for the support that I have received from them during this my time as a Ph.D. student, cheers to Rich, for sharing a corner of a big office, to Theo and Matt for sharing a big flat with little heating, to Ruth and Pete for sharing ideas on many things. Cheers also to Jack, Kamila, Don and Zoe, for your lasting friendship and guidance.

I have saved the most important acknowledgement for last, and it goes to Katy H. if it were just for being the proof reader of my thesis, then it would be a very big thank you, but for inspiring me, making me smile, and giving me the encouragement that I needed, I'm not sure what to say, other than thank you.

Contents

List of figures

List of tables

Chapter 1

Introduction

1.1 Environmental magnetism

Understanding the environment that we live in is becoming increasingly important. Decisions that will affect the future of the planet have to be made with the strongest grounding in science and with the largest amount of relevant information possible. Climate change in particular is an issue that causes grave concerns. Our present understanding of past changes in the global climate has been based mostly upon interpretation of from sea sediment and ice cores. However, loess deposits and lake sediments provide information on past climate variability too. Because loess deposits are land-based they are more easily acquired than sea sediment cores. Because lacustrine sedimentation rates tend to be higher than oceanic sedimentation rates, climate data retrieved from lake cores will tend to be of a higher resolution. In this study I develop an application that will aid in the environmental interpretation of magnetic measurements made on lake sediments, and further investigate a proposed link between rainfall and soil magnetic properties.

Palaeomagnetists use magnetic measurements made on rock and sediment samples to gain insights into the past intensity and direction of the Earth's magnetic field. In order to make these measurements, sensitive magnetometers and powerful magnetisers have been developed. As a result of the work of palaeomagnetism, an understanding of the magnetic properties of materials and minerals in nature has been developed. The knowledge gained by palaeomagnetists and the equipment developed for investigating the Earth's magnetic field have provided a toolbox for the environmental magnetist.

Environmental processes can affect the magnetic properties of materials (Figures 1.1 and 1.2). This being the case, measuring the magnetic properties of materials could help in the investigation of environmental processes. By using the tools and techniques developed for palaeomagnetism, a wealth of magnetic measurements is available to help characterise and understand the environment.

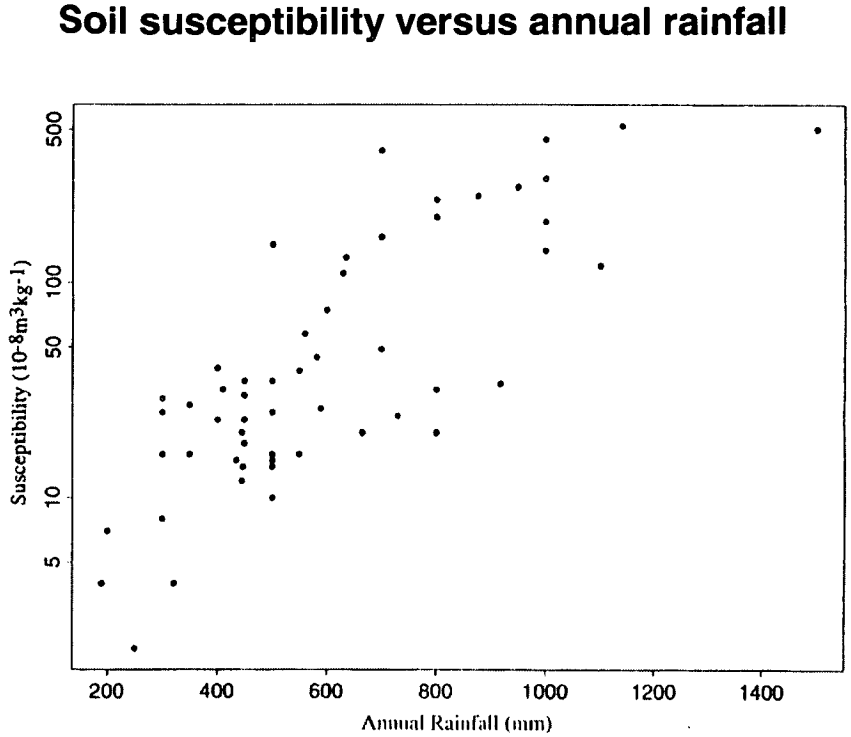

Figure 1.1. Graph of soil magnetic susceptibility plotted against rainfall for northern hemisphere soils (after Maher and Thompson, 1995).

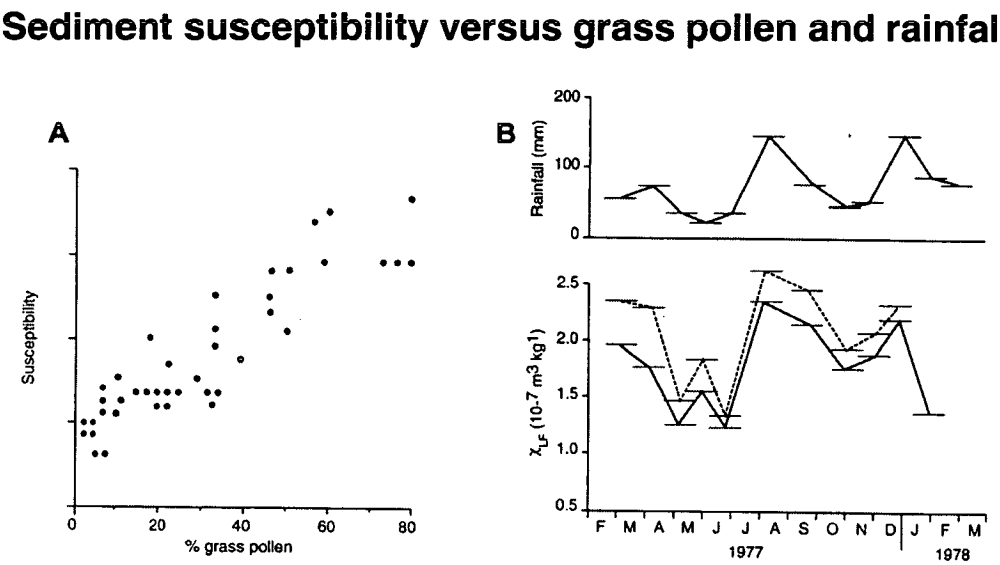

Figure 1.2. A) magnetic susceptibility of lake sediments plotted against the grass pollen relative abundance for those sediments (Thompson *et al.*, 1975). B) Susceptibility of sedimenting material (mass specific, solid line and allegoric, dashed line) with monthly rainfall (Dearing and Flower, 1982).

Environmental magnetism, as a distinct field, was first discussed in 1980 (Thompson *et al.*, 1980). Since then, much research has been undertaken to understand the magnetic properties of materials in terms of environmental processes. One of the advantages of environmental magnetism over other techniques is the relative ease and rapidity of data acquisition: hundreds of magnetic measurements can be made in a single day. The equipment required for making basic magnetic measurements is

relatively cheap and, in the case of susceptibility measurements, portable. In addition to the speed and ease of acquisition, most magnetic measurement techniques are non-destructive. This means that further studies can be made on a sample that has had its magnetic properties measured. Environmental magnetism can also be used to investigate questions which cannot be answered by chemical and physical techniques (Oldfield, 1991).

Two particular interests of environmental magnetism have been soils and lake sediments. Environmental investigation of the magnetic properties of lake sediments have been carried out on lakes from all over the world. Magnetic measurements of lake sediments have been used to: identify, and quantify erosion within lake catchments (O'Hara, *et al.,* 1993; Erikson and Sandgren, 1999), make quantitative identifications of sediment sources (Thompson, 1986; Yu and Oldfield 1989; Maher and Thompson, 1992 (Loess); Walden *et al.,* 1997; Lees, 1997), and investigate changes in climate (Sagnotti *et al.*, 1998; Ortega-Ramirez *et al.*, 1998). In each of these studies one of two techniques has been applied:

1. A comparative assessment of the magnetic properties of lake sediment material.
2. Iterative constrained least squares magnetic end-member unmixing using SIMPLEX.

In the first of these techniques, the magnetic properties of sedimentary material being analysed are either compared to the magnetic properties of other sediment horizons or catchment material. This comparison is done in a qualitative way and allows the identification of broad trends. O'Hara, *et al.,* (1993), for instance, suggest high susceptibility in Lake Pátzcuaro's sediments (central Mexico) indicates soil erosion, assuming the soils in the Lake Pátzcuaro catchment have a higher susceptibility than organic material produced within the lake during low erosion periods. Erikson and Sandgren, (1999) use a slightly more detailed approach, linking the remanence properties of lake sediments to depositional environments (Figure 1.3). They propose that sediments with remanence properties similar to haematite were deposited in swamp conditions, suggesting that dissolution had removed the dominant magnetite signal that was seen in the catchment's soils (Figure 1.3).

The second of the two techniques for the environmental analysis of lake sediments uses quantitative computer modelling. Quantitative modelling allows sediment samples to be unmixed, or separated, in terms of catchment end-members. Constrained least squares iterative modelling using the SIMPLEX technique has been used to quantitatively identify likely sediment sources. The quantitative identification of lake sediment sources facilitates a greater understanding of past environmental processes. However, the SIMPLEX method has a grave drawback: because SIMPLEX is an iterative technique, it is not guaranteed to converge on a global minimum solution. SIMPLEX is discussed further in Chapter 4.1.2.

The magnetic properties of lake sediments have also provided a quick method of correlating between sediment cores (Thompson and Oldfield 1986).

Summary diagram of environmental magnetic techniques applied to lake sediments from central Tanzania

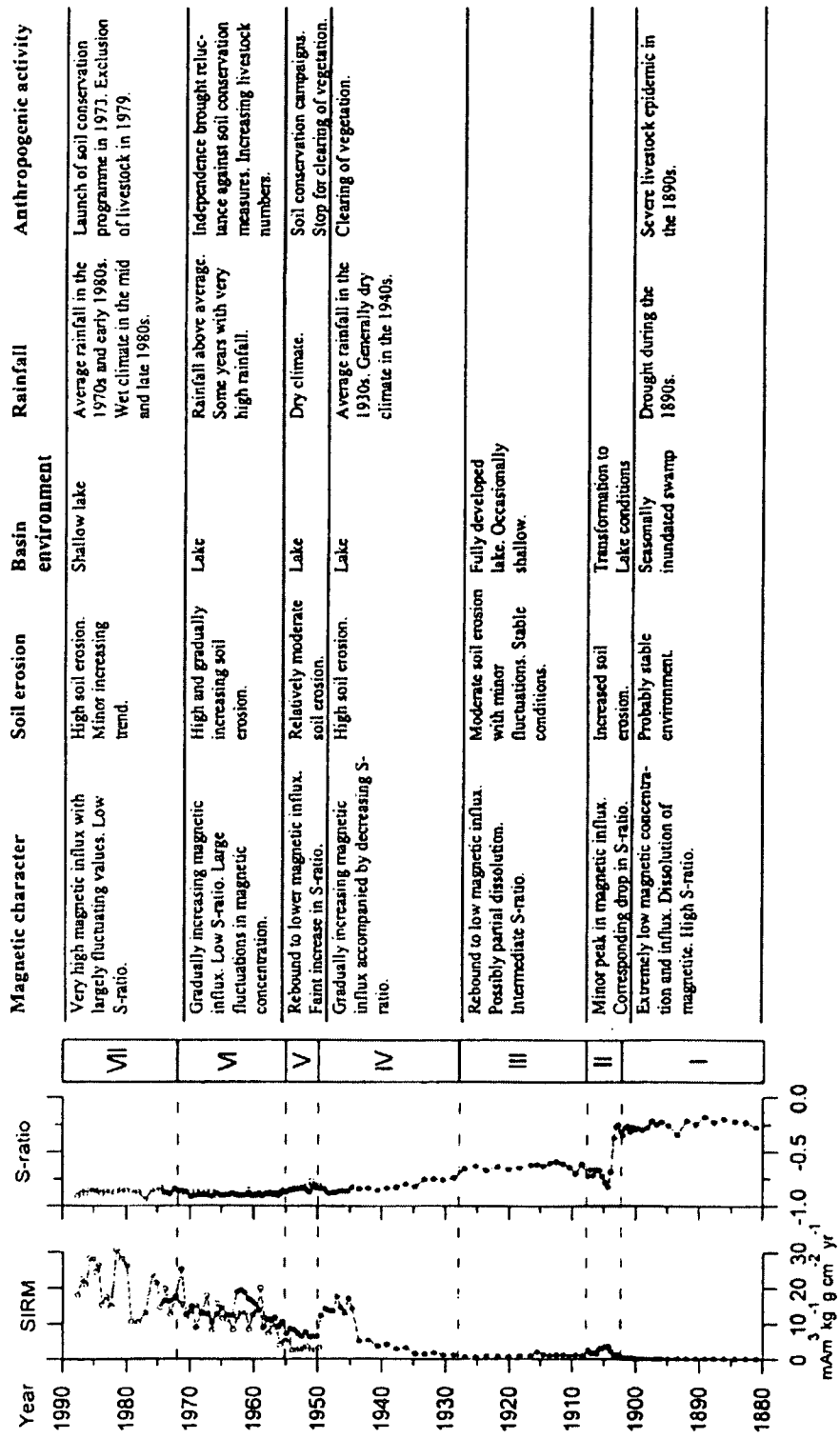

Figure 1.3. Summary diagram of comparative assessment environmental magnetic techniques applied to lake sediments from central Tanzania. Columns show magnetic parameters of saturation IRM, and S-ratio, plus a summary of the interpretation of the magnetic properties of the lake's sediments. The interpretation is given in terms of soil erosion and basin environments plus historical data from the catchment, which includes rainfall and anthropogenic activity (after Eriksson and Sandgren, 1999).

A link between the magnetic properties of soil profiles and the annul rainfall at the soil profile site has been suggested (Maher, *et al.*, 1994) (Figure 1.1). However the relative importance of climate on the magnetic properties of soils as compared to other soil-forming factors like time and parent material is a point of contention. One location where a relationship between the magnetic properties of soils and rainfall is of particular interest is the loess plateau in China. The magnetic properties of loess and palaeosol sequences in the loess plateau in China have been interpreted in terms of past climates (Maher *et al.*, 1994). The connection between the magnetic properties of the loess deposits and climate potentially give access to the longest land-based climate record in the world (the loess deposits have been accumulating for approximately 2.5 million years (Heller and Liu, 1982)). The relationship between soil magnetics and climate is further discussed in Chapter 3.4.

1.2 The aims of this project

This study has two main aims:
1) To develop and apply an improved magnetic unmixing technique.
2) To investigate the relationship between rainfall and soil magnetic properties.

The first aim is achieved through the development of new unmixing routine that uses non-negative least squares and a stepwise F-testing function to generate parsimonious best-fit models that unmix the magnetic properties of a sediment sample in terms of selected end-members. The new unmixing technique is applied to sediments from two lakes in Mexico: Lake Pátzcuaro, in the central Mexican volcanic belt, and Lake Babicora, in the northern Mexican plateau. In both cases, the results of the unmixing models are interpreted in terms of environmental processes that have affected the magnetic properties of the lake's sediments.

To achieve the second aim, the magnetic properties of 89 soil samples, which were collected from across large rainfall gradients in Mexico, are measured, and compared to the rainfall at the soil profile sites. I generate multiple component models relating the magnetic properties of the soil profiles to the annual rainfall in order to understand better the effect of rainfall on the magnetic properties of soils.

1.3 Climate of Mexico

Mexico was chosen as the field location for this project due to the large diversity in climates that it experiences at present and has experienced in the past. Mexico is climatically sensitive (Kutzbatch and Street-Perrott, 1985; Liverman 1993), having experienced climate changes on both long (Bradbury 1989; Metcalfe *et al.*, 1991) and short (Jauregui and Klaus, 1976, O'Hara and Metcalfe, 1997) time-scales. Two major atmospheric circulation features affect the climate in Mexico at present: the trade winds and the sub-tropical high-pressure belt. The wet and dry seasons in Mexico are associated with the position of the inter tropical convergence zone (ITCZ). During the northern hemisphere summer (Figure 1.3a), April to October, the ITCZ moves northwards, along with the Bermuda Azores and East Pacific highs. These features bring the majority of Mexico's rainfall by generating a monsoon-type circulation. Conversely in the Northern hemisphere's winter (Figure 1.3b), the ITCZ

moves south, bringing the sub-tropical high pressure belt over Mexico. This results in stable dry conditions over much of the country.

The region of high precipitation on the precipitation map of Mexico (Figure 1.5), has been described as a highly deformed "U" (Mosiño and García, 1974) (Figure 1.5): the left stroke of the U runs down the western side of the Sierra Madre Occidental mountain range, the right stroke runs down the east side of the Sierra Madre Oriental mountain range and the tail of the U is found in the south east lowlands and the Yucatan peninsular. Mosiño and García (1974) describe the causes of these three high rainfall zones. The cause of the high rainfall region to the east of the Sierra Madre Oriental mountain range is moisture-laden trade winds from the east being forced to rise over the central Mexican plateau. The high rainfall in the south east of Mexico is caused by three factors: i) orographic effects, similar to those affecting the area to the east of the Sierra Madre Oriental, ii) tropical cyclones from the Caribbean sea and the Gulf of Tehuantepec and iii) the ITCZ, which can reach this far north in the northern hemisphere summer. The high rainfall experienced on the west side of the Sierra Madre Occidental mountain range is caused by tropical cyclones moving along the western coast of Mexico. The central Mexican plateau has lower rainfall than the coastal lowlands, because most of the moisture has been removed from the air masses moving over this region. The precipitation effects described above combine to produce very large climate gradients across Mexico. The precipitation of Mexico ranges from over 4,500mm per year in the Southeast to less than 300mm per year in the Northwest. The variability of climate across Mexico has led to a great variety of ecosystems in the country (Figure 1.6).

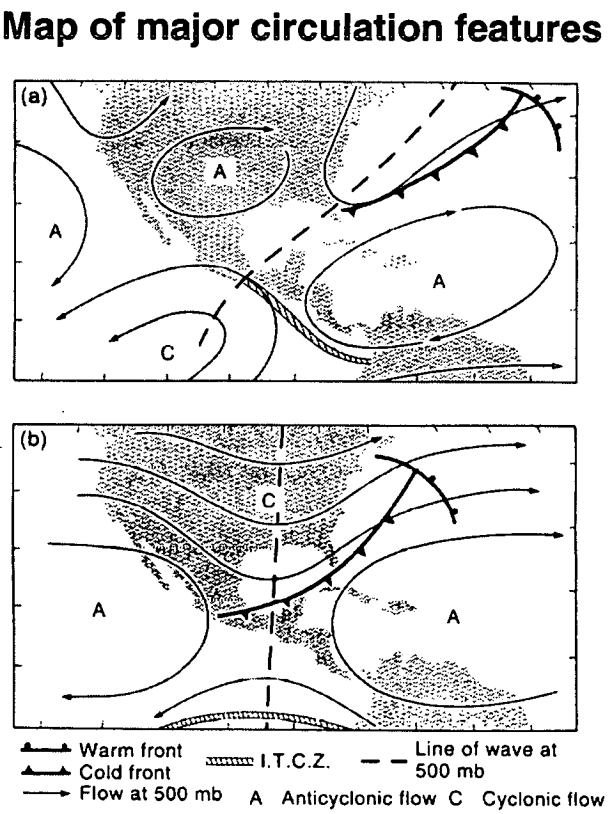

Figure 1.4. Map of the major atmospheric circulation features for summer (a) and winter (b) in Mexico (after O'Hara and Metcalfe, 1997).

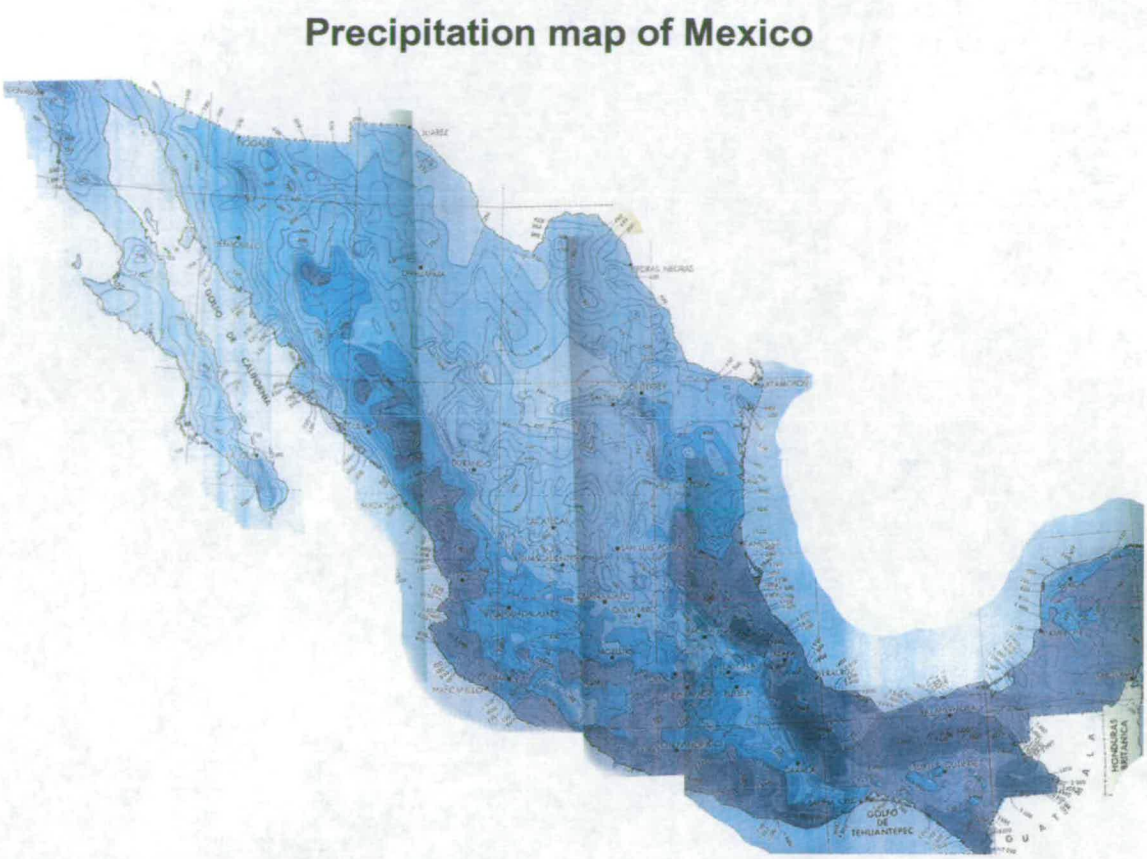

Figure 1.5. Precipitation map of Mexico with precipitation contours every 100mm year^{-1}. Darker shades indicate higher rainfall. (Map compiled by Dirección Geografía y Meteorología)

Figure 1.6. Five of the major ecosystems present in Mexico (Robles, 1994).

1.4 Thesis layout

In this study I start by giving background information on the magnetic measurement techniques used and the most significant magnetic minerals found naturally (Chapter 2). I then review previous work on environmental magnetics as applied to soils and lake sediments (Chapter 3). Chapter 4 contains an explanation of the magnetic unmixing technique that I have developed. Also in Chapter 4 are descriptions of error analysis and skill measure techniques that are used to asses the results of the magnetic unmixing routine. I apply the new magnetic unmixing routine to the magnetic properties of two sediment cores taken from Lake Pátzcuaro (Chapter 5), and two sediment cores taken from Lake Babicora (Chapter 6). The investigation of a link between the magnetic properties of soil samples collected during two field seasons in Mexico and the annual rainfall at the soil sample sites is discussed in Chapter 7. Chapter 8 comprises the conclusions of the thesis.

Chapter 2

Mineral magnetism

This chapter provides a brief introduction to the magnetic properties of natural minerals. It covers basic mineral magnetic properties and measurements, and introduces some useful parameters and graphs. The information in this chapter is included as background for following chapters, which use rock magnetic properties to describe and aid in the understanding of the environment.

2.1 Magnetic mineral classification

There are three classes of minerals, diamagnetic, paramagnetic and ferromagnetic. Each type of mineral can be characterised by its behaviour in a magnetic field (Thompson and Oldfield, 1986):

Paramagnetic minerals are attracted towards a positive magnetic field gradient. The attraction into a magnetic field is due to permanent magnetic dipole moments within the paramagnetic mineral, which are normally randomised by thermal activity. An external magnetic field supplies the energy necessary to align the magnetic dipoles. The randomisation due to thermal activity still persists within a magnetic field. The number of the material's magnetic dipoles aligned with the external field, and hence the force of attraction, depends on both the temperature and the strength of the applied field. When a paramagnetic mineral is removed from a magnetic field, it immediately loses its magnetism.

Diamagnetic minerals are repelled from a positive magnetic field gradient. The repulsion of a diamagnetic mineral from a magnetic field is caused by the generation of magnetic dipole moments within the atoms of the mineral. These dipoles are formed by the disruption of electron orbits within the material due to the presence of the magnetic field. The repulsion of a diamagnetic mineral from a magnetic field gradient is far smaller than the attraction of a paramagnetic mineral. Like a paramagnetic mineral, a diamagnetic mineral loses its internal magnetic field once it has been removed from an external magnetic field.

Ferromagnetic minerals are attracted into a positive magnetic field gradient. The strength of attraction is far larger for ferromagnetic minerals than it is for paramagnetic minerals. Ferromagnetic minerals have permanent internal magnetic dipole moments due to the spin of electrons within the mineral. The individual dipoles within a ferromagnetic mineral, when aligned by an external magnetic field,

will tend to remain aligned even when the field is subsequently removed. The persistence of the dipole alignment is called remanence and is caused by quantum mechanical effects arising from the ferromagnetic mineral's crystal lattice structure.

2.2 Hysteresis

Remanence means that the magnetic properties of a ferromagnet depend not only on the present conditions affecting it, but also on the past magnetic fields to which it has been subjected. In Figure 2.1 the magnetic field that a ferromagnetic material is being subjected to is plotted on the horizontal axis, against the magnetisation induced within the material on the vertical axis. Also shown is the low field magnetic behaviour. Up to a certain applied magnetic field ferromagnetic materials exhibit no hysteresis effects, when the external field is removed the material returns to an unmagnetised state. Beyond this reversible stage, the material will remember the field that it has been subjected to. Low fields will result in low remanence in the sample. Higher external fields will induce higher values of remanence, until the material reaches saturation remanence. Saturation remanence is the state where a further increase in the applied magnetic field will not increase the remanence of the sample.

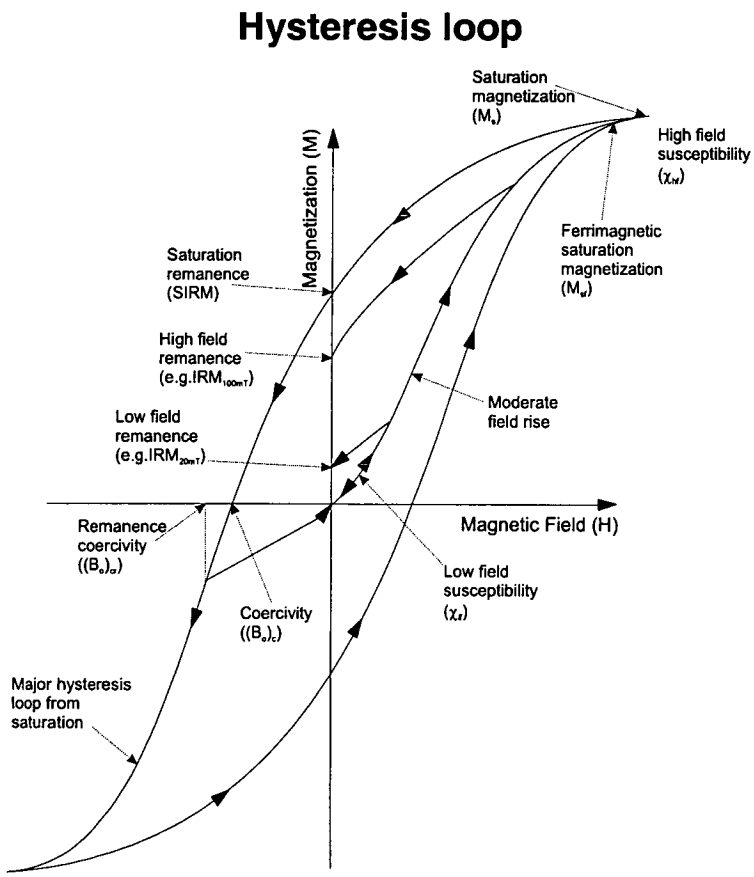

Figure 2.1. After Maher *et al.*, (1999) Some important parameters on the hysteresis curve are: Saturation Magnetisation (M_S), which is the largest magnetisation that can be imparted to a given ferromagnetic mineral. Saturation Remanence (B_S), which is the remanent magnetisation of a material that has been magnetised in a saturating field and is the same as SIRM discussed later. Coercive force (B_{cr}), which is the magnetic field that has to be applied to reduce the saturation remanence to zero magnetisation when measurement is made in the presence of the field (Thompson and Oldfield 1986).

2.3 Ferrimagnetism and antiferromagnetism

The majority of natural magnetic minerals with which palaeomagnetism and environmental magnetism are concerned are the ferrimagnets and imperfect antiferromagnets. Ferrimagnets and imperfect antiferromagnets are special classes of ferromagnet and owe their magnetic properties to the alignment of the electrons in their 3d shell. The relative direction and intensity of the magnetic dipoles of individual atoms at different crystal sites, and the interactions between these sites, determines the different classes of magnetic properties of the ferrimagnetic and antiferromagnetic minerals. The various types of ferrimagnets and antiferromagnets and their crystal lattice interactions are best represented graphically (Figure. 2.2).

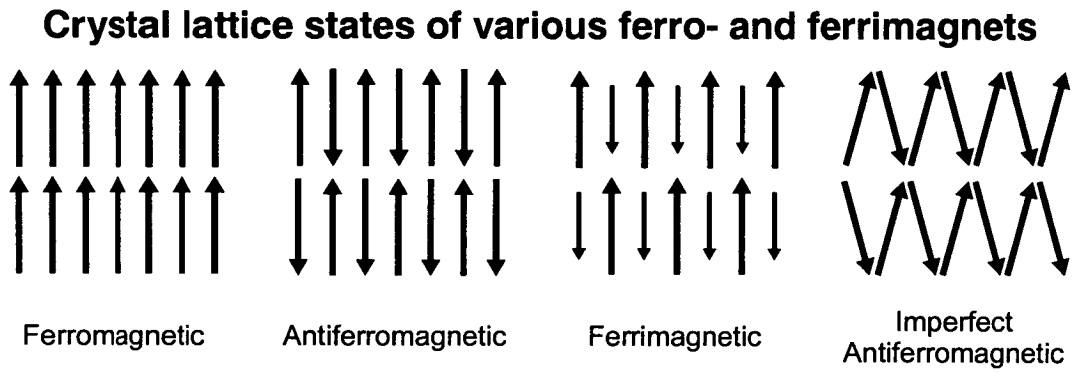

Figure 2.2 Arrangement of magnetic moments in ferrimagnets ferromagnets and anti ferromagnets (Stacey, 1992)

Ferrimagnetic minerals have two types of magnetic crystal lattice sites that naturally align themselves to be antiparallel. The net magnetic moment within the ferrimagnet is due to either a difference in the ionic make up of different crystal sites, or a crystallographic inhomogeneity between different sites (Figure 2.2). In antiferromagnetic minerals there are two different magnetic crystallographic sites, however the magnetic moments of the ions at different sites entirely cancel, to give zero net magnetic moment (Figure 2.2). A net magnetic moment can only exist within an antiferromagnet if its individual magnetic ion sites are not entirely antiparallel, this is called imperfect or canted antiferromagnetism (Figure 2.2). In practice ferrimagnets have strong magnetic properties and moderate coercivities. Imperfect antiferromagnets have weaker magnetic properties but very high coercivities. These differences can be used to detect them in natural materials (Thompson and Oldfield, 1986).

2.4 Magnetic parameters

Here I shall explain the three basic magnetic parameters that have been used in this work to characterise the magnetic properties of natural samples. Although there are alternative magnetic measurements available, like high and low temperature remanence, and thermal demagnetisation. These techniques were considered either too time consuming to apply to the large number of samples analysed, or else they were destructive in nature; the sample would not be available for other techniques after the measurement. The magnetic parameters used in this study are:

1. Susceptibility
2. Isothermal remanent magnetisation (IRM)
3. Anhysteretic remanent magnetisation (ARM)

2.4.1 Susceptibility

The susceptibility of a sample is the ratio of the magnetic field induced within it to the magnetic field required to produce that magnetisation. In this project susceptibility has been measured using a Bartington susceptibility bridge. The susceptibility bridge generates a high frequency low amplitude alternating magnetic field to induce a field in the sample. Magnetic crystals at some sizes are sensitive to the frequency of an applied field. For these crystals a susceptibility measurement at a high frequency will be lower than a susceptibility measurement at a low frequency. This effect is called frequency dependence and shall be discussed in more detail below (Section 2.6). I measured both low and high frequency susceptibility on all the samples in this study.

2.4.2 Isothermal remanent magnetisation (IRM)

The IRM of a sample is the magnetisation retained by that sample when it has been subjected to a known field at a known temperature (usually room temperature). IRM can be measured at varying field strengths, typically between 20mT and 3T. IRMs may be measured at several different fields by either: increasing the field that a sample is subjected to in stages and measuring the samples remanence between each stage, or, by magnetising the sample at a high field and then applying increasing fields in the opposite direction to remove the original magnetisation. In this study the former technique was used.

The saturation IRM or SIRM is the maximum remanence that a sample can acquire by IRM magnetisation and is equivalent to M_s measured at room temperature (the saturation magnetisation Figure 2.1). The field at which SIRM is induced can be very diagnostic of a material's composition. For example magnetite will usually reach saturation at approximately 300mT whereas Haematite is often still unsaturated at applied fields of 2T or 3T, and goethite has been known to still be gaining remanence above 9T (Dekkers, 1988). The overall shape of the IRM acquisition curve (the IRMs gained through the application of successive magnetic fields of increasing intensity) contains information about the magnetic composition of a sample. All the samples in this study had IRM's imparted at 20, 40, 60, 80, 100, 200, 300, 1000, 2000, and 3000mT, with remanence measurements made between each magnetisation.

2.4.3 Anhysteretic remanent magnetisation (ARM)

The ARM of a sample, sometimes called its perfect magnetisation, is similar to the IRM in that it is a measurement of the remanent magnetisation of a sample after it has been subjected to a known field. To impart an ARM, the sample, is magnetised within an alternating (ac) magnetic field, with a smaller steady (dc) field superimposed. The ac field is increased to a known maximum and then smoothly reduced to zero. ARM drives the magnetisation of the sample backward and forward around the origin of its hysteresis loop. A net magnetisation is imparted by creating a statistically preferred remanence direction with the small dc field. ARM is generally imparted at a high alternating field, measured, and then demagnetised using smaller alternating fields, without the application of the steady field. The demagnetisation of the sample using known fields builds up an ARM demagnetisation curve. The ARM demagnetisation curve gives similar information to the IRM curve, however ARM

properties are more strongly influenced by grain size and magnetic interactions. In this study samples were magnetised with an alternating field of 99mT and a steady field of 0.1mT, before being demagnetised in fields of 5, 10, 20, 40 and 80mT.

2.4.4 Measurement sequence

The sequence in which magnetic measurements are made is very important. Remanence means that measurements previously made on a sample can influence future measurements. In this study the magnetic measurements have been made in a strict order

1. Susceptibility (low frequency then high frequency).
2. ARM (imparted at 99mt then demagnetised at 5, 10, 20, 40 and 80mT).
3. IRM (20, 40, 60, 80, 100, 200, 300, 1000, 2000 then 3000mT)

2.4.5 Remanence notation

The names of IRM and ARM measurements shall be abbreviated by the remanence type followed by the magnetising, in the case of IRM's, and demagnetising, in the case of ARM's, field. So a IRM imparted at 100mT will be written IRM_{100} and an ARM demagnetised at 10mT as ARM_{10}. IRM magnetisation at 3000mT and ARM magnetisation are referred to as SIRM (saturation IRM) and SARM (saturation ARM).

2.5 Magnetic properties of ferromagnetic materials

Ferromagnetic crystals will seek to balance or minimise three different energies: thermal, magnetic moment, and surface magnetic tension, caused by "free poles" at the surface of the magnetic crystal (Tauxe, 1998). The point at which these energies balance will determine the magnetic properties of a sample.

2.5.1 Temperature

Ferromagnetism is a temperature-dependent phenomenon. In fact ferromagnetism and paramagnetism are at different ends of a thermal energy / magnetic energy scale. At a low enough temperature paramagnetic behaviour can become ferromagnetic due to the lack of randomising thermal energy. Likewise at a high enough temperature ferromagnets can become paramagnetic due to thermal energy randomising the direction of individual ionic dipoles. The temperature at which ferromagnetism breaks down is called the Neel or Curie Temperature and is dependent on mineral composition. Indeed it is often used to identify minerals (Nagata, 1961).

2.5.2 Magnetic grain-size

Magnetic crystal grain size is, as with temperature, a balance between opposing energies. The larger the magnetic crystal the greater the magnetic tension caused at its surface by "free poles" (Tauxe, 1998). As the grain size increases, the number of free poles at the surface of the crystal also increases. At a certain size, this magnetic surface tension overcomes the magnetic moment of the crystal and splits it into two or more magnetic domains. There are five different magnetic states that are

dependent on the size of the ferromagnetic crystal. These are superparamagnetism (SP), viscous magnetism, single domain (SD), pseudo single domain (PSD) and multidomain (MD).

Superparamagnetic (SP) materials are so small that thermal energies overcome stable magnetic energies. Minerals of SP size are not capable of holding remanence at room temperature. As the name suggests these very small minerals exhibit strong paramagnetic properties.

Viscous materials are in a grain size between supperparamagnetic and single domain, they can hold remanence for a short period of time, the exact amount of time depends on the grain-size and temperature.

Single domain (SD) crystals overcome the randomising effect of thermal energy by the magnetic energy of larger volume, a very stable magnetic moment results.

Pseudo single domain (PSD) crystals are larger than single domain crystals. They balance the extra magnetic tension over their surfaces that their increased size generates by dividing their magnetic moment into a few magnetic domains. Each magnetic domain will have its own magnetic moment and will be separated by a domain or block wall. PSD crystals in many ways act similarly to single domain crystals, with similar saturation and stability (Thompson and Oldfield 1986).

Multi domain (MD) crystals have more strongly developed domain structures than PSD crystals. The magnetisation properties of MD crystals are severely reduced as the domains tend to cancel out each others magnetic moments. However MD grains can still hold remanence, as an applied magnetic field will tend to move the domain walls to favour a magnetic moment in alignment with the applied field.

2.6 Frequency dependent susceptibility

The induced magnetic field of sub-micron sized magnetic crystals near the SP/SD boundary is sensitive to the frequency of the applied field (Bloemendal and Barton, 1985). A higher frequency applied field produces a lower response field in these samples. By measuring the susceptibility at two different frequencies (1kHz and 10kHz) it is possible to get a measure of its frequency dependence (Equation 2.1). Frequency dependence therefor gives an indication of the amount of small magnetic grains there are in a given sample. A suggested limit to χ_{fd} of 8% was given by Mullens (1977), however results above 10% have been reported (Verosub and Roberts, 1995) and I have been informed of frequency dependence approaching 15% (Maher, Pers. comm.).

$$\chi_{fd}(\%) = 100 * \left(\frac{\chi_{lf} - \chi_{hf}}{\chi_{lf}} \right)$$

Equation 2.1

where:

χ_{fd} = Frequency dependence as a percentage of χ_{lf}.

χ_{lf} = Susceptibility measured at low frequency.

χ_{hf} = Susceptibility measured at high frequency.

2.7 Magnetic stability (hardness)

Magnetic stability or hardness is a qualitative measure of the ease with which a sample can have a remanence imparted or removed. A material is said to be magnetically hard if a relatively high field is needed to magnetise or demagnetise it, and soft if a low field will do the same. The relative "hardness" of ferromagnetic minerals can be linked to their magnetic crystal size. A sample consisting of predominantly single domain crystals will be relatively hard requiring high fields to influence its magnetic remanence. A sample containing mostly multidomain grains will be magnetically soft and it will be easy to impart a remnant magnetisation (Thompson and Oldfield, 1986). Viscous materials are generally magnetically soft, so both the largest and smallest crystals display soft magnetic properties, and can therefor be difficult to distinguish without other measurements like frequency dependent susceptibility and ARM.

2.8 Magnetic parameter ratios

Although much information can be obtained from individual magnetic parameters and the shapes of remanence acquisition and demagnetisation curves, the sheer volume of magnetic data can be prohibitive. It has been found that ratios of magnetic measurements and in particular biplots of two ratios can make magnetic data more accessible. Biplots of SIRM/B_r against B_{cr}/B_c have been used to identify magnetic grain sizes (Day, Fuller and Schmidt, 1977) as has the ratio of SIRM/χ (Tauxe, 1993). However for both of these estimations of grain size it has to be assumed that the only minerals within the samples being plotted are magnetite and that there is only one grain size present in the sample. In many natural samples these assumptions can be misleading. Figure 2.3 is an example of a Day plot with the zones of various size fractions marked out.

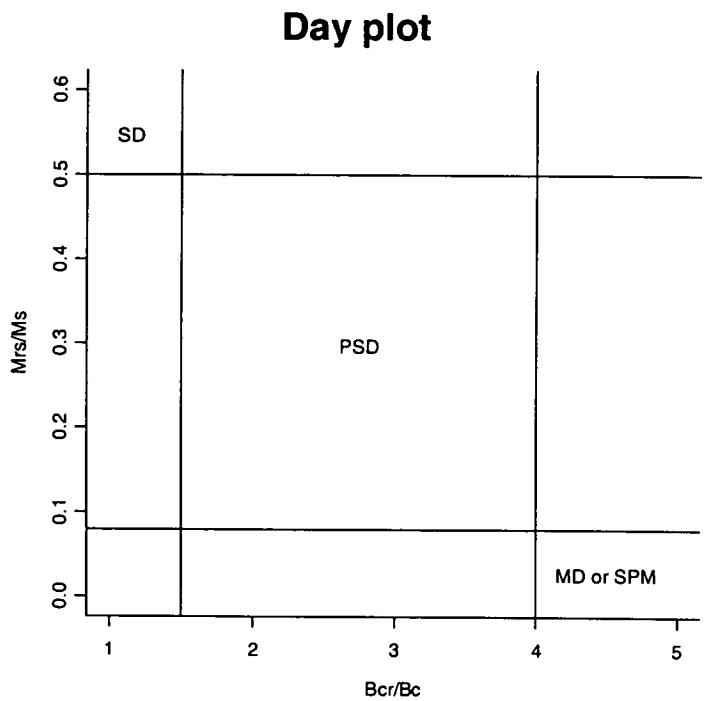

Figure 2.3 The Day plot gives an indication of the magnetic grain size for materials that contain only one size fraction of magnetite. Diagram after Day *et al.* (1977)

In this study I shall use a variety of biplots to help visualise the magnetic properties of sediments. I shall include magnetic mixing curves on these biplots that describe the magnetic properties of varying concentration mixtures of two magnetic minerals. Although the magnetic properties of minerals in low concentration are considered to add linearly (Chapter 4.1), the difference in magnetic remanence intensities for different minerals leads to a curved mixing line. These mixing curves aid the interpretation of the magnetic properties of various materials, and give a feel for the multi-dimensional space described by remanence and susceptibility measurements. The shape of the mixing curves is characterised on the biplots (Figure 2.4 and 2.5) as grey dots between each set of two minerals. Each dot on the mixing curve represents a 5% increase in the concentration of one of the minerals that the dot lies between. The magnetic measurements used to characterise the minerals on these biplots have come from many sources and experiments, which have been collated over the career of Roy Thompson.

The first of the biplots (Figure 2.4) shows ARM hardness against IRM softness, these two parameters show some degree of correlation. We do however see a wide separation of the magnetic minerals within this biplot alone. The second biplot (Figure 2.5) shows squareness against IRM softness. This biplot is particularly good at identifying magnetotactic bacteria magnetosome chains (Chapter 3.1) and viscous magnetite.

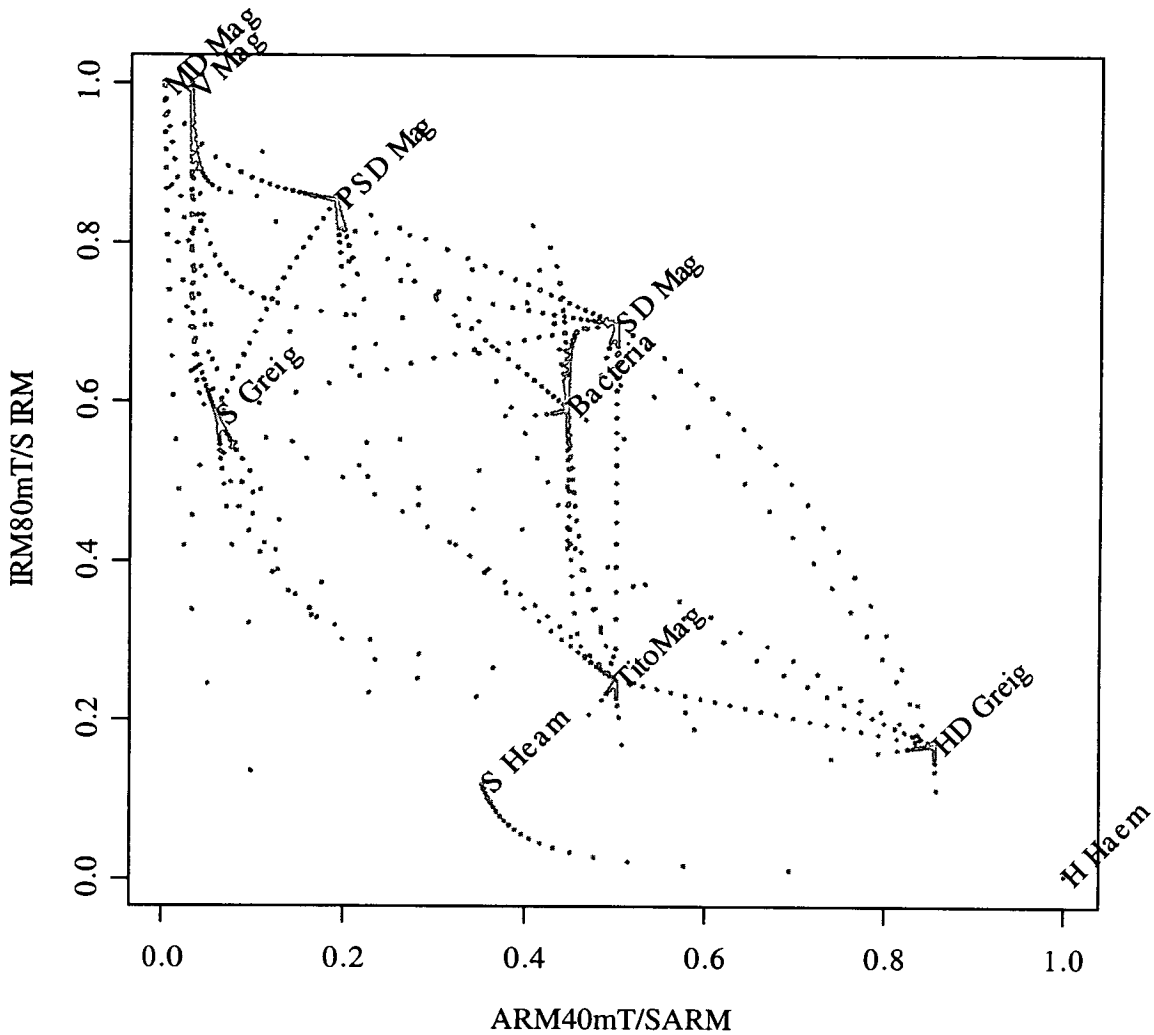

Figure 2.4 Biplot showing the SARM demagnetised in an alternating field of 40mT divided by SARM against IRM acquired at 80mT divided by SIRM. Increasing values on the X-axis denote higher ARM hardness. Increasing values on the Y-axis denote increasing IRM softness. The dots represent the magnetic properties of mixtures of materials between each of the minerals. Each dot represents a 5% change in concentration between the two end members. Abbreviations used in this plot are, S = soft, H (HD)= hard, V = viscous boundary, Mag = magnetite, Greig = greigite Haem = haematite and TitoMag = titanomagnetite.

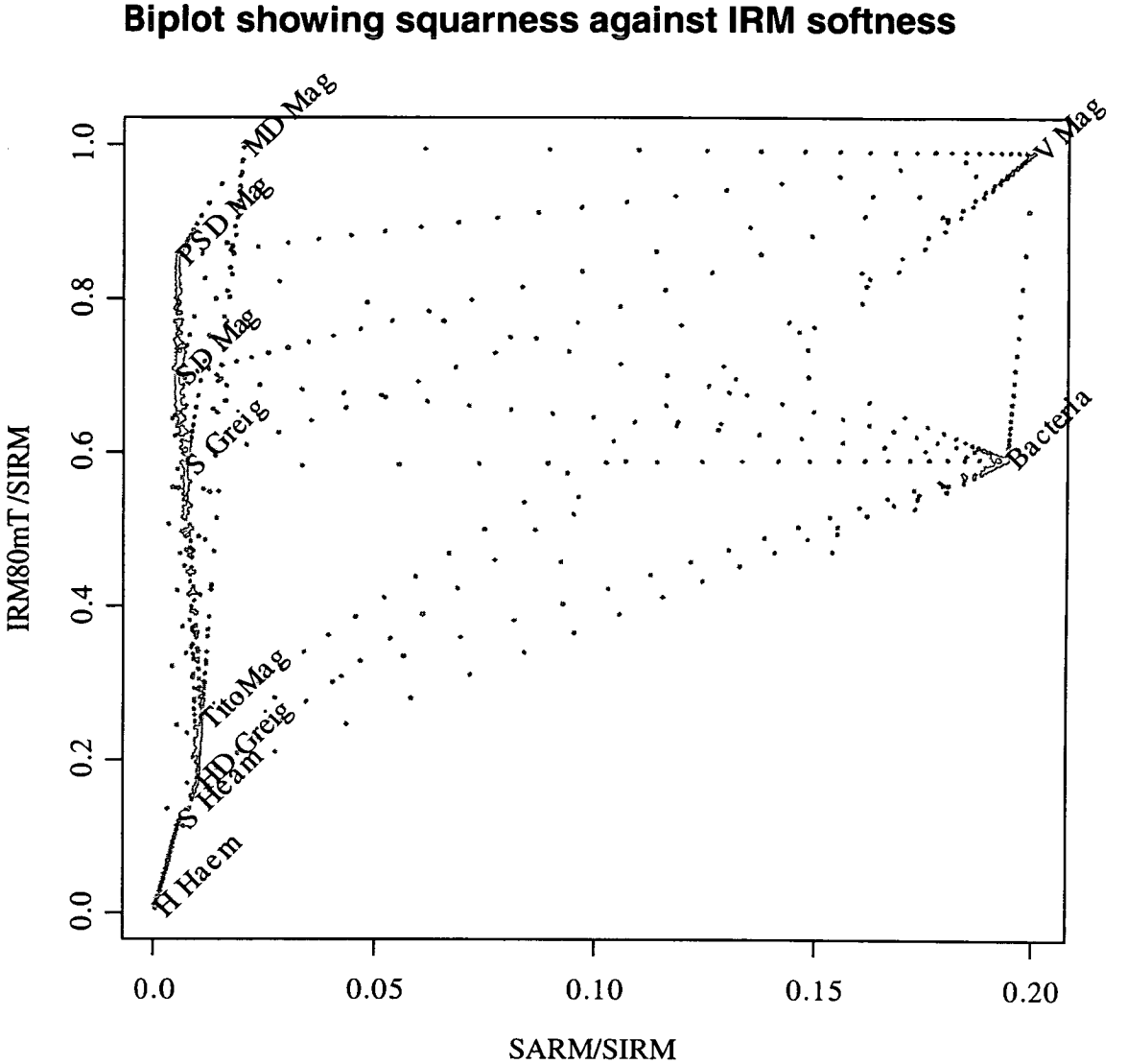

Figure 2.5 Biplot showing the SARM / SIRM which is related to the squarness of the hysteresis loop, against IRM acquired at 80mT divided by SIRM. Increasing values on the X-axis denote higher SARM to SIRM importance, or squareness. Increasing values on the Y-axis denote increasing IRM softness. The dots represent the magnetic properties of mixtures of materials between each of the minerals. Each dot represents a 5% change in concentration between the two end members. Abbreviations used in this plot are, S = soft, H (HD) = hard, V = viscous, Mag = magnetite, Greig = greigite Heam = haematite and TitoMag = titanomagnetite.

2.9 Natural magnetic minerals

What follows is a brief summary of the properties of some natural magnetic materials, starting with the most common, the iron oxides and then looking at the iron sulphides and hydroxides. The minerals chemical formulae and distinguishing features are given. The magnetic properties of these minerals are summarised in Table 2.1.

2.9.1 Iron oxides

The iron oxides form the majority of all natural magnetic minerals. The combination of iron, oxygen and titanium has many magnetic phases, and attached to some of

these phases are the names magnetite, Haematite, maghaemite, titanomagnetite and titanohaematite. In reality there is a smooth transitions between these end-members, they form a solid solution series. A good summary of this group of minerals can be seen in the ternary diagram (Figure 2.6)

Ternary phase diagram for the iron and titanium oxides

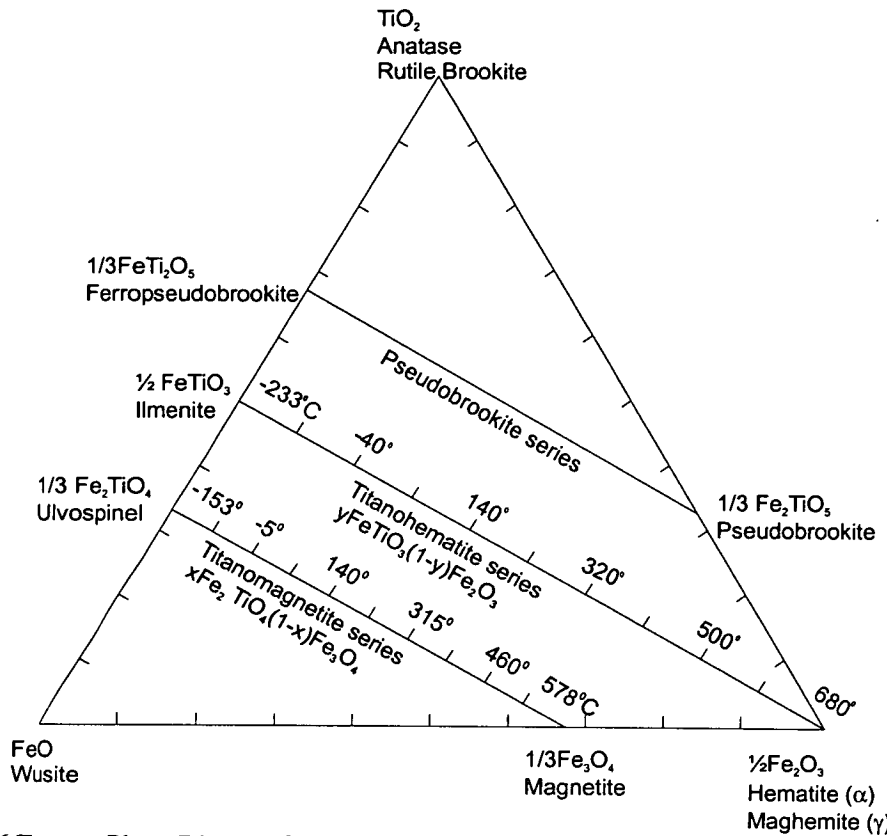

Figure 2.6 Ternary Phase Diagram for the iron and titanium oxides, with Curie temperatures for the ferromagnetic minerals (McElhinny and McFadden, 2000).

Magnetite (Fe_3O_4) is the strongest and most abundant natural magnetic mineral on Earth: it is a ferrimagnet. In its single domain form magnetite holds a stable remanence for millions of years. The presence of magnetite in most sediments and rocks has allowed workers in the field of palaeomagnetism to make retrodictions of continental movements and field reversals. It has a cubic inverse spinel structure and a Curie temperature of 578^0 C.

Haematite. (Fe_2O_3) is a canted antiferomagnet with magnetic properties weaker than magnetite. Haematite is the second most abundant magnetic mineral on Earth. It can be characterised by its IRM hardness, very stable magnetic remanence, resistance to ARM magnetisation and high Curie temperature, 675^0 C.

Maghaemite (αFe_2O_3) has the same composition as Haematite but has the cubic structure of magnetite. This mineral has very similar magnetic properties to magnetite, but with a higher SIRM and Curie temperature. In the natural environment it generally occurs where magnetite has been oxidised at low-temperature and is indicative of weathering.

Titanomagnetite ($Fe_3O_4 \rightarrow Fe_2TiO_4$) from magnetite ($Fe_3O_4$) to ulvöspinel ($Fe_2TiO_4$) (a paramagnet at room temperature). The titanomagnetites form a continuos series and their magnetic properties vary smoothly between the magnetite and ulvöspinel end-members. TM60 is near the centre of the titanomagnetite series with a composition of $Fe_{2.4}Ti_{0.6}O_4$ and has been used in this study to characterise the properties of titanomagnetites.

Titanohaematites ($Fe_2O_3 \rightarrow Fe_1Ti_1O_3$) this series ranges from haematite (Fe_2O_3) to ilmenite ($Fe_1Ti_1O_3$) (a paramagnetic mineral at room temperature). Unlike the titanomagnetites, titanohaematites do not have a smooth transition in their magnetic properties between their end-members. With increasing titanium concentration, the magnetic properties go from canted-antiferromagnetic (haematite) to strongly ferrimagnetic and finally antiferromagnetic (ilmenite).

2.9.2 Iron sulphides

The next most common group of natural magnetic minerals are combinations of iron and sulphur. These minerals are less common than the magnetic oxides and are generally formed in environments that lack oxygen.

Pyrrhotite (FeS_1) despite the chemical formula, pyrrhotite occurs in nature with slightly less iron than sulphur, typically ranging between Fe_7S_8 to Fe_9S_{10}. The resulting vacancies in the crystal lattice are well ordered and lead to a net ferrimagnetic moment by reducing the magnetic moment of one of the magnetic sub-lattices. Pyrrhotite typically has a Curie temperature of between 290^0 and 330^0 C

Greigite (Fe_3S_4) has recently become acknowledged as a contributor to the magnetic properties of both lake sediments and soils (Roberts *et al.* 1996). Its magnetic properties are similar to those of pyrrhotite, as is its Curie temperature.

2.9.3 Iron hydroxides

Goethite (FeOOH) is the only iron hydroxide which holds a room temperature remanence. It is an imperfect antiferromagnetic mineral. Goethite is very common in nature and occurs as a weathering product of iron-bearing minerals. Goethite will dehydrate to haematite. It has very high coercivity and low Curie temperature (150^0 C).

Magnetic properties of selected natural minerals

Mineral	T_c (^0C)	M_s ($Am^2 kg^{-1}$)	C ($um^2 kg^{-1}$)	SARM ($mA\ m^2 kg^{-1}$)	SIRM ($mA\ m^2 kg^{-1}$)
Magnetite (MD)	575	92	560	18	9
Magnetite (SD)	575	92	400	110	22
Titanomagnetite (MDt)	200	24	170	80	7
Titanomagnetite (SD)	200	24	200	480	12
Haematite	675	0.5	0.6	0.002	0.24
Ilmenohaematite	100	30	25	480	8
Greigite	300	20	120	110	11
Pyrrhotite	300	17	50	80	4.5
Goethite	150	0.5	0.7	0.005	0.05
Iron	770	220	2000	800	80
Ferrihydrite ($5Fe_2O_3 \cdot 9H_2O$)	1/T	-	0.4	0 Paramagnetic	0 Paramagnetic
Lepidocrocite ($\gamma FeOOH$)	1/T	-	0.7	0 Paramagnetic	0 Paramagnetic
Diamagnet	const.	-	-0.006	0 Diamagnetic	0 Diamagnetic

Table 2.1 Summary of the magnetic properties of selected magnetic minerals. Table compiled from data by Maher and Thompson (1999) and Maher (1998).

2.10 Magneto-crystalline anisotropy

Magneto-crystalline anisotropy occurs as most magnetic materials have different magnetic properties along various crystal axis (Thompson and Oldfield, 1986). This effect arises from the internal geometry of magnetic crystals (Thompson and Oldfield, 1986). Magneto-crystalline anisotropy is strongest in imperfect antiferromagnets (Thompson and Oldfield, 1986). Some magnetic crystals can be said to have an easy axis, this refers to a crystal axis along which it is most easy to magnetise the crystal (Nagata, 1961).

2.11 Magnetic interactions

When a magnetic material has a low concentration of strongly magnetic materials, which are well dispersed, there will be relatively few magnetic field interactions (Lees, 1999). This will be the case for most natural sediments and soils (Lees, 1999). In the case of well dispersed magnetic materials the magnetic remanence and susceptibility properties of the material will add linearly (Maher and Thompson, 1999). However in a few cases, materials may be present in high concentrations or clustered. In these cases, magnetic interaction can be expected between grains. When grains are randomly orientated in clusters, a decrease in coercivity, and ARM, can be expected (Dankers, 1981; Maher, 1988). This decrease in ARM is due to negatively interacting magnetic fields between grains, and is most commonly found in the fine grained SP material (Dankers, 1981; Maher, 1988). However in the case where grains are arranged in an ordered fashion, with their magnetically easy axis in the same direction, positive interactions between grains will increase coercivity, and ARM, properties. This is most effectively seen in magnetotactic bacteria magnetosome chains (Blakemore, 1975; Moskowitz *et al.*, 1993) (Chapter 3.1).

2.12 Magnetic extractions

Several techniques have been developed to extract the magnetic materials from sediments and soils; these techniques are summarised in Hounslow and Maher (1996). In this thesis I have used the Petersen *et al.* (1986) technique for magnetic extraction using a magnetised probe. Once the magnetic materials have been extracted from a sample it is possible to study them using optical and electron microscopy, as well as X-ray diffraction. The analysis on magnetic extracts can facilitate the identification of the remanence carrying materials within a soil or sediment (Hounslow and Maher, 1996). It is important when looking at extracts to look not just at the material extracted, but also at the magnetic properties of the non-extracted material, or extract residue (Hounslow and Maher, 1999). The extract residue will contain the non-magnetic material that was in the sample as well as the magnetic material that was not extracted. It is possible to quantify the efficiency of the extraction process, by comparing the magnetic properties of the extract residue to the properties of the original sample (Hounslow and Maher, 1996). Equation 2.2 gives extraction efficiency in terms of the percentage of any given magnetic measurement (Hounslow and Maher, 1999). The efficiency of the extraction may vary between measurements if the magnetic extraction process does not extract a representative array of magnetic materials. It has been reported that the magnetic probe extraction method can preferentially extract low coercivity material (Hounslow and Maher, 1996). The bias towards low coercivity material may mean materials like haematite may not be extracted in representative quantities (Hounslow and Maher, 1996).

$$\text{Efficiency}(\%) = \frac{\text{Pre Extraction Measurement - Measurement on Residue}}{\text{Pre extraction Measurement}} * 100$$

Equation 2.2

The magnetised probe extraction technique (Petersen *et al.* 1986) uses a small magnetic field, less than 100mT, induced on a sharp probe. Large magnetic field gradients are induced at the tip of the probe. The sample is suspended in solution and pumped past the probe for several days (Figure 2.7). The magnetic extract can be collected on a daily basis throughout the extraction process from the probe. Great care must be taken throughout preparation and extraction processes in order to avoid contamination of the sample. All reagents used to disaggregate and suspend the sample are filtered at 0.2μm to remove contaminants (Hounslow and Maher, 1999). At all stages of the process, distilled water is used. Once the main extract is separated, it is possible to extract the finer magnetic material from it. The finer magnetic extract is recovered by mixing the main extract and allowing it to settle for an hour. The fluid in the container is then siphoned off and left to settle in a beaker with a magnet attached to the side. The fine grained magnetic material that collects by the magnet is termed the E_{MPT} material and the coarse material left after the fine magnetic extract has been removed is called the E_{MP} material. E_{MPT} material is typically around 2 μm or less in size and the E_{MP} fraction is larger than this.

Diagram of the extraction apparatus

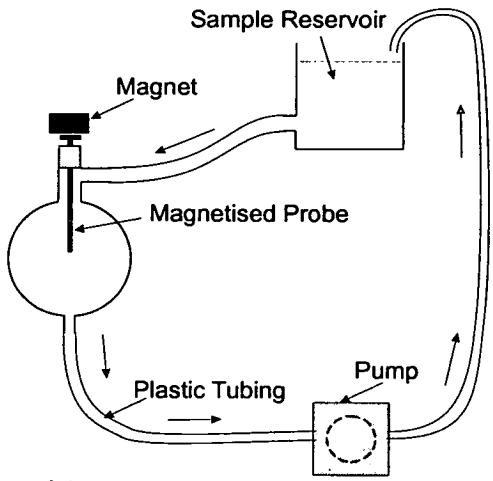

Figure 2.7 Schematic diagram of the extraction apparatus for the magnetic probe extraction technique. The sample is pumped for several days through the apparatus, with the extract collected from the probe on a daily basis. (Hounslow and Maher, 1996)

2.13 Summary

Ferromagnetic materials are abundant in the natural environment, their magnetic properties are well documented, their natural remanences have been widely used for palaeomagnetic reconstructions of plate motions and magnetic field reversals. One outcome of such studies in palaeomagnetism is a wealth of rock magnetic knowledge and instrumentation. By using the knowledge of the magnetic properties of materials in our environment and the instruments available in palaeomagnetics laboratories, it is possible to gain insight into environmental processes. In the next chapter I shall discuss some of the work that has been undertaken in the field of environmental magnetism.

Chapter 3

Magnetic properties of the environment

This chapter is a summary of previous work that has been carried out on the magnetic properties of soils and lake sediments. The interpretation of magnetic properties of sediments and soils has facilitated a greater understanding of past environments, environmental processes and the impact of humans on the natural environment. The magnetic properties of soils and lake sediments are of great importance to the ideas that will be developed through this thesis.

3.1 Biogenic magnetic material

Biogenic magnetic material is important both in soil and sedimentary environments (Vali and Kirschvink, 1989; Fassbinder *et al.*, 1990; Peck and King 1996; Konhauser 1998; Maher 1998). Two families of bacteria exist that are responsible for the creation of ferrimagnetic materials. Magnetotactic bacteria (Blakemore, 1975) (Figure 3.1) and iron-reducing bacteria (Lovley *et al.*, 1987). Magnetotactic bacteria, first discovered by Blakemore (1975), form magnetite or greigite (Roberts *et al.*, 1996) crystals within their bodies in order to orientate themselves to the Earth's magnetic field. The synthesised magnetite crystals, called magnetosomes, are commonly arranged in a linear fashion along the motive axes of the bacteria. Magnetosomes when organised in this way are often referred to as magnetosome chains. The ability of magnetotactic bacteria to align their bodies to the Earth's magnetic field helps them find either oxic or anoxic environments. Although most species of magnetotactic bacteria are thought to prefer anoxic environments (Konhauser, 1998), some have been found to thrive in oxic waters (Hesse, 1994). Magnetotactic bacteria have great control over the shape and size of the individual magnetosomes that they produce (Konhauser, 1998). The majority of magnetosomes are in the optimal single domain state 0.03 and 0.12μm in diameter (Bazylinski *et al.*, 1994). The arrangement of the single domain magnetosomes in a chain maximises the torque experienced by the bacteria when not aligned to the Earth's field (Konhauser, 1998). Magnetotactic bacteria have been found in almost every aquatic environment where they have been looked for, from the sediments in a Baltic lake (Peck and King, 1996) to the Tasman sea (Hesse, 1994), and even top soils (Fassbinder *et al.*, 1990; Maher, 1998). The intact magnetosome chains of magnetotactic bacteria have very strong ARM's , with SARM/SIRM ratios of up to 0.3 (Moskowitz *et al.*, 1993). Such a high SARM / SIRM ratio is due to the positive magnetic interactions between the individual magnetosomes (Moskowitz *et al.*,

1993). The high SARM/SIRM ratio of magnetotactic bacteria chains, coupled with their stable single domain magnetite IRM curve makes them readily identifiable.

Magnetotactic bacteria and magnetosome chains

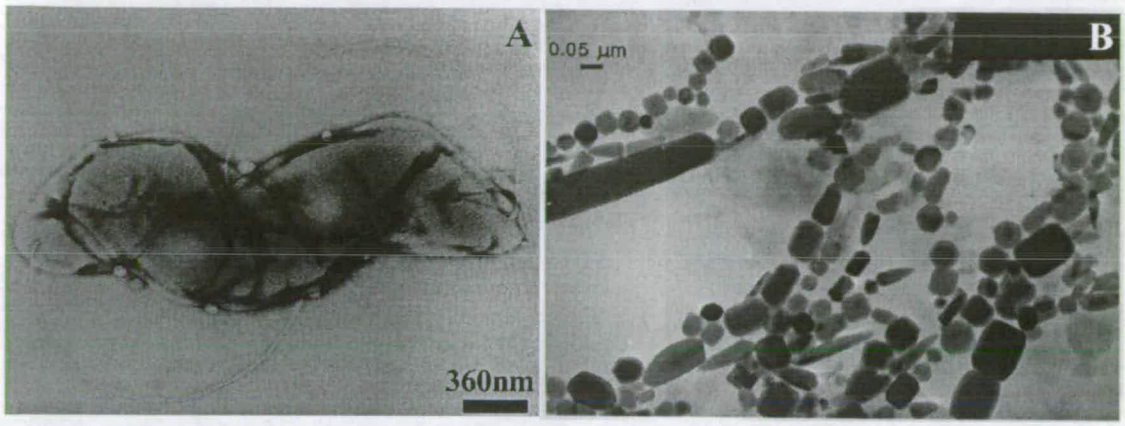

Figure 3.1 Magnetotactic bacteria A) a transmission electron microscope (TEM) image of a magnetotactic marine spirillum cell, with a visible magnetosome chain (Konhauser, 1998). B) TEM of bacterial magnetosome chains from sea sediments (from Maher *et al.*, 1999).

Iron-reducing bacteria have been found in soils around the world. Maher (1998) explains how iron-reducing bacteria do not directly produce magnetite, they use Fe^{3+} ions from their environment as a source of Fe atoms for metabolism or as an electron sink during respiration in anaerobic environments. The bacteria then excretes Fe^{2+} ions back into its environment. The Fe^{2+} ions produced by iron reducing bacteria can then go on to oxidise in the presence of Fe^{3+} to form magnetite crystals. Single bacteria have been photographed (Figure 3.2) surrounded by hundreds of these magnetite crystals (Lovley *et al.*, 1987). The magnetite produced by these bacteria is far less restricted in grain size than that produced by magnetotactic bacteria. Typically the grains produced by iron-reducing bacteria vary in size between 0.0001 and 0.05μm (Lovley *et al.*, 1987). The material from these bacteria is prone to oxidation to maghaemite as it is very fine grained and therefore has a large surface area to volume ratio (Maher, 1998).

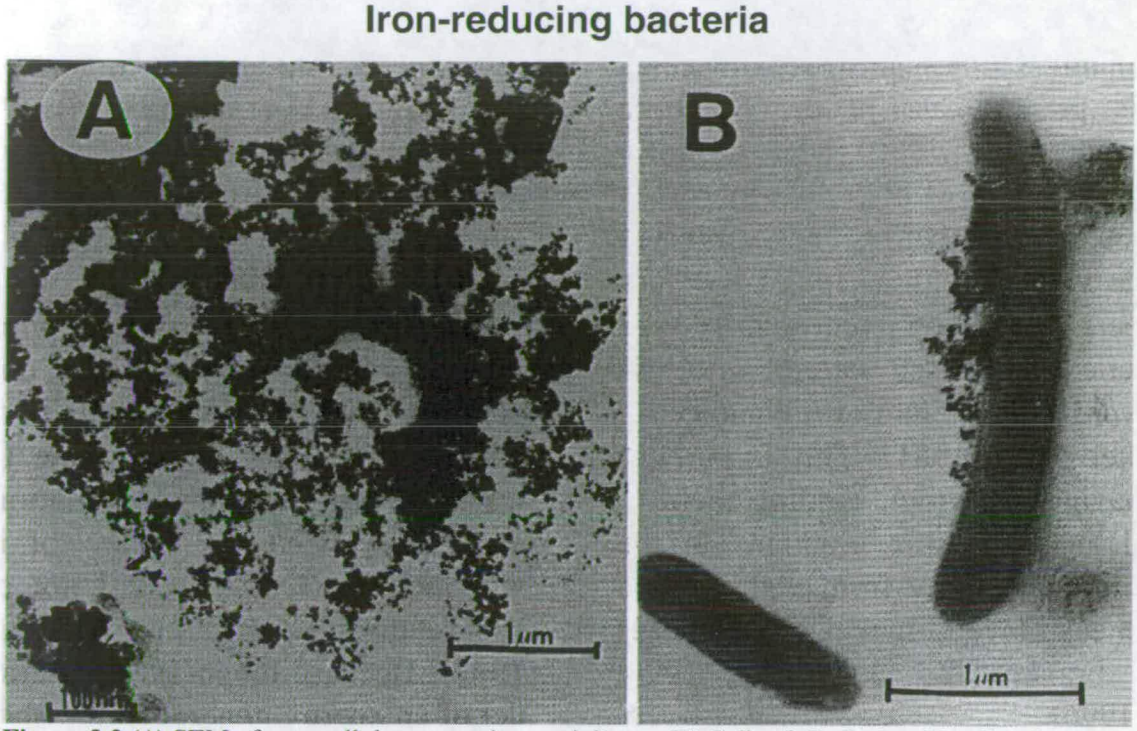

Figure 3.2 (A) SEM of extracellular magnetite precipitates. (B) Cells of *Geobactor Metallireducens* (GS-15), with extracellular magnetite particles (Loveley *et al.*, 1987).

3.2 Magnetite spherules

Two types of magnetic spherules, cosmogenic and anthropogenic, have been observed in nature. The first originate from meteorite dust (Crozier, 1960; Kukla *et al.*, 1988), and rain out through the atmosphere across the whole planet. The other type of magnetic spherule comes from the burning of fossil fuels (Maher *et al.*, 1999). The spherules associated with the burning of fossil fuels have been found in high concentrations by roadsides and industrial areas (Maher *et al.*, 1999; Kapicka *et al.*, 1999; Abdul-Razzaq and Gautam, 2001). These materials are characteristically spherical with unusual surface textures when viewed under SEM (Figure 3.3) and are generally multidomain in grain size.

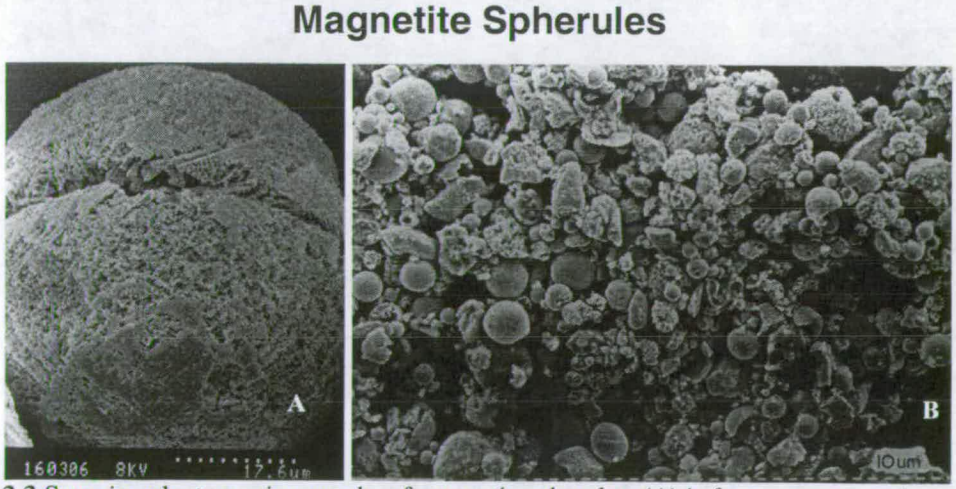

Figure 3.3 Scanning electron micrographs of magnetic spherules, (A) is from a cosmogenic source (B) shows abundant anthropogenic spherules in an American roadside soil (Maher *et al.*, 1999).

3.3 Magnetic inclusions

Magnetic materials can exist both as exposed crystals, which are referred to as detrital magnetic material, or as inclusions within non magnetic materials such as quartz and feldspar (Hownslow and Maher, 1996). Recently magnetic inclusions have been found which display very strong ARM properties (Hounslow and Cox, In press). Figure 3.4 (Hounslow and Cox, In press), shows the magnetic properties of a wide variety of grains with magnetic inclusions. Some of these materials have very high SARM/SIRM ratios. The very high SARM/SIRM ratios of some magnetic inclusion material may dominate the bulk sediment magnetic properties when strong dissolution of the detrital magnetic material has taken place.

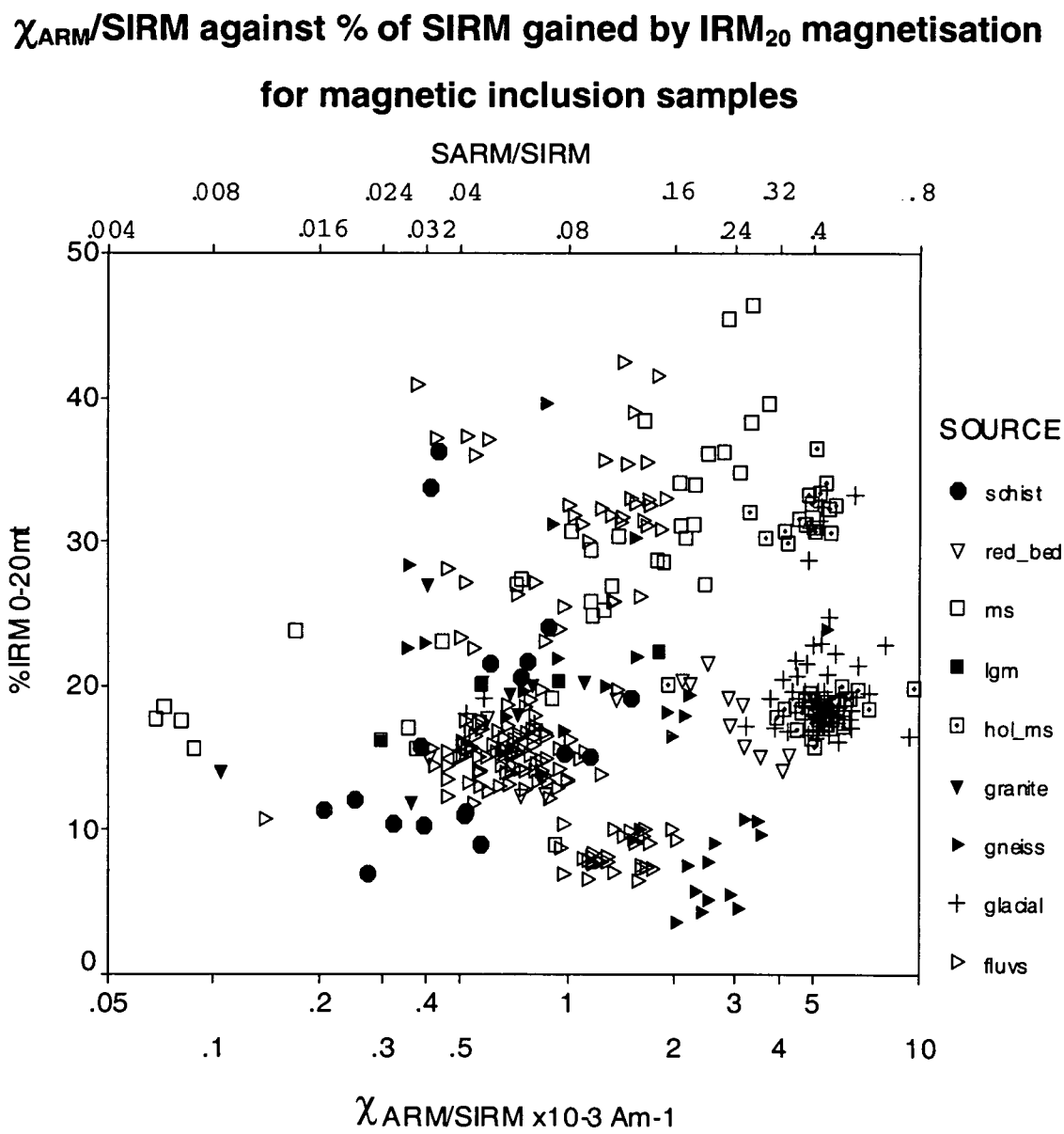

Figure 3.4. Adapted from Hounslow and Cox, (In press) shows the χ_{ARM}/SIRM (and SARM/SIRM equivalent for a 0.1mT dc ARM magnetisation) against % of SIRM gained with a 20mT magnetisation for inclusion samples.

3.4 Soil magnetics

Soils are very complex systems; indeed the definition of what constitutes a soil, is something that can still be debated. Jenny (1941) states that any property of a soil is related to five factors. These are:

1. Parent material
2. Climate
3. Vegetation
4. Time
5. Topography

Depending on the soil and the property being measured, some of these factors can be considered more significant than others (White, 1997).

3.4.1 Topsoil magnetic enhancement and depletion

Leborgne (1955) was the first to report that the upper profile of many soils shows a greater magnetic susceptibility than the lower horizons *"La couche superficielle du sol présente souvent une susceptibilité magnétique beaucoup plus importante que celle de la roche mère sous-jacente"*, this effect has since been referred to as magnetic enhancement. The enhancement effect has since been seen in soils world-wide (as reported by Maher, 1998). Many explanations for the magnetic enhancement effect have been suggested, and here I shall discus some of them.

The difference in susceptibility (and remanence properties) between the various iron oxides, sulphides, hydroxides and the paramagnetic materials commonly found in soil (specifically lepidocrocite and ferrihydrite) (Table 2.1) indicate that it only takes a small quantity of ferrimagnetic material to substantially alter the magnetic properties of a soil (Maher, 1998). Thus it is not the iron content of a soil that dominates its magnetic properties, so long as it is above a threshold value, which Maher (1998) indicated should be around 10g/kg (Figure 3.5), but rather the mineral assemblage within which the iron is contained. This is illustrated by Dearing *et al.*, (1996) with respect to the iron content and susceptibility of British soils (Figure 3.5). In Figure 3.5 we see very little relationship between overall iron content and magnetic susceptibility for all but the most iron-depleted soils. The magnetic properties of a soil are dependent on processes that increase its magnetic content, *magnetic enhancement*, and those that decrease or dilute its magnetic content, *magnetic depletion*, as well as the raw magnetic materials found in the soils parent material (Maher, 1998).

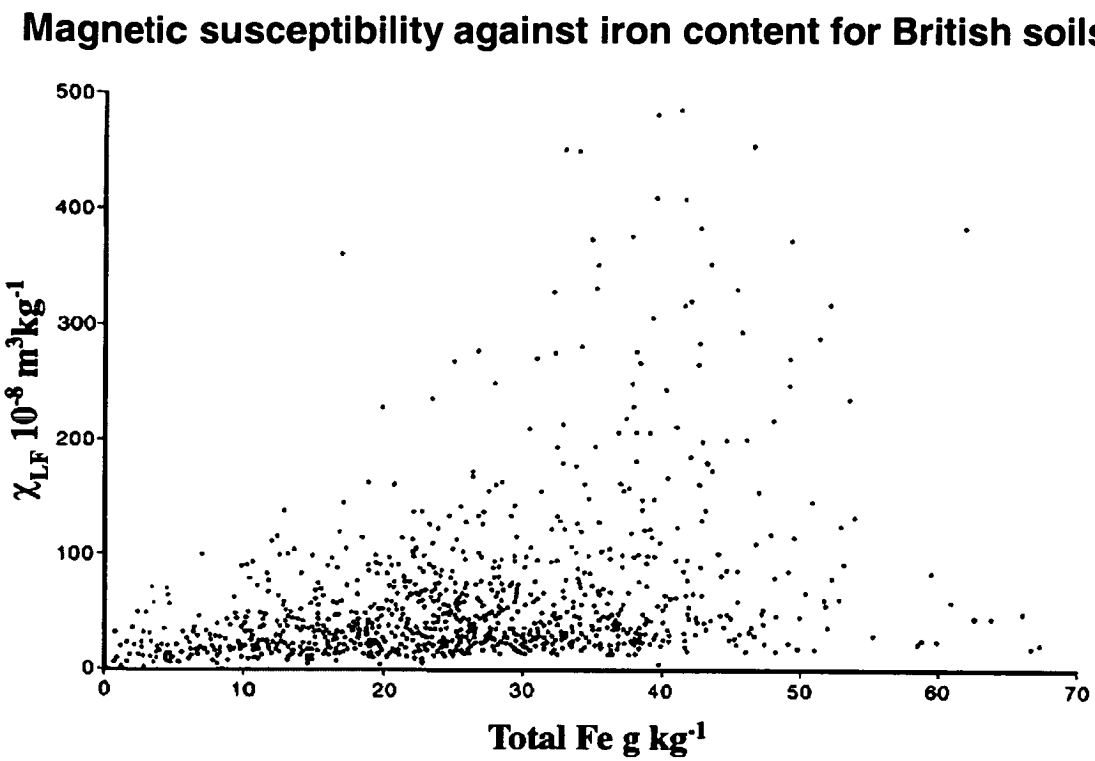

Figure 3.5 Magnetic susceptibility against iron content for British soils, after Dearing *et al.*, (1996).

Maher (1998) outlines the necessary conditions for magnetic enhancement as:

1. Conversion of some of the weakly magnetic iron oxides or other Fe sources into the strongly magnetic iron oxides.
2. Subsequent persistence of these ferrimagnets in the soil profile.
3. Selective concentration of any weathering-resistant detrital ferrimagnets.

The third of these will magnetically enhance one part of the soil profile at the expense of another. For the overall magnetic enhancement of the soil profile the first condition is of obvious importance. Several processes for conversion of weakly magnetic iron compounds into strongly magnetic compounds have been suggested. These include:

1. Burning of soils (Oldfield *et al.*, 1981).
2. The action of magnetotactic and Fe reducing bacteria (Lovley *et al.*, 1987; Fassbinder *et al.*, 1990; Maher and Thompson 1991; Maher and Thompson 1992).

Another way to increase the strongly magnetic Fe-oxide content of the topsoil is to add new material in the form of extra-terrestrial magnetic spherule fallout. Crozier (1960) and Kukla et al. (1988) propose this explanation of topsoil enhancement.

The effects and causes of magnetic enhancement have been of particular interest in the study of the loess deposits in China. There a link between enhancement and annual rainfall has been found (Maher *et al.*, 1994).

3.4.2 Chinese loess plateau

Wind blown dust deposits have been collecting in the loess plateau of north-central China almost constantly for > 2.5 million years (Heller and Liu, 1982). In some areas these deposits reach a thickness of around 300m of interbedded loess and palaeosols (Thompson and Maher, 1995). Magnetic analysis of the palaeosol loess sequence indicated that the palaeosols are magnetically enhanced, with higher susceptibility and NRM than the loess deposits (Heller and Liu, 1982, 1984). Heller and Liu (1984) suggested that the palaeosols were enhanced as a result of climatic actions. This suggestion was enforced when striking similarities between the magnetic susceptibility of loess palaeosol sequences and the $\delta^{18}O$ isotope records of a North Pacific deep sea core were reported by Hovan *et al.* (1989). However the similarity between $\delta^{18}O$ is most clearly seen in the diagram from Maher and Thompson, (1995) reproduced here as Figure 3.6.

Oxygen isotope record for marine sediments compared to susceptibility record from Chinese loess

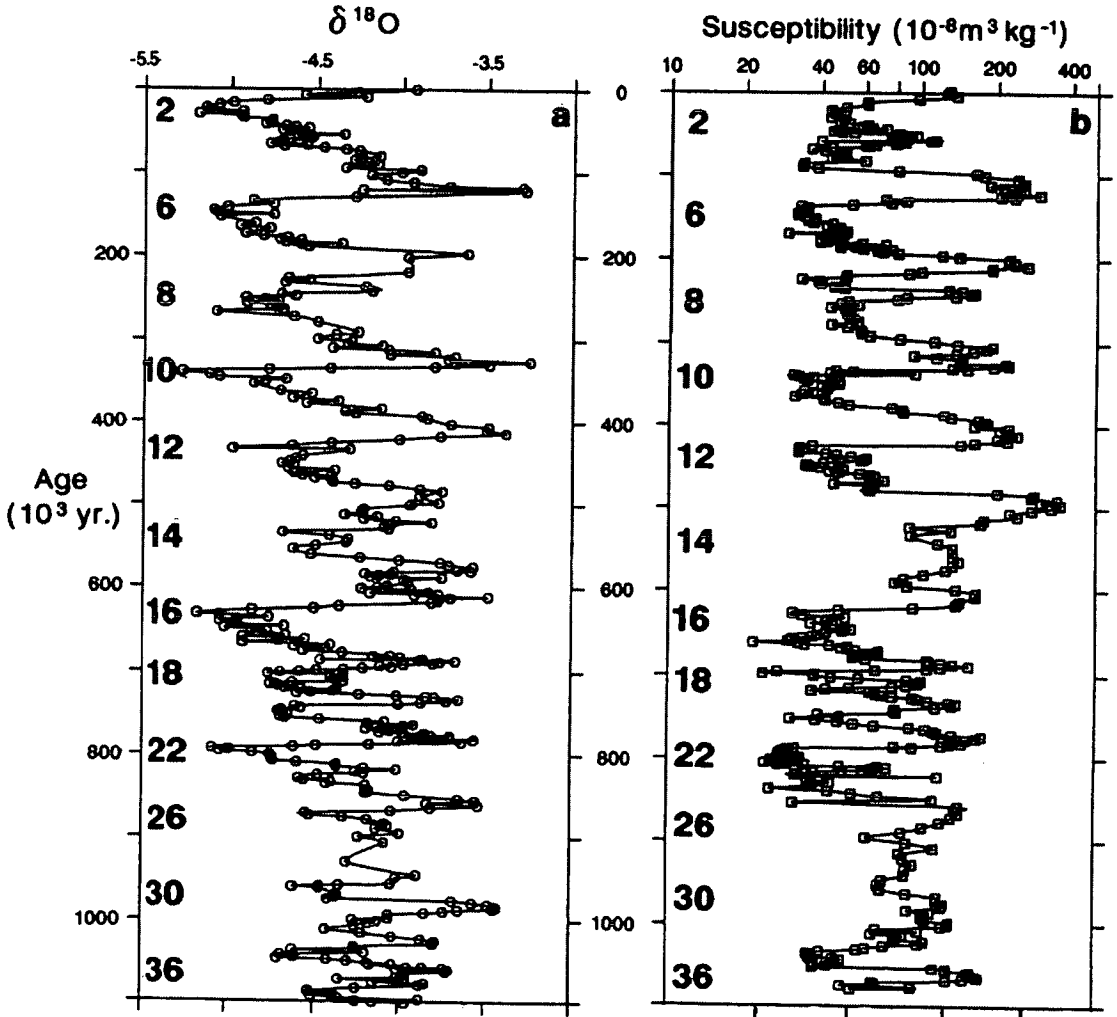

Figure 3.6. Oxygen isotope record of deep sea core against magnetic susceptibility from loess deposits in the central loess plateau, after Maher and Thompson (1995).

In the 1980s two different explanations for the relative enhancement of palaeosols were proposed. Heller and Liu (1986) suggested the enhancement was the result of soil compaction and decalcification within the palaeosol layers due to higher rainfall in interglacial periods. In contrast, Kukla *et al.* (1988) proposed that the relative enhancement of the palaeosols was due instead to the combined effects of lower loess accumulation rates coupled with constant input of cosmogenic magnetic dust. In the theory proposed by Kukla *et al.* (1988), the majority of the magnetic properties of the loess deposits is accounted for by magnetic spherules. The suggested mechanisms for the enhancement of palaeosols proposed by Kukla *et al.* (1988) and Heller and Liu (1986) could not account for any change in the magnetic composition of the loess palaeosol sequence. Both explanations can only account for changes in the relative concentration of the magnetic materials and not for any mineralogical changes. Subsequent studies of the loess palaeosol sequences found several notable differences between the magnetic composition of the palaeosols and loess. The palaeosols display higher frequency dependence of susceptibility and a greater SARM/SIRM ratio than the loess deposits (Zhou *et al.*, 1990; Heller *et al.*, 1991; Maher and Thompson, 1992) (Figure 3.7 Maher and Thompson, 1999). Both of these parameters are sensitive to ultra fine SP/SD magnetite grains. The magnetic differences between the palaeosols and loess indicate that an increase in the SP/SD concentration in the palaeosols is responsible for their higher magnetic susceptibility. This conclusion is strengthened by low temperature magnetic susceptibility and remanence work (Liu *et al.*, 1994; Hunt *et al.* 1995), which show that the palaeosols exhibit classic low temperature SP/SD behaviour. The susceptibility of the palaeosols increases as temperature increases from -192^{0}C (liquid nitrogen temperature) to room temperature (Figure 3.8 Maher and Thompson, 1999). This behaviour is indicative of SP magnetite grains, which "unblock" on warming. The magnetic properties of the loess material are very different. The low temperature properties of the loess material show a multidomain, Verwey transition, indicating that their magnetic material is of a larger grain size than that seen in the palaeosols (Figure 3.8, Maher and Thompson, 1999).

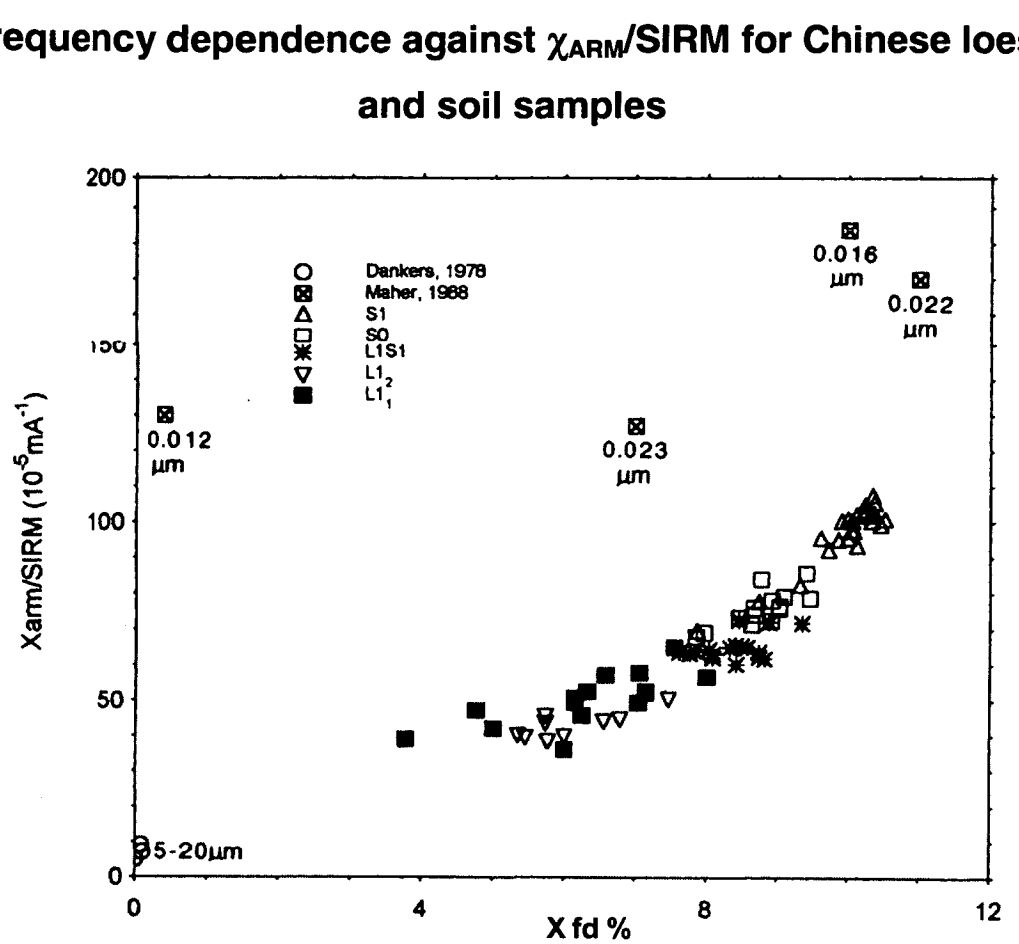

Figure 3.7 Frequency dependence of susceptibility against χ_{ARM} /SIRM for soil (S) and loess (L) samples. Also plotted are some grain-sized ferrimagnets (Maher and Thompson, 1999).

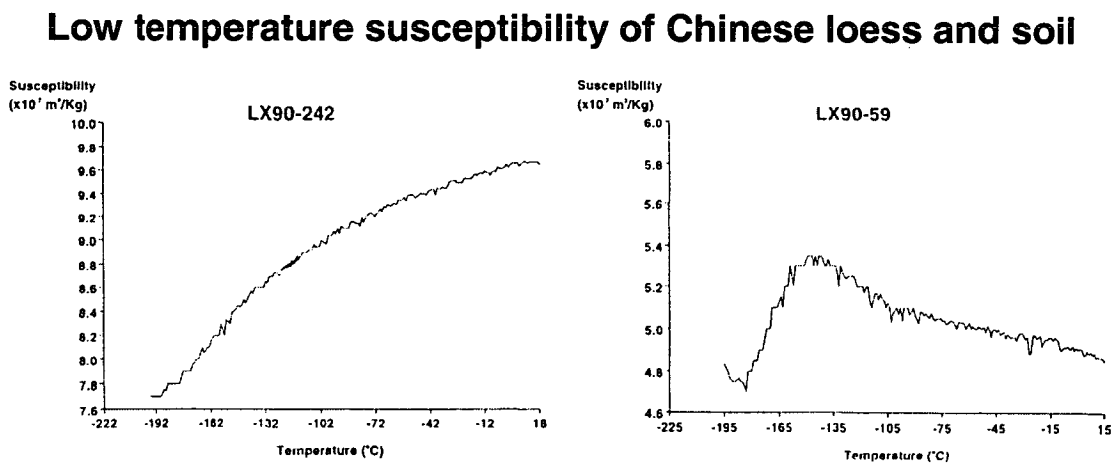

Figure 3.8 Low temperature susceptibility from Chinese palaeosol (left) and loess sample (right). Note Verwey transition (Maher and Thompson, 1999).

Because Kukla *et al.* (1988) and Heller and Liu's (1986) explanations for the magnetic enhancement of the palaeosols in the Chinese loess sequence could not account for a difference in the magnetic materials in the palaeosols and loess deposits, a new explanation was needed. This had to be able to explain the formation of very fine magnetic particles within the palaeosols. Three possible mechanisms have been suggested, note that these are the same mechanisms suggested for enhancement of modern soils.

1. The action of magnetotactic bacteria (Fassbinder *et al.*, 1990).
2. The action of iron reducing bacteria (Maher, 1998).
3. Burning of soils (Folkoff, 1987; Kletescha and Banerjee, 1995; lu, *et al.* 2000).

Magnetic extraction work carried out by Maher and Thompson (1995) shows that although there are bacteria magnetosomes present in the palaeosol material, they are found in insufficient quantities to explain the magnetic enhancement of these layers. Dearing *et al.* (2001) also report that due to the low number of magnetotactic bacteria, (less than 100 cells per gram of soil) within several English soil profiles, bacteria would not contribute significantly to the enhancement of those soils. The action of fire undoubtedly enhances the magnetic susceptibility of soils (Folkoff, 1987; Kletescha and Banerjee, 1995; lu, *et al.* 2000). However, enhanced modern soils have been found where there had been no fires (Maher, 1998). So fire cannot be the sole reason for the magnetic enhancement of soils. Iron reducing bacteria would be capable of producing both the very fine size fraction (0.001-0.05μm) and the quantity of fine grained magnetite found in the palaeosols of the Chinese loess plateau (Maher and Thompson, 1995). For this reason iron-reducing bacteria are considered the most likely source of the enhancement of the palaeosols, and are suggested as an important contributor to the magnetic enhancement of topsoil (Maher, 1998).

3.4.3 Magnetic enhancement to rainfall climo-function

Maher *et al.*, (1994) studied thirty six modern soil profiles from the Chinese loess plateau. The soils were collected from across a climate gradient ranging from the wetter (700mm $year^{-1}$ precipitation) and warmer southern and eastern areas to the cooler and more dry (350mm $year^{-1}$ precipitation) west. Maher *et al.* (1994) found that the soils from the wetter regions had a greater enhancement of their upper horizon. The lateral variation in the soil enhancement in modern soils formed on Chinese loess is also apparent in the palaeosols in the loess sequence (Maher *et al.*, 1994). Further analysis of the modern soil profiles led to a correlation between the soil enhancement ($\chi_{B\ horizon} - \chi_{C\ horizon}$) and annual rainfall (P) of the form:

$$P\ mm\ year^{-1} = 222 + 199 \log_{10} (\chi_{B\ horizon} - \chi_{C\ horizon}) 10^{-8}\ m^3\ kg^{-1}$$

Equation 3.1

Where
P = Mean annual rainfall.
$\chi_{B\ horizon}$ = Susceptibility of the B horizon.
$\chi_{C\ horizon}$ = Susceptibility of the C horizon.

This relationship was found to have a correlation coefficient of r = 0.95 for the soils studied (Maher *et al.* 1994).

The study of the relationship between susceptibility enhancement and rainfall for soils developed on Chinese loess was extended to other soil profiles in the Northern hemisphere (Maher and Thompson, 1995). A good relationship between magnetic enhancement and annual rainfall was found below an annual precipitation rate of 1500mm $year^{-1}$, at which point the enhancement was found to fall (Maher and

Thompson, 1999) (Figure 3.9). The high correlation between rainfall and magnetic enhancement was in spite of the fact that the soils included in the study were not considered optimal, as they did not necessarily exclude soils, that were (Maher and Thompson, 1999):

1. Burnt (burning enhances a soil's susceptibility);
2. Poorly drained (iron reduction in waterlogged soils counters fine magnetite production);
3. Acidic (acidic soils are unfavourable for magnetite precipitation (Taylor *et al.*, 1987));
4. Eroded soils (these may have lost their enhanced upper layer);
5. Soils containing strongly magnetic materials from tephra falls or atmospheric pollutants;
6. Soils inheriting strongly magnetic minerals from parent substrates;
7. Soils on slowly weathering or iron-deficient parent substrates.

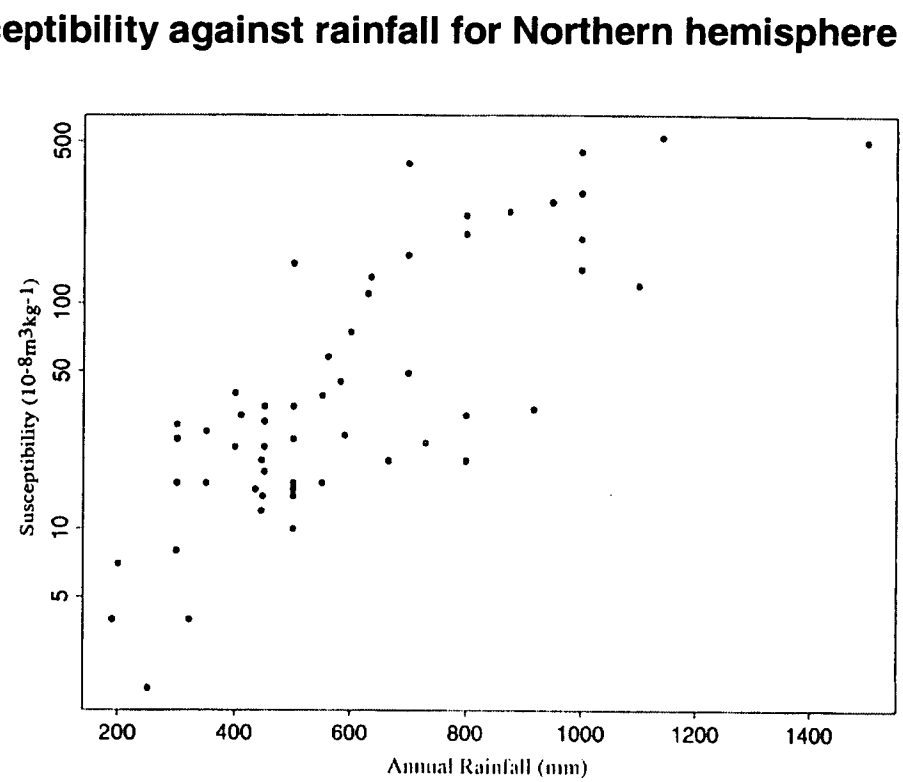

Figure 3.9 The magnetic susceptibility against rainfall for soils taken from various sites in the northern hemisphere (Maher and Thompson, 1995).

Maher and Thompson (1995) explain the soil enhancement rainfall relationship in terms of the magnetic content of the upper soil profile reaching a steady state. They suggest a balance is reached between the generation of fine grained magnetite from the action of iron-reducing bacteria in successive wet and dry conditions, and magnetite oxidation to lower susceptibility forms such as haematite and goethite in dry conditions. The exact point of balance is determined by precipitation, which is the limiting factor on the action of iron-reducing bacteria. In order for this steady state to occur, the soil in question should be "well drained, moderately buffered, and have a source of Fe" (Maher and Thompson, 1999). It has been found that in areas where there is very high rainfall, over 1500mm $year^{-1}$, this relationship will breakdown (Maher, 1998). The breakdown of the precipitation-susceptibility

relationship in high rainfall areas is either due to the soil being leached and becoming acidic or becoming saturated. In a saturated soil Fe^{2+} ions are less likely to be oxidised and a reducing environment not conducive to magnetite formation, is likely (Maher and Thompson, 1999).

It has been suggested that the magnetic enhancement of topsoils is a time dependent phenomena (Singer and Fine, 1989; Singer *et al.*, 1992; Fine *et al.*, 1992). This comes from the study of soils that have a known age and display enhancement. It was found by Singer *et al.*, (1992) that soils younger than 40,000 years showed very little magnetic enhancement. This is in direct contrast to the findings of Maher *et al.*, (1994) who report enhanced palaeosols formed on loess of far younger ages. Fine *et al.*, (1992) attribute the magnetic enhancement of their soil sequences to pedogenic processes that are influenced by climate, age and parent material. They see age as being the dominant controlling factor. However the strong relationship between soil enhancement and rainfall (Maher and Thompson, 1999, Figure 3.9) does not take account of the age of a soil, indicating that age is not the dominant controlling factor for the soils studied.

3.5 Lake sediments

Palaeolimnology, the study of lake sediments, facilitates a greater understanding of past environments. Lake sediments generally have higher sedimentation rates than sea sediments, which means they provide a higher resolution sediment record. Many different techniques exist for the analysis of core materials gathered from past and present lakes. Grain size, chemical analysis, pollen and diatom assemblage analysis, as well as loss on ignition and sedimentation rate, through dating, have all contributed to the understanding of the lakes and catchments. Lake sediments offer an important window on the past, both in terms of climatic and vegetation changes and in recording the action of humans in the catchment area.

There are a number of difficulties with standard limnological techniques. Many techniques used to analyse core sediments are destructive, they change the properties of the sample, restricting further analyses. Two of the major techniques used for lake and catchment environmental processes are pollen and diatom analysis. Both give insights into lake ecology and the abundance and type of local flora. This knowledge allows reconstructions of past climates and environments, as well as anthropological information on populations, farming methods and crop types. Pollen and diatom analysis are extremely time consuming; they require an expert to identify and count several hundred pollen grains or diatoms for any given horizon. By contrast magnetic analysis of lake cores is rapid: up to one hundred samples can be processed in a single day. Magnetic analysis is also non-destructive: the samples are unchanged in all but their magnetic properties, allowing other types of analysis to be carried out on the same sample. The main difficulty in the magnetic analysis of lake cores is in the interpretation of the results. To date, magnetic measurement of sediment cores, both from lacustrine and marine sediments, have been undertaken to investigate soil erosion (O'Hara, *et al.*, 1993; Eriksson and Sandgren, 1999) and climate change (Sagnotti *et al.*, 1998; Ortega-Ramirez *et al.*, 1998). These studies have used rock magnetic measurements to identify likely sediment source material and to identify changes in the magnetic properties of sediments.

Dearing (1999) provides a summary of past research into environmental magnetics applied to lake sediments. In this summary he proposes five factors which effect the magnetic properties of lakes:

Allogenic (coming from outside the lake)
- Atmospheric particles (pollution particles, wind erosion, tephra)
- Fluvial borne detrital material

Authigenic (generated within the lake)
- Bacterial mgentosomes
- Authigenic iron sulphides
- Reductive diagenesis

3.5.1 Allogenic material

Atmospheric particles

The two main transportation processes that will deliver material to a lake are water and air. Air transported material has proved of great significance in some studies of sea core material (Hovan *et al.,* 1991; Hovan and Rea, 1991; Maher and Hounslow, 1999). It should be noted however that in many deep-sea environments, aeolian material is the only significant allogenic sediment source, and accumulation rates are very low. In a core from the Northwest pacific near the significant loess deposits in China the dust fluxes range from 43, to 718 mg $(cm^2kyr)^{-1}$ over the past 530,000 years (Hovan *et al.*, 1991). Even in this high aeolian input environment the dust material alone would produce a maximum sedimentation rate of 0.0205mm yr^{-1} (assuming a density of 3.5gcm^{-3}). Indeed the deepest part of the Chinese loess plateau is around 300m thick, and accumulated over more than 2.5 million years (Heller and Liu, 1982), this produces a rough figure of 0.12mm of dust accumulation a year for one of the thickest dust deposits known on Earth. However, the local transportation of material by wind could have a more significant effect. Rea (1994) summarises three general principles in the generation and transport of aeolian dust.

1) Except in the limiting case of less than 200mm of rainfall a year, higher production of dust material is expected at the dust source with reducing rainfall (Figure 3.10 , Pye, (1989)).
2) The distance that a given size of dust grain can be transported by wind is dependant on the strength of the wind. Increases in grain size of the aeolian component for a sediment source can be interpreted as an increase in wind strength at that time.
3) Dust flux does not necessarily correlate with average wind speed, seasonal winds may transport larger grains to an area than would be expected given the dust accumulation rates at the site.

Therefore, aeolian input of wind eroded material may become significant in a lake when sedimentation rates are low due to reduced fluvial input, and the lake area is experiencing dry conditions and high winds. Dust delivered from short distances is more likely to produce an effect on lake sediments than material from further afield. Lake sediments significantly supplied by wind blown material would generally have a finer grain size than water borne lake sediment material.

Airborne pollutants with strong magnetic signatures have been reported (Chapter 3.2). These materials could make significant contributions to the magnetic properties of recent sediments in highly industrial areas. Industrially derived magnetic materials would typically display multi-domain magnetite properties.

Another aolian transported material which could have significance in magnetic studies of lake sediments is tephra. Tephra derived material becomes increasingly significant with proximity to its volcanic source. In the studies of lake Pátzcuaro (Chapter 5) local tephra samples have been included as end-members in the unmixing model. These tephra samples displayed magnetic properties similar to titanomagnetite.

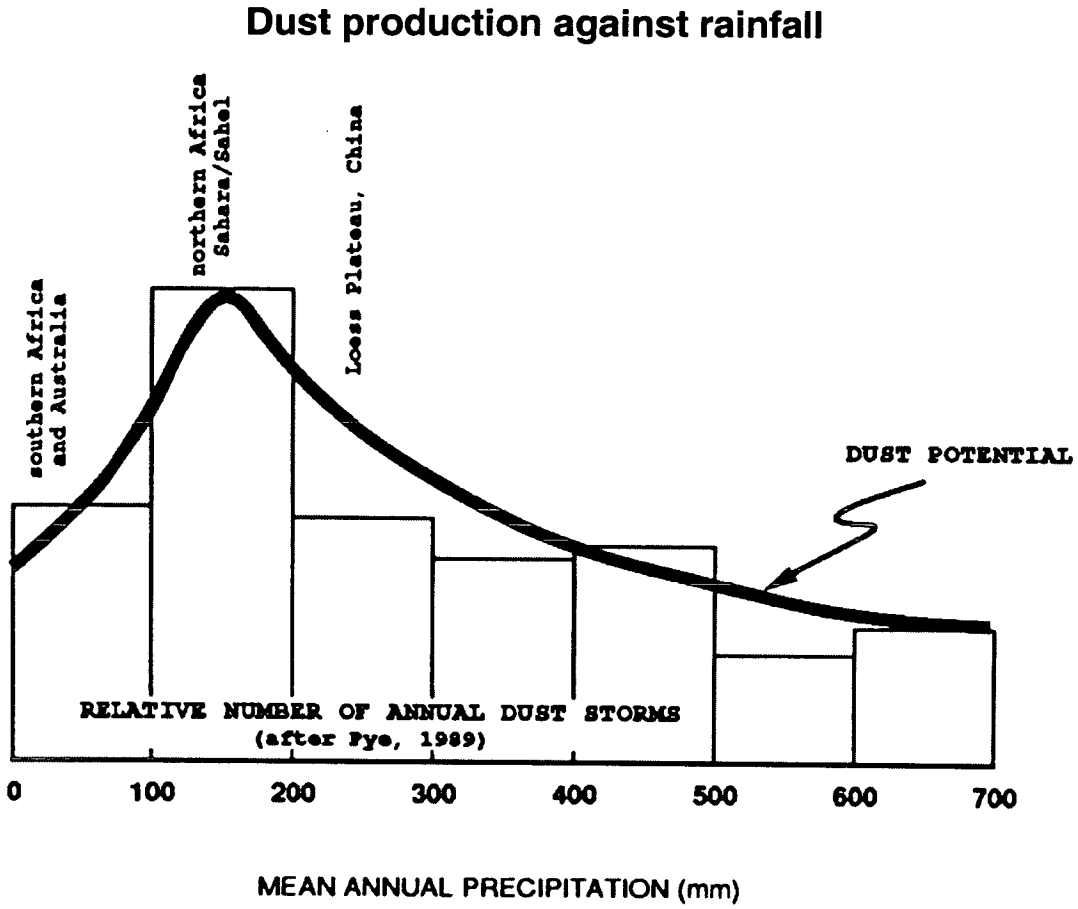

Figure 3.10. Schematic diagram of volume of dust production against annual rainfall (after Pye, 1989).

Fluvial borne detrital material

Material transported by water from the lake catchment can make a significant contribution to the magnetic properties of the lake's sediment. Any material found in a lake's catchment can be transported by water into the lake. The exact composition of the fluvialy transported material is dependent on several processes.

- Erosion of catchment materials.
- Transportaion of these materials to the lake site.
- Sorting of these materials during transportation and deposition.

Slope (steepness and length), vegetation cover, rainfall (annual rainfall, and rainfall seasonality and intensity) and wind speed are all important factors in the quantity and depth of erosion within a catchment. The effects of some of these factors are obvious, long steep slopes will tend to erode faster than short shallow slopes. Vegetation cover will tend to reduce soil erosion (a protected surface can have up to $1/100^{th}$ of the material eroded under the same rainfall conditions as an unprotected surface (Hudson, 1981)). Higher wind speed will increase wind erosion (White, 1997). More complicated relationships are encountered with rainfall. Although rainfall has a direct effect on soil erosion, it can also have an effect on the vegetation cover in the catchment. The relationship between degree of rainfall and erosion can be seen when looking at the sediment loads in rivers related to annual rainfall (Figure 3.11 after Langbein and Schumm, 1958). We see that up to an annual precipitation of around 500mm soil erosion increases with increasing precipitation. After this the effect of increased vegetation arising from the higher rainfall leads to a reduction of soil erosion. However we can see that in catchments where the vegetation has been removed there is an increase in soil erosion with increasing annual precipitation beyond 500mm. The seasonality of rainfall can have a large effect on vegetation cover. Even if the mean annual rainfall is high, if all the rain falls in only a few months less vegetation and a greater degree of erosion will result, compared to the rain falling evenly over the year (Bridges, 1997).

When precipitation rates fall below 25mm h^{-1} they are considered non-erosive (White, 1997), this means that the intensity of rainfall is an important factor in erosion of soils. In temperate regions only 5% of rainfall is above this threshold, as compared to 40% of rainfall in tropical regions (White, 1997).

When erosion rates become particularly high, for instance when vegetation cover is low, and or rainfall seaonality and intensity are high in a steeply sloping region, rill erosion may be seen (White, 1997). Rills are small streams of surface water. Rills, if fed by more rainfall, will tend to deepen and form erosional gullies. These features will erode deeper soil material than surface run-off alone (Figure 3.12).

Annual precipitation and erosion rates

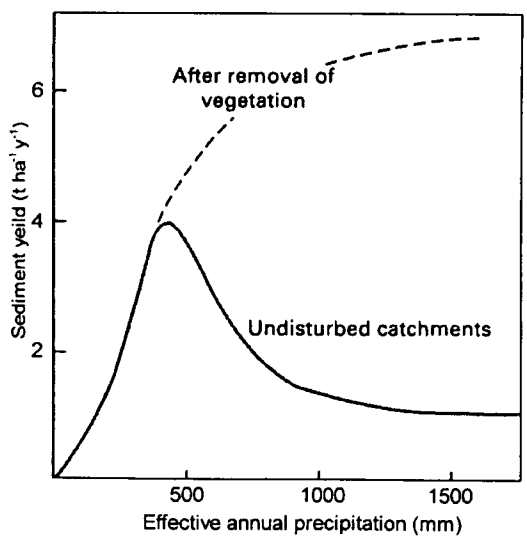

Figure 3.11. Sediment yield taken from sediment loads in rivers, in relation to annual precipitation (adjusted for differences in temperature) (after Langbein and Schumm, 1958).

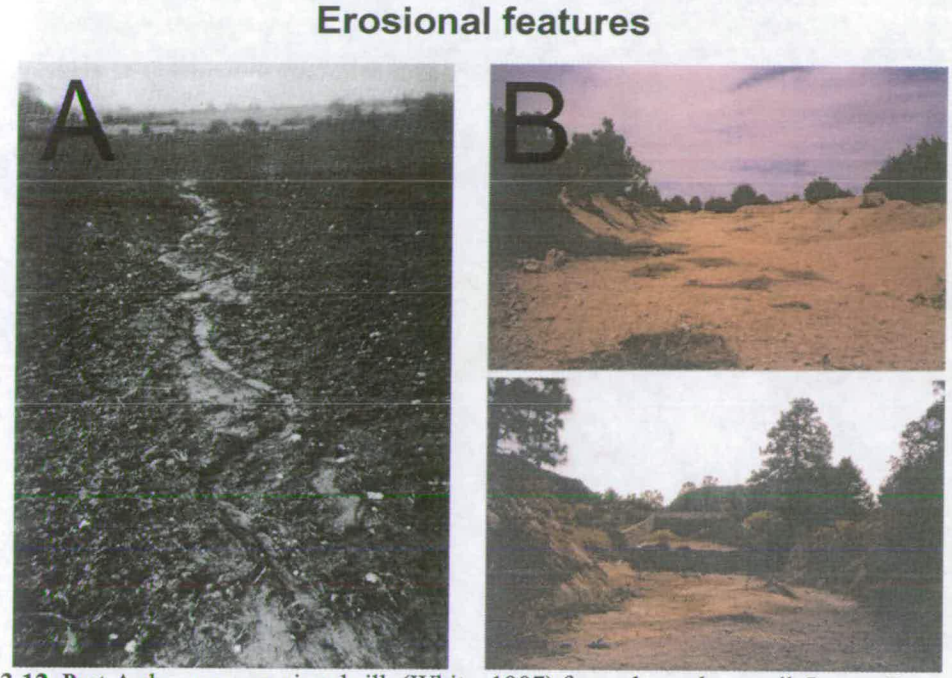

Figure 3.12. Part A shows an erosional rill, (White, 1997) formed on a bare soil. In part B are two wadis in the Lake Babicora catchment area, these deep wide erosional features are common in this catchment, along with smaller gulies. Note in the lower picture from part B the erosion that has taken place around the base of the road bridge.

Sorting

Material that is eroded form a lake's catchment may be transported directly to the lake, or re-deposited within the lake catchment. Material transported by wind, surface runoff or in rivers and streams will tend to become size sorted as it move through the catchment and enters the lake system. Coarser materials require more energy to be moved, this means that lake sediments close to the edge of a lake tend to be coarser than those found in the centre of the lake. The exact degree of sediment sorting is dependent on; the manner of sediment erosion, transportation and the size of the lake in which the material is deposited. In general terms the shorter the distance between the sediment source and the lake, and the smaller the lake the less effect sorting will have. Sorting can have a major effect on the magnetic properties of sediments. Dearing (1999), reports that as much as a five fold difference in the magnetic concentrations of sediments can occur due to sorting. Depending on how the magnetic properties of catchment material vary according to size, the magnetic properties of lake sediments may not be accurately reflected by the magnetic properties of bulk sediments.

3.5.2 Authigenic materials and processes

Bacteria

Materials generated within the lake are generally organic in origin (Jones and Bowser, 1978) and include animal shells and plant matter. These organic materials rarely contribute to the magnetic properties of the lake sediment as they are iron poor. However, significant for the magnetic analysis of lake sediments are magnetotactic bacteria, and more specifically the magnetite grains that they use to orientate themselves to the Earth's field (Section 3.1). The magnetotactic bacteria

magnetosomes can contribute significant quantities of magnetic material to lake sediments, especially where low sedimentation rates facilitate the concentration of magnetosomes (Peck and King, 1996; Konhauser, 1998). Hilton (1986) suggests that magnetotactic bacteria contributions would be unmeasurable if sedimentation rates were above 0.1mm yr^{-1}. However, other studies summarised in Dearing (1999), indicate bacterial presence in sediments accumulating at over 1.6mm yr^{-1}. Note that magnetotactic bacteria, when present, will make a more significant contribution to the magnetic properties of a lake when sedimentation rates are low.

It has been suggested that iron-reducing bacteria may also be active in lake sediments (Oldfield, 1999). One of the locations where the presence of iron-reducing bacteria has been inferred had highly specific conditions (sediments deposited during a period when sewage was treated with paramagnetic iron salt) (Oldfield, 1999). If iron-reducing bacteria were active in lake sediments, and if oxidising conditions were also present, the bacteria may have a similar effect on the magnetic properties of lake sediments as they do on topsoils. If this is the case then sediment material may be miss classified as originating from topsoils.

Iron sulphides

Iron sulphides, specifically greigite, have been found in lake sediments. Snowball and Thompson (1988) noted the first occurrence in sediments from Loch Lomond. Since then may occurrences of authigenic greigite in both brackish and fresh water lakes have been noted (Oldfield, 1999). However, the authigenic production of greigite has only been observed in very slowly accumulating sediments (<< 0.5mm yr^{-1}) with relatively high organic and carbon content (Dearing, 1999). When greigite is present in lake sediments one would expect to observe very hard magnetic properties, with IRM's still being gained at over 1T. Authigenic production of large quantities of greigite could substantially alter the magnetic properties of lake sediments from those seen in the surrounding catchment.

Reduction diagenesis

Diagenesis is defined as "Reactions which take place within a sediment between one mineral and another, or between one or several minerals and the interstitial or supernatant fLiuds" (Selley, 2000). Or more simply as "Chemical and physical changes occurring in sediments during and after their deposition, but before consolidation." (Parker, 1994).

Material that is transported from the lake catchment into the lake system and then deposited as sediment can undergo several phases of chemical alteration (Jones and Bowser, 1978). It has been found that the finer grained the material in question, the greater the degree of alteration that will take place during transport and deposition (Sly, 1978). The length of time for which the material is transported will effect the degree to which it is altered. Once the material has reached the lake bed, diagenesis may occur (Jones and Bowser, 1978). If the sediment-water interface is oxygenated, this will lead to the breakdown of organic material by the action of bacteria and other benthic organisms (Sly, 1978). An anoxic environment will lead to the better preservation of sediments (Sly, 1978). However, anoxic bacteria may still breakdown the organic material present in the sediment, with some of this material being released as gas into the water column (Sly, 1978). Anoxic environments can have a large effect on the magnetic properties of exposed magnetic grains, especially in

alkaline conditions. In these anoxic alkaline conditions strongly magnetic iron oxides may break down to form weakly magnetic materials. Canfield and Berner, (1986) state

"With a fair degree of assuredness we can say that magnetite dissolution should be a ubiquitous phenomenon in sediments supporting active sulphate reduction and H_2S formation. The degree of dissolution is a function of the surface area of the magnetite, the concentration of dissolved sulphide and the time with which magnetite is in contact with the sulphide pore fLiuds."

Reduction diagenesis has been found to remove magnetite at depth within the sediment column (Karlin and Levi, 1983; Canfield and Berner, 1986; Leslie *et al.*, 1990; Peck and King, 1996). However, most of the studies on the effect of reduction diagenesis have been carried out on marine not lake sediments. Where reduction diagenesis has been observed, it has generally had a very strong effect on the magnetic materials in the sediment. Typical indicators are sharp reductions in magnetic susceptibility and SARM/SIRM as magnetites are preferentially removed and more stable minerals like hematite are left behind (Oldfield, 1999). The effects of diagenasis are illustrated in Figure 3.13 (After Oldfield, 1999).

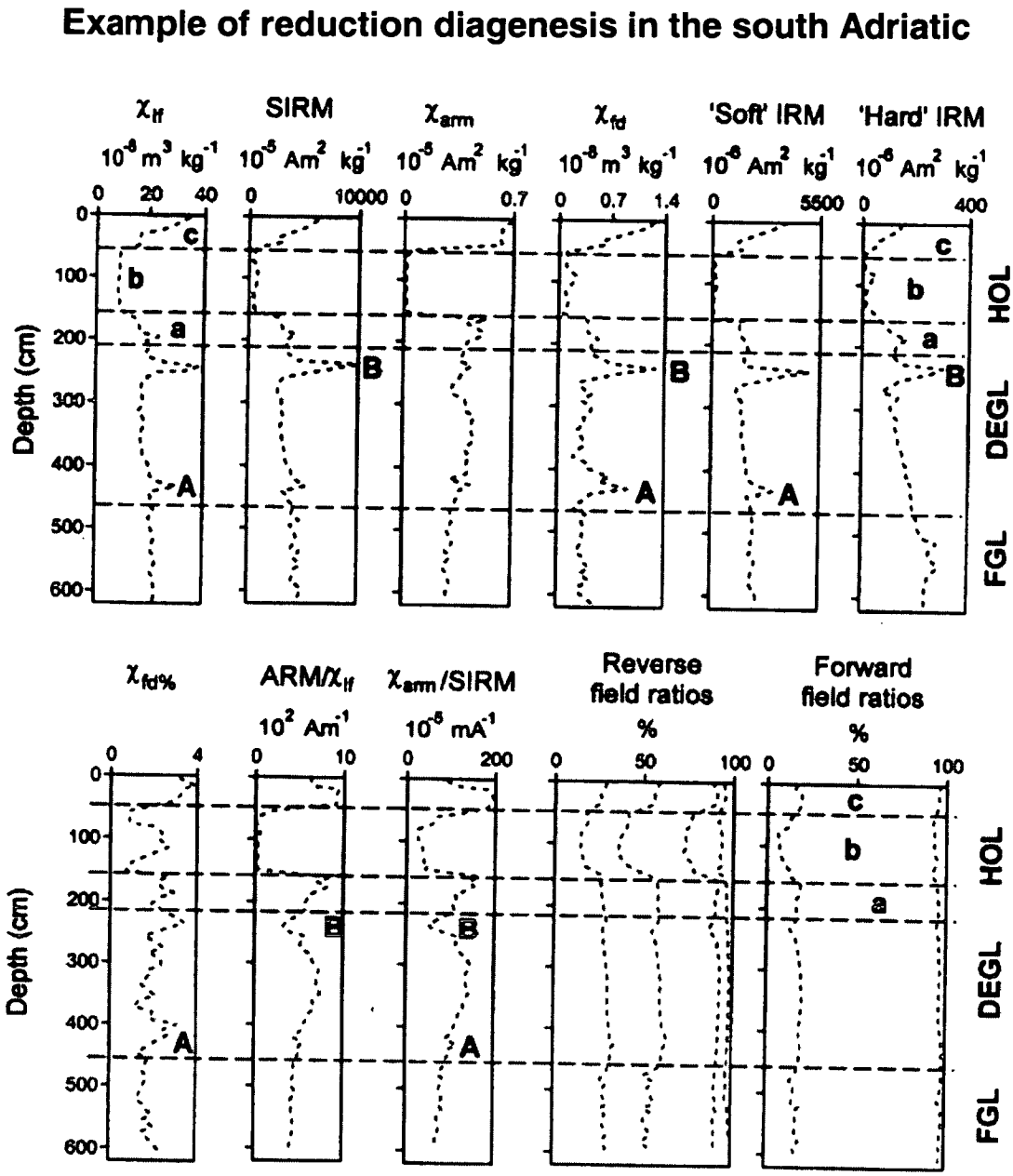

Figure 3.13. Routine magnetic susceptibility and remanence measurements and quotients from samples from a Late Pleistocene and Holocene core from close to the deepest point in the S Adriatic. The major zone of minimum concentrations spanning much of the early-mid Holocene (Zone 'b') represents a period of magnetic dissolution in which all but the paramagnetic and some imperfect anti-ferromagnetic minerals are absent from the record (Oldfield, 1999).

Bioturbation

Once sediment has been buried below the sediment-water interface it will become progressively more stable (Reading and Levell, 1996). However, the action of benthic organisms may lead to bioturbation, effectively mixing the sediment. Bioturbation may occur until below the depth where these organisms live, typically a few centimetres (Jones and Bowser, 1978). However most of the studies on the effect of bioturbation have been carried out on marine not lake sediments. The action of diagenesis and bioturbation will both tend to alter the properties of the original material that was eroded from the catchment (Reading and Levell, 1996).

3.5.2 Sediment source identification

The quantitative identification of the different materials present in lake sediments is not presently possible using standard techniques. That said some chemical indicators, K, Na and Mg, can be used to get an idea of the amount of catchment erosion that is taking place (Jones and Bowser, 1978). Thompson and Oldfield (1986) suggest a link between magnetic susceptibility of lake sediments and catchment erosion for lakes where the catchment material has a high susceptibility. This observation has been used to identify high and low catchment erosion phases in several limnological studies (O'Hara *et al.*, 1993; Eriksson and Sandgren, 1999; and Ortega-Guerrero *et al.*, 2000). Some attempts at using magnetic measurements to identify the source materials of lake sediments have been undertaken (Thompson, 1986; Yu and Oldfield 1989; Maher and Thompson, 1992; Walden *et al.*, 1997; Lees, 1997). These are discussed below (Chapter 4). It is worth noting here however that attempting to link the magnetic properties of lake sediments to catchment materials is not without its difficulties. These difficulties have been well summarised by Deering (1999):

"*It is probably true to say that early attempts at sediment-source tracing failed to appreciate the range of factors which need to be excluded or evaluated; such as, losses of sediment to storage zones upstream of the lake; non-detrital magnetic components such as magnetosomes or reduction diagenesis; failure to sample the true sediment sources; a large atmospheric pollution component in the sediments; and over long timescale of the sediment record.*"

3.6 Summary

Magnetic measurements can provide information that would otherwise be unavailable both for the analysis of soils and lake sediments. Research has been undertaken to better understand relationships between magnetic properties of materials found in the environment and the processes that have acted on those materials. It is, however, noticed that the quantitative identification of lake sediments through the analysis of magnetic measurements has not yet been satisfactorily achieved. Also, the relationship between soil magnetic enhancement and rainfall needs to be tested on a larger data-set of soils, from a large range of climatic regions.

Chapter 4

End-member unmixing

This chapter introduces mathematical and statistical techniques used throughout the following chapters. Of particular note is the end-member unmixing routine developed. This routine uses magnetic remanence and susceptibility data to unmix the magnetic properties of a sample in terms of given end-members. In Chapters 5 and 6, I use the unmixing technique to model the magnetic properties of lake sediments in terms of catchment end-members. Magnetic unmixing of lake sediments allows the identification of sediment sources and facilitates a better understanding of catchment processes.

4.1 Previous work on unmixing

The underlying assumption in magnetic unmixing is that for materials containing a low concentration of magnetic crystals, the magnetic properties of a bulk sample are the same as the sum of the magnetic properties of each of the constituent magnetic crystals (Kneller and Luborsky, 1963; Lees, 1999). This additivity supposition breaks down when individual magnetic grains become close to each other, allowing magnetic interactions between grains (Lees, 1999) notably in the case of magnetotactic bacteria (Blakemore, 1975). However, in most natural sediment samples magnetic grains are sufficiently dispersed for magnetic interactions to be considered negligible (Lees, 1999). The additive nature of magnetic samples allows linear modelling of a sample (Lees, 1999) (Figure 4.1).

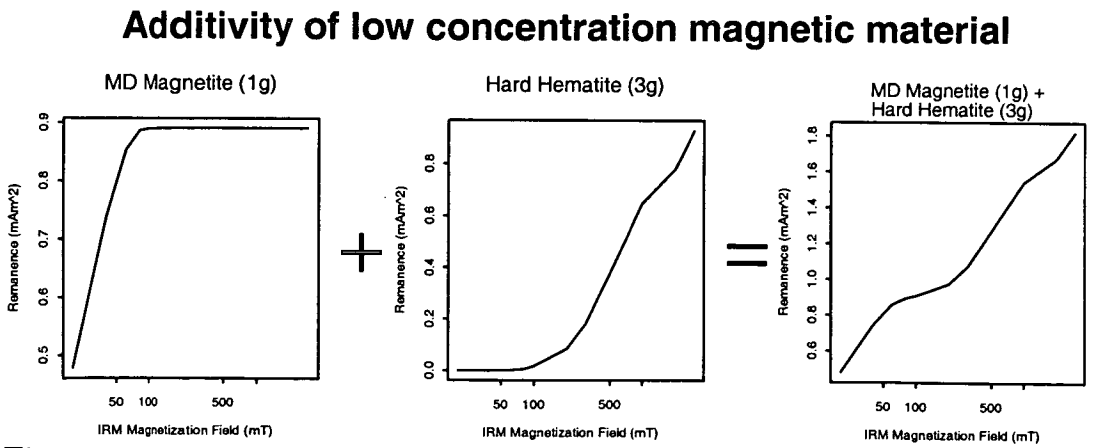

Figure 4.1. Diagrammatic representation of additivity, showing the theoretical result of combining multidomain magnetite and hard hematite.

Linear modelling unmixes the magnetic properties of a sample by summing the magnetic properties of given end-members at different concentrations. Linear modelling optimises the fit of an end member concentration model to the original sample by minimising the residuals (ε) between the model and the sample (Equation 4.1).

$$\varepsilon_j = \sum_i \left(A_{ij} * x_j\right) - y_j$$

Equation 4.1

Where
ε = A vector of magnetic measurement residuals.
y = A vector of magnetic measurements from the sample that is to be "unmixed".
x = A vector of concentrations of the End-members. All possible values of these define the "solution space".
A = End members matrix, each row representing an end member, each column an observation (magnetic measurement).
j = The j^{th} measurement.
i = The i^{th} end-member.

In matrix format this can be written,

$$\varepsilon = xA - y$$

Equation 4.2

Where:
ε = Residuals.
y = A vector of magnetic measurements from the sample that is to be "unmixed".
x = A vector of concentrations of the End-members.
A = End members matrix.

A best fit can be achieved by minimising the difference between the model and the actual magnetic data. However the model must stay within physical constraints, a negative concentration of any end-member is not possible. To date the most popular way to minimise the residuals of the unmixing model is to use constrained least squares using the SIMPLEX routine (Thompson, 1986; Yu and Oldfield 1988; Maher and Thompson, 1992; Walden *et al.*, 1997; Lees, 1997).

4.1.1 Constrained least squares

The constrained least squares unmixing technique makes use of the very well developed least squares approximation theory. Least squares minimises the square of the residual between the model and measured data. In constrained least squares unmixing, penalties are imposed on the selection of undesirable concentrations of end-members. These constraints are used to prevent negative concentrations and to constrain the model to include end-members whose total mass equals the mass of the sample. However in order to add these constraints the least squares technique has to be made iterative, which introduces grave problems with local minima and non convergence, as well as increasing computational time.

4.1.2 SIMPLEX

SIMPLEX modelling (Nedler & Mead 1965) was suggested by Thompson (1986) for the modelling of magnetisation data. The SIMPLEX modelling technique can be

visualised as "rolling" a shape (the SIMPLEX) with one more vertex than the dimensionality of the solution space (i.e. a triangle in a two end-member model) "down hill" through the solution space. The intention is to find the minimum of g in Equation 4.2. The SIMPLEX technique is iterative so it can suffer from the problem of not reaching the global minimum due to the SIMPLEX becoming stuck in a local minimum (Thompson, 1986). Running the model several times, changing the starting point of the SIMPLEX, can reduce the local minimum problem. However multiple runs are highly computer intensive and time consuming, requiring detailed analysis of each model produced and do not guarantee finding the global minimum.

In order for the SIMPLEX technique to create models that do not include negative concentrations of end-members, penalties are imposed on negative concentration selection. These penalties create an uneven solution space, which can increase the problems with local minima. The SIMPLEX method has no way of reducing the number of end-members that are being considered, so the selection of end-members that are going to be included in the model is critical. The limitations of the SIMPLEX technique mean that only simple unmixing models have been considered with a maximum of three end-members (Thompson 1986; Walden *et al*, 1997), hence, extreme care must be taken in end-member selection.

4.2 My unmixing model

I have used weighted non-negative least squares as the basis of my unmixing model. Non-negative least squares combined with a stepwise, F-testing end-member selection routine allows the modelling procedure to select from a large array of end-members without over-fitting. Because the non-negative technique produces a least squares model, it is possible to apply standard error analysis techniques to quantify uncertainty in the concentration vector x (Equation 4.2).

4.2.1 Non-negative least squares

The non-negative least squares technique ensures concentration of any end-member in a model will be positive (Lawson and Hanson, 1995). Here I present a brief explanation of the non-negative least squares method; a full explanation can be found in Lawson and Hanson (1995).

The non-negative least squares technique can be thought of in terms of two computational loops. The first loop selects end-members that will have a positive concentration in a least squares model, one at a time, preferentially selecting those that minimise residuals in the least squares model. The second loop is only entered if the inclusion of a new end member forces the least squares model to make a previously selected end-member negative. The second loop is essentially the opposite of the first. The second loop removes end members, preferentially selecting those that will minimise the increase in residuals of the least squares model, one at a time. It can be proved that this technique will converge on the global minimum non-negative least squares model within a finite number of iterations (Lawson and Hanson, 1995). The non-negative least squares routine exists as a set command within the S-Plus language and was accessed from there.

4.2.2 Parsimony

One important aspect of any modelling technique is to try and find the least complicated solution that accurately models the observed data. In the unmixing technique that I have developed parsimony is achieved by using a stepping routine. Stepping is a process that uses a formal statistical test to decide if the addition or removal of an end-member significantly improves the fit of a model. The test used in my modelling routine was an F-test between the fit of the original and altered models, when stepping up or down by one end-member this looks like:

$$F = \frac{(RSS_1 - RSS_2) \times (N - K)}{RSS_1}$$

Equation 4.3

Where
F = The F-statistic (high values indicate significant change).
RSS_1 = The residual sum of squares for the original model.
RSS_2 = The residual sum of squares for the new model.
N = Number of magnetic measurements (or effective parameters).
K = Number of end-members in the new model.
N-K = Degrees of freedom of the new model.

The result of the F-test can be compared to a table of standard F-test values to decide if a given change in the degrees of freedom can be justified by the change in the models fit.

The stepping technique in its simplest form consists of adding, or removing an end-member, and validating the action taken. The addition of an end-member is called stepping up and the removal of an end-member stepping down. It is possible to combine the upward and downward techniques into a stepwise stepping routine. It is unusual, except in the most basic of cases, for upwards stepping and downward stepping to converge on the same model (Ramsey and Schafer, 1997). Generally, stepping up leads to simple models relatively few end members, stepping down leads to models containing more end members, while stepwise stepping will lead to similar models to either stepping up or down depending on whether it is started with all or none of the end-members (Johnson, 1998). I decided to use an upward stepping stepwise end-member selection process, thus sacrificing some fit for a simpler, more interpretable model.

4.3 Validation and error analysis

A model is only of use if fits the data well and it can make good predictions. In the modelling process I have developed there are three tests of the goodness of fit,

1. **Correlation coefficient**: Shows how well a model is fitting the data.
2. **Covariant matrix error analysis**: Shows how errors in the data propagate through to the final model giving an estimate of the confidence limits of the final model.
3. **Skill**: Determines the predictive power, a powerful method of demonstrating parsimony.

Fourthly the stratigraphic continuity may be considered for down core modelling

4.3.1 Correlation coefficient

The correlation coefficient (r) is a dimensionless quantity that provides a measure of how two variables are associated. The possible values of the correlation coefficient vary between -1 and 1, with positive values denoting a positive relationship, i.e. high values of one variable corresponding to high values of the other, and negative values an inverse relationship. The closer the value of the correlation coefficient to either 1 or -1 the greater the linear correlation between the variables. For example, if the value of r were equal to 1 a plot of any variable against the other would fall on a straight line with a positive gradient.

The value of r for two series of numbers x_i and y_i where i ranges from 1 to N can be obtained from the following equation (Pearson coefficient of correlation, Ryan and Joiner, 1994).

$$r = \frac{\sum(x-\bar{x})*(y-\bar{y})}{\sqrt{\sum(x-\bar{x})^2 * \sum(y-\bar{y})^2}}$$

Equation 4.4

Where
r = Correlation coefficient.
x = 1st set of variables.
y = 2nd set of variables

For this thesis, correlation between variables will be reported as R^2; this is the square of the correlation coefficient and ranges between 0 and 1 (Equation 4.4).

4.3.2 Error analysis

The error on the concentration of any given end-member for any given sample is a vital statistic for an unmixing model. It is important to know how sensitive the modelling routine is to the input data. It is possible to determine the mathematical stability of the modelling routine by examining the covariance matrix of the inverse matrix that solves the least squares problem.

In order to find the solution of the least squares part of the non-negative least squares technique, it is necessary to identify the inverse of the end-member measurements matrix.

$$y = Ax - \varepsilon$$
$$A^{-1}y = A^{-1}Ax - A^{-1}\varepsilon$$
$$A^{-1}y = x - A^{-1}\varepsilon$$

Equation 4.5

where:
y = A vector of magnetic measurements from the target sample.
x = The vector of concentrations of the end-members (the non-negative least squares solution).
A = End members matrix (each row representing an end-member each column an observation).
A^{-1}= The inverse of the end-member matrix.
ε = The vector of magnetic measurement residuals.

The covariance of the inverse matrix is defined as:

$$Cov\left(A^{-1}\right)_{lm} = \sum_{p}\left(A_{lp}^{-1} - \overline{A}_{l}^{-1}\right)*\left(A_{pm}^{-1} - \overline{A}_{m}^{-1}\right)$$

Equation 4.6

Where
l = the l^{th} column of the inverse matrix
m = the m^{th} row of the inverse matrix
p = dummy variable, varies between 1 and K (total number of end-members)
A^{-1}= The inverse of the end-member matrix.

The covariance matrix of the inverse matrix gives information on how sensitive the inverse matrix is to errors in the data to be unmixed (y). The i=j^{th} diagonal of the covariance matrix when combined with the variance of the residuals of the unmixing model indicates the error on the x_i^{th} concentration (Meju, 1994):

$$err(x_i) = \frac{\left(\sum_{j=1}^{N}\left((Ax_j - y_j) - \overline{(Ax - y)}\right)^2 * Cov(A^{-1})_{ii}\right)^{1/2}}{N - K}$$

Equation 4.7

where:
y = A vector of magnetic measurements from the target sample.
x = The vector of concentrations of the end-members (the non-negative least squares solution).
A = End members matrix (each row representing an end-member each column an observation).
A^{-1} = The inverse of the end-member matrix.
j = The j^{th} measurement.
i = The i^{th} end-member.
N = Number of measurements.
K = Number of end-members in the model.

The off diagonals of the covariance matrix give the correlation between the end-members that are being used in the modelling (Meju, 1994). In terms of unmixing models it is possible to use the error estimates obtained above to indicate instability in the model. In turn, this error gives an estimation of the uncertainty attached to the estimates of the concentrations of any given end-member. However, these error estimates assume that the right end-members have been chosen in the model.

4.3.3 Skill

As well as being able to estimate confidence limits on the end-member concentrations for a given model, it is also important to know how reliable that model is. If the modelling processes selection of end-members is dependent on only a couple of measurements the resultant model may be unstable. An unstable model could give misleading information. It is vital to know when model instability due to end-member selection is a problem, as it may highlight over- and under-fitting or indicate missing end-members in the modelling routine. The skill of a model is a measure of how well a model can predict new data. In the absence of new data, the predictive capability of a model can be tested by temporarily removing data. A model is then generated with the remaining data. The resulting model can then be compared with the data that was set aside. This process, often referred to as cross validation, can be repeated, in turn, for every magnetic measurement, so making full

use of the original data. In the case of magnetic data, there can be high degrees of correlation between measurements. Due to this high auto correlation between magnetic measurements, instead of removing one measurement at a time, five sequential measurements were removed at once, and the middle one was predicted. The skill parameter compares the goodness of fit between the predicted measurements and the actual measurements. When testing the skill of unmixing models, the zero skill model was taken to be the mean of the magnetic measurements of the sample that was being unmixed (Equation 4.8) (Cook et al, 1999).

$$Skill = 1 - \frac{\sum (x_i - \hat{x})^2}{\sum (x_i - \bar{x})^2}$$

Equation 4.8

where

x_i = The i^{th} magnetic measurement.

$\hat{x}$ = The predicted value of x_i.

$\bar{x}$ = The mean value of x.

The skill equation (Equation 4.8) gives a value between 1 and $-\infty$ with 1 being a perfect prediction, 0 a skill level equal to the zero skill level and a negative skill is worse than the zero skill level. From the analysis of the fit of many different skill levels a skill above 0.7 was considered satisfactory for a magnetic unmixing model. The skill parameter has also been used to estimate the number of effective parameters within the end-member and core sample data. Figure 4.2 shows examples of various levels of skill.

The cross validation process above, where five sequential measurements are removed and the middle one predicted can be referred to as "leave five out" cross validation. In Chapter 7, "leave one out" cross validation is used to measure skill for models which link rainfall to soil magnetics. The "leave one out" cross validation is the same as "leave five out" cross validation except only one measurement is removed.

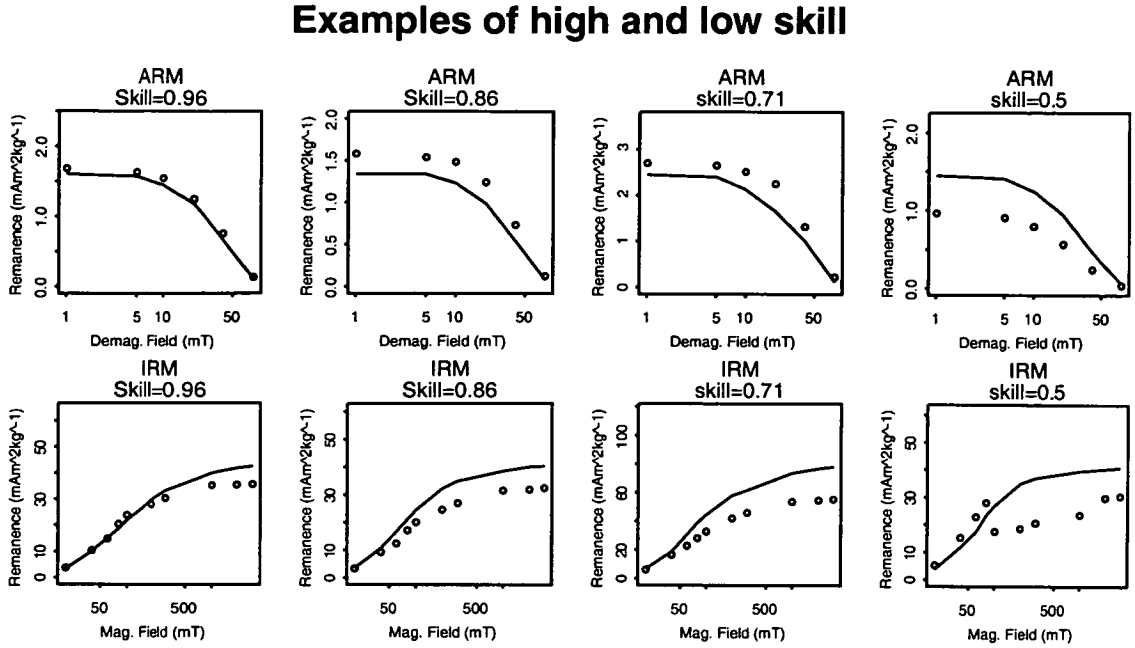

Figure 4.2. Examples of high and low skill levels. Plotted are magnetic results (lines) for ARM demagnetisation (top) and IRM magnetisation (bottom) and the predicted value of these measurements when leaving five measurements out and predicting the middle measurement (circles) for models with skills of (from left to right) 0.96, 0.86, 0.71 and 0.5.

4.3.4 Effective number of parameters

The F-test statistic used in the stepping routine assumes that all observations (magnetic measurements) are independent, however remanence data can be highly auto correlated, suggesting that the effective number of degrees of freedom should be lower than the number of magnetic measurements minus the number of end-members in the model. In order for auto correlation in the remanence data to be taken into account, a variable that could be manually altered was introduced. This variable the "effective number of measurements" was used in the F-test in place of the normal degrees of freedom. The result of changing the effective number of measurements parameter on the skill level of a model can be seen in Figure 4.3.

The main reason for using a stepwise model is to avoid under- or over-fitting. For most levels of the Pátzcuaro core, a good skill level has been achieved irrespective of the chosen value of effective parameters (Figure 4.3). The robust high level of magnetic measurement prediction is an artefact of the non-negativity requirement of the modelling process. In effect the model's choice of end-members is limited not only by the stepwise routine, but also by the non-negativity, making over-fitting less likely. In Figure 4.3 the removal of the non-negativity requirement has led to reduced skill, due to over-fitting. However, for some horizons, even with a non-negativity constraint the modelling procedure has over-fit and under-fit, depending on the chosen value of effective parameters. For the final unmixing models, the effective number of parameters is allowed to vary down-core and has been chosen at each horizon by maximising skill.

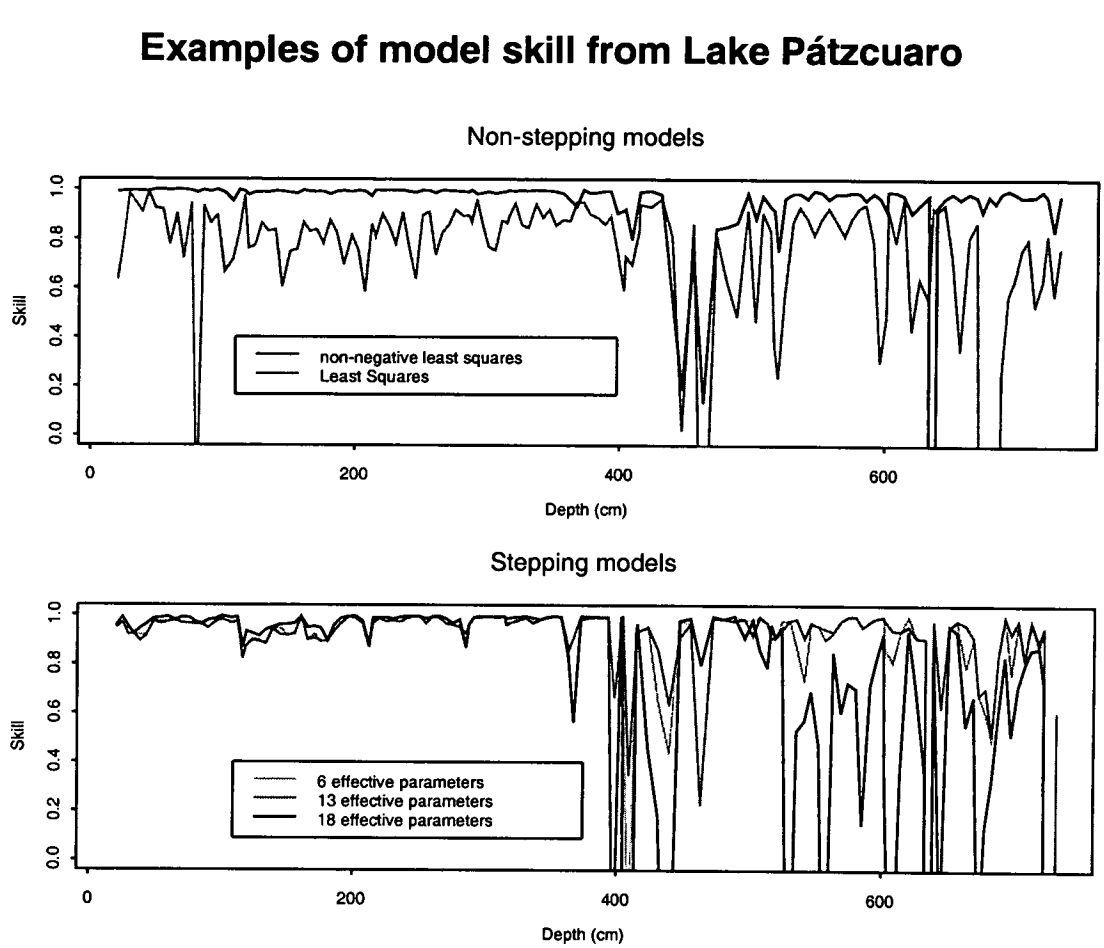

Figure 4.3. Examples of the skill levels of unmixing models from Lake Pátzcuaro. The top graph shows skill levels for models which did not use a stepping function, the lower plot shows the effect of different choices of effective parameters on the skill of models that do use a stepping function. Higher numbers indicate greater degrees of skill.

4.4 End-member classifications and model output

Magnetic measurements on cores from two lakes in Mexico have been unmixed using the method developed. The end-members used to unmix the two Mexican lakes were collected from within the lakes catchment. These catchment end-members have been classified as topsoil, subsoil, bedrock, tephra, or dust. A magnetotactic bacteria magnetosome chain end-member was also included in some unmixing models. The unmixing models convert the magnetic measurements on the lake cores into masses of each end-member for each core horizon. Where an end-member type is represented by more than one end-member sample, for instance if a core horizon has been modelled with two different topsoil samples, the mass of each topsoil sample is summed. The final unmixing model is presented as a down-core plot for each end-member type. Each down-core plot shows the percentage of the cores mass which is accounted for by that end-member type.

4.5 Testing of the unmixing model

In order to test the magnetic unmixing model, a set of unmixing models were run on magnetic data generated using the measurements made on lake catchment end-members. For these unmixing tests, magnetic measurements made on catchment samples were mathematically combined, two samples at a time. For instance to generate a 50% mixture of topsoil and subsoil, the magnetic measurements of each sample were halved and then added together. Random errors were then generated on the mixtures measurements, this process was repeated to generate fifty mixtures with random errors. The resulting fifty synthetic mixture measurements were then unmixed in terms of seven end-members, two topsoils, one subsoil, two bedrocks and two tephra samples. Four samples, one of each end-member type, were used to generate the synthetic mixtures. The magnetic measurements for the topsoil subsoil bedrock and tephra samples used to generate the synthetic mixtures are shown in Figure 4.4. For reference the R^2 between the magnetic measurements of the four end-members used to generate the synthetic mixtures is given in Table 4.1.

R^2 between end-member types used in mixture tests

	Topsoil	Subsoil	Bed-Rock	Tephra
Topsoil	1	0.9942898	0.9882714	0.9001846
Subsoil		1	0.9952311	0.9311770
Bed-Rock			1	0.9527537
Tephra				1

Table 4.1 R^2 between the four end-members used in the mixture tests. Highest correlation is between subsoil and bedrock, the lowest correlation is between tephra and topsoil.

Using two samples, selected form topsoil subsoil bedrock and tephra, six different mixtures could be generated. For each type of mixture nine different combinations of the two end-members were modelled. The concentrations were based on the mass of the end-member samples. The concentrations used were set to 1, 10, 15, 30, 50, 70, 85, 90 and 99%, with the second end-member making up the rest of the sample. For each end-member concentration mixture, errors were synthesised at five different percentages 1, 3, 5, 7 and 10%. I have shown three of the six possible mixtures of the four end-member types (Figure 4.5, 4.6 and 4.7). The other three can be found in Appendix A. The output of the unmixing tests is given in terms of the summed end-member contribution of each end-member type with error bars to indicate the variance in the fifty repetitions of each unmixing experiment (Figure 4.5, 4.6, and 4.7).

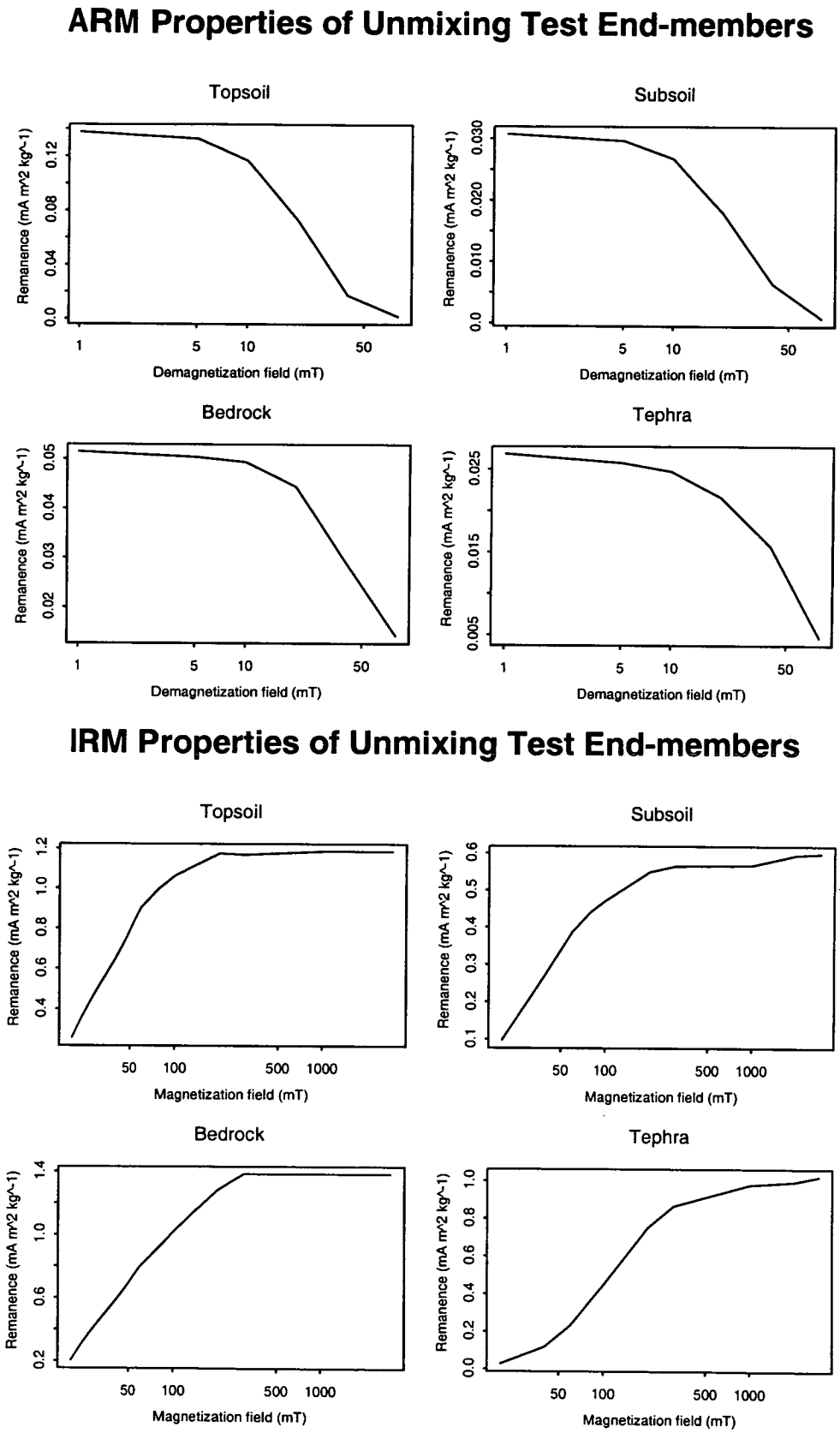

Figure 4.4. ARM and IRM properties of Pátzcuaro catchment material used in the unmixing tests plotted against demagnetising field (for ARM's) and magnetising field (for IRM's).

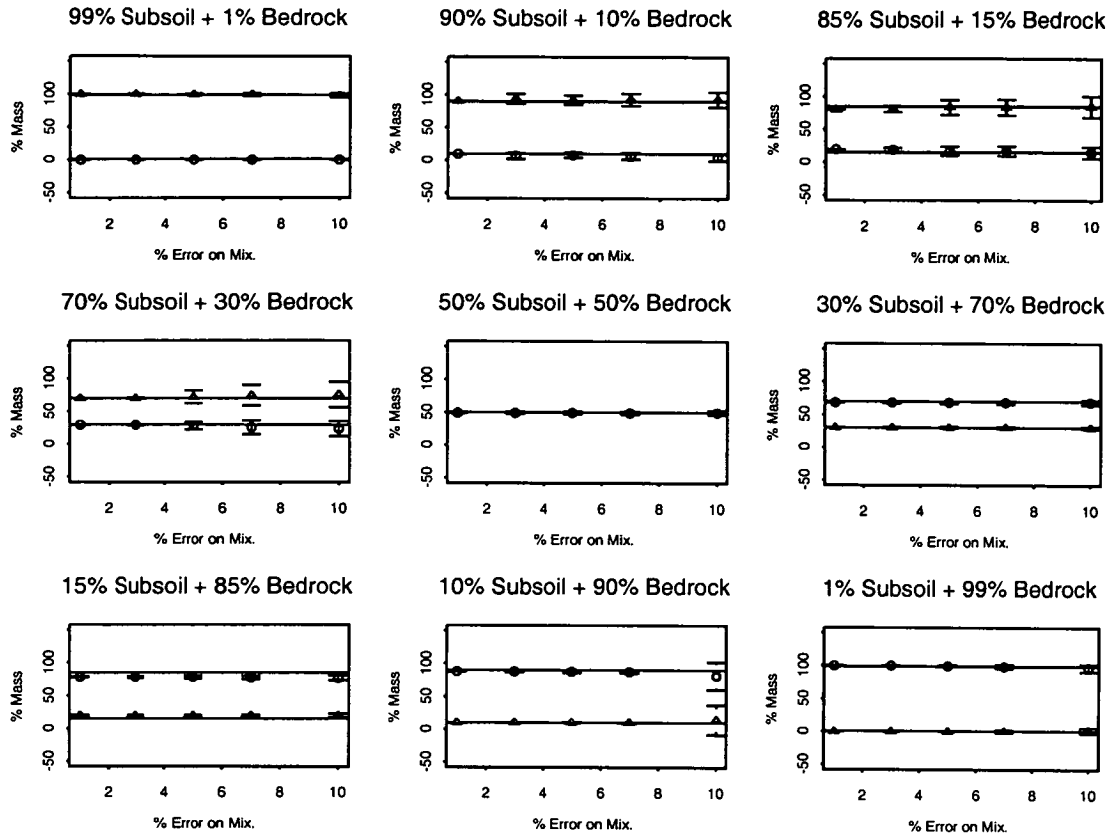

Figure 4.5. Unmixing test results for nine different concentrations of subsoil and bedrock. On each plot five different percentage error tests are plotted along the horizontal axis and the modelled percentage mass of both end-members on the vertical axis (triangle for subsoil, circle for bedrock). Horizontal lines show the actual mixture that was being unmixed. Symbols show mean result of fifty different unmixing experiments, error bars show standard deviations.

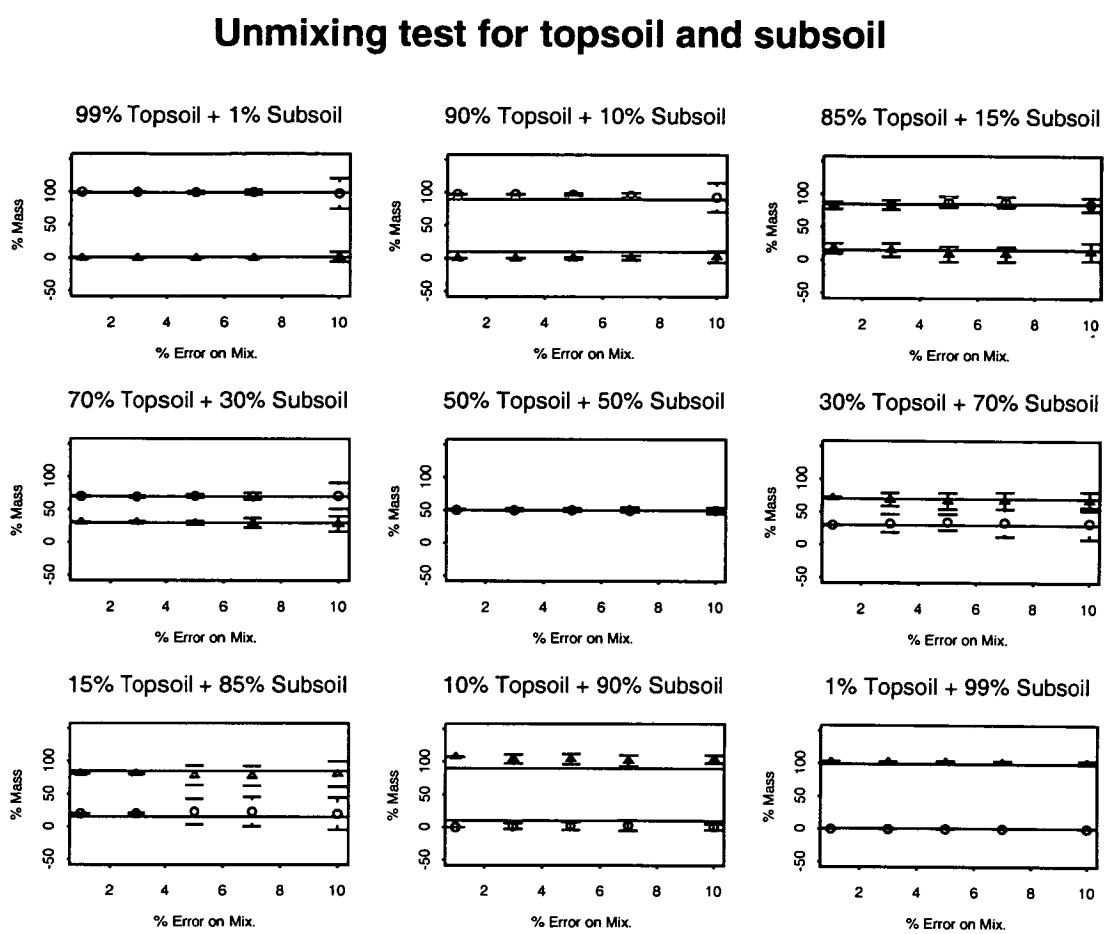

Figure 4.6. Unmixing test results for nine different concentrations of topsoil and subsoil. On each plot five different percentage error tests are plotted along the horizontal axis and the modelled percentage mass of both end-members on the vertical axis (triangle for subsoil, circle for topsoil). Horizontal lines show the actual mixture that was being unmixed. Symbols show mean result of fifty different unmixing experiments, error bars show standard deviations.

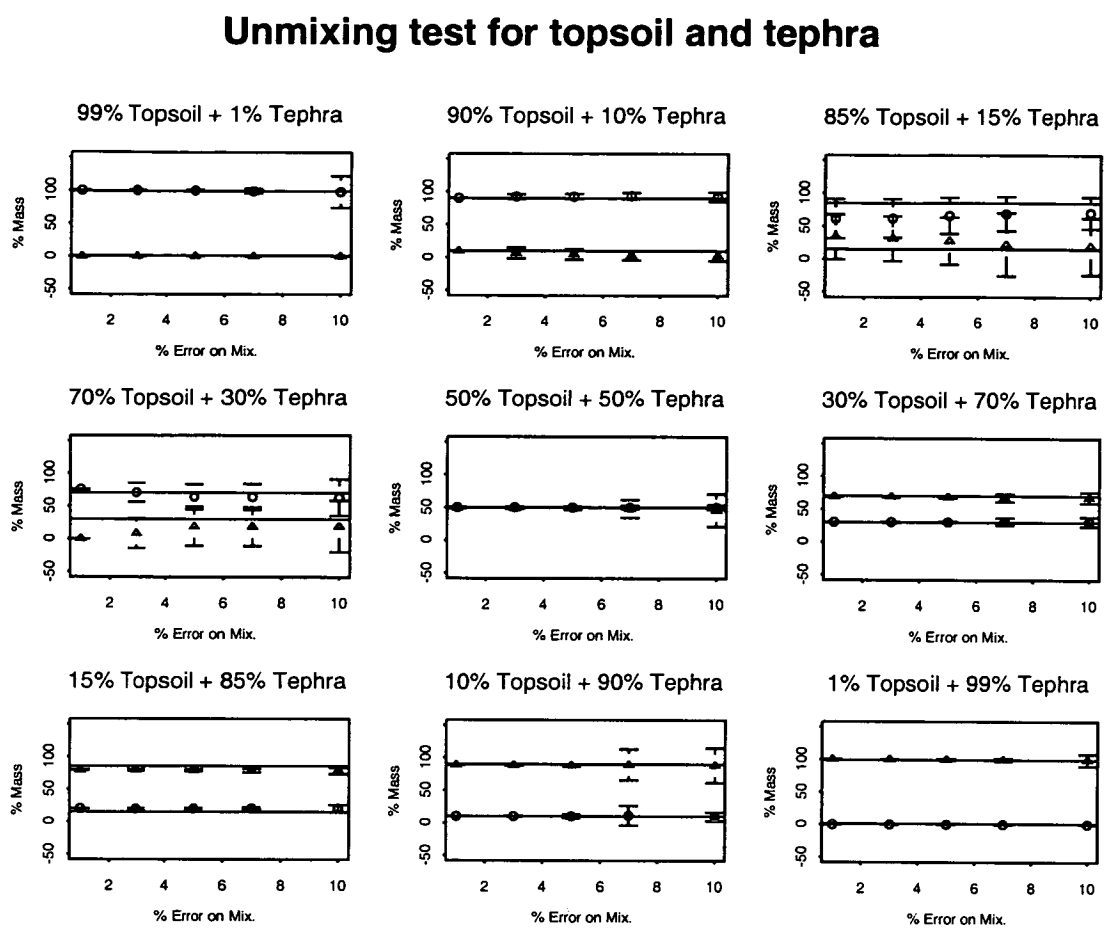

Figure 4.7. Unmixing test results for nine different concentrations of topsoil and tephra. On each plot five different percentage error tests are plotted along the horizontal axis and the modelled percentage mass of both end-members on the vertical axis (triangle for tephra, circle for topsoil). Horizontal lines show the actual mixture that was being unmixed. Symbols show mean result of fifty different unmixing experiments, error bars show standard deviations.

All three sets of unmixing tests (Figure 4.5, 4.6 and 4.7), show that the modelling routine is capable of differentiating between magnetically similar materials. The main point that is highlighted by these tests is the need for caution when a small quantity of material is mixed with a much larger quantity of magnetically similar material (Figure 4.6). Even introducing random errors of up to 10% on the magnetic measurements does not greatly effect the mean model. However there is a general increase in the standard deviations of the multiple experiments with increased measurement error.

An attempt to identify the size of errors in the measurement of remanences was made. Two samples, the present spinner magnetometer calibration sample and an older spinner magnetometer calibration sample, were repeat measured in the Molspin one hundred times on three attenuator settings. The Molspin used was calibrated each time the attenuator setting was changed, and had been left on for a long period, over six months, to reduce instrument drift. Examination of the results from the repeat measurements showed very little instrument drift during the period of the 100 repeat measurements. The instrument drift was removed by subtracting from the data the gradient of least squares line fitted to the data. The results of the repeat measurement tests with instrument drift removed are shown as histograms (Figure 4.8).

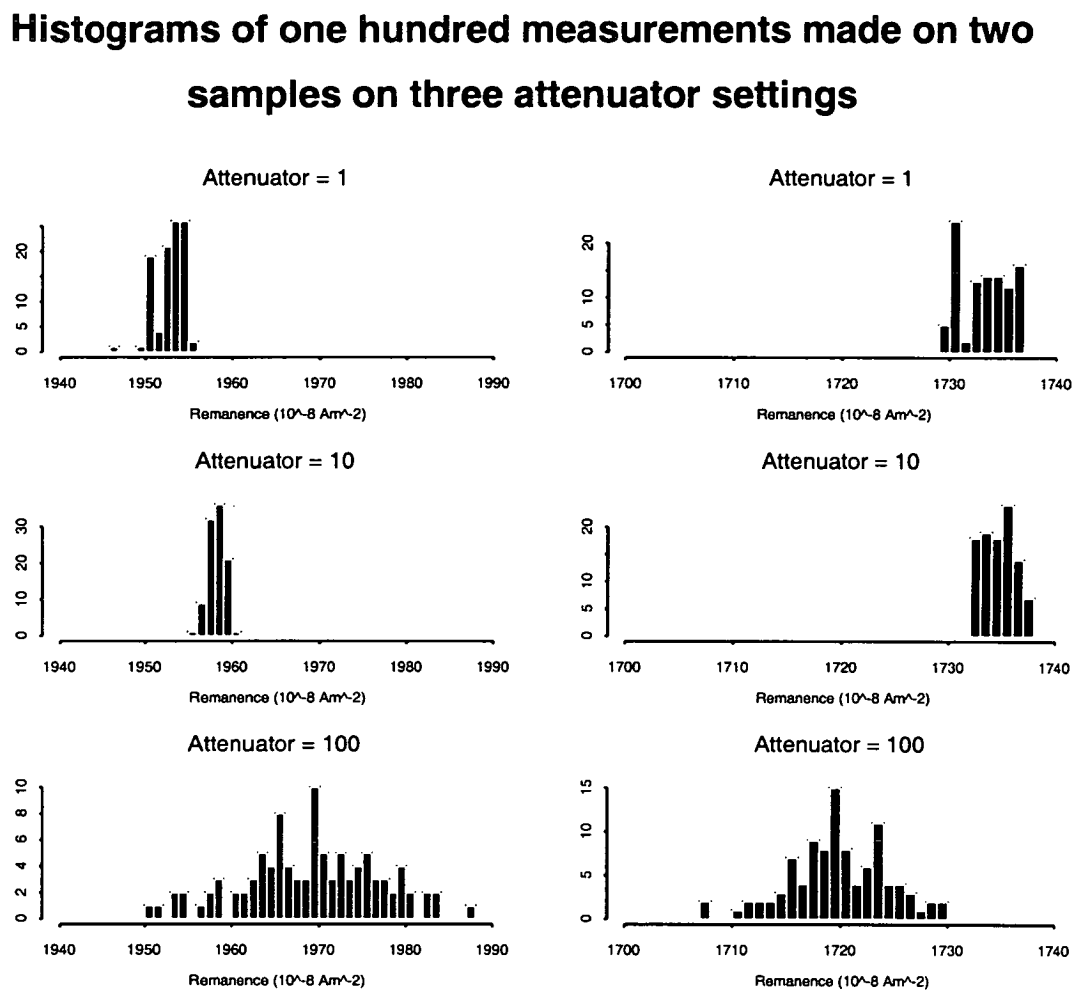

Figure 4.8. One hundred measurements made on two calibration samples at three different attenuator settings. Sample on the left is the current calibration sample (19.6 mAm^-2), sample on right is an old calibration sample.

The results of the attenuator test indicate that the measurement errors associated with the Molespin magnetometor are small. The standard deviations and percentage errors are summarised below in Table 4.2. We can see from Table 4.2 that the percentage error on the remanence measurements can be confined to below 1%. There is a systematic difference between the results for different attenuator settings (Figure 4.8). The difference between attenuator settings may be due to calibration problems. However directional effects should be minimal, as the results given are magnetic intensities. The difference between the three attenuator settings amounts to a percentage error of 0.8% for the both calibration samples. In order to reduce the error associated with different attenuator settings, all the ARM measurements in this thesis have been made at an attenuator setting of ten and all IRM measurements at an attenuator setting of one hundred.

Summary of Repeat Measurements of Molespin Calibration Samples

		Atten. = 1	Atten. = 10	Atten. = 100
Current Calibration Sample	Mean	1952.89	1958.19	1969.08
	Standard Deviation	1.61	0.93	7.73
	% Error	0.01	0.05	0.4
Old Calibration Sample	Mean	1733.29	1734.66	1719.23
	Standard Deviation	2.25	1.52	4.47
	% Error	0.12	0.09	0.26

Table 4.2. Mean, standard deviation and percentage error for two calibration samples measured one hundred times on three different attenuator settings, in a molespin magnetometor.

4.6 Assumptions of End-member magnetic unmixing

There are several assumptions that are made when catchment sample end-member magnetic unmixing is attempted. In chapters five and six where the new unmixing technique is applied to lake sediments from Lakes Pátzcuaro and Babicora, attempts have been made to address these assumptions. Here for the sake of clarity the assumptions are listed:

1. A representative set of catchment end-members has been collected.
2. Where magnetic interactions occur, their effects are accounted for by interactions seen in the catchment material.
3. Particle size sorting during transportation and deposition has not altered the characteristic magnetic properties of materials seen in the lake catchment.
4. Authigenic production of greigite does not significantly contribute to the magnetic properties of the sediment.
5. Reduction diagenesis has not significantly altered the magnetic properties of the sediment.
6. Iron-reducing bacteria have not made a significant change to the magnetic properties of the sediment.
7. Magnetotactic bacteria have not made a significant contribution to the magnetic properties of the sediment.
8. Inputs of aeolian material, either from industrial pollution or from sources not sampled are not significant.

The validity of these assumptions can be assessed using a number of different approaches. Point one requires selective sampling from as much of the catchment as possible. However, where end-members are missing, this should become apparent by poor fit and low skill in the modelling. Point two, additivity, is discussed in Section 4.1. Particle size analysis of the lake sediments, and analysis of how catchment magnetic properties vary with size could be used to address points three and eight. Points four and five can be addressed by an examination of the magnetic properties of the lake sediments. Reduction diagenesis would lead to a sharp reduction in magnetic intensity, coupled with low SARM/SIRM ratios. Authigenic greigite production would be indicated by IRM acquisition at very high fields. Point seven can be addressed by including a magnetotactic bacteria end-member in the magnetic unmixing. This leaves the question of iron reducing bacteria in the lake sediment, which cannot be addressed simply by use of magnetic measurements.

4.7 Summary

The new unmixing routine developed here solves the problems associated with previous magnetic unmixing techniques of local minima, non-convergence between multiple model runs with different starting points and highly constrained end-member selection. The unmixing technique is entirely non-negative through the use of non-negative least squares and parsimonious through a stepwise F-testing technique. Using the error analysis techniques described in Section 4.4.1 and 4.4.2 it is possible to evaluate the goodness of fit of models and to estimate the errors involved. The unmixing tests on catchment samples from the Pátzcuaro basin show that the unmixing technique can differentiate between magnetically similar materials. For example a mixture of 15% subsoil and 85% topsoil can be unmixed successfully even with a 7% error applied to the magnetic measurements (Figure 4.6). However, where any magnetic unmixing is attempted the assumptions listed in Chapter 4.6 should be considered, and where possible accounted for.

Chapter 5

Pátzcuaro Basin

In this chapter, the magnetic unmixing technique described in Chapter 4 is applied to magnetic measurements made on two cores from Lake Pátzcuaro. The results are discussed in the context of previous studies of the sediments from Lake Pátzcuaro, and are interpreted in terms of past environmental processes.

5.1 Introduction

Lake Pátzcuaro has been the focus of many scientific studies, from remote imaging (Chacón *et al,* 1992) and climatic trends (Chacón and Iribe, 1997; Bridgwater, *et al.,* 1999; Bradbury, 2000) to human impact (O'Hara *et al.,* 1993; O'Hara *et al.,* 1994) and water quality assessment (Chacón, 1993). It is the most studied lake in Mexico (Bridgwater, *et al.,* 1999) and has been described as one of the most important highland lakes in that country (Chacón, 1993). Due to the importance of Lake Pátzcuaro and the previous studies carried out there, it was chosen as a good location to run the unmixing methods that I have developed. It is hoped that the analysis of the magnetic properties of cores from Lake Pátzcuaro, and especially the identification of sediment sources through end-member unmixing, will increase our understanding of the processes that have affected Lake Pátzcuaro.

5.2 Location and history

Lake Pátzcuaro is located in the central Mexican highlands in an enclosed volcanic basin in the state of Michoacán (Figure 5.1). The lake is 2,036 meters above sea level and covers an area of 126 km^2. Its surrounding catchment covers an area of 927 km^2 giving a catchment area to lake area ratio of 7.4. The lake is situated in a sub-humid region; receiving a mean annual rainfall of 1,000mm per year. The rainfall in central Mexico is highly seasonal, with 80% falling between the months of May and October (Figure 5.2). Lake Pátzcuaro lies in a climatically sensitive region due to its geographical location, altitude and orographic effects (Chacón and Iribe, 1997). Lake Pátzcuaro is a shallow water body with a mean depth of only 4.6 m, it is most shallow in the south (1-2 m) and deeper in the north, up to 12 m. Lake Pátzcuaro's catchment is dominated by volcanoes. The surrounding geology consists of Cenozoic volcanic rocks and fluvial-lacustrine sediments (Chacón, 1993). Soil types have been influenced by the volcanic bedrock and are typically andosols and luvisols on the mountain slopes and lowlands, and gleysols at the lake's shore. Andosols and luvisols are both very susceptible to erosion (Bridges, 1997). Figure 5.3 shows a

view over Lake Pátzcuaro's catchment, note the bare soil and erosional features in the photograph. This image is typical of much of the Lake Patzcuaro catchment.

Lake Pátzcuaro has no outlet and no permanent major inlets, it is fed by temporary surface streams, surface runoff, rainfall and groundwater seepage (Chacón and Iribe, 1997). Lake Pátzcuaro is almost unique amongst Mexican lakes, in that there is no indication that it has dried out at any time during the Holocene (Bradbury 2000). This means the sediments taken from Lake Pátzcuaro represent an uninterrupted sediment record.

Lake Pátzcuaro has been an important source of water for drinking, irrigation, cleaning and sewage disposal, as well as a source of fish, for the local inhabitants. The presence of maize pollen in the lake's sediments indicates that there has been farming within the catchment from 3,500 ^{14}C yr B.P. (Watts and Bradbury, 1982). Agriculture dominates the present land use in the Lake Pátzcuaro catchment (O'Hara, 1991).

The Pátzcuaro basin was the focal point of the Tarascan empire from 1,000 yr B.P. until the Spanish conquest in AD 1521 (O'Hara, *et al.*, 1993). It is estimated to have been home to between 60,000 and 105,000 people immediately before the arrival of the Spaniards in AD 1521. The Tarascans are known to have used great quantities of wood, both for ceremonial fires and building which has led to extensive deforestation of the lake's catchment (O'Hara *et al.*, 1993). Presently the population residing close to Lake Pátzcuaro has been estimated at 80,000. This estimate is based on the major population areas of Pátzcuaro and Quiroga (Terrett, 2000).

Lake Pátzcuaro is now a highly eutrophic water body due to the large amounts of sewage and soil being washed into the lake system (Rosas *et al.* 1985). The pollution of Lake Pátzcuaro is a major problem as it causes health problems and has reduced fish populations, especially that of the "white fish" which is the symbol of the state of Michoacán. A captive breeding programme has been instigated in an attempt to re-stock the lake with the white fish, but continuing deterioration in the lake's water quality is hampering the restocking of the lake.

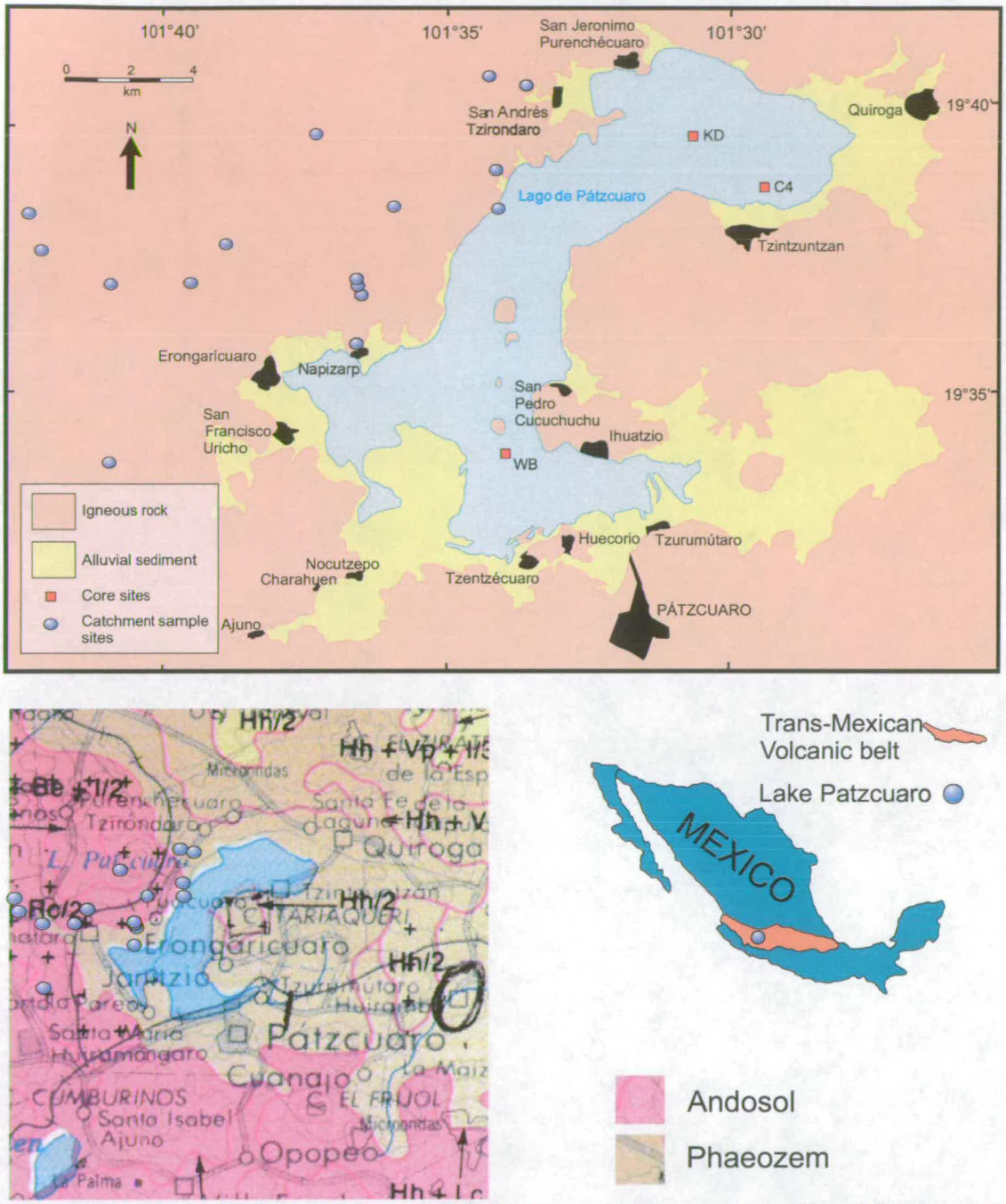

Figure 5.1 Geology and soil maps, showing Lake Pátzcuaro. Locations of cores KD and C4 (the cores used in this study) are shown, together with the location of the Watts and Bradbury (1982) core (WB) and the catchment samples taken for the magnetic unmixing.

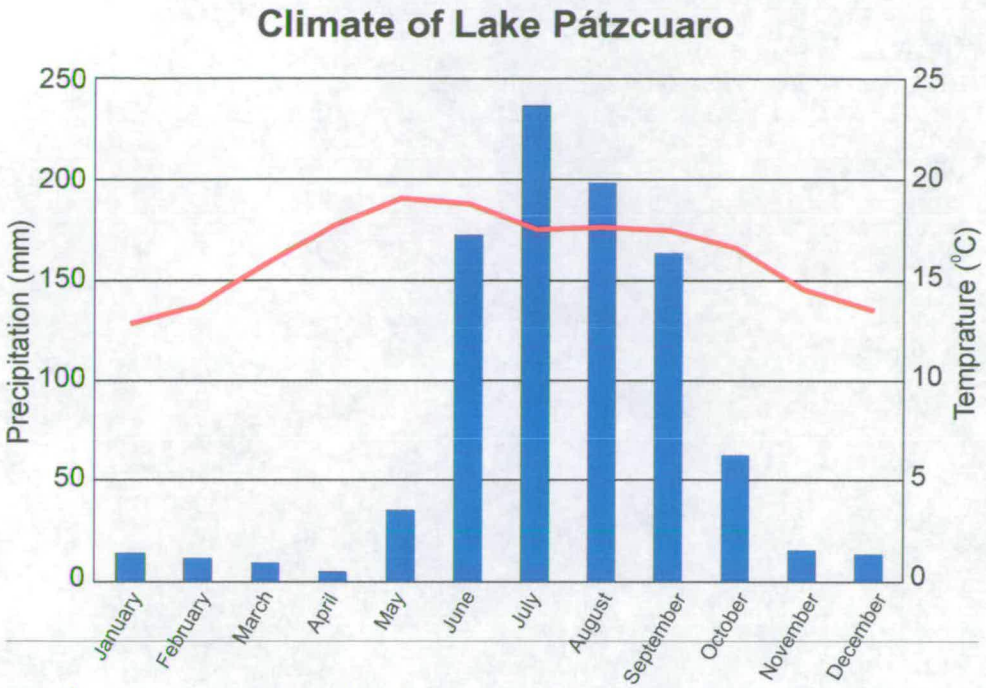

Figure 5.2 Shows mean monthly precipitation (bars) and temperature (line) data for Pátzcuaro over the last 30 years. Note the pronounced difference in winter and summer precipitation.

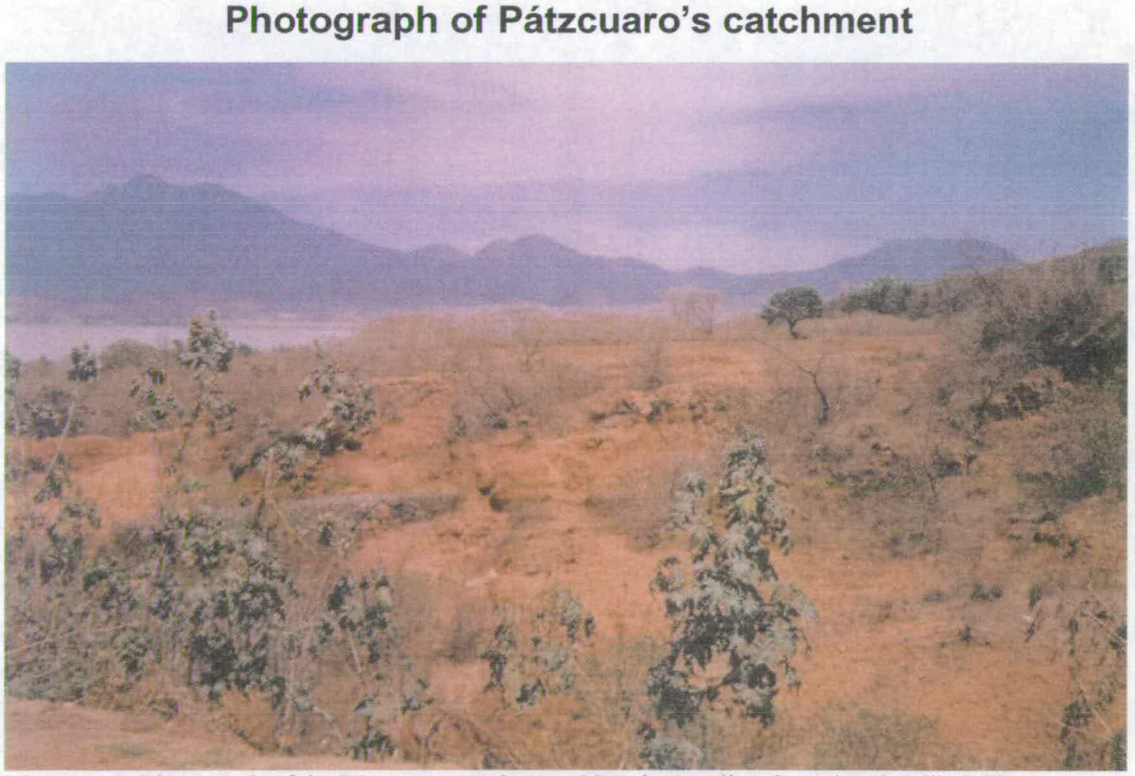

Figure 5.3. Photograph of the Pátzcuaro catchment. Note bare soil and erosional gullies. These features are common in this catchment, and indicative of deep soil erosion.

5.3 Previous work on sediments from Lake Pátzcuaro

Bradbury (2000) studied the diatom assemblage and Watts and Brabury (1982) studied the pollen assemblage of a 14m core from the south of the Pátzcuaro basin that covered 48 thousand years of sedimentation. Changes of climate and the effects

of human inhabitation are reported in both the pollen (Watts and Brabury, 1982) and diatom (Bradbury, 2000) records. The main conclusions reported by Bradbury (2000) are as follows:

- 38,000 to 25,000^{14}C yr B.P. deep freshwater conditions.
- 30,00, to 10,000^{14}C yr B.P., highest precipitation in winter and early spring.
- After 10,000^{14}C yr B.P., shallowing, and eutrophication of the lake with low rainfall and increased salinity.
- 4,000^{14}C yr B.P., agriculture around lake, increased soil erosion and nutrient inputs into the lake system.

However care should be taken with the dating of these episodes. Only four radio carbon dates were available from the period of sedimentation represented here.

O'Hara *et al.*, (1993) report results from 20 short sediment cores from Lake Pátzcuaro that ranged in length from 1.24 to 2.85 m. Analysis of these surface cores indicated that human activities were responsible for increased soil erosion within the Pátzcuaro catchment, leading to high sedimentation rates in the lake. The soil erosion was found to occur in three distinct phases. The first of these erosion periods started 3,640 ± 80^{14}C yr B.P. and finished by 2,890 ± 80^{14}C yr B.P.. A second and more intense erosion period lasted from 2,530 ± 60^{14}C yr B.P. until 1,190 ± 70^{14}C yr B.P. (O'Hara *et al.*, 1993). After these two periods of high erosion, there was a third high erosion episode that started approximately 850^{14}C yr B.P. and has continued until the present. Between the periods of high erosion the lake sediments were reported to have high organic content and be rich in ostrocods. In the two most recent erosion periods it was found that the rate and overall volume of eroded material was greater in the north of the basin than in the south. It is believed that the higher erosion rate in the north of the basin was due to a higher population there (O'Hara *et al.*, 1993). The high erosion rates from pre-Hispanic times indicated that indigenous farming techniques had similar soil erosion problems to the present agricultural methods introduced by the Spanish (including the use of the plough) (O'Hara *et al.*, 1993).

O'Hara *et al.*, (1993) hypothesised that the bulk magnetic susceptibility of the Pátzcuaro sediment gave a good indication of the amount of soil erosion within the catchment. These authors suggested that the relationship between lake sediment magnetic susceptibility and soil erosion was due to the high ferromagnetic content of the soil-derived sediment as opposed to the ferromagneticly weak sediments associated with high organic content and calcium carbonate rich ostracod shells. Note that a limitation of the O'Hara *et al.*, (1993) study was that the only magnetic parameter measured was susceptibility and no catchment sample studies were made.

Bridgwater *et al.* (1999) used floral and stable-isotope records from Lake Pátzcuaro to infer past climates using ostrocod shells extracted from the same 20 cores that were used for the soil erosion analysis by O'Hara *et al.* (1993). The cores covered a maximum time span of 4,100 yrs. Bridgwater *et al.* (1999) divide the climate over this period into five distinct episodes:

Period (yr B.P.)	Climate
0 – 220	Wetter Conditions
300 – 800	Drier Conditions
1,190 – 1,330	Wetter Conditions
1,330 – 2,340	Drier Conditions
2,390 – 3,530	Wetter Conditions

The distinction between these periods was found both in the $\delta^{18}O$ record within ostracod shells and the particular species of ostracods found within different core horizons (Bridgwater *et al.*, 1999). These shifts in climate were not just found on a local scale: similar changes have been noted in the Caribbean and East Mexico (Jauregui and Klaus, 1976; Hastenrath, 1976).

Terrett (2000) completed a diatom analysis of core C4, one of the two cores that this study of the magnetic properties of Lake Pátzcuaro is based on. Her major findings were:

- Deep, cool and stratified conditions 19,000 to 10,000^{14}C yr B.P..
- Shallow warm and dry, fluctuating lake levels, increased turbidity 10,000 to 3,500^{14}C yr B.P..
- Dry environment, shallow lake 3,500 to 3,250^{14}C yr B.P..
- Fluctuating lake levels climate changing between dry and humid 3,250 to 2,500^{14}C yr B.P..
- Drier conditions 2,500 to 2,200^{14}C yr B.P..
- Low lake levels, warm and dry increasingly eutrophic 2,200yr to 1300^{14}C yr B.P..

The interpretations of Terrett (2000), Watts and Bradbury (1982), Bradbury (2000), O'Hara *et al.* (1993), and Bridgwater *et al.*, (1999) are given in Figure 5.4 (modified from Terrett (2000)). We can see in Figure 5.4 that although there is some disagreement between the different methods and cores, there are several similar features, summarised below:

- Cool and wet period from 18,000 to either 15,000 or 13,000^{14}C yr B.P..
- Warm and dry period between 10,000 and either 5,000 or 4,000^{14}C yr B.P..
- Fluctuating periods of wet and dry conditions in the last 4,000 years.
- A pronounced arid period approximately 2,000^{14}C yr B.P..
- Eutrophication and high erosion from approximately 3,500^{14}C yr B.P..

A point of note in Figure 5.3 is the dating control on the studies in question. There are only four ^{14}C dates to constrain dating on both the Watts and Bradbury (1982) and Bradbury (2000) studies; these dates are shown in the left column of Figure 5.4. Age constraints for the short cores taken by O'Hara *et al.*, (1993) are provided by 16 ^{14}C dates on the cores and also cross correlation between cores.

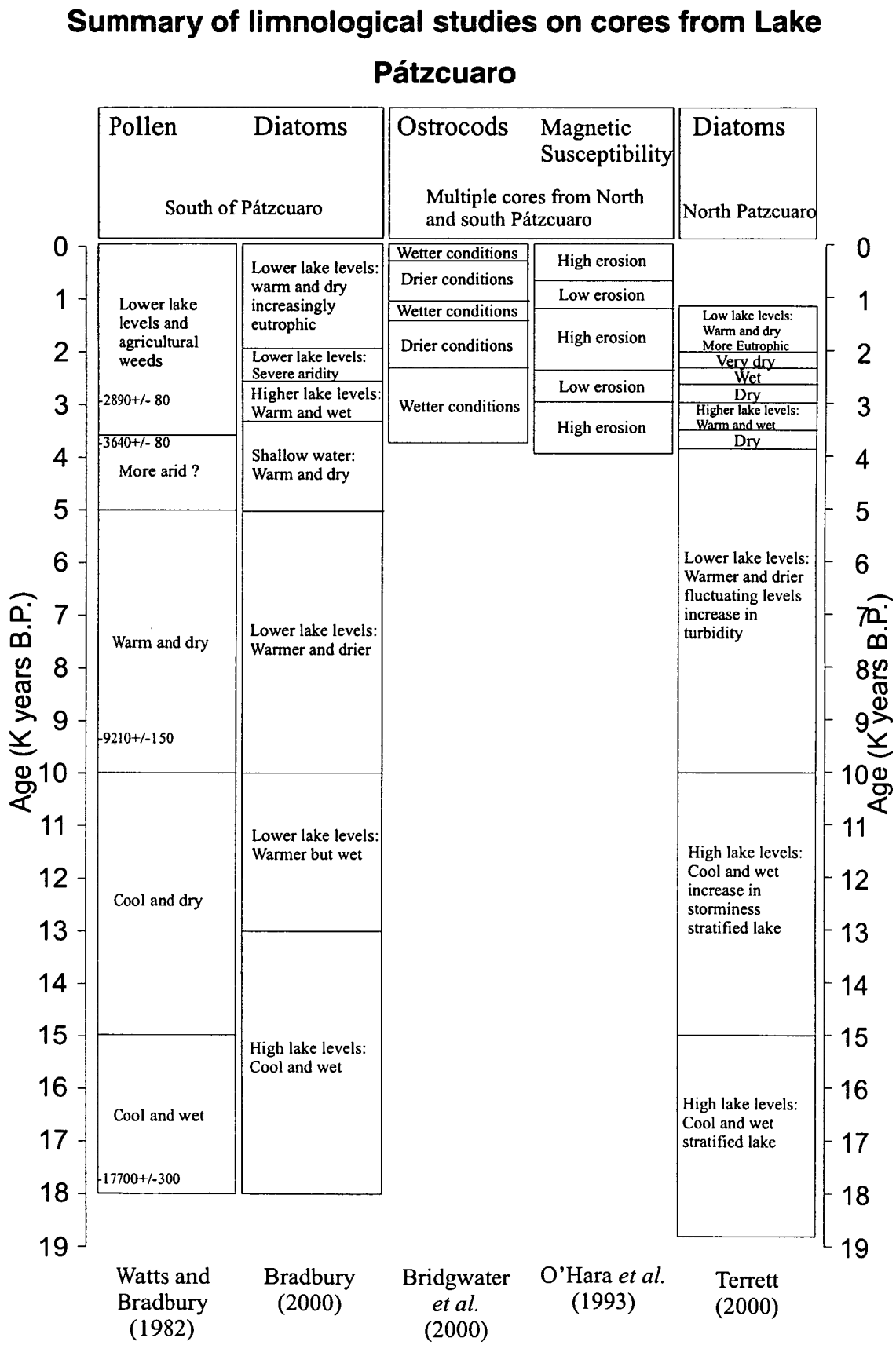

Figure 5.4 Summary plot of limnological studies carried out on cores taken from Lake Pátzcuaro. The C4 column comes mostly from diatom analysis, but magnetic susceptibility and XRD results were taken into account. This figure is a modified version of Figure 8:4:1 from Terrett (2000).

5.4 Description of cores C4 and KD

Two cores have been used to study the magnetic properties of Lake Pátzcuaro. Both cores were taken from the deeper north part of the lake (Figure 5.1). The first core, core C4, is a 735cm long Livingstone core taken by Kingston University. The second core, core KD, is a 78 cm long Kullenberg core taken by the University of Edinburgh Geography department. The Livingstone core appears to be missing the uppermost part of the sediment sequence, so together the two cores are thought to represent a sequence of over 8m in length. The stratigraphy of the two cores is shown in Figure 5.6 and Figure 5.9. The Livingstone core has been dated at ten points (Figure 5.6) using the ^{14}C method. Based on these ^{14}C dates, the core is found to provide a record covering 19,000 years of sedimentation. An age depth profile has been drawn using these ten radio carbon dates (Figure 5.5). The Kullenberg core has a ^{14}C date from near its base of 960 ± 45 ^{14}C yr B.P., which transfers to AD 1073 +171/-34 (Stuiver and Reimer, 1993), and a tephra sample from the top of the core has been identified as coming from the eruption of Paricutin in AD 1943.

To aid the description of core C4, I have divided it into three sections:

1. **Section one** from the bottom of the core to 530cm, 19,000 – 13,600 ^{14}C yr B.P.;
2. **Section two** from 530cm to 360cm, 13,600 – 3,200 ^{14}C yr B.P.; and
3. **Section three** from 360cm to the top of the core 3,200 – 1,300 ^{14}C yr B.P..

The dates on these sections are approximations inferred from the available ^{14}C dates on the core. These sections were chosen in order to split the core into magnetically similar material. These three sections remain the same throughout the description of the core and the unmixing models that I develop.

5.5 Age depth profile and sedimentation rate of Core C4

The age depth profile for core C4 (Figure 5.5) shows that the lake has undergone large changes in sedimentation rate. Sections one and two of the C4 core have a lower sedimentation rate than section 3. However, the sedimentation rate for core KD, at 0.085cm year^{-1}, is significantly lower than the sedimentation rate seen in section three of the C4 core. However, note that the C4 core is closer to the shore line than the KD core, and so it should be expected to have a higher sedimentation rate. The generally high sedimentation rates seen in Lake Pátzcuaro, would make both reduction diagenesis and the authigenic production of iron sulphide minerals unlikely (Chapter 3.5.2).

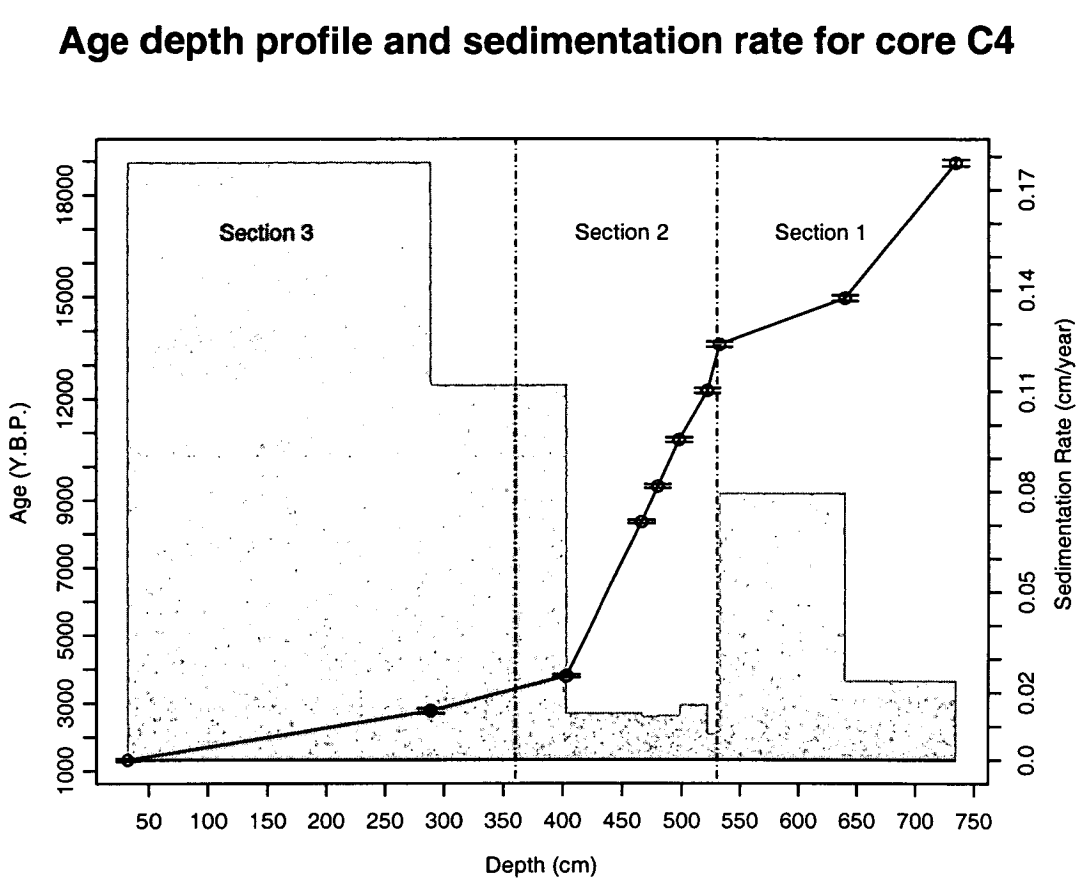

Figure 5.5. The age depth profile (black line) and sedimentation rates (grey blocks) for core C4 plotted against depth. Data comes from 10 ^{14}C dates on the core. The sedimentation rate in C4 can be compared with a sedimentation rate of approximately 0.085cm/year in core KD. The sections used for core description are marked for reference.

5.6 Results

Both cores C4 and KD were sub-sampled to provide material for magnetic measurements. Core KD was sampled at 2cm intervals for its entire length. Core C4 was sampled at approximately 5cm intervals. For some horizons of the C4 core material was unavailable because it had been used for other techniques. Each of the 157 sub-samples from C4 and the 33 sub-samples from KD were placed into 2 cm plastic cylinders and then subjected to 18 magnetic parameter measurements. The magnetic measurements started with 2 susceptibility measurements (high and low frequency), followed by ARM magnetisation (99mT ac field with 0.1 mT dc field) then ARM demagnetisations (at 5, 10, 20, 40, and 80mT), and finally ten IRM magnetisations (at increasing fields of 20, 40, 60, 80, 100, 200, 300, 1000, 2000, and 3000 mT). A more detailed description of the magnetic measurements can be found in Chapter 2.4.

5.6.2 Stratigraphy and organic content of core C4

The stratigraphy of the C4 core (Figure 5.6) is dominated by dark brown silty clay. The lower section of the core is finer-grained, coarsening up from clays to silty clays.

The colours of core C4 vary between very dark-grey clay and olive-grey clay. There are a few horizons of silty clay in section one of the core, the largest being between 600cm and 680cm. Section three of the core consists almost entirely of dark brown silty clay. This upper core material is similar to the material found in the lower portion of the KD core. The stratigraphy was provided by Sarah Metcalfe (pers. com.). Unfortunately loss on ignition and calcium carbonate curves do not exist for either of the two Pátzcuaro cores. However spot measurements indicate that the organic content of the cores is generally low varying between 10 and 20% of their mass (Sarah Mtetcalfe, pers. com.).

5.6.3 Results of Magnetic Measurements on C4

Here I shall describe the magnetic properties of each of the three sections of core C4 in order from one to three. Throughout the description of the magnetic measurements made on core C4 I shall refer to Figure 5.6, which shows some selected magnetic measurements and measurement ratios. Dates have been extrapolated from the available radio carbon dates on the core, assuming a constant rate of sedimentation between each date.

Section one of core C4, 19,000 – 13,600 yr B.P.; (Figure 5.6) is characterised by low (in proportion to the rest of the core), although still measurable magnetic susceptibility high frequency dependence and high SARM/SIRM. The hardness of section one of the core is quite variable, this is apparent in both the ARM40mT/SARM and IRM80mT/SIRM ratios. Although the SARM/SIRM ratio is generally high in section one of the core, it is also highly variable from horizon to horizon. It is interesting to note that many of the tephras in section one are coincident with reductions in the SARM/SIRM ratio, as are the two areas of ostrocod shell abundance.

Section two, (13,600 – 3,200^{14}C yr B.P.), of core C4 also has a low susceptibility (Figure 5.6). The sediment in section two is generally magnetically harder than section one, with hardness reaching a peak at around 4.70 m (dated to 8,600^{14}C yr B.P.). This peak in magnetic hardness is most apparent in the ARM_{40}/SARM ratio curve. It coincides with several tephra events. The frequency dependence of the C4 core reaches zero at three horizons in section two. The first zero in frequency dependent susceptibility is at 496cm, close to horizons containing rootlets and tephra. The second is at 431cm, coinciding with a layer of charcoal found in the core. The third zero in the frequency dependence curve occurs at 367cm which would appear to coincide with an abundance of ostrocod shells. The third zero in frequency dependence coincides with reductions in susceptibility and SARM/SIRM, this may be an indication of reduction diagenesis. Note also that the first zero in frequency dependence, at 496cm, coincides with a peak in SARM/SIRM and a fall in IRM and ARM hardness. A peak in susceptibility at 520cm directly coincides with a tephra. The low susceptibility and SARM/SIRM ratios and the high magnetic hardness of much of section two of the core may be an indication of removal of detrital magnetic material by reduction diagenesis (Chapter 3.4).

Section three of the core (3,200 – 1,300^{14}C yr B.P.), is characterised by a three to five-fold increase in magnetic susceptibility (Figure 5.6). The core material of section three is dominated by magnetically soft material, as can be seen from the

IRM and ARM ratios. A particularly striking feature is that both the IRM and ARM ratios in this section of the core are stable with little variation over the three and a half meters of sediment represented here. We see that the frequency dependence in section three of the core is reasonably high being consistently around 6% to 7%. The SARM /SIRM ratio is also high and moderately stable at 0.1. The susceptibility, SARM/SIRM and frequency dependence all trough at 212cm (2,200^{14}C yr B.P.). This fall in susceptibility and frequency dependence coincides with an abundance of ostrocod shells, and again may be an indication of reduction diagenesis. Note also a fall in susceptibility at around 285cm which would appear to be associated with a tephra layer at that level.

For almost the entire core saturation IRM has been reached by 1T. This would indicate that iron sulphides are not a major factor in the magnetic properties of the core (Chapter 3.5).

5.6.4 Biplots of core C4

To further investigate the magnetic properties of core C4, and to compare the magnetic properties of the core's three sections, Two biplots of magnetic measurements from core C4 are shown (Figures 5.7 and 5.8). These two biplots show ARM hardness (ARM40mT/SARM) against IRM hardness (IRM80mT/SIRM), and IRM hardness (IRM80mT/SIRM) against SARM/SIRM (squareness). Envelopes have been drawn bounding the three core sections to indicate the general trend of each core section's magnetic properties. Section two contains four outliers, which plot in the section three area. These outliers were not included in the section two envelope, but are still plotted. The outliers are all from close to the boundary between sections two and three.

In the first biplot (Figure 5.7), which shows ARM hardness (ARM40mT/SARM) against IRM hardness (80mT/SIRM), the first section of core C4 plots between the hard titanomagnetite and hard magnetite end-members. In some places, the first section material overlaps with material from the second core section. However the first core section tends to be more drawn out towards the bacteria and very hard magnetite end-members. The second core section is widely spread in a "banana" shape that spans a large range of magnetic hardnesses from near the hard titanomagnetites to the hard magnetites. The material from the third section of the core sits in a tight area near the hard magnetite mineral end-member.

The second biplot (Figure 5.8), of IRM hardness (80mT/SIRM) against SARM/SIRM (squareness), is less discriminatory between the three core sections. However, the section three material is once again more uniform in its magnetic properties than the section one and two materials. Also, the section one material is generally closer to the bacteria end-member than either of the other two sections. In this biplot, the same four outliers have been excluded from the bounding box for section two.

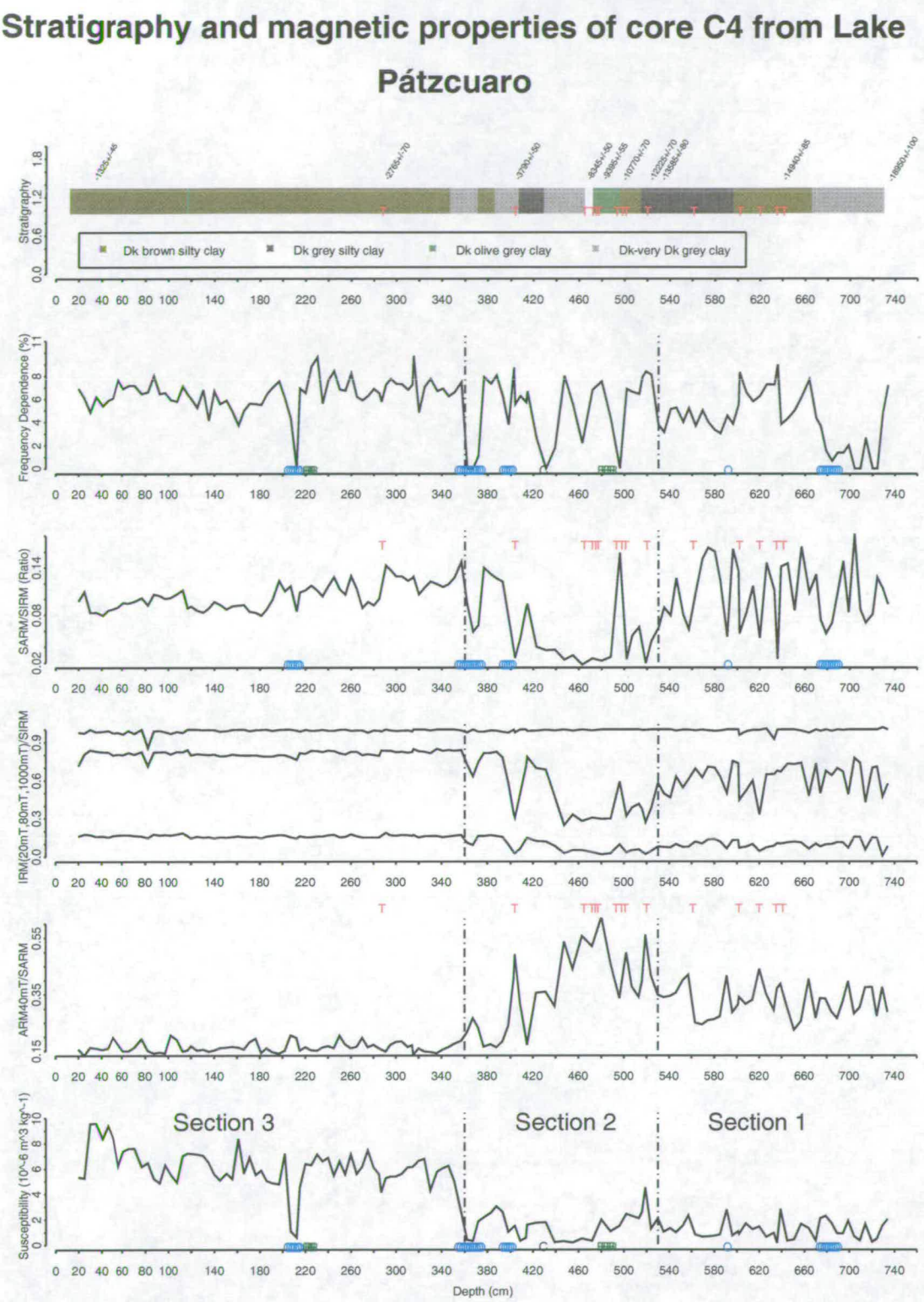

Figure 5.6. The stratigraphy and some magnetic results and ratios from the C4 core plotted against depth. The broken vertical lines separate the core into the three sections described in the text, from the bottom of the core to the top these are Section 1, Section 2 and Section 3. O = ostrocod rich layer, R = layer with rootlets, T= tephra layer and C = layer with charcoal present. Also shown are the 10 ^{14}C dates.

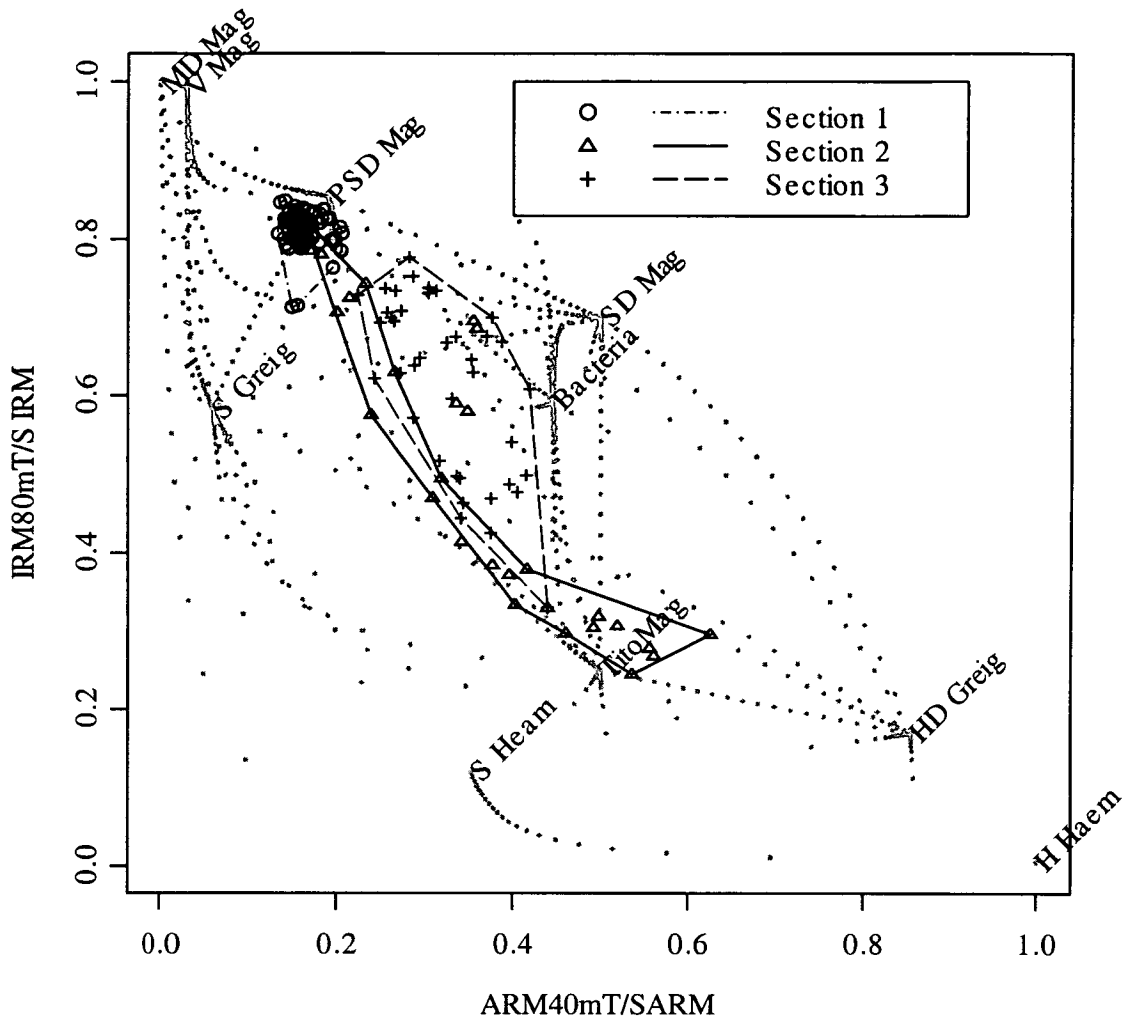

Figure 5.7. Biplot of the magnetic hardness of the material from the Pátzcuaro C4 core. IRM hardness increases downwards, ARM hardness increases to the left. The core has been separated into three sections. These sections have been bounded to emphasise differences and similarities between them. The section two bounding box has been drawn without the inclusion of four points that come from near the section 2, section 3 boundary. Also plotted are mineral magnetic end-members for reference, and points on the mixing curves between these end-members. For a further explanation see Chapter 2.8.

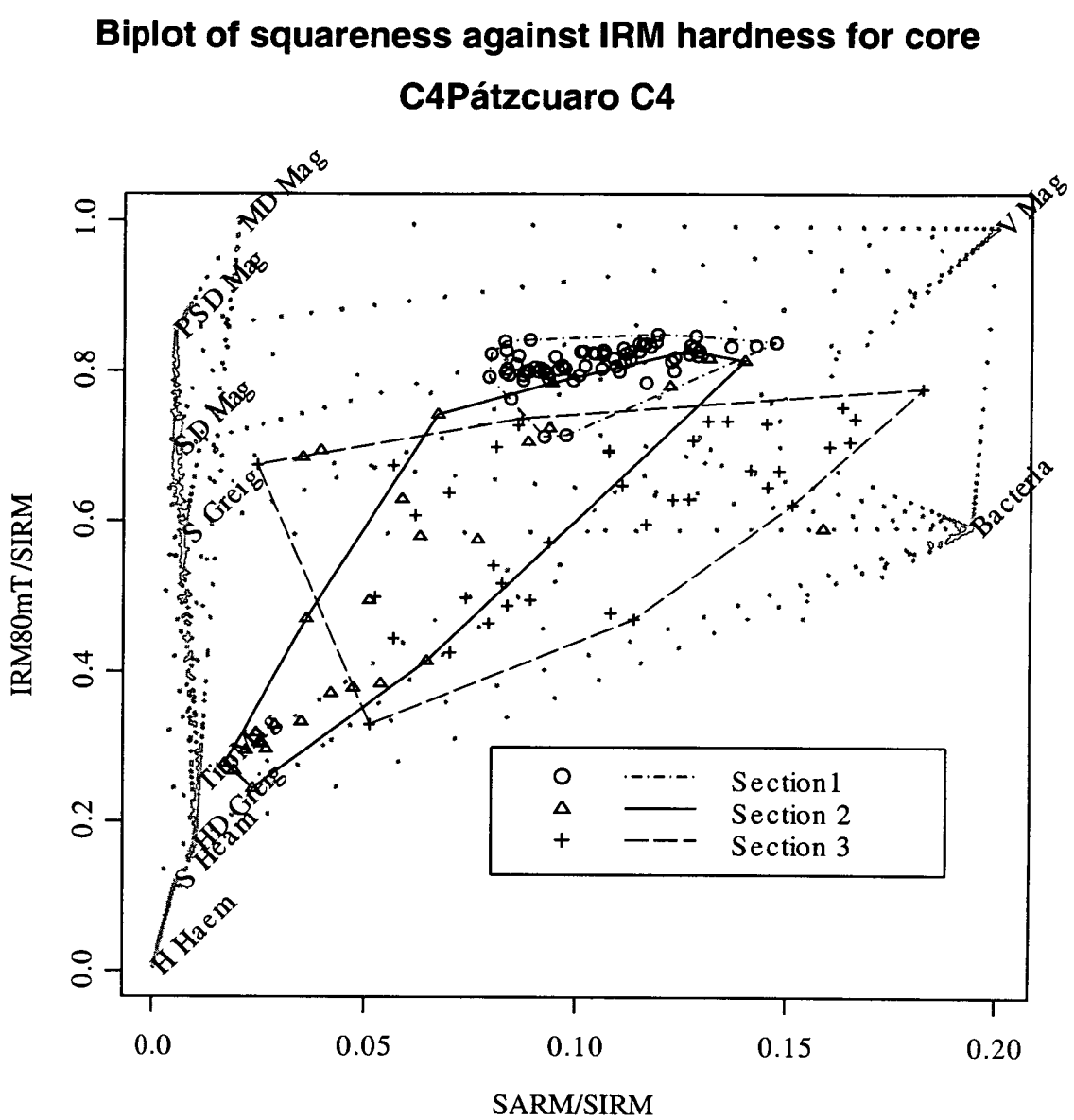

Figure 5.8. Biplot of the magnetic squareness against IRM hardness of the Pátzcuaro KD core. IRM hardness increases downwards, and squareness increases to the right. The core has been separated into three sections. These sections have been bounded to emphasise differences and similarities between the various sections. The section two bounding box has been drawn without the inclusion of four points that are believed to be outliers. Also plotted are mineral magnetic end-members for reference, and points on the mixing curves between these end-members. For a further explanation see Chapter 2.8.

5.6.5 Stratigraphy of KD

The stratigraphy of the KD core (Figure 5.9) is very consistent. Almost the entirety of core KD is dark, greyish brown clay. There is one horizon where this clay becomes more grey (41 to 43cm depth). The base of core KD is a dark-brown, silty clay, similar to the material at the top of the C4 core. Two dates have been obtained for the KD core: a ^{14}C date of $960^{14}C$ yr B.P. (AD 1037 +171/-34, (Stuiver and Reimer, 1993)) from near the base of the core and a dated tephra layer from the eruption of volcano Paricutin in 1943, from near the top of the core. Using these two dates, the sedimentation rate for the core has been calculated to be 0.085cm $year^{-1}$.

5.6.6 Magnetic Results of Core KD

The magnetic properties of core KD are as homogenous as its stratigraphy (Figure 5.9). Most of the magnetic parameters reveal a difference in the lower core material compared to the upper core. The lower core material has lower magnetic susceptibility, frequency dependence and SARM/SIRM, but its hardness is similar to the upper core material. Other trends of note are a general increase in susceptibility and frequency dependence up-core.

Stratigraphy and magnetic properties of core KD from Lake Pátzcuaro

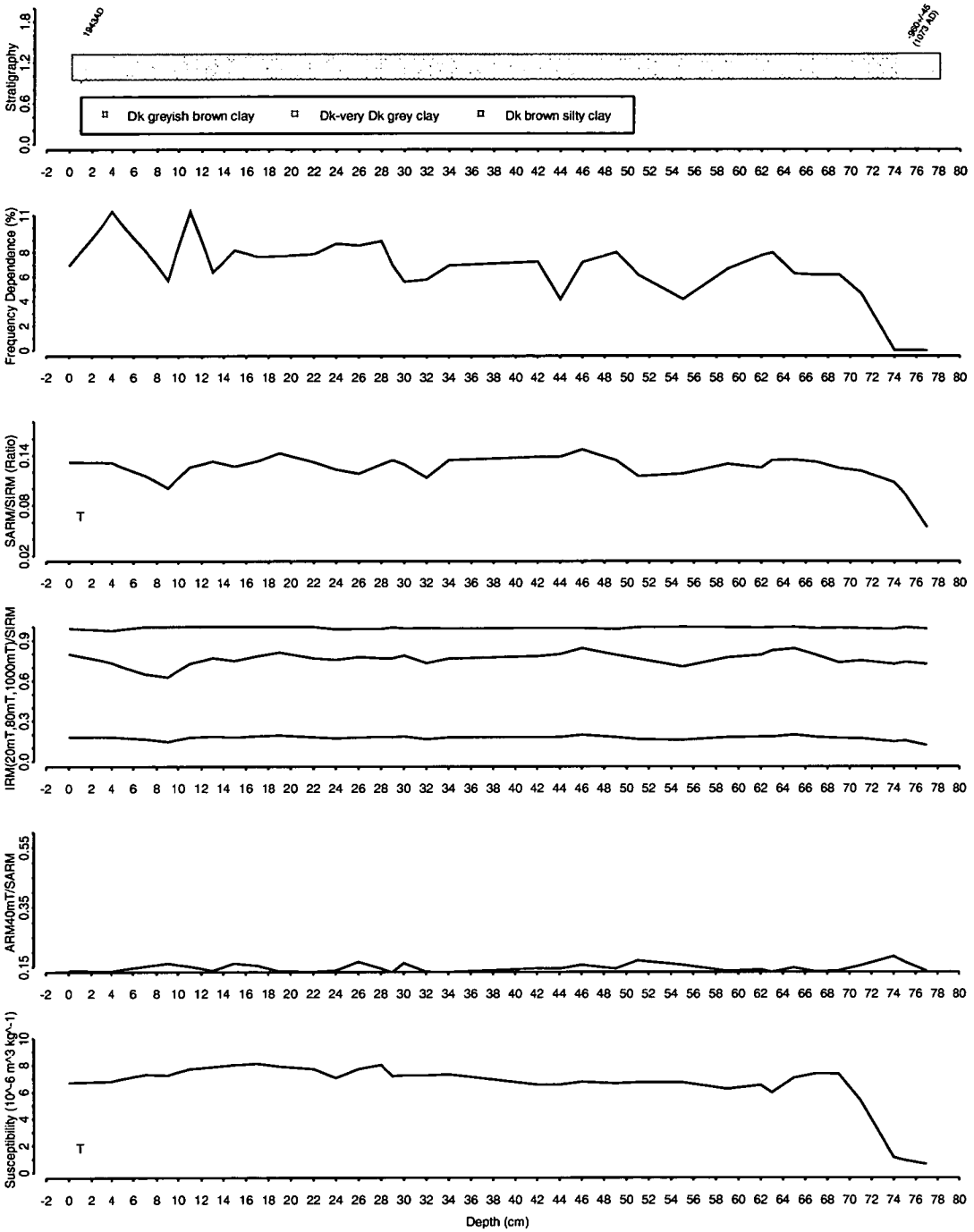

Figure 5.9. The stratigraphy and magnetic properties of the Pátzcuaro KD core, against depth in cm. T = Tephra layer.

5.6.8 Catchment samples

In order to interpret the magnetic properties of the lake sediments and to provide data for unmixing, 36 catchment samples were collected from the Lake Pátzcuaro basin. Dr. Anthony Newton, University of Edinburgh Department of Geography, kindly

collected these samples. The 36 catchment samples were subjected to exactly the same magnetic measurements as the core material. The catchment samples were classified into four different end-member types depending on the material they were thought to represent. These end-member classifications were topsoil, subsoil, bedrock and tephra. Note, however, that misclassification, especially in regard to topsoil and subsoil material, is likely, as these distinctions can be somewhat subjective. Attempts were made to gather material from as many different catchmnet environments as possible, but of course it is possible that distinctive catchment material is missing from this set of samples. The magnetic properties of the catchment materials are most easily seen on biplots (Figs 5.11 and 5.12). In the first of these two biplots (Figure 5.11), there is a good separation between bedrock, tephra and the soils. However there is little discernible difference between topsoil and subsoil. The second of the two biplots (Figure 5.11) shows a similar case; however, bedrock and soils are more alike in this plot. Note in the second biplot that the soils generally lie between the tephra and bedrock samples and viscous magnetite.

If we compare the catchment sample biplots, Figures 5.10 and 5.11, to the two biplots of the lake material, Figures 5.7 and 5.8, we can see that the catchment samples plot in and around the lake sediment biplots. The fact that the catchment samples cover the range of magnetic properties exhibited by the lake core material is an encouraging sign for the unmixing process.

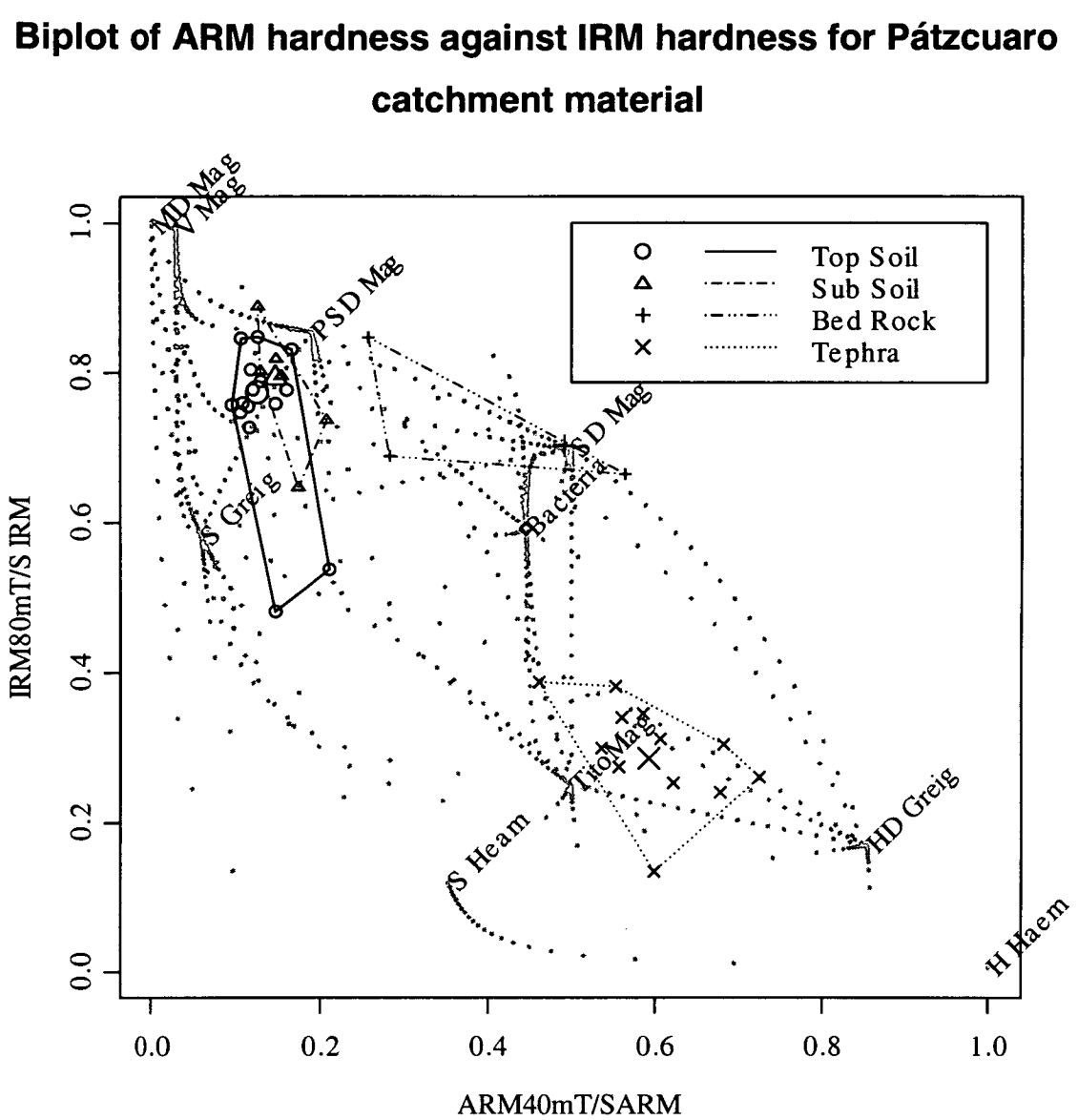

Figure 5.10. Biplot of the magnetic hardness of the material from the Pátzcuaro catchment. IRM hardness increases downwards, ARM hardness increases to the left. The catchment material has been separated into four types. These have been bounded to emphasise differences and similarities between them. Also plotted are mineral magnetic end-members for reference, and points on the mixing curves between these end-members. For a further explanation see Chapter 2.8.

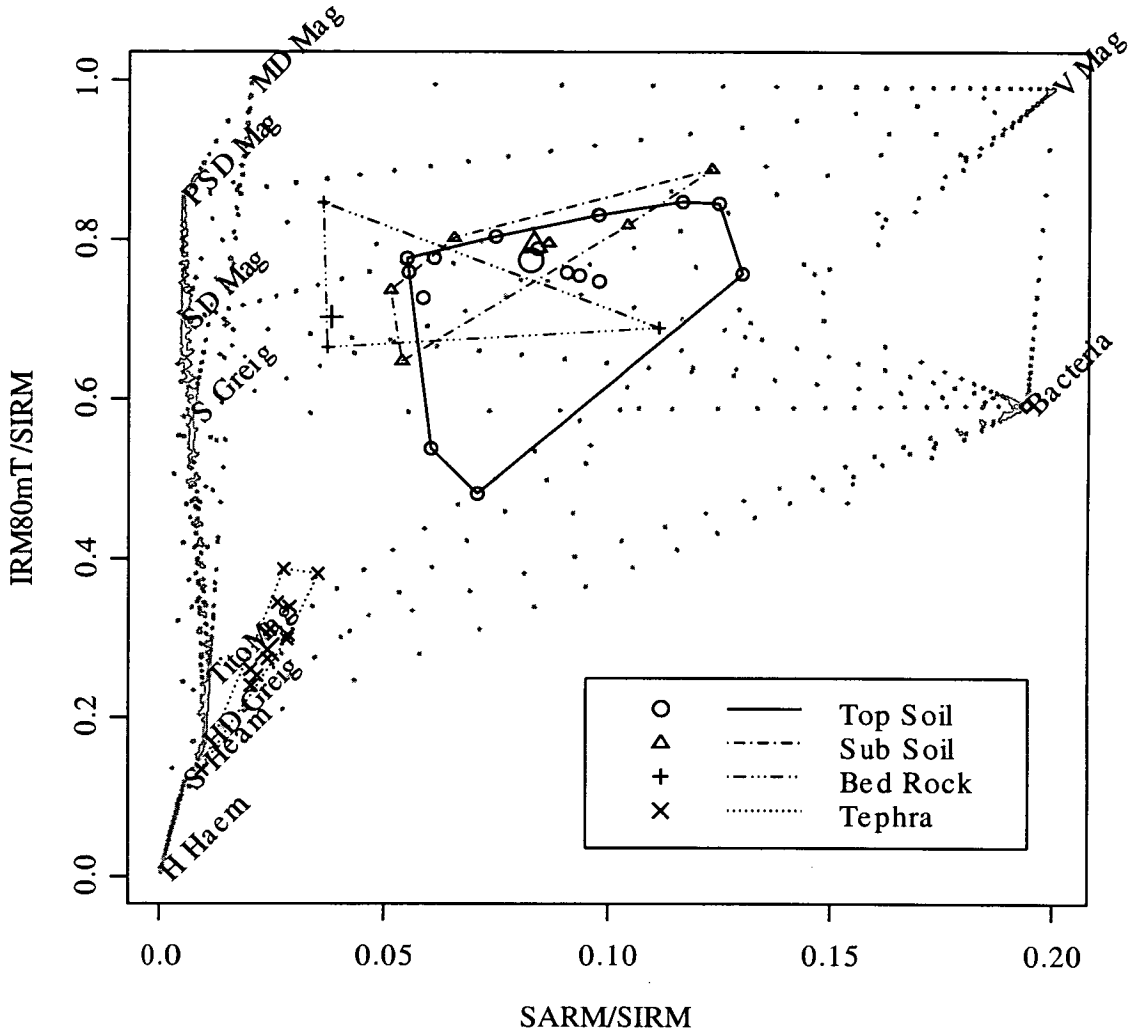

Figure 5.11. Biplot of the magnetic squareness against IRM hardness of the material from the Pátzcuaro catchment. IRM hardness increases downwards, and squareness increases to the right. The catchment material has been separated into four types (Topsoil, Subsoil, Bedrock and Tephra). These catchment types have been bounded to emphasise differences and similarities between them. Also plotted are mineral magnetic end-members for reference, and points on the mixing curves between these end-members. For a further explanation see Chapter 2.8.

5.6.9 Catchment sample sieving

In order to more fully understand the catchment materials, I sieved the twelve soil end-members: eight topsoils and four subsoils, which were selected by the modelling procedure to be included in the 1st unmixing model (Section 5.7.1), and a sediment sample from deep in the core (700cm). The samples selected for sieving were soaked in sodium hexametaphosphate (4% solution) for three days, and then placed in an ultrasonic bath for five minutes to disperse. The samples were then separated into five size fractions; >500μm, >63μm, >10μm, >2μm and <2μm, by sieving and centrifuging. After separation, the soil sample splits were subjected to

the same eighteen magnetic measurements made on the bulk sample. Unfortunately the sediment sample split did not have these measurements made, as it was used for magnetic extraction. For each soil sample the sum of the magnetic properties of the five size fractions was compared to the magnetic properties of the bulk sample. It was found that the summed IRM properties of the sieved samples were generally similar to the IRM properties of the bulk sample before sieving. However, the summed ARM properties of the sieved samples were consistently lower than the ARM properties of the bulk samples pre-sieving (Figure 5.12). This unexpected reduction of the ARM properties of the soils on sieving was most pronounced for topsoils. It is very difficult to find an explanation for the reduction of ARM when the IRM remains constant.

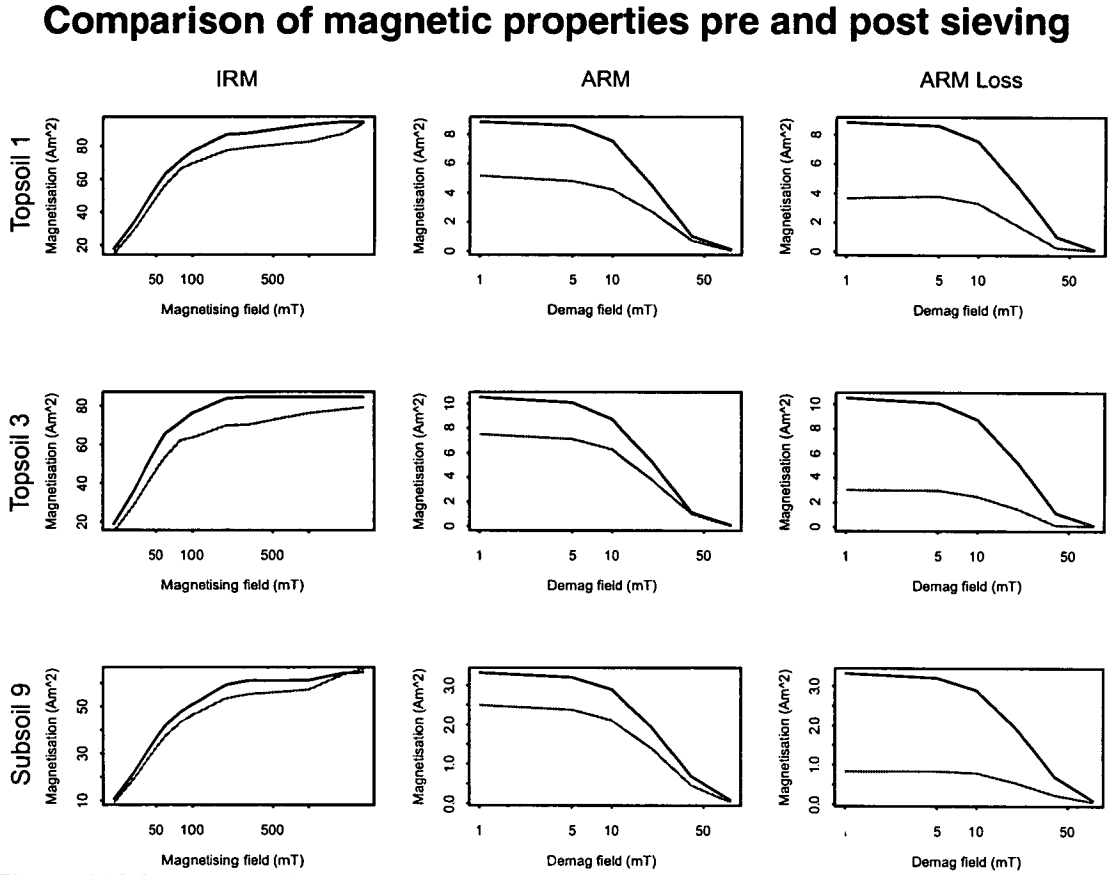

Figure 5.12 Comparisons between the magnetic properties of bulk samples pre-sieving (black) and the sum of the magnetic properties of the size fractions post-sieving (grey). Shown are the IRM properties, ARM properties and the difference between the ARM properties pre- and post-sieving (ARM loss).

As might be expected, the sieved subsoils and topsoils showed a different size fraction composition (Figure 5.13). The subsoils have a larger percentage of sand (>63μm) and coarse silt (>10μm) than the topsoils. The subsoils also have much less fine silt (>2μm) and clay material (<2μm) than the topsoils. The >500μm material is not plotted here, as it did not account for more than 1% of the total sample mass for any of the samples that were sieved. A wide variety of size fractions are present in single core sample analysed. This variety in the particle size make up of this sediment is greater than would be expected from the stratigraphic interpretation of this material as being clay. There is a higher concentration of fine silt in this material than the soil samples from the catchment. The difrence in the size make-up of the

sediment material compared to the catchment soils may have implications for the unmixing of these sediments. Ideally unmixing should be done using catchment material which represents the size fraction make up of the core material. This could be achieved by using individual size fractions for unmixing end-members. This approach was not possible here as the magnetic properties of the catchment material were altered by sieving (Figure 5.12).

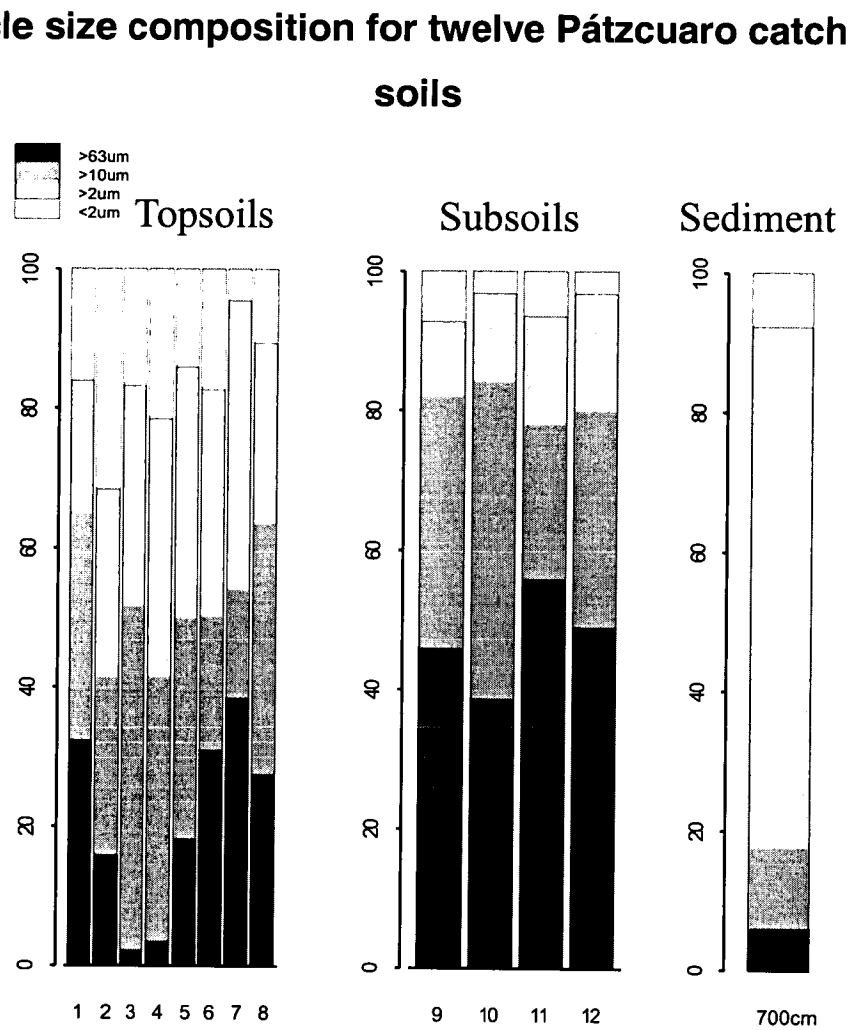

Figure 5.13. Particle size composition of the 12 soils and sediment sample that were sieved presented as a mass percentage of the bulk sample.

5.7 Unmixing

In order to aid the environmental interpretation of the magnetic properties of the Pátzcuaro cores, magnetic unmixing models were generated. The first of the models used all the catchment samples available to unmix the magnetic measurements made on cores C4 and KD. However it became apparent that this initial model had difficulties in differentiating between catchment end-members, in particular, between topsoil and subsoil. Three new models were generated with end-members selected from the end-members which the first model used. End-members were chosen for these three new models in order to optimise the differentiation between the catchment end-member types. Each model is defined by the choice of catchment

samples to be used as end-members. The models can be summarised in terms of catchment end-members as:

1. All catchment samples.
2. Mean magnetic properties of each catchment sample type.
3. Most extreme catchment sample from each catchment sample type.
4. Set of extreme catchment samples from each catchment sample type.

In each of these four models, an additional end-member representing the properties of magnetotactic bacteria was also included.

The magnetic unmixing results are given in terms of the percentage of the core's mass at each sample horizon that is accounted for by a given magnetic end-member. The contributions of each catchment sample type (e.g. topsoil or bedrock) are summed to give the total mass of that end-member. In some horizons, the total mass of the end-members is more than the mass of the core at that horizon, this is discussed in more detail in section 5.10.3. The models are presented as down-core graphs for each end-member type. Each graph shows the summed percentage of the core's mass that is accounted for by a given end-member. Also plotted on the graphical representation of each model are the stratigraphy of the core and the skill of the model. One point to note when looking at the percentage of the core's mass accounted for by each end-member type is the relatively low contribution made by the bacteria end-member to the mass of the core. This contribution is low because the bacteria end-member represents pure magnetotactic bacteria magnetosomes, whereas the catchment end-members are bulk samples which are made up of mostly non-ferromagnetic material.

5.71 Model one for core C4 (All catchment samples)

I shall describe the attributes of the first model for core C4 (Figure 5.14) using the same three sections that were used for the description of the core's magnetic properties. Section one of unmixing model one has been modelled predominantly with bacteria magnetosome chains, although both topsoil and tephra material are present. The second section of the core has relatively weak magnetic properties. The modelling of the second section of core C4 contains very little catchment material. At the bottom of section two, tephra has been used in the modelling, with four high concentration peaks, and an ongoing lower concentration. The third section of model one for core C4 is dominated by the topsoil and subsoil groups of catchment samples. The model routine switches between topsoils and subsoils from horizon to horizon, but there is generally a higher concentration of subsoil type material. Model one of core C4 has a high skill level, with a mean skill of 0.931 and only two horizons have a skill below 0.7.

5.7.2 Model one for core KD (All catchment samples)

The first model generated for core KD (Figure 5.15) identifies topsoil as being the major component of the magnetic properties of the core. The bacteria magnetosome end-member is occasionally present, especially towards the top of the core. One horizon, at the bottom of the very base of the core is modelled with subsoil material and a horizon between 10cm and 5cm depth is modelled with bedrock material.

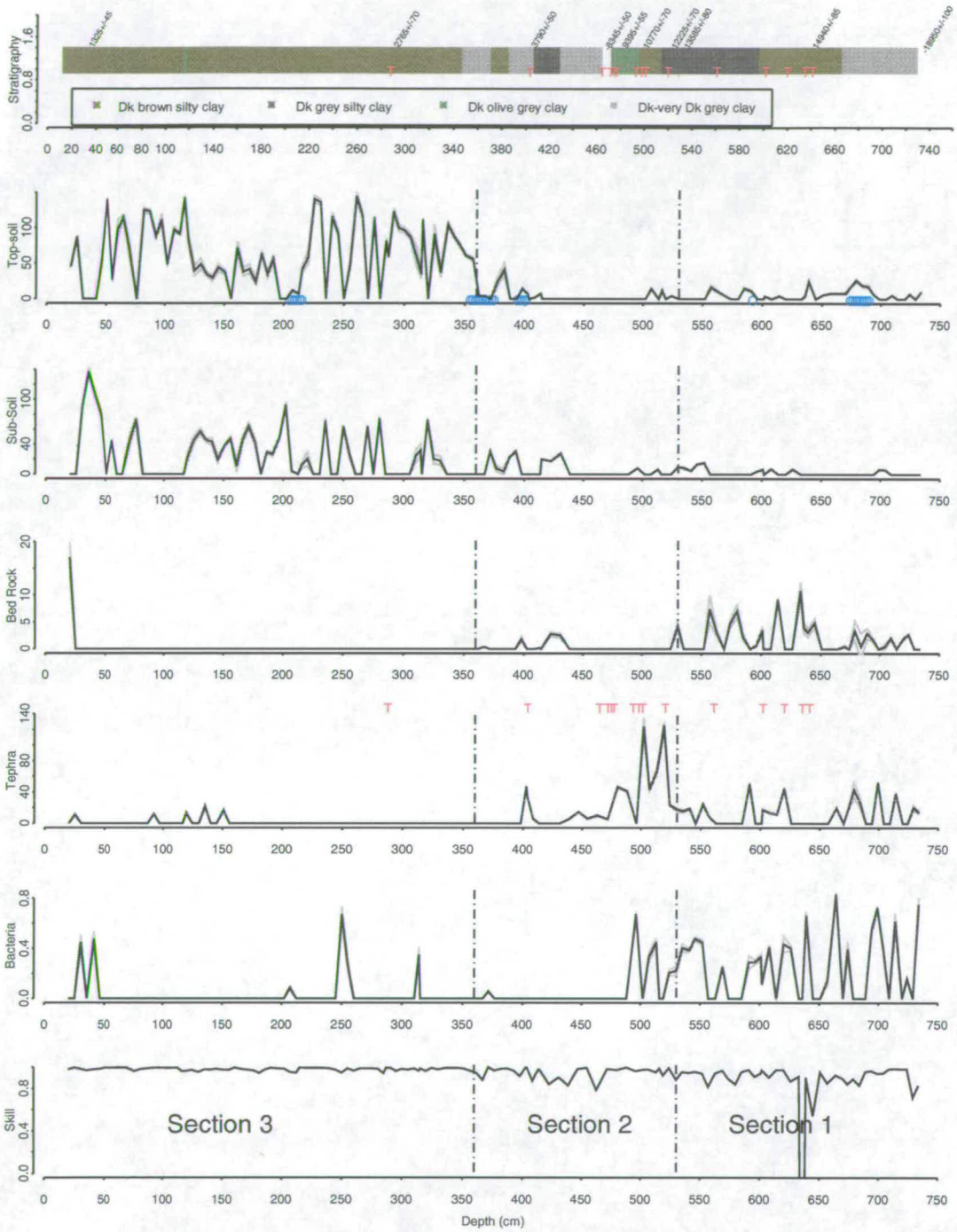

Figure 5.14. Magnetic unmixing model 1 for core C4, with the percentage of the cores mass explained by each end-member type against depth in cm. Broken lines show limits of sections, which are labelled 1-3 from the bottom of the core up. Grey lines show the extent of errors from the stability of the unmixing inverse matrix. Also plotted is the skill of the model, the stratigraphy, ostrocod rich layers (O) and tephra layers (T).

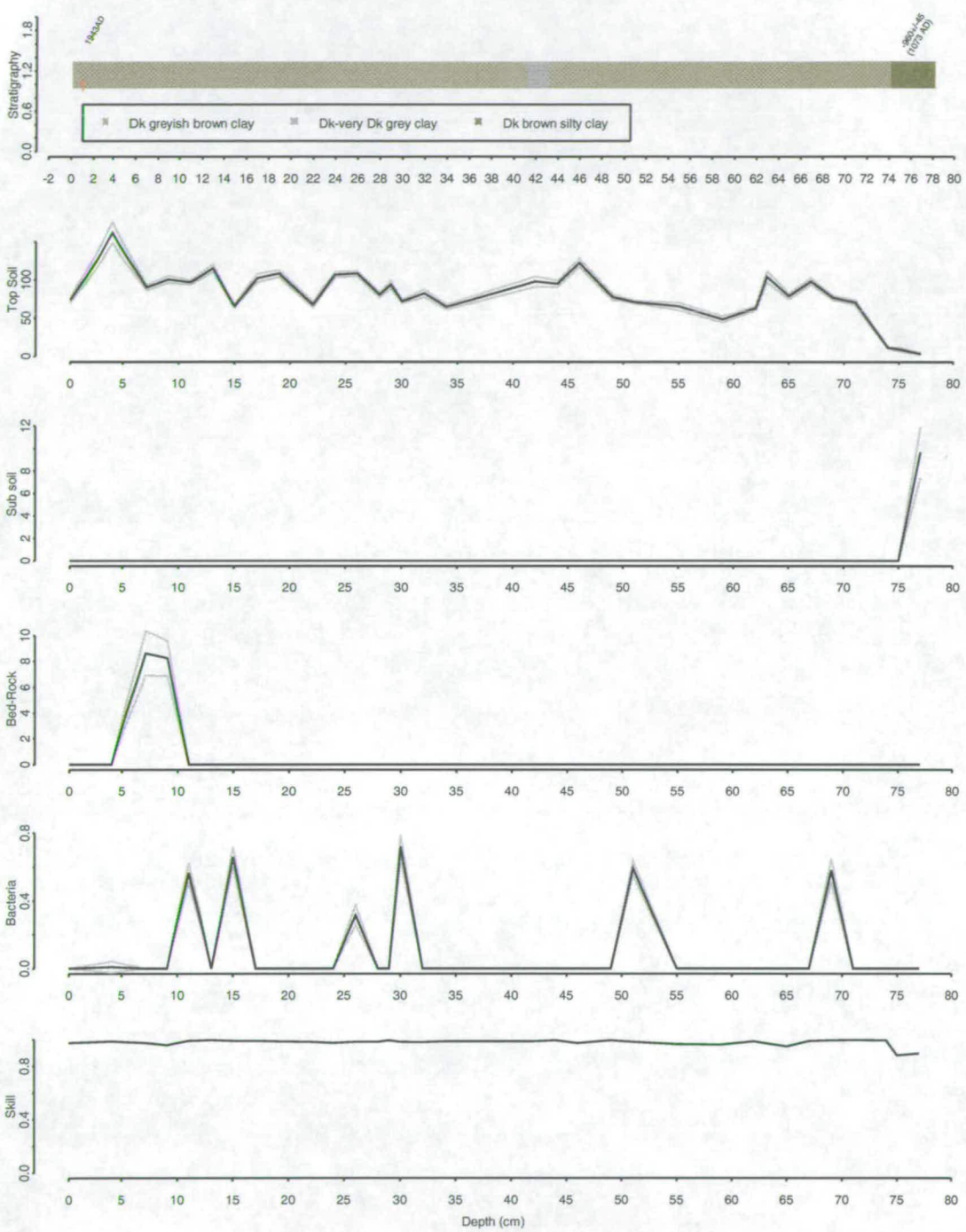

Figure 5.15. Magnetic unmixing model 1 for core KD, with the percentage of the cores mass explained by each end-member type against depth in cm. Grey lines show the extent of errors from the stability of the unmixing inverse matrix. Also plotted is the skill of the model.

5.7.3 Concerns with the initial models

Looking at the initial C4 model more closely (Figure 5.14), it is of concern that the topsoil and subsoil components are not being very clearly distinguished: the model

tends to flip from horizon to horizon between topsoil and subsoil. The difficulty which the model has in separating topsoil and subsoil in the lake sediments probably stems from the fact that, although it is convenient to classify soils as being either topsoil or subsoil, the actual catchment soils consist of a gradation of material between these two end-members. In order to unmix the magnetic properties of the Lake Pátzcuaro's sediments, the magnetic properties of these topsoil and subsoil end-members must be identified. I have attempted to do this in three ways, and the next three models have been analysed to decide which is the best method of end-member selection. The next three models' end-members have been chosen as being:

2. The mean properties of each catchment type.
3. The single most extreme catchment material for each catchment type.
4. The bounding samples most distant from the magnetic properties of another classification of catchment material.

The first of these methods of end-member selection is relatively straightforward, the other two require the identification of the extremes in magnetic properties of the four catchment sample types. In order to do this, a principal component analysis has been carried out on the full data set of soils that were sieved, as well as all the tephra and bedrock samples from the catchment. Figure 5.16 shows plots of the 1st, 2nd and 3rd components of this PCA.

From these PCA plots it is possible to identify both:

a) The most extreme sample, i.e. the materials that are most different from all the other catchment types, and
b) A bounding set of samples for each catchment type that is most distant from all the other catchment types.

For (a) the set of single most extreme samples for each catchment type, I chose tephra sample T7, bed rock sample B1, topsoil 3 and subsoil 9. For (b) the bounding set of samples for each catchment type that is most distant from all other catchment types, I chose: tephra samples T3 and T4, bed rock samples B1 and B2, topsoil samples 3 and 4 and subsoil sample 9. Only one subsoil end-member was chosen as the rest of the subsoils plotted too close to the topsoils to be differentiated.

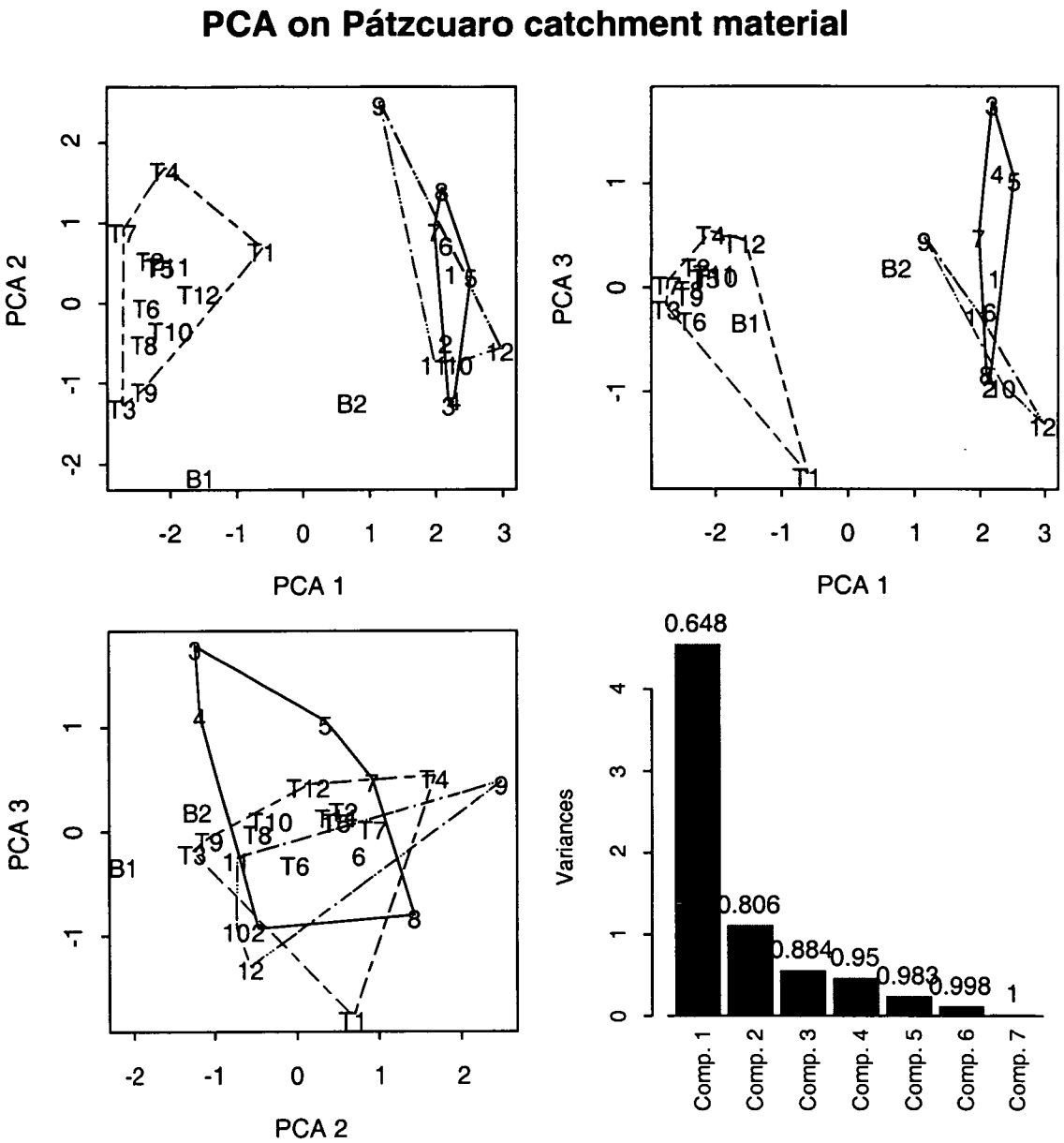

Figure 5.16. Diagram of the 1st, 2nd and 3rd PCA components of the magnetic properties of the Lake Pátzcuaro catchment samples plotted against one another. B1 and B2 are bed rock samples, T1-T12 are tephra samples, 1-8 are topsoil samples and 9-12 are subsoil samples. Each catchment type has a convex hull plotted around it. The bar chart shows the total of the entire data-set's variance that is accounted for by the PCA components.

5.7.4 Models two, three and four

The next three models were generated for core C4 using the end-members selected above. Equivalent models were also generated for core KD. The most effective unmixing procedure was chosen on the basis of the C4 models, and for this reason, the KD core models are included in Appendix B and are not further discussed here.

5.7.5 C4 core model two (Mean end-member properties)

In section one of model two for core C4, magnetotactic bacteria are the most significant end-member, although subsoil and topsoil end-members are present in low concentrations. The second section of the model also contains some topsoil, subsoil, and bacteria, but is dominated by tephra. The tephra presence is sustained throughout the second section of the model. Similar to model one, there are four high tephra concentration spikes in section two of model two for core C4. The third section of model two is dominated by subsoil, although there are sporadic appearances of bacteria and topsoil. The three horizons that include topsoil are not modelled with subsoil. We can see from Figures 5.9 and 5.10 that the mean magnetic properties of topsoil and subsoil are very similar. The similarity between the mean magnetic properties of topsoil and subsoil make the differentiation of these two end-members difficult for model two. The skill level for model two is not as good as for model one, with eight horizons having a skill below 0.7. The skill is generally higher in section three than in the rest of the model.

5.7.6 C4 core model three (Most extreme end-member)

The first section of model three (Figure 5.18) is, like model one and two, high in material derived from magnetotactic bacteria, there is also a presence of subsoil material. Four tephra spikes again dominate the second section of the model. Topsoils and subsoils, as for models one and two, are present in the second section of the model and there are a few isolated occurrences of magnetotactic bacteria material. The third section of the model is dominated by topsoil and subsoil. The concentration of subsoil is generally greater than topsoil for section three. The sporadic inclusion of subsoil at the bottom of section three, 350cm to 200cm, indicates difficulties in the separating these two end-members. The occurrences of magnetotactic bacteria in section three of model three are sporadic and spiky and show some correlation with the inclusion of subsoil in the model. The skill level for this model is very good in section three, but there are five horizons that fall below a skill of 0.7 in sections one and two.

5.7.7 C4 core model four (Bounding end-member samples)

Bacterial magnetosomes and subsoil material dominate the first section of model four (Figure 5.19), although there are sporadic horizons where the model has included topsoil bedrock and tephra material. Four tephra concentration spikes again dominate the second section of model four, much like the second section of the other C4 models. Topsoil and subsoil end-members are present towards the top of the second section of the model. Section three of model four is dominated by topsoil. The concentration curve of topsoil in section three is relatively smooth, compared to the other models. Subsoil and bedrock materials seem to be included in almost alternate horizons towards the top of section three. Tephra material is present in several horizons and magnetotactic bacteria derived material is indicated in isolated horizons towards the bottom of section three. The skill level of model four is generally better than models two and three, although it is not as good as model one for C4. This model has four horizons with a skill below 0.7.

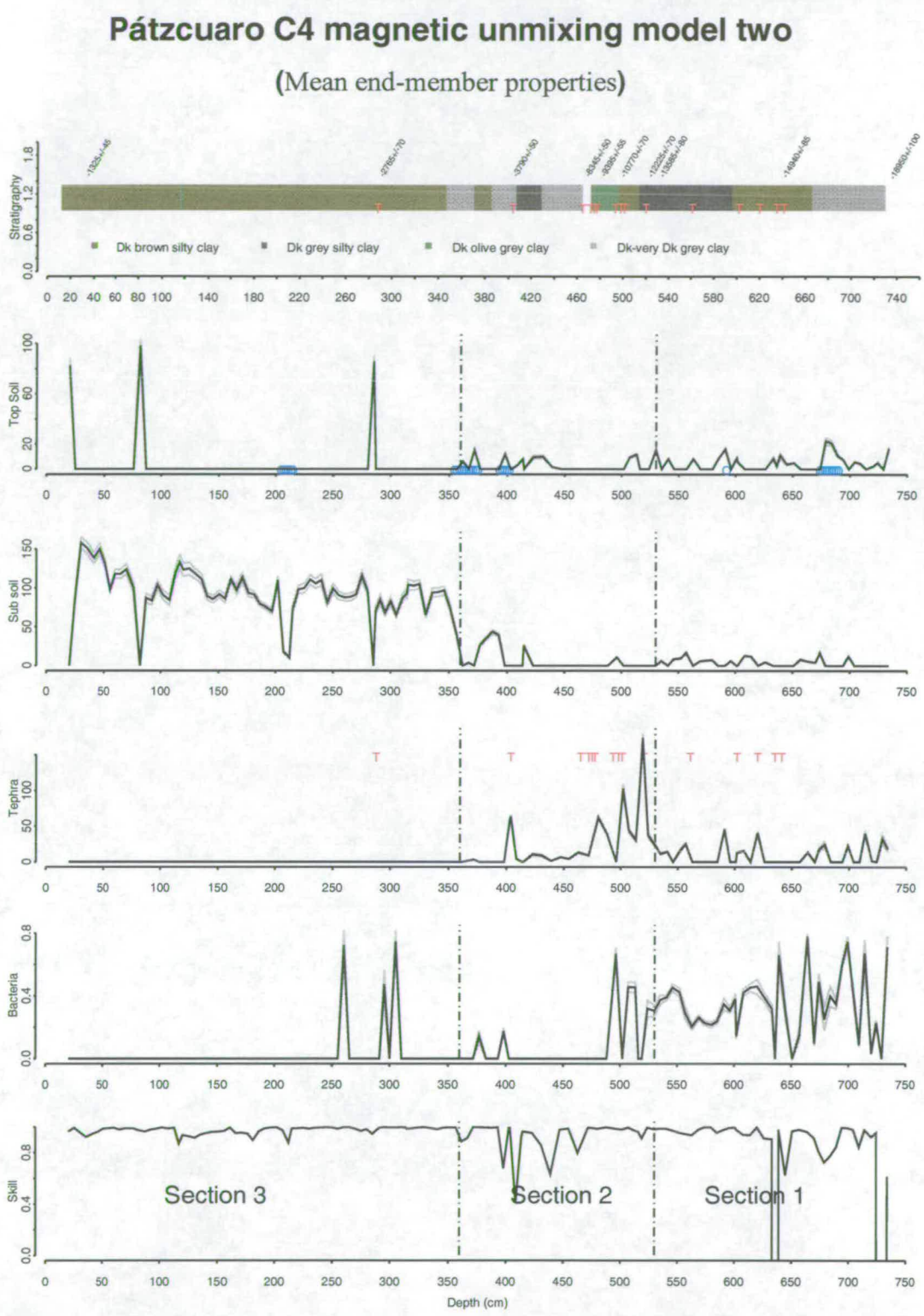

Figure 5.17. Magnetic unmixing model 2 for core C4, with the percentage of the cores mass explained by each end-member type against depth in cm. Broken lines show limits of sections, which are labelled 1-3 from the bottom of the core up. The grey lines show the extent of the errors from the stability of the inversion matrix. Also plotted is the skill of the model, the stratigraphy, ostrocod rich layers (O) and tephra layers (T).

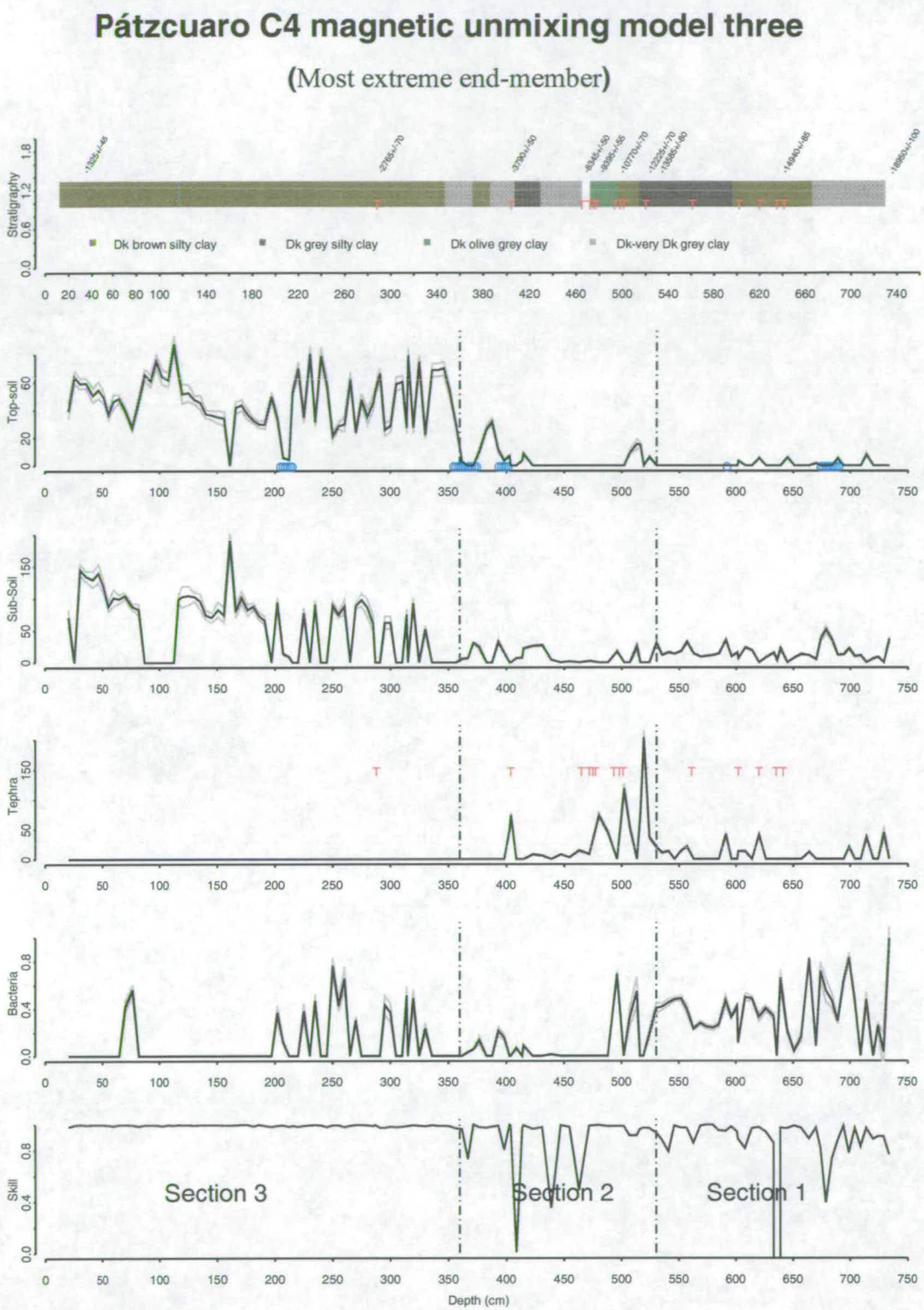

Figure 5.18. Magnetic unmixing model 3 for core C4, with the percentage of the cores mass explained by each end-member type against depth in cm. Broken lines show limits of sections, which are labelled 1-3 from the bottom of the core up. The grey lines show the extent of the errors from the stability of the inversion matrix. Also plotted is the skill of the model, the stratigraphy, ostrocod rich layers (O) and tephra layers (T).

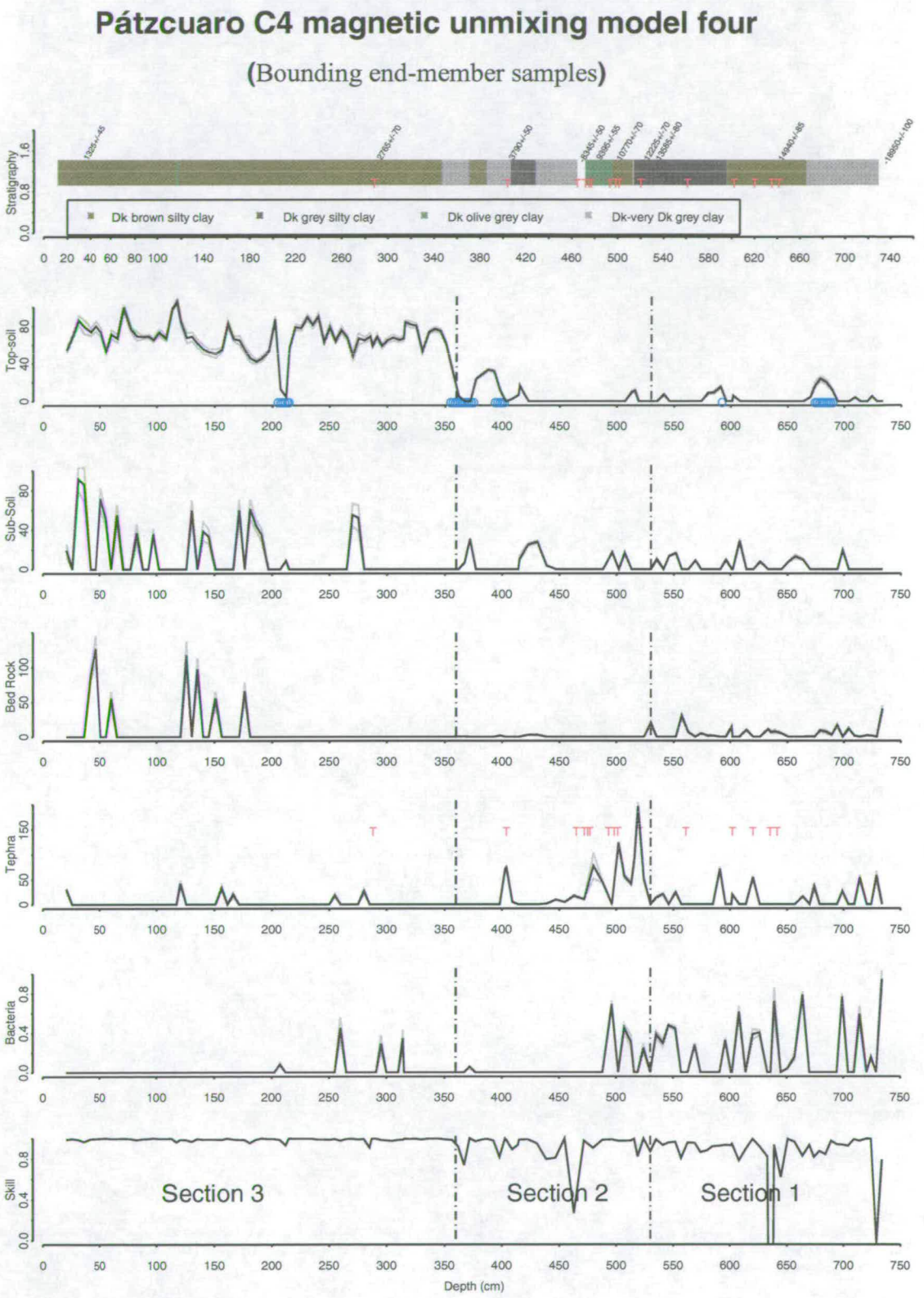

Figure 5.19. Magnetic unmixing model 4 for core C4, with the percentage of the cores mass explained by each end-member type against depth in cm. Broken lines show limits of sections, which are labelled 1-3 from the bottom of the core up. The grey lines show the extent of the errors from the stability of the inversion matrix. Also plotted is the skill of the model, the stratigraphy, ostrocod rich layers (O) and tephra layers (T).

5.8 Model selection

Table 5.1 is a summary of the four unmixing models for cores C4 and KD. The correlation between the topsoil and subsoil is included to identify models that have problems differentiating between these two end-member classifications. A high negative correlation indicates that the model was swapping between including topsoils and subsoils because it could not differentiate between them.

Summary of the C4 and KD models

	Mean skill	Number of horizons with skill less than 0.7	Correlation between topsoil and subsoil	Mean skill with low skill horizons removed
C4 Model 1	0.9312	2	-0.1544	0.9619
C4 Model 2	0.2823	8	-0.2522	0.9630
C4 Model 3	0.8283	5	0.2328	0.9566
C4 Model 4	0.9124	4	0.1578	0.9555
C4 Model 5	0.9090	5	0.195	0.9523
KD Model 1	0.9752	0	-0.4169	0.9752
KD Model 2	0.9751	0	-0.5855	0.9751
KD Model 3	0.9682	0	-0.7363	0.9682
KD Model 4	0.9463	1	-0.5285	0.9547
KD Model 5	0.9460	1	-0.3452	0.9544

Table 5.1. Model comparison showing the mean skill level, number of horizons with a skill less than 0.7, the correlation coefficient between topsoil and subsoil end-members and the mean skill after removing horizons that have lower than 0.7 skill. Model 5 is discussed is Section 5.10.

I have chosen model four as the best model for unmixing Lake Pátzcuaro core C4 in terms of bulk catchment samples and bacteria. Model 4 has a positive correlation between topsoil and subsoil end-member inclusion, whist still retaining a high skill level, and few horizons that fall below the 0.7 skill level. One problem with this model is that it has difficulties differentiating between subsoil and bedrock. However, as this problem is limited to a few horizons it can be accepted.

5.9 Magnetic extraction

Although subsoil, topsoil and bedrock contributions cannot be directly measured, we can test if bacterial magnetosomes are actually present in the core horizons where the magnetic modelling has identified them. Based on the results of the model 4 unmixing on core C4, two consecutive core samples that were modelled with high concentrations of material derived from magnetotactic bacteria were subjected to magnetic extraction (samples came from 700cm depth). The resulting magnetic extract was subjected to optical and transmission electron microscopy in order to try to identify the remanence-carrying material within the samples. The extraction efficiency achieved on this sample is summarised in Table 5.2. As the extraction

efficiency is close to 50% for all of the parameters measured, the extraction shall be taken as being representative of the bulk magnetic materials within the sample.

Extraction efficiency on C4 core sample

	Susceptibility (10^{-9} SI)	SIRM (10^{-9} A m^2)	SARM (10^{-9} A m^2)
Before extraction	5.0	167.8	12.7
Extraction Residue	2.6	76.8	77.9
Efficiency	48.2%	54.2%	38.8%

Table 5.2. Susceptibility, SIRM and SARM extraction efficiency for core sample from core C4. Efficiency is measured by subtracting the magnetic properties of the non-extracted residue, from the magnetic properties of the sample before measurement. Efficiency is expressed as the percentage of the magnetic properties of the extracted material to the original sample (Equation 2.2).

During transmission electron microscope analysis, no magnetosome chains or magnetosomes were identified in the fine grained part of the extract from core C4. The lack of material derived from magnetotactic bacteria in the extract indicates that the selection of the bacteria end-member by the unmixing algorithm is a misclassification of the magnetic material present in the core. The bacteria end-member was most likely selected by the modelling routine to represent section one of core C4 because this part of the core displays high SARM/SIRM ratios combined with low susceptibility.

High concentrations of quartz and feldspar crystals with magnetic inclusions (Figure 5.20) were seen during optical microscope analysis of the magnetic extract from the C4 core. Magnetic inclusions have previously been associated with high SARM/SIRM ratios (Hounslow, in press) (Chapter 3.3). Magnetic inclusions could become the dominant remanence-carrying material in a lake sediment, if dissolution were to remove detrital magnetic material. The dissolution effect is plausible for core C4 section one because samples from this section showed high concentrations of quartz and feldspar crystals with magnetic inclusions compared to small amounts of detrital material during optical microscope analysis (Figure 5.20 and 5.21).

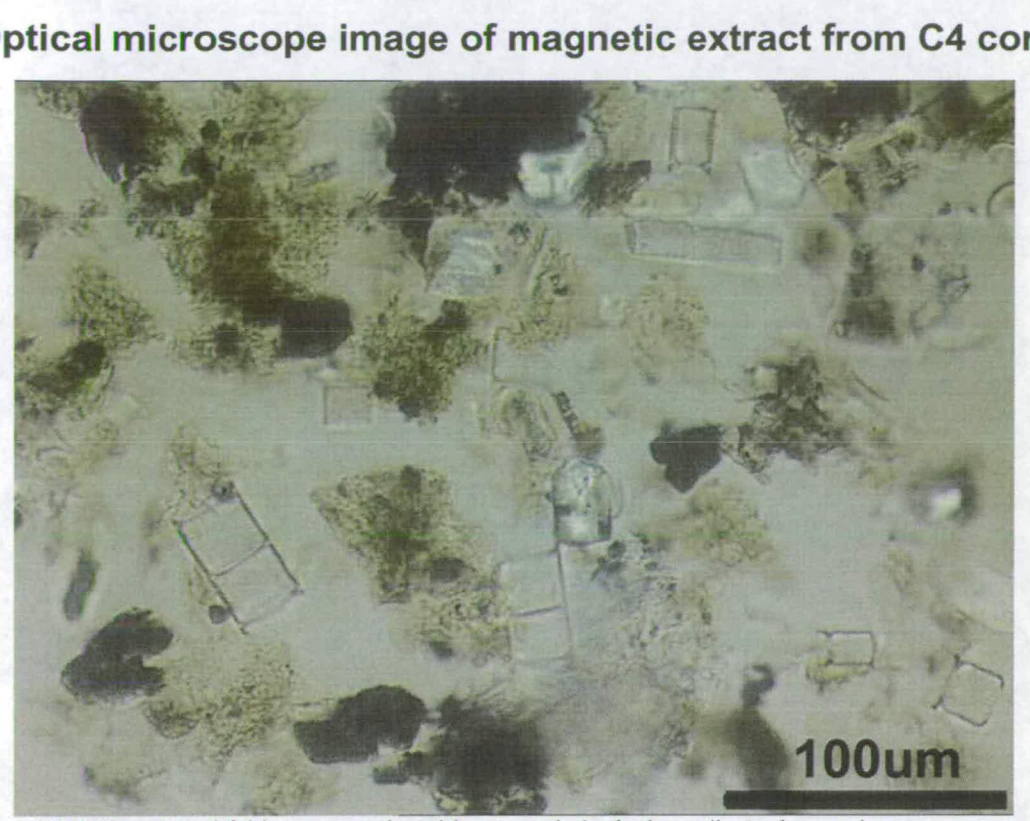

Figure 5.20. Quartz and feldspar crystals, with magnetic inclusions, (irregular semi-transparent grains with dark micron sized inclusions) also diatom fragments (regular curvilinear outlines). From magnetic extract taken from section one of core C4.

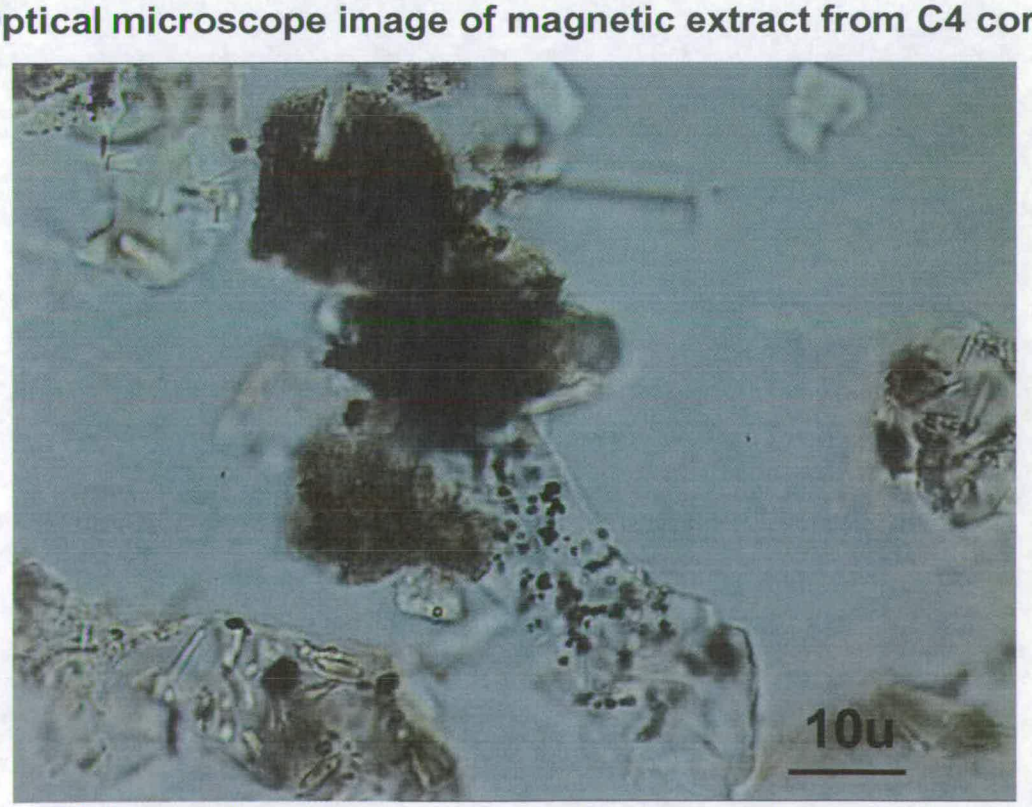

Figure 5.21. A particularly good example of a quartz grain with magnetic inclusions of about 1μm in length sits in the lower middle portion of this micrograph. Micrograph comes from a magnetic extract taken from section one of core C4.

Four samples were chosen to test if inclusion material within Lake Pátzcuaro's sediments, or catchment, exhibited high SARM/SIRM behaviour. The four samples chosen represented a topsoil, a subsoil, material from C4 core section one and material from the middle of the KD core. These samples were boiled in concentrated HCl for twenty minutes, in accordance with Hounslow (in press), in order to remove all detrital magnetic material. The samples then had their magnetic properties re-measured. None of the four samples showed any significant increase in SARM/SIRM (Table 5.3). On the basis of this experiment, magnetic inclusions are not a likely cause of the high SARM/SIRM ratios in section one of C4.

SARM SIRM and SARM/SIRM properties of four samples before and after HCl treatment

	SARM (10^{-9} A m^2)	SIRM (10^{-9} A m^2)	SARM/SIRM
Topsoil (before)	9.27	131	0.071
Topsoil (after)	1.18	51.8	0.023
Subsoil (before)	89.5	729.	0.12
Subsoil (after)	5.89	6.68	0.088
C4 section one (before)	12.35	167	0.074
C4 section one (after)	0.31	5.02	0.062
KD (before)	24.39	182	0.13
KD (after)	1.21	64.8	0.019

Table 5.3. The SARM and SIRM properties and the SARM/SIRM ratio of a topsoil subsoil and core samples from C4, section one and KD, before and after 20 minutes in boiling concentrated HCl.

5.10 Model five

A fifth model, that uses the same end-members as model four but with the magnetotactic bacteria end-member removed, has been made. This model is presented in Figure 5.21 for core C4 and Figure 5.23 for core KD. From Table 5.1 we can see that the removal of the bacteria end-member from model 4 has resulted in model five having a slightly lower skill for both the C4 and KD cores.

5.10.1 C4 Core model 5 (End-member bounding samples without Bacteria)

There is little difference between model five (Figure 5.22) and model four (Figure 5.19) for the C4 core. The only major change occurs in section one, as this is the section that was previously modelled with magnetotactic bacteria magnetosomes. Comparing section one of model five to section one of model four, we see an increase in the topsoil and tephra components, and a reduction in the subsoil component. Both topsoil and tephra are almost continuously present in section one of model five. The rest of model five for the C4 core is almost identical to model 4 for the C4 core.

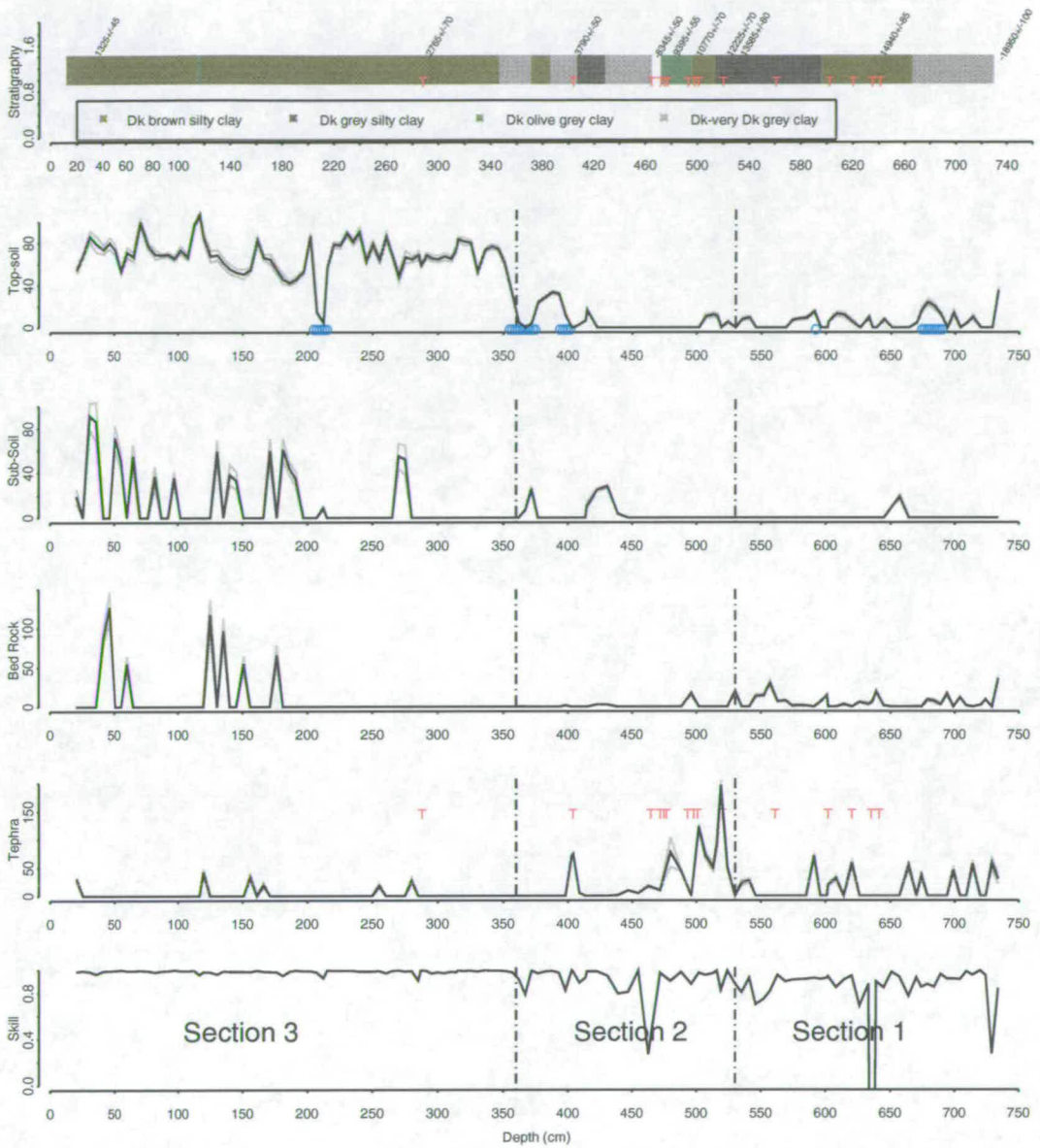

Figure 5.22 Magnetic unmixing model 5 for core C4, with the percentage of the cores mass explained by each end-member type against depth in cm. Broken lines show limits of sections, which are labelled 1-3 from the bottom of the core up. The grey lines show the extent of the errors from the stability of the inversion matrix. Also plotted is the skill of the model, the stratigraphy, ostrocod rich layers (O) and tephra layers (T).

5.10.2 KD core model 5 (End-member bounding samples without Bacteria)

Unmixing model five uses topsoil end-members to match the magnetic characteristics of core KD for almost its entire length (Figure 5.23). The

concentrations of the topsoil end-member are low in two of the horizons of this model. The first of these is at the base of the core; the second occurs at a depth of 55cm, roughly equivalent to a date of AD 1300. This trough in topsoil material corresponds to a peak in subsoil material. There are a few subsoil material peaks towards the top of the model, along with one bedrock end-member horizon. The skill for this model is generally very high, except for one horizon at 75cm depth.

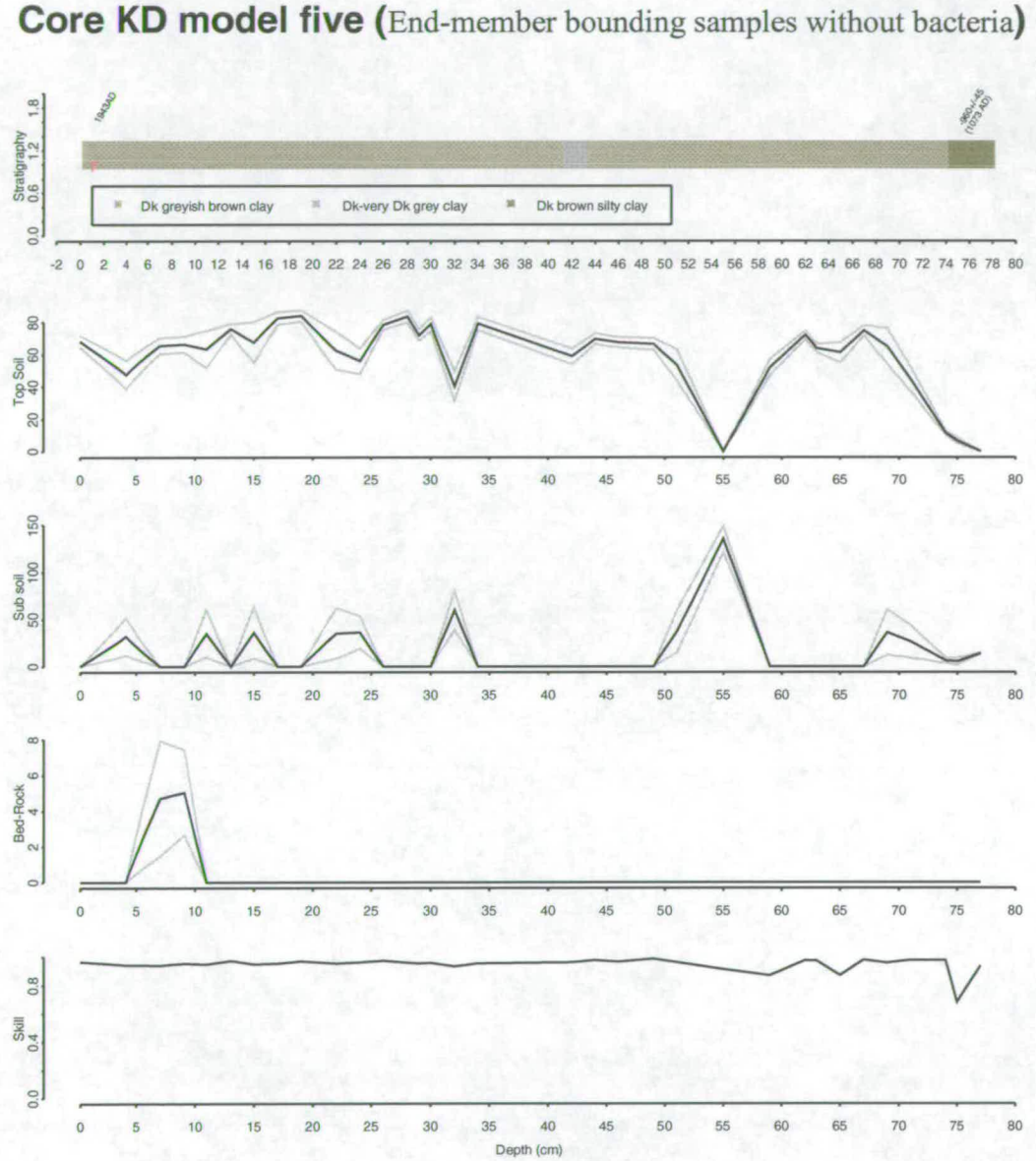

Figure 5.23. Magnetic unmixing model 5 for core KD, with the percentage of the cores mass explained by each end-member type against depth in cm. Broken lines show limits of sections, which are labelled 1-3 from the bottom of the core up. The grey lines show the extent of the errors from the stability of the inversion matrix. Also plotted is the skill of the model, the stratigraphy, and tephra layers (T).

5.10.3 Combined mass contributions for model five on core C4

Figure 5.24 shows three combined mass contributions of the model 5 end-members. The three plots show combined contributions of: all end-members; catchment erosion end-members (topsoil subsoil and bedrock), and bedrock and subsoil, also plotted is the topsoil end-member. For several horizons, the combined contributions of the model elements account for more than 100% of the mass of the core (Figure 5.24). Although more than 100% of the core's mass being accounted for causes complications for the quantification of sediment erosion, it should be expected, as bulk samples found in the catchment are unlikely to be delivered to the core site whole (Chapter 3.5). The magnetic properties of different grain size fractions vary, so the action of preferentially removing either coarse or fine material during transportation and deposition is likely alter the magnetic properties of the remaining material. Figure 5.25 shows the mean saturation IRMs for the various grain sizes of sieved catchment material. We can see that the removal of either the finest or the coarsest material will increase the SIRM per kg of the remaining material. This sorting effect means the bulk masses that I have used for the catchment end-members are likely to be an over-estimation of the mass contribution of the catchment end-member to the material occurring in the core. Unfortunately, this problem, and the problem of unmixing using bulk magnetic properties which may also be affected by sediment size sorting, could not be solved by unmixing in terms of catchment size splits. The size split material could not be used for unmixing because the sieving process altered the magnetic properties of the catchment samples (Section 5.6.9, Figure 5.11). However, the problem of unmixing using bulk magnetic properties may may not be too great because:

i) The largest and smallest size fraction material in the catchment makes the weakest magnetic concentration (Figure 5.25).

ii) The unmixing model could chose between catchment material with varying size fraction properties.

iii) The particle size distribution of the one sediment horizon contained material from a range of size fractions despite being classified as clay in the stratigraphy.

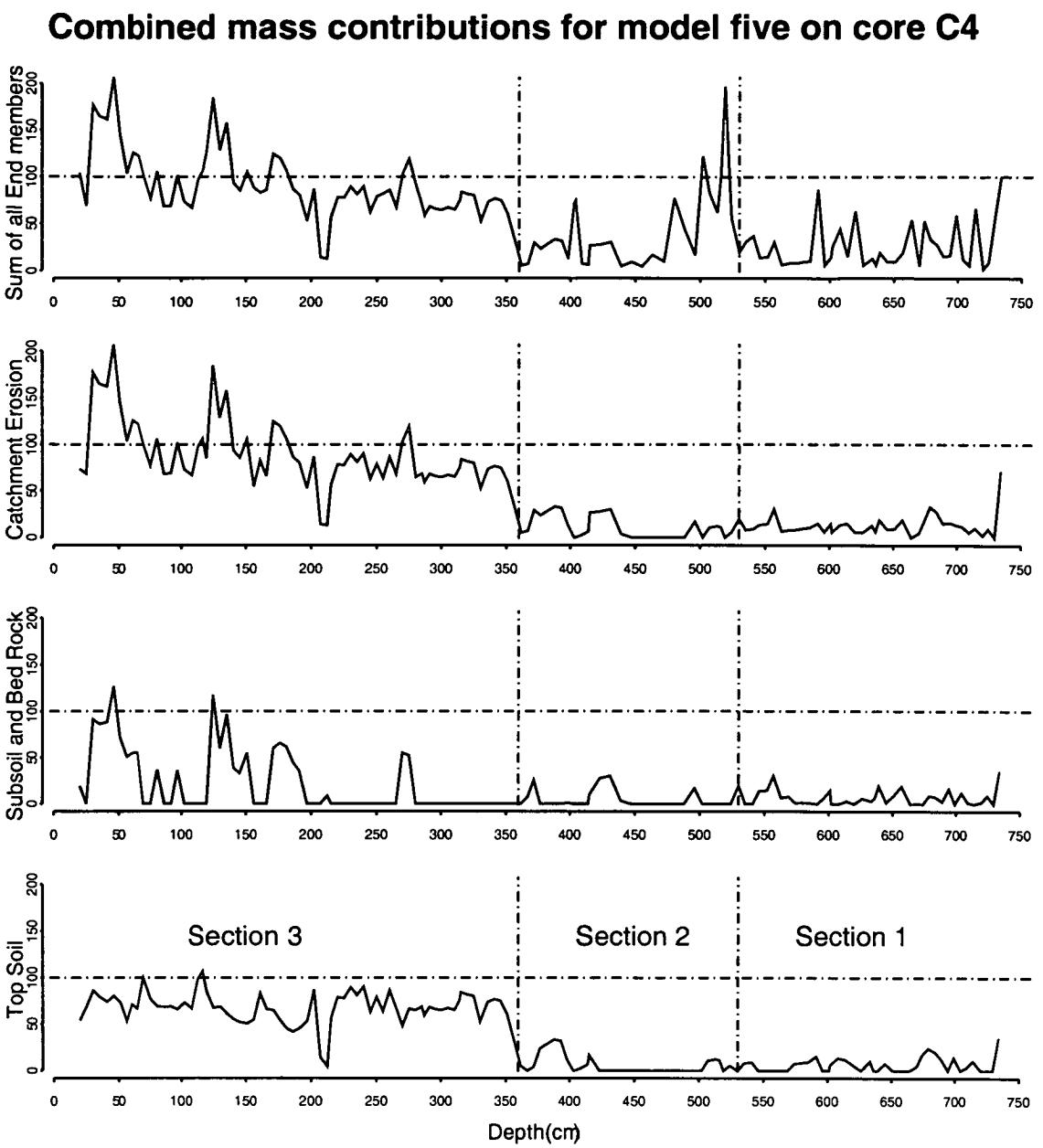

Figure 5.24. Combinations of different elements of model 5 for C4, as a percentage of the core sample's mass accounted for by given sets of end-members against depth. The top plot shows the combined contribution of all the end-members in the model. The second plot shows a sum of all the catchment erosion end-members (topsoil, subsoil and bedrock). The third plot is the sum of the subsoil and bedrock components and the final plot is the topsoil erosion plot. On all plots, a horizontal line is drawn at 100% concentration and two vertical line separating core sections one, two and three.

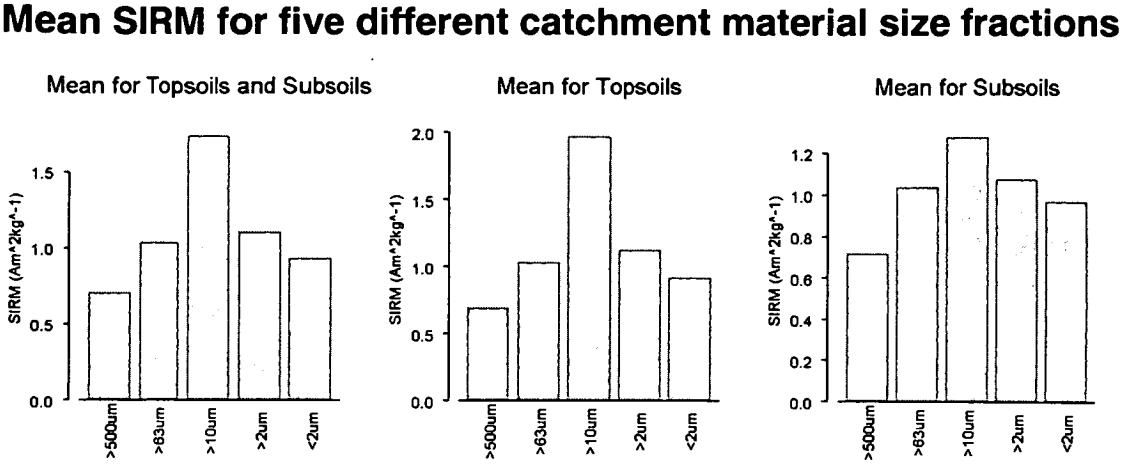

Figure 5.25. The mean SIRM for five size fractions of material from Lake Pátzcuaro's catchment, and the profiles for the mean SIRM of size fractions of topsoil and subsoil on their own.

5.11 Interpretation of the unmixing of cores C4 and KD

Here I interpret the results of the fifth unmixing model on cores KD (Figure 5.22) and C4, (Figure 5.23) in an attempt to identify the processes that were acting on the catchment during the time of deposition of the sediment. I start by giving a brief overview of the core as a whole, and then a section-by-section interpretation of horizons of interest. All dates given here have been extrapolated from the available radio carbon dates on the cores, assuming constant sedimentation between dated horizons. It should be noted that the extrapolation of a study made on two cores to processes affecting an entire catchment is not ideal.

Model five for core C4 (Figure 5.22) shows that the magnetic properties of section one of C4 can be modelled with topsoil erosion and tephra input and those of section two mostly with tephra input. The upper part of the core, section three, is dominated by catchment erosion signals, namely: topsoil, subsoil and bedrock.

5.11.1 C4 section one

Section one (19,000 – 13,600^{14}C yr B.P.) of model five on the C4 core (Figure 5.22) has a persistent inclusion of the topsoil end-member and occasional peaks in the tephra and bedrock end-members. There are nine distinct tephra peaks in section one of the model; these occur at 18,500, 18,000, 17,200, 16,200, 15,500, 14,700, 14,400, 14,100 and 13,700^{14}C yr BP. The peaks that occur at 14,700 and 14,400^{14}C yr BP correspond to tephra layers noted in the stratigraphic record.

In this section of the model, (19,000 – 13,600^{14}C yr B.P.) erosion material (topsoil, subsoil and bedrock end-members) makes up on average less than 30% of the mass of the sediment (Figure 5.22). This low contribution of erosion material could be an indication of either high production of organic material within the lake or low levels of catchment erosion. However, as the sedimentation levels for this part of the core are generally low (Figure 5.5), low erosion is considered the most likely explanation. Bedrock material horizons in section one of the model may indicate occasional deep erosion episodes within the catchment. From extrapolation of the three available radio carbon dates in section one of the C4 core, the three most notable periods of

bedrock material inclusion are dated at 18,800, 15,000 and 14,100 ^{14}C yr B.P.. The horizons modelled with bedrock material may represent higher energy periods within the catchment, perhaps indicating more stormy weather or more seasonal rainfall leading to deeper erosion, e.g. gullies.

Section one of model five on core C4 corresponds to a stable catchment and a generally low energy environment. This is consistent with the findings of Bradbury (2000) and Terrett (2000) who report evidence of a stable well stratified lake in the diatom record. The occasional presence of bedrock material in the model may be the result of high intensity rainfall, stormy periods, where gullies are created on the steep slopes surrounding the lake.

5.11.2 C4 section two

Topsoil and bedrock are almost absent in section two of model five for the C4 core (13,600 – 3,200^{14}C yr B.P.) (Figure 5.24). Topsoil is apparent in low quantities (less than 15%, at the top of section two up to a depth of 500cm which corresponds to a date of 11,000^{14}C yr B.P.). Topsoil is then absent from section two of the model until a depth of 375cm, which corresponds with a carbon age of 3,600^{14}C yr B.P. where higher quantities, over 30% of the mass of the core, are included in the model. The subsoil end-member is apparent in section two of model five in two horizons that correspond to dates of 4,500 – 6,500^{14}C yr B.P. and 3,500^{14}C yr B.P.. However, by far the most abundant material in section two of model five is the tephra end-member. Four distinct peaks in the tephra end-members are immediately apparent. These peaks occur at 12,100, 11,000, 9,300 and 3,900^{14}C yr B.P.. The tephra end-member horizons in section two of model five match with several tephra layers noted in the core stratigraphy (Figure 5.24).

Terrett (2000) (Figure 5.4) describes the period from 15,000 to 10,000^{14}C yr B.P. as being associated with high lake levels and the period from 10,000 to 5,000^{14}C yr B.P. with lower lake levels. The change from a deep lake to a shallow lake can also be inferred from the end of topsoil associated sediment at 11,000^{14}C yr B.P. in section two of model five on the C4 core. The cessation of soil erosion material in model five until a depth of 450cm, which corresponds to a date of 6,500^{14}C yr B.P., could indicate a reduction in precipitation. Reduced precipitation could both reduce erosion on steep surfaces in the catchment and lower the lake level, preventing eroded material getting to the core site. However, the annual levels of precipitation would have had to stay above 500mm otherwise loss of vegetation cover could be expected to contribute to higher erosion (Figure 3.11). This interpretation is supported by the work of Terrett (2000) and Bradbury (2000), who both report lower lake levels and drier conditions in the Pátzcuaro catchment after 10,000^{14}C yr B.P.. An alternative explanation for the low level of erosional material in this section of the unmixing model could be the action of reduction diagenesis. Reduction diagenesis (Chapter 3.5) could have removed the magnetic signature of detrital material deposited in this section of the core. Reduction diagenesis is more likely to occur if sedimentation rates were low, organic content high and the lake is deep, well stratified and not mixed. Although sedimentation rates in this section of the core are low (Figure 5.5) diatom evidence indicates that the lake would have been shallow and turbulent during this period (Terrett, 2000) making reduction diagensis less likely.

The generally low levels of topsoil and subsoil material represented in section two of model five are interrupted by subsoil erosion from 6,500 to 4,500^{14}C yr B.P.. This period of deep erosion is followed by another stable period, when ostrocod shells accumulate in the core. At 3,600^{14}C yr B.P., model five, of section three, indicates a period of topsoil erosion followed by subsoil erosion at 3,500^{14}C yr B.P.. After 3,500^{14}C yr B.P., there is a horizon where no soil end-members are seen. The erosion events seen at the top of model five section two, indicate a change in climate within the catchment to a higher energy environment causing higher erosion. This higher energy environment as seen in the magnetic unmixing model is not reported in any of the previous studies. Watts and Bradbury (1982), Bradbury (2000) and Terrett 2000 all describe the lake and catchment during the period between 5,000 and 3,500 as being shallow and dry. It is possible that this erosion event is caused by wind erosion or by increased water based soil erosion due to low plant cover during a particularly dry period (Figure 3.11). However, as the lake has not dried out entirely in the Holocene (Bradbury, 2000) there are limits to the levels of aridity in the catchment. The model five horizon after 3,500^{14}C yr B.P., which has no soil erosion end-members, corresponds to a dry period seen by Terrett (2000) (Figure 5.3).

5.11.3 C4 section three

Catchment soil erosion increases dramatically in the third section (3,200 – 1,300^{14}C yr B.P), of model five on core C4 (Figure 5.22). Most of section three's core material, according to model five, is derived from the catchment's topsoils. The dramatic increase in topsoil erosion seen in section three coincides with the first occurrence of maize pollen in the sediments of Lake Pátzcuaro (Watts and Bradbury, 1982). The scale of topsoil erosion represented in the magnetic unmixing model is unprecedented in the rest of the sediment core. At points, the topsoil end-member in section three of model five accounts for over 80% of the mass of the core. This huge input of topsoil material would account for the increased sedimentation rate seen in section three of the Pátzcuaro C4 core (Figure 5.5). The occurrence of maize pollen at the same date of increased topsoil end-member concentration in the Pátzcuaro, magnetic unmixing model implies that human activities led to topsoil erosion, as suggested by O'Hara *et al.,* (1993).

Two phases of topsoil erosion can be seen in section three of this model. A low erosion zone at approximately 210cm depth separates these two topsoil erosion periods. Extrapolation of available radio carbon dates would indicate an age of 2,300^{14}C yr B.P. for this gap between the two high topsoil erosion periods. However, as the sedimentation rate between the high topsoil erosion periods is likely to be far lower than seen during the topsoil erosion periods, this date has to be viewed with some caution. The zone of decreased erosion coincides with a layer of high ostrocod concentration. O'Hara *et al.,* (1993) also report a period of high catchment erosion, followed by low catchment erosion with increased ostrocod concentration, before a resumption of high catchment erosion. O'Hara *et al.'s,* (1993) dating for these events is more tightly constrained than the dating on core C4. Table 5.4 shows their dating of these events. O'Hara *et al.*, (1993) associate the two low erosion periods with decreased precipitation in the catchment.

Catchment erosion dates from O'Hara *et al.*, (1992)

Catchment Erosion	Beginning date (^{14}C yr B.P.)	Ending date (^{14}C yr B.P.)	Duration (years)
High	3,640 ±80	2,890 ± 80	750 ± 113
Low	2,890 ± 80	2530 ± 60	360 ± 100
High	2530 ± 60	1,190 ±70	1340 ± 93
Low	1,190 ±70	850	340 ± 70
High	850	Present	850 (still occurring)

Table 5.4. Dates and duration of catchment erosion events for Lake Pátzcuaro, from O'Hara *et al.*, (1993).

The second phase of high soil erosion seen in section three of the magnetic unmixing model of core C4 (2530 ± 60 to 1,190 ±70; dates from O'Hara *et al.*, (1993)) seems to have been more severe than the first. High concentrations of subsoil and bedrock material accompany the topsoil end-member in this part of the unmixing model. The subsoil and bedrock end-member inclusion (in the upper part of the third section of model five of core C4) indicates deep erosion was occurring in the catchment. The deep erosion hypothesis is supported by the high sedimentation rates: 0.18cm year^{-1} seen for this part of the core (Figure 5.5), which is the highest sedimentation rate seen in the C4 core. O'Hara *et al.*, (1993) describe this period of erosion as being "more intense" than the period preceding it.

5.11.4 KD core

After an initial horizon of low erosion, at the base of model five for the KD core (Figure 5.23), the modelled concentration of the topsoil end-member is similar to section 3 of C4 model five. The low topsoil end-member concentration seen at the bottom of model five on core KD is not obvious at the top of the C4 model five. It is therefore likely that a sediment gap exists between these two cores. Core KD covers the top of the second low erosion period and the whole of the third high erosion period reported by O'Hara *et al.*, (1993) (Table 5.4).

The model for core KD suggests that topsoil erosion is continuing in a manner similar to that seen in section three of model five for the C4 core. According to this magnetic unmixing model for the KD core, topsoil generally accounts for between 40% and 80% of the mass of the core. There is one horizon at 55cm, which corresponds to a date of approximately AD 1300 (based on the assumption of a constant sedimentation rate), where subsoil erosion dominates the model. However, in general the unmixing model on core KD indicates that erosion in the Pátzcuaro catchment is not as great as it was at the top of section two. The reduction of subsoil material in the unmixing model for core KD as compared to the same model for section three of the C4 also suggests that soil erosion is less severe at present, and in recent history, than it was between 2530 ± 60 and 1,190 ±70 (dates from O'Hara *et al.*, (1993)).

5.12 Summary of the magnetic unmixing model

The application of magnetic unmixing to Lake Pátzcuaro has given an insight into the erosional history of the lake's catchment. By unmixing the magnetic properties of

Lake Pátzcuaro in terms of catchment samples I have been able to identify periods of both surface and deep catchment erosion. The erosion signatures identified by the unmixing models have been interpreted in conjunction with the previous work carried out on Lake Pátzcuaro, the main points of the interpretation are summarised in Figure 5.26 and listed here:

1. 19,000 – 11,000 ^{14}C yr B.P. Stable catchment with low level topsoil erosion and occasional deep erosion events, which were probably connected to more stormy climatic periods.
2. 11,000 – 6,500 ^{14}C yr B.P. No topsoil material making it to core site, drier conditions with reduced lake level and stable catchment.
3. 6,500 – 3,500 ^{14}C yr B.P. Fluctuating shallow and deep soil erosion followed by a period of very low catchment erosion associated with changing precipitation.
4. 3,500 – 2,900 ^{14}C yr B.P. Dramatic increase in topsoil erosion caused by farming and deforestation in the catchment.
5. 2,900 – 2,500 ^{14}C yr B.P. Reduced catchment erosion due to reduction in precipitation.
6. 2,500 – beyond 1,325 (gap in core record) Very high erosion of catchment material and deep catchment erosion caused by human activity in the catchment.
7. Before AD 1073 (Gap in core record) – AD 1,100. Reduced erosion caused by lower precipitation.
8. AD 1,100 – present. Renewed high levels of catchment erosion, but not as severe as seen previously.

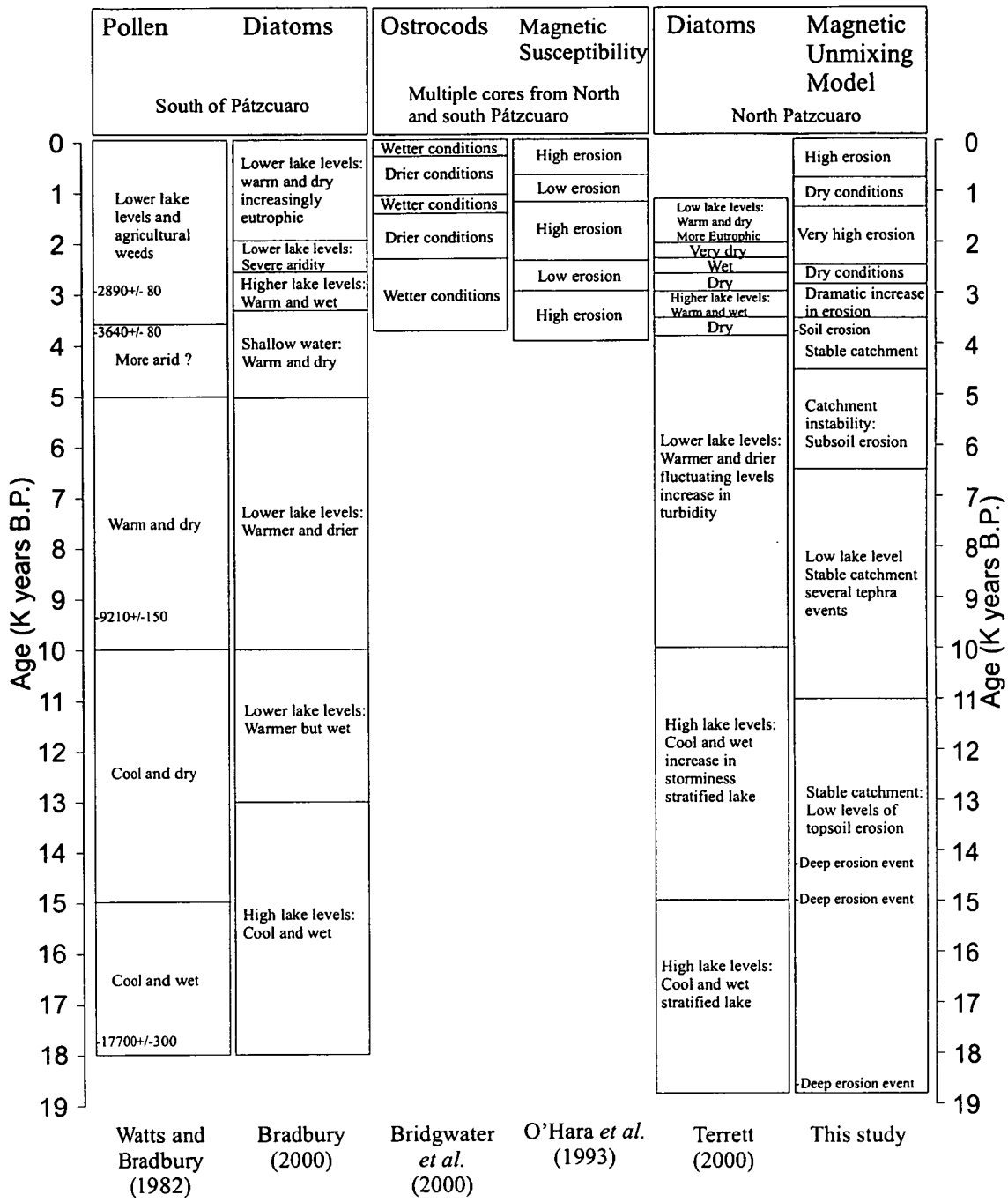

Figure 5.26. Summary of magnetic unmixing model on the KD and C4 cores compared with summaries of previous work on cores from Lake Pátzcuaro. Dotted lines denote uncertainty in dates.

5.13 Discussion

A key test of the unmixing technique is whether it reflects known climatic events, as reported in the literature. Previous studies of sediments from Lake Pátzcuaro have identified a reduction in lake level at approximately 10,000yr B.P. (Bradbury, 2000;

Terrett, 2000), which was associated with an increase in temperature and reduction in precipitation. This reduction in lake level intensified at around 5,000yr B.P. (Watts and Bradbury, 1982; Bradbury, 2000). After 3,500yr B.P., the sediment record of Lake Pátzcuaro is dominated by a series of three high erosion events (O'Hara *et al.*, 1993). The second of these high erosion events was described as "more severe" (O'Hara *et al.*, 1993) than the other two. Between the high erosion periods, the catchment stabilises and there is an accumulation of ostrocods in the lakes sediments. Analysis of the ostrocods (Bridgwater *et al.*, 2000) deposited between and during the high erosion periods after 3,500yr B.P., suggests that the low erosion periods occurred during times of drought.

Analysis of the magnetic unmixing models on Lake Pátzcuaro has also identified the broad trends that were seen in the previous studies. The reduction in lake level at 10,000yr B.P. is apparent in the unmixing model as a reduction in topsoil and subsoil erosion in the catchment. Although this reduction in the modelled concentrations of topsoils and subsoils could be due to reduction diagenesis. The further reduction of lake level at 5,000yr B.P. coincides with a period where soil erosion is again low, according to the unmixing model, although some soil erosion is apparent at 3,600^{14}C yr B.P.. The three high erosion events occurring after 3,500 yr B.P. are indicated by topsoil and subsoil in the magnetic unmixing model. The second high erosion period contains large quantities of subsoil material, consistent with O'Hara *et al's* (1993) assertion that this event is the most severe of the three. The interpretation of the magnetic unmixing model of Lake Pátzcuaro has identified all of the major climate trends reported by previous palaeolimnological studies.

The five unmixing models generated for Lake Pátzcuaro all show broadly similar trends, with low accumulation of soil-derived sediments in section one, tephra events in section two, and a large quantity of material associated with soil erosion in section three. However, the difficulties that models one, two and three had in differentiating between the topsoil and subsoil end-members highlights the problem with categorising catchment material. It is essential when unmixing to identify end-members correctly, and to not attempt to unmix with material which is itself a mixture of the end-member classifications one is trying to differentiate.

5.14 Conclusions

1. Magnetic unmixing has been successfully applied to the sediments from two cores that cover 19,000 years of sedimentation in Lake Pátzcuaro, Mexico.
2. Magnetic unmixing, carried out in terms of catchment end-members, gives an insight into catchment processes recorded within a sediment core.
3. Care must be taken in the selection of end-members to be used in an unmixing model and the subsequent classification of those end-members. When selecting catchment unmixing end-members, it is best to choose samples whose magnetic properties are extreme representations of the class of material being classified.
4. The miss-identification of magnetotactic bacteria magnetosomes in the first four unmixing models indicates that skill cannot always be relied upon to identify problems in unmixing.
5. The interpretation of the unmixing models are in broad agreement with previous studies on Lake Pátzcuaro.
6. The three soil erosion events reported by O'Hara *et al.*, (1993), have been positively identified as high concentrations of topsoil and subsoil material in the unmixing models. It has also been found that the second period of high erosion (2,530 to 1,190 ^{14}C yr B.P.) delivered substantial quantities of subsoil material to the core site.

Chapter 6

Babicora basin

In this chapter I analyse magnetic measurements on two sediment cores taken from Lake Babicora, in the northern plateau of Mexico. Lake Babicora is the second of the two lakes to have its magnetic properties unmixed using the new unmixing procedure introduced in Chapter 4. The results of the unmixing models on magnetic properties of Lake Babicora, are interpreted in terms of environmental process that were active at the time of sediment deposition.

6.1 Introduction

Although other studies have investigated the sediments of Lake Babicora (Metcalfe, *et al.*, 1997; Urruitia-Fucugauchi, *et al.*, 1997; Ortega-Ramirez, *et al.*, 1998; Metcalfe *et al.*, in press), less research has been carried out on Lake Babicora than Lake Pátzcuaro. I have made magnetic measurements on 274 sediments samples taken from two cores: one from the north and one from the centre of the lake basin and 21 samples from within the lake's catchment. Combining the magnetic data from the cores and catchment material I have constructed four magnetic unmixing models for Lake Babicora. The results of the magnetic unmixing models give an indication of the rate and depth of erosion in the lake's catchment; this has been used to make inferences on the past climatic conditions of the region.

6.2 Location and history

Lake Babicora is located in the highlands of the Chihuahuan desert in the state of Chihuahua, North Mexico (Figure 6.1). The lake is situated in the foothills of the Sierra Madre Occidental (29^0N, 108^0W) and is 2138m above sea level. The lake catchment and surrounding area have a mean annual precipitation of 500mm in the east, rising to 1000mm in the west. The rainfall is very seasonal, with the majority falling between July and October. The average annual temperature is 11.3^0C. The general climatic regime of the area is one of hot humid summers (mean temperature 20^0C) and cold, dry winters (mean temperature 3.5^0C). Lake Babicora is a hydrologically closed system. The geology of the catchment area is dominated by Tertiary rhyolites, with some Quaternary basalts in the north west of the basin (Figure 6.1). Although no soil maps of this region have been acquired, analysis of a soil map from near the basin indicates that the geology of Babicora is associated with regosols. The vegetation in the area surrounding Lake Babicora has been

characterised by Ortega-Ramirez *et al.,* (1998) as arid tropical scrub, below 2200m above sea level, and woodlands composed mostly of *Juniperous* (juniper), *Quercus* (Oak), *Pinus cembrodies* and *Pinus oocarpa* (Pine) above 2200m above sea level.

During the dry season (November to June), standing water is limited to two areas in the north of the basin. During the wet season, the inundated area of Lake Babicora increases, forming a single water body (Figure 6.1). The wet season inundated area has been calculated at 158km^2 (Metcalfe *et al.,* in press). During particularly wet conditions, extensive flooding of the basin can occur. The last reported flooding of the Babicora basin occurred in 1986, when 774mm of rain fell in Gomez Farias (a town to the east of the lake Figure 6.1). This compares to the long-term average of 552mm for that town (Metcalfe, *et al.,* in press). Erosional features, gullies and steep-sided dry river beds (Figure 3.12) are common in this catchment. Land use is mostly devoted to free range low intensity cattle grazing, although small pockets of agriculture do exist (Metcalfe, pers. comm.).

Geology map of Babicora with core sites and catchment sampling sites marked

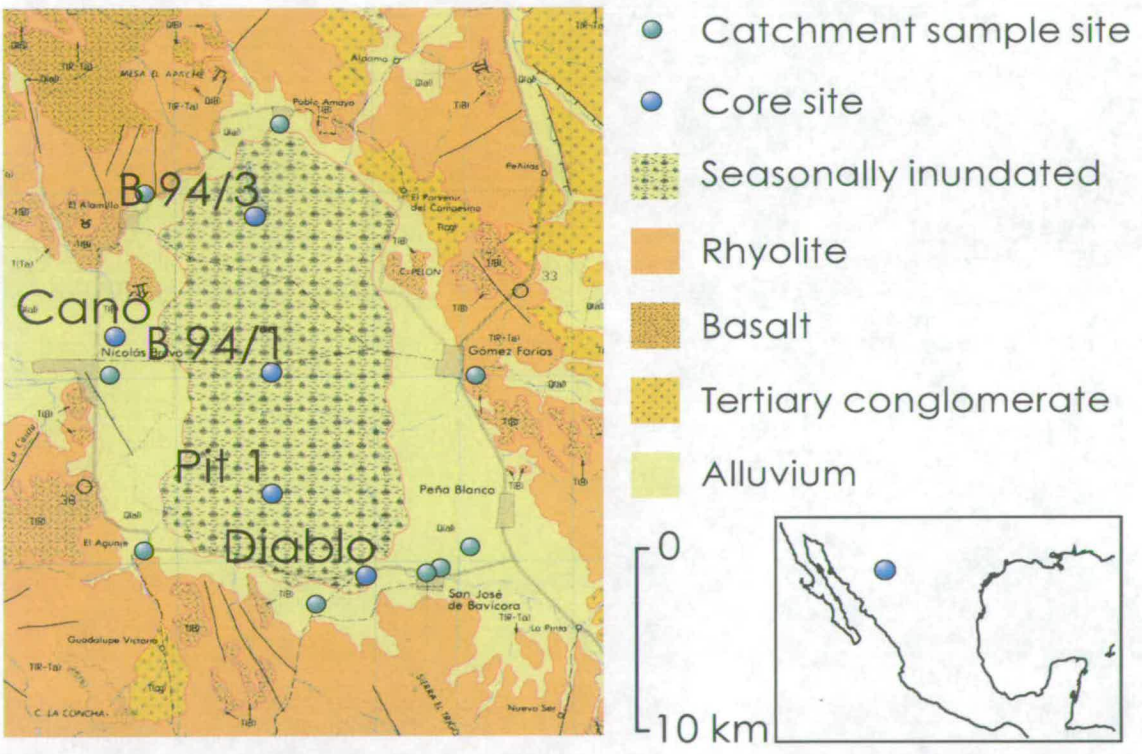

Figure 6.1. Geological map of the Babicora catchment with core sites and catchment sample sampling sites marked.

6.3 Previous work

Palaeolimnological studies have been undertaken on various cores and pits from within the Babicora basin. These studies have included stratigraphic (Ortega-Ramirez, *et al.,* 1998), diatom (Metcalfe *et al.,* 1997; Metcalfe *et al.,* in press), pollen (Metcalfe *et al.,* in press), chemical (Metcalfe, *et al.,* 1997; Ortega-Ramirez *et al.,* 1998; Metcalfe *et al.,* in press), particle size (Urruitia-Fucugauchi *et al.,* 1997;

Ortega-Ramirez *et al.*, 1998) and magnetic (Urruitia-Fucugauchi *et al.*, 1997) analysis of the lakes sediments. The results of these four studies are summarised in Figure 6.2.

The results of the previous studies on sediments from Lake Babicora can greatly depend on the site of the study in question (Figure 6.1). The present extent of Lake Babicora is much smaller than it has been in the past. Sites closer to the present day lake are likely to have received more recent lacustrine deposits than sites further away. Also sites further from the present lake are more likely to have been effected by recent erosion and pedogenesis.

Of the four studies summarised here, the results from the B94/3 core provide the longest sediment record for Lake Babicora (Metcalfe *et al.*, in press). Dating of the B94/3 core is provided by four AMS ^{14}C dates and five U-series dates on diatom silica (Metcalfe *et al.*, in press). Figure 6.4 shows an age depth profile and sedimentation rates for core B94/3.

Pollen and diatom analysis on B94/3 show a distinct change at around 29,000yr B.P. from a deep lake with occasional shallow episodes to a shallower lake, with drier, colder conditions (Metcalfe *et al.*, in press). Unfortunately, pollen and diatom analysis of the upper part (after 10,500yr B.P.) of core B94/3 have been impossible due to low concentrations of intact diatoms and pollen (Metcalfe *et al.*, in press). Further south in the basin, at the Pit 1 (Metcalfe *et al.*, 1997), Cano and Diablo (Urruitia-Fucugauchi, *et al.*, 1997; Ortega-Ramirez *et al.*, 1998) sites there is evidence of the existence of a deep lake until approximately 11,000 yr B.P.. At around 11,000yr B.P. all three sites see a reduction in lake level. There is an increase in effective moisture that is dated at 5,400yr B.P. in Pit 1 (Metcalfe *et al.*, 1997), and either 5,600yr B.P. (Urrutia-Fucugauchi *et al.*, 1997) or 4,000yr B.P. (Ortega-Ramirez *et al.*, 1998) in the Cano and Diablo sites. This wet period is thought to last until roughly 2,800yr B.P. (Metcalfe *et al.*, 1997; Urrutia-Fucugauchi *et al.*, 1997) or possibly 2,000yr B.P. (Ortega-Ramirez *et al.*, (1998)). The Pit 1 site's dating is constrained by five ^{14}C dates, the Cano and Diablo each have three ^{14}C dates.

The combined picture of the Babicora basin represented by sediments from the B94/3, Pit1, Cano and Diablo sites is one of a large lake at 65,000yr B.P., which becomes shallower at around 29,000yr B.P. but still extends over a large area of the Babicora basin. At approximately 11,000yr B.P., the extent of Lake Babicora reduced dramatically. Then, for a period between 6,000 and 2,000yr B.P., the lake level seems to increase again. This is followed by a second dry period that starts at some point between 2,200 and 2,800yr B.P., and lasts to the present day.

Summary of previous work on sediments from Lake Babicora

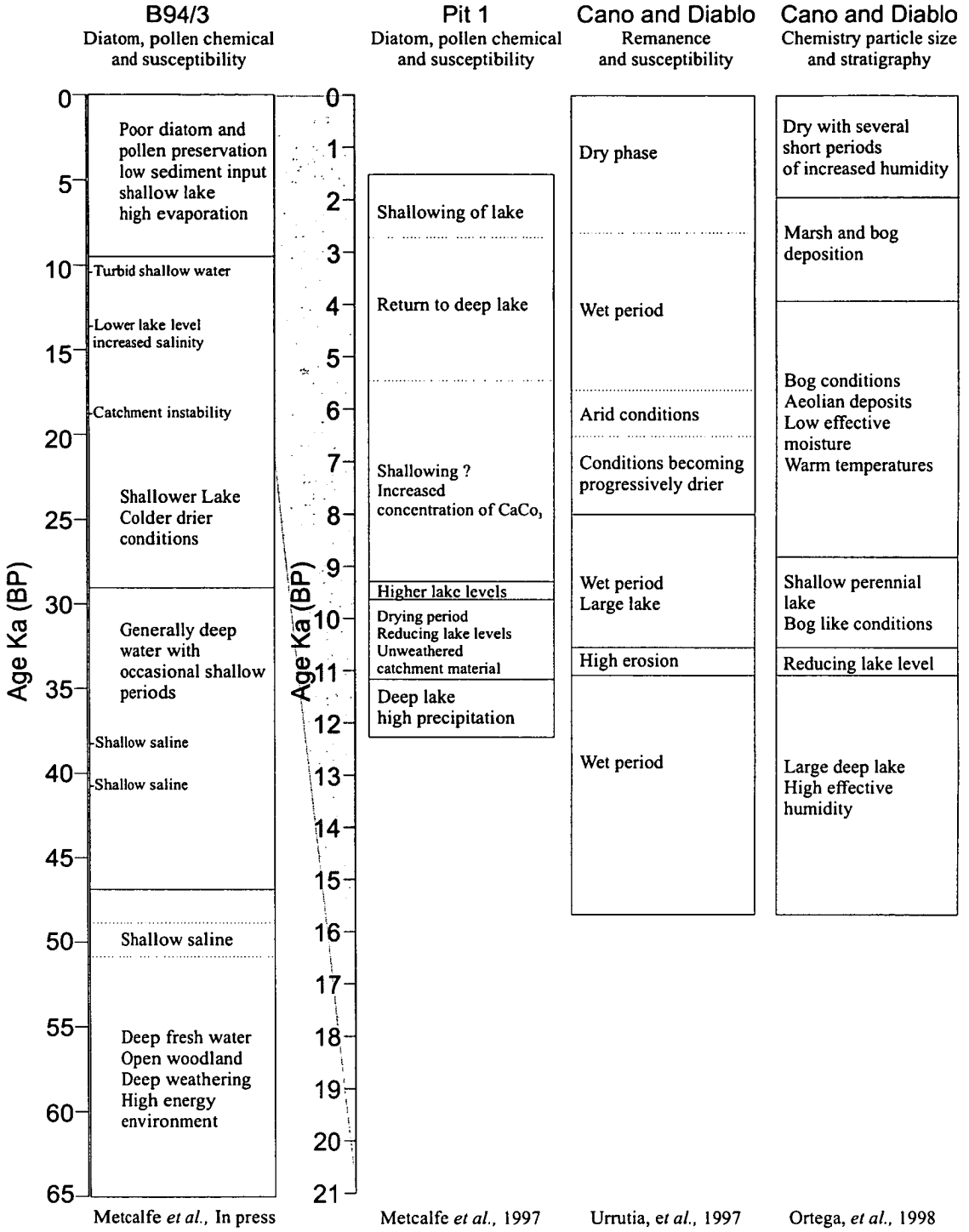

Figure 6.2. Summary of previous studies on sediments from Lake Babicora. Broken lines show areas of dating uncertainty.

6.4 Cores B94/1 and B94/3

Both cores B94/1 and B94/3 are percussion cores taken from the Babicora basin in 1994. B94/1 comes from near the centre of the seasonally inundated area of the Babicora basin and B94/3 comes from the north of the Babicora basin, from close to the edge of one of the two permanent water bodies (Figure 6.1). B94/1 is 490cm long, and was sub-sampled at roughly 5cm intervals producing 120 samples that were each subjected to the standard 18 magnetic measurements (Chapter 2.4). Unfortunately no dates are available for the B94/1 core. However, diatom analysis of B94/1 suggests that it may cover a similar period of sediment accumulation to that represented by B94/3 (Figure 6.5).

Core B94/3 is composed of two percussion cores that were taken within 1m of each other. The first of the B94/3 cores is called B94/3a; it covers sediment from the surface to a depth of 366cm. The second core is called B94/3b. The top of B94/3b starts at 355cm depth and goes down to 549cm below the surface. Both B94/3a and B94/3b were sub-sampled at 2cm intervals. For B94/3a this sampling produced 157 samples and for B94/3b, 97 samples were produced. The samples from B94/3a and B94/3b were subjected to the standard 18 magnetic measurements described in Chapter 2.4. Unfortunately the material from core B94/3b was dry at the time of sub-sampling, which may have altered its magnetic properties.

Originally, it was believed that B94/3a and B94/3b made a continuous sequence, with a short sediment overlap (Metcalfe *et al.*, in press). Constraining the extent of the overlap between the two cores was complicated by differences in the stratigraphy of the top of B94/3b and the bottom of B94/3a. The magnetic susceptibility and SARM/SIRM of the bottom 75cm of B94/3a seem to mirror those at the top of B94/3b (Figure 6.3), so I suggest that these two cores overlap by approximately 75cm. The overlap in the B94/3a and B94/3b cores is also apparent in some of the chemical and diatom abundance data (Metcalfe *et al.*, in press). The similarity is less obvious in the chemical and diatom abundance data due to the lower resolution of these studies.

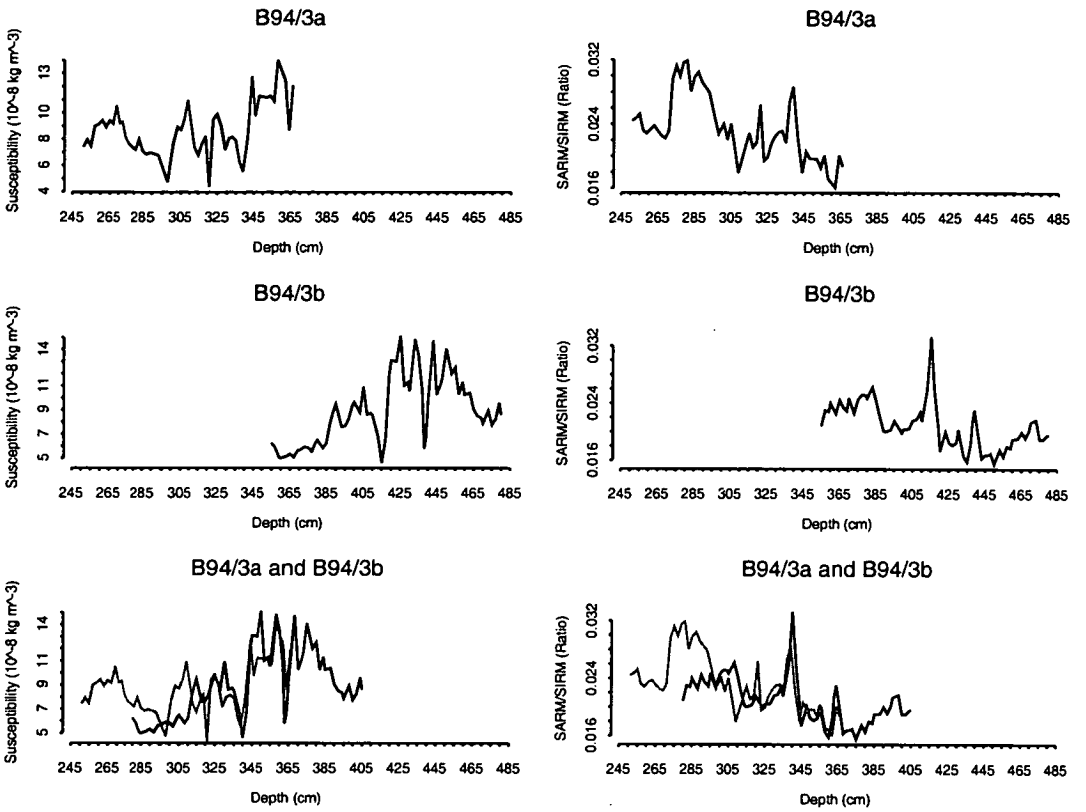

Figure 6.3. A core overlap of 75cm between cores B94/3a and B94/3b is shown by high resolution (every 2cm) magnetic susceptibility and SARM/SIRM measurements. For each measurement the top graph shows the results for B94/3a, the middle graph for B94/3b with original depths, and the bottom graph for B94/a (grey) and B94/3b (black) with depth corrected by 75cm.

6.5 Age depth profile for B94/3

The age depth profile and sedimentation rates for B94/3 (Figure 6.4) show that the rate of sedimentation in the core has generally been reducing through time. There is a marked decrease in sedimentation between 380cm to 320cm, which is between a U series date of 54,600 +3,600/-3,480yr B.P. and a ^{14}C 35,860 ± 390 ^{14}C yr B.P.. However, the sedimentation rate calculated at this point could be in error because this period falls on the cross over between cores B94/3a and B94/3b, and the cross over between dating techniques, and the U series date has particularly large error bounds. Taking the error bounds of the dating techniques into account gives a sedimentation rate of 26.7 (+6.9/-4.7) μm yr^{-1}. Given all the factors that are changing at this point in the core, care should be taken when interpreting this apparent low sedimentation period.

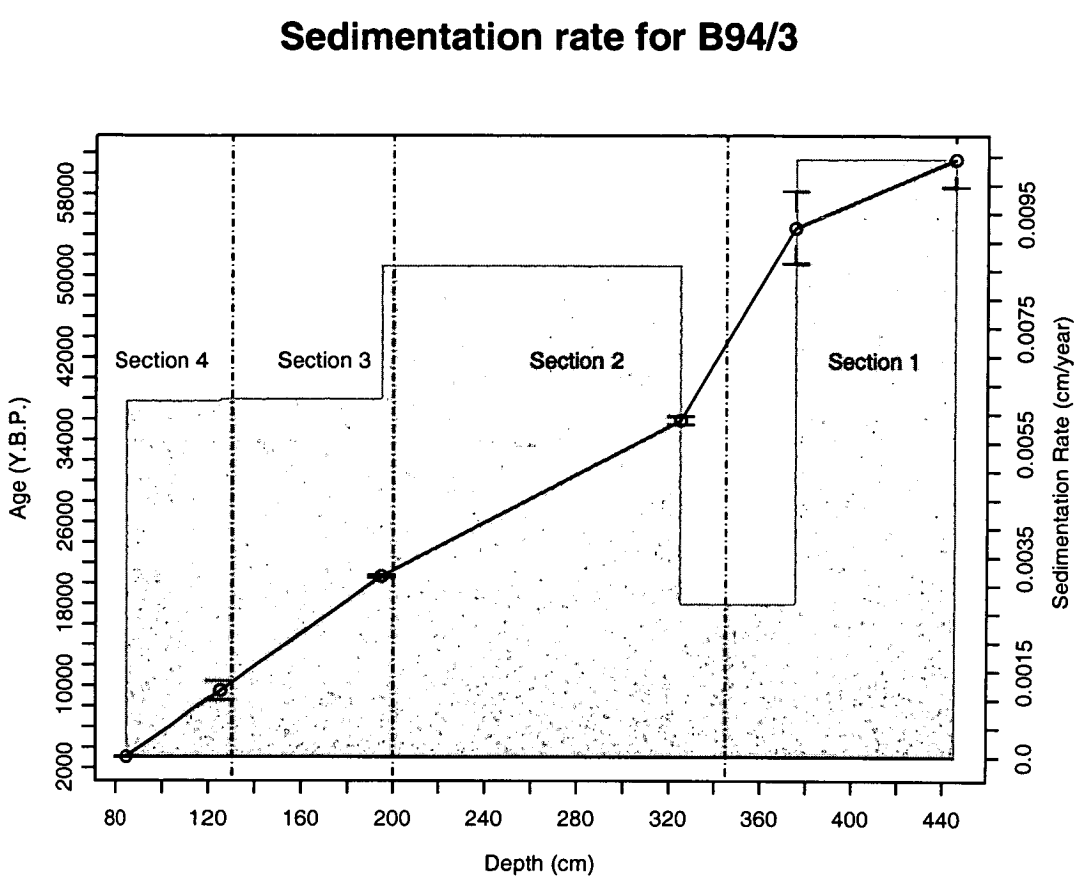

Figure 6.4. sedimentation rate and age depth profile for core B94/3. Sedimentation rate as grey columns, age depth profile is black line. Radio carbon dates and U series dates given as plotted points with error bars.

6.6 Diatom comparison between cores B94/1 and B94/3

Interpretations of the processes which have affected lake sediments are much more useful when attached to accurate dates. Unfortunately core B94/1 has no dating control. However some of the diatom counts for the B94/1 and B94/3 cores have similar features, so it was suggested by Metcalfe (Pers. comm.) that the two cores may represent a similar sediment accumulation period. Figure 6.5 shows an attempt I have made to correlate the diatom abundance of three diatom species between the two cores. Although these diatom species have some elements that seem to match between the two cores, other species are not so convincing, and there is little similarity in the down core variation of magnetic properties of the two cores. If the match between B94/1 and B94/3 is to be accepted then B94/1 would seem to cover over 36,000 years of sedimentation (from the radiocarbon date on B94/3 at 340cm depth). However, without proper dating on core B94/1, chronological constraints on the environmental models resulting from this core are speculative at best.

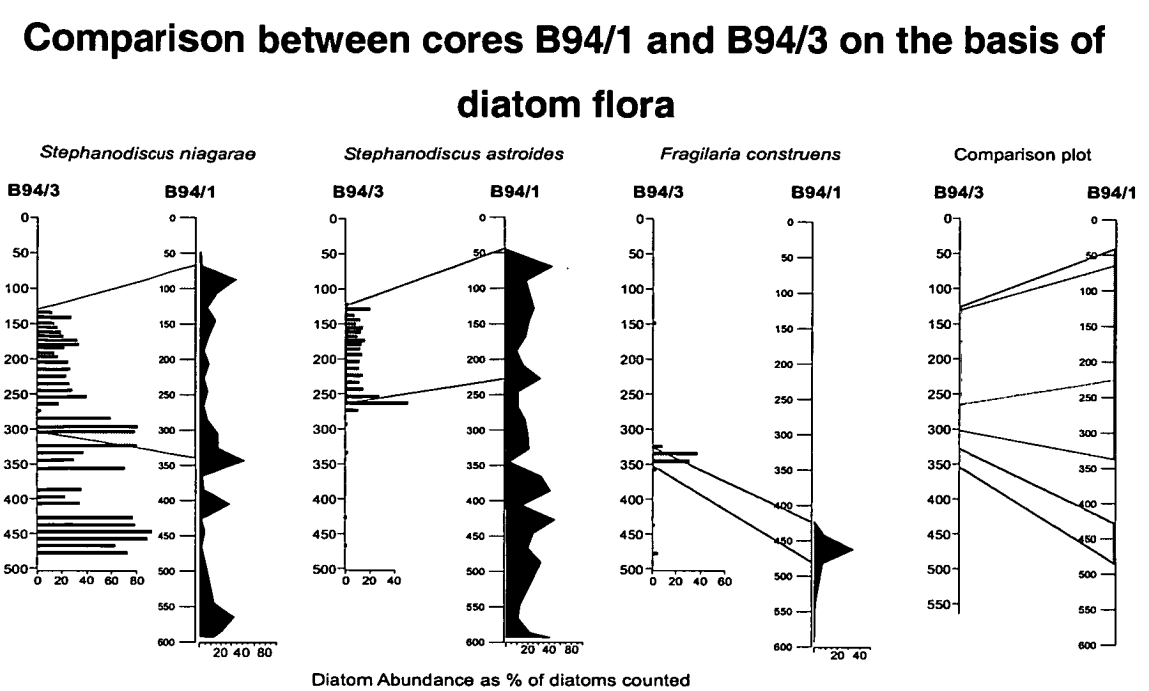

Figure 6.5. Comparison of diatom flora for three selected species in core B94/1 (D. Heath Pers. comm.) and B94/3 (A. Say Pers. comm.). Grey boxes show an attempt to link the diatom abundance plots between cores.

6.7 Catchment samples

Twenty-one samples were taken from around the Babicora catchment, the locations of the catchment sample sites are indicated in Figure 6.1. The catchment samples were divided into five categories: enhanced topsoil, topsoil, subsoil, bedrock, and wind-blown dust. The categorisation of each sample was based on both field observations and subsequent magnetic analysis. The enhanced topsoil category consisted of soils that showed similar properties to viscous magnetite in Figures 6.13 and 6.14. Enhanced topsoils were grouped as a separate category because they clustered so far from the magnetic properties of topsoils. Each catchment sample was subjected to the same eighteen magnetic measurements as the core samples from B94/1 and B94/3, (Chapter 2.4).

6.8 Results

The results of the magnetic measurements on the cores B94/1 and B94/3 are plotted in Figure 6.6 and Figure 6.7. Here I give a brief description of the magnetic properties and stratigraphy of the cores and the catchment samples.

6.8.1 Core B94/1 magnetic properties and stratigraphy

To aid the description of the magnetic properties of core B94/1, I have divided it into three sections (Figure 6.6). Section one goes from the bottom of the core (490cm) to a depth of 355cm, the second section goes from 355cm to 225cm, and the third section from 255cm to the top of the core. Below I describe the magnetic properties and stratigraphy of each section of the core in turn from section 1 to section three.

The susceptibility of the first section of the core (Figure 6.6), is initially high, with two peaks over $7*10^{-6}$kg m^{-3} at 467cm and 432cm. Between the two high susceptibility peaks, the susceptibility is lower and highly variable. After the two initial high susceptibility peaks, the susceptibility falls to around $2*10^{-6}$kg m^{-3} at a depth of 360cm. Section one of B94/1 exhibits slowly increasing IRM and ARM hardness. The ARM hardness is very variable. The SARM/SIRM ratio of section one of B94/1 is low, averaging around 0.03. SARM/SIRM increases to almost 0.035 by the top of the section. Section one of B94/1 is made of clay material, the lower and upper parts of the clay in this section contain shell fragments and other carbonate material.

At the beginning of section two (Figure 6.6), the susceptibility of the core jumps to approximately $4*10^{-6}$kg m^{-3} then steadily drops to $3*10^{-6}$kg m^{-3} by the top of the section. There is a period of increased susceptibility at 280cm where it rises to $4.5*10^{-6}$kg m^{-3}. Section two of B94/1 has a steadily increasing SARM/SIRM ratio, and also exhibits increasing IRM hardness. ARM hardness is again variable, but not as variable as in section one. Like section one, section two of B94/1 consists of clay material. The first half of section two also contains shell fragments and other carbonates.

Section three of B94/1 (Figure 6.6), generally has lower susceptibility than seen in sections one and two. The IRM hardness continues to increase throughout this section. The ARM hardness decreases at first. However, after a depth of approximately 100cm, the ARM hardness steadily increases to the top of the core. The SARM/SIRM ratio of section three of B94/1 is higher than either of the previous two sections. SARM/SIRM peaks at 165cm and 140cm, and reaches a plateau of 0.055 at the top of the core. The bottom of section three is made of clay material, which becomes a silty clay at 200cm depth and a clayey silt at 170cm. Between 100cm and 75cm the core reverts to silty clay. The top of the core is described as inorganic, friable sediment (Metcalfe (pers. comm.)).

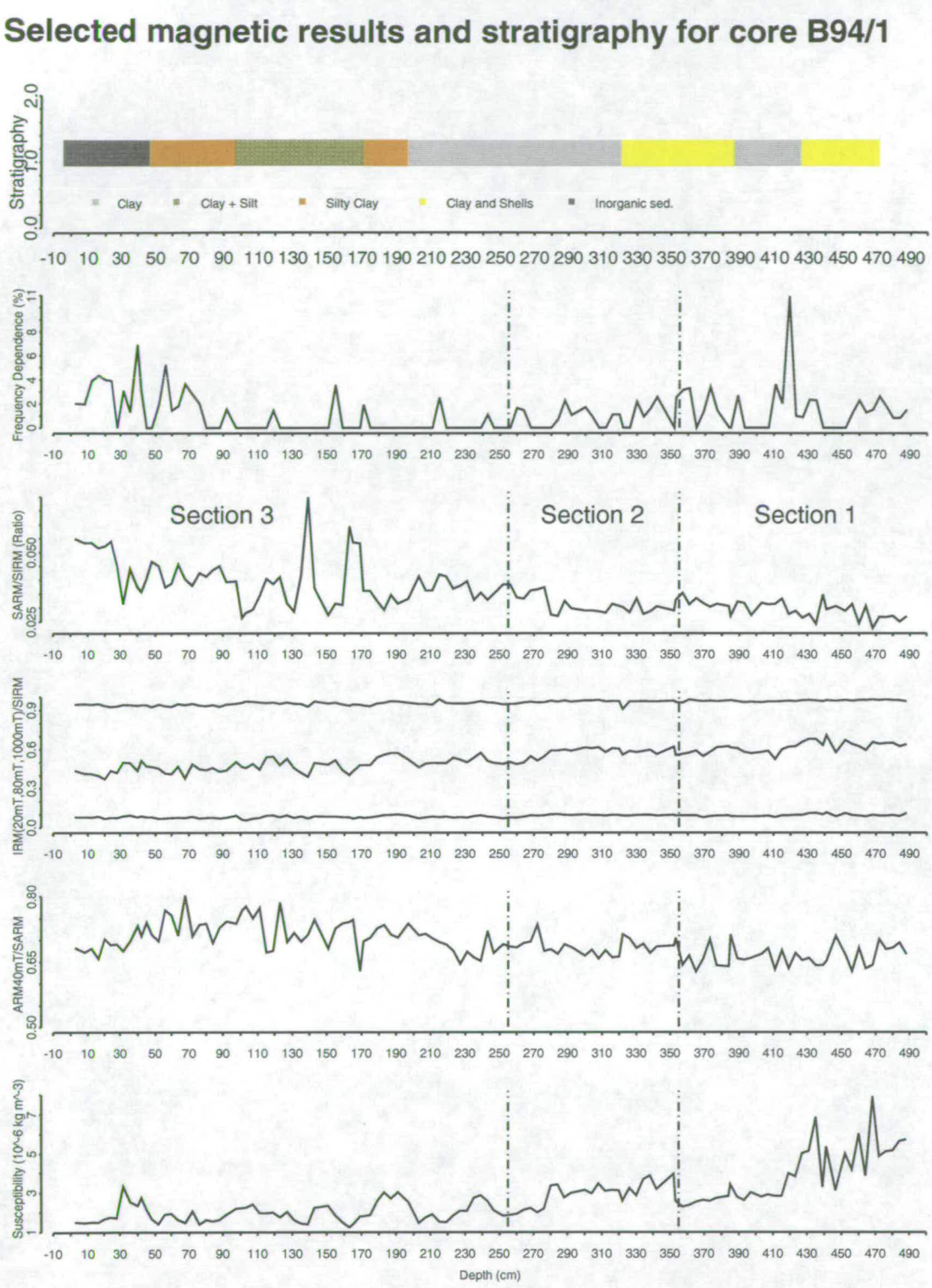

Figure 6.6. The stratigraphy and selected magnetic results and ratios for core B94/1, plotted against depth. Broken vertical lines separate the core into three sections, section one at the bottom of the core and section three at the top.

6.8.2 Core B94/3 magnetic properties and stratigraphy

The composite core B94/3 comes from the combination of B94/3a and B94/3b with a 75cm overlap (Figure 6.3). To aid the description of the magnetic properties of this core I have separated it into four sections. These sections are defined as:

- **Section 1** from the bottom of the core to a depth of 345cm extrapolating the available radio carbon and U series dates gives an approximate time span of 65,000 – 43,000yr B.P.,
- **Section 2** from 345cm to 200cm extrapolating the available radio carbon dates gives an approximate time span of 43,000 – 21,000ry B.P.,
- **Section 3** from 200cm to 130cm, extrapolating available radio carbon dates gives an approximate time span of 21,000 – 10,000yr B.P. and,
- **Section 4** from 130cm to the top of the core, this section covers a period from approximately 10,000yr B.P. to present (Figure 6.4).

Section one of B94/3, (approximately 65,000 – 43,000yr B.P.) shows generally high susceptibility (Figure 6.7). However there is great variation of the magnetic susceptibility from the base of the core up to 440cm depth. From 440cm to 380cm, the susceptibility increases steadily from about $2*10^{-6}$kg m^{-3} to around $9*10^{-6}$kg m^{-3}. After 380cm, the susceptibility plateaus up to the top of this section of the core. There is one large susceptibility trough at 363cm where the susceptibility drops to less than $2*10^{-6}$kg m^{-3} then returns to over $9*10^{-6}$kg m^{-3}. The ARM hardness increases steadily over section one of core B94/3. The SARM/SIRM ratio shows a general decrease from the base of the core up to the top of section one. IRM hardness is generally stable in this section, however there is a trough in the IRM_{100mT}/SIRM at 404cm. The stratigraphy of the lower part of section one, from the bottom of the core up to 380cm, is dominated by silty clay. Above this there is a narrow sand horizon, followed by finer clay material.

Section two of B94/3, (approximately 43,000yr – 21,000yr B.P.), has a lower average susceptibility than seen in section one (Figure 6.7). The stratigraphy of section two of core B94/3 is almost entirely dominated by clay material. The bottom of section two has a prolonged horizon of silty clay with fine sand that lasts from 340cm up to 315cm deposited between 42,000 and 36,000yr B.P. (by extrapolation of U series dating) there is a radiocarbon date of 35,860 ± 390 ^{14}C yr B.P. just above this material. Another departure from the predominantly clay stratigraphy of section two of the core occurs in the centre of the section, where there is a horizon with a large number of shells and shell fragments. The shell rich horizon lasts from roughly 270cm to 260cm depth. Extrapolating the available radio carbon dates would place the period of deposition of this shell rich material between 29,000 to 28,000yr B.P.. The lower part of section two has a more variable susceptibility than is seen in the upper part of the same section. The zone of large susceptibility variations seems to start in the silty clay and fine sand horizon at the bottom of section two, but extends beyond this region at a depth of 280cm. There is a peak in susceptibility at around 270cm which reaches $11*10^{-6}$kg m^{-3}. There is a slight decrease in both IRM and ARM hardness through section two of B94/3, and two distinct troughs in the ARM hardness, at 300cm and 272cm. The SARM/SIRM ratio of section two of B94/3 is generally quite steady with an average value of around 0.023. There is one prolonged peak in the SARM/SIRM ratio between 298cm and 272cm, this peak occurs at the

point of high shell content in the core, and before the peak in susceptibility at 270cm, and reaches a SARM/SIRM ratio of 0.03.

Section three of core B94/3, (Figure 6.7) covers the period 21,000 – 10,000yr B.P. and again mostly consists of clay material. At around 185cm this material is replaced by coarser silty clay with fine sand, which fines upwards to silty clay. Extrapolation of radio carbon dates gives a date of 19,000yr B.P. for the changeover between clay and silty clay with fine sand. At 160cm, (roughly 15,000yr B.P.) the core material has returned to the clay size fraction. Section three of B94/3 has a highly variable susceptibility. The bottom of section three has three peaks in susceptibility, which increase in intensity. The first susceptibility peak is at 195cm, the second at 187cm and the third and largest is at 181cm their maximum susceptibility vales are $6*10^{-6}$kg m^{-3}, $7*10^{-6}$kg m^{-3}, and $9.5*10^{-6}$kg m^{-3} respectively. After the three susceptibility peaks, susceptibility drops to around $3.5*10^{-6}$kg m^{-3}, there are then two susceptibility troughs, where the susceptibility falls to approximately $1*10^{-6}$kg m^{-3}. The first of the two susceptibility troughs is prolonged and goes from 165cm to 158cm, approximately 16,000yr B.P. from extrapolation of radio carbon dates , the second occurs at 150cm or 12,500yr B.P., from the extrapolation of radio carbon dates . ARM and IRM hardnesses generally increase throughout section three of B94/3. There is a pronounced ARM hardness trough at 145cm. The SARM/SIRM ratio for section three is mostly steady at around 0.25, however there are two peaks in the SARM/SIRM ratio which reach values of around 0.04. The peaks in SARM/SIRM ratio are coincident with the two susceptibility troughs in this section of the core, and so occur between 165cm and 158cm, and at 150cm.

Section four of B94/3, (approximately 10,000yr B.P. to present), has a lower susceptibility than any other section of the core (Figure 6.7). The predominantly clay size of this section of the core is interrupted by coarser silty clay material between 95cm and 85cm. Rootlets are found in the top 10cm of the core. A carbon date near the upper limit of the silty clay horizon indicates that it was deposited before 3,070±60 ^{14}C yr B.P. The susceptibility of section four of B94/3 is always less than $2*10^{-6}$kg m^{-3}. The bottom of this section of the core displays a gradual increase in ARM and IRM hardness. Above a depth of 50cm, the increasing hardness reverses, with IRM and ARM hardness decreasing towards the top of the core. There are several pronounced ARM hardness troughs in section four of B94/3; the largest of these occur at the bottom of this section, around 110cm and 87cm, with smaller troughs towards the top of the core at around 32cm, 15cm and 7cm. The SARM/SIRM ratio in section four is far greater than seen in any previous section. SARM/SIRM increases steadily from the bottom of section four, plateauing at 95cm at a value of 0.05 before decreasing after a depth of 30cm.towards the top of the core.

For the whole of B94/3 there is little magnetic evidence of reduction diagenesis or authigenic iron sulphide production. Although susceptibility falls sharply in section four, this fall is accompanied by a rise in SARM/SIRM indicating that a selective dissolution of magnetite over haematite has not occurred. The fact that for the whole of the B94/3 core IRM saturation has nearly been reached by 1T makes authigenic iron sulphide production unlikely.

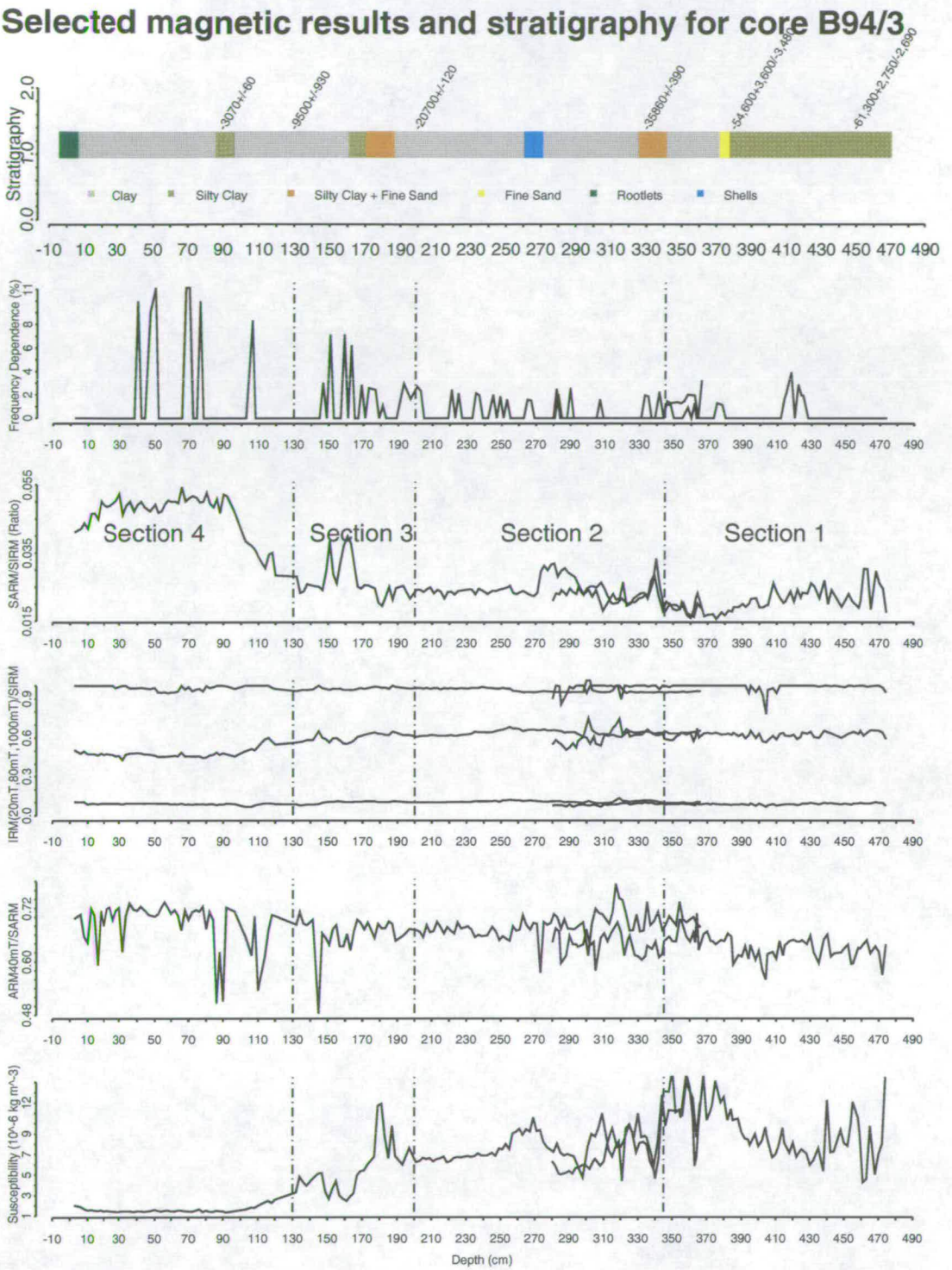

Figure 6.7. The stratigraphy and selected magnetic measurements and ratios for core B94/3, plotted against depth. Broken vertical lines separate the core into four sections, section one at the bottom of the core and section four at the top. Stratigraphy includes four ^{14}C dates (the top four dates) and two U series dates (the lowest two dates) on the cores.

6.8.3 B94/3 loss on ignition

Figure 6.8 shows the loss-on-ignition (l.o.i.) data for the B94/3 core (Metcalfe *et al.*, in press). These values of l.o.i. are considered very low for lake sediments (Metcalfe,

pers. comm.) The indication of low organic content in the core and the lack of magnetic evidence, make both dissolution diagenesis and iron sulphide production unlikely in spite of the low sedimentation rates seen for B94/3.

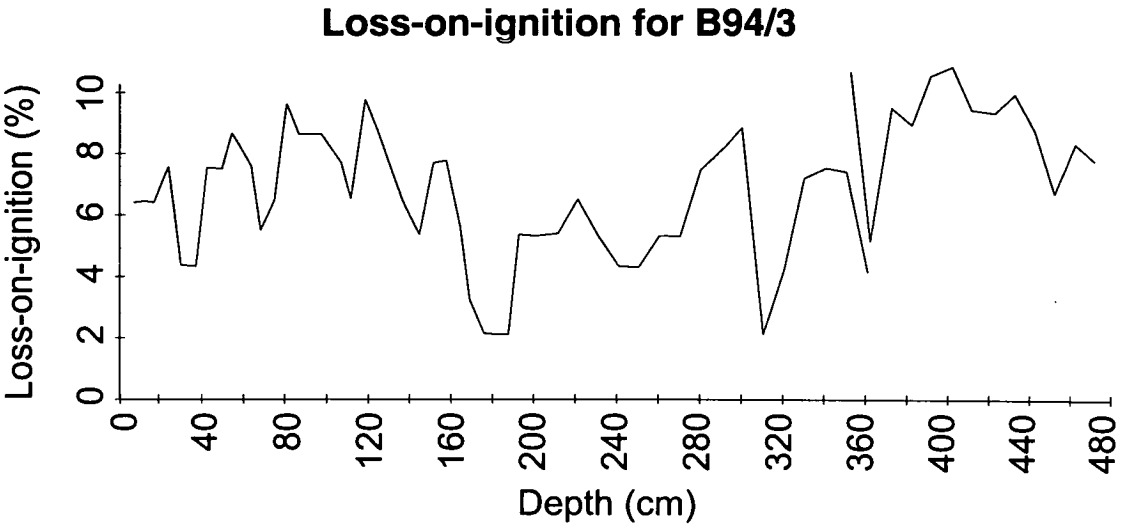

Figure 6.8. Loss on ignition curve for B94/3. Loss-on-ignition was determined by ignition at 550^{0}C (Metcalfe *et al.*, in press).

6.8.4 Babicora core biplots

Two biplots have been drawn for each of the two Babicora cores (B94/1 and B94/3) (Figure 6.9 6.10, 6.11 and 6.12). These biplots show ARM against IRM hardness and SARM/SIRM against IRM hardness. The sections into which the cores have been divided, are marked on these diagrams.

ARM versus IRM hardness for B94/1

The IRM hardness against ARM hardness biplot for B94/1 (Figure 6.9) shows an increase in hardness moving up the core. Section three has the greatest hardness both in ARM and IRM, section one displays softer magnetic properties. In this biplot, the whole of the B94/1 core falls in a mixing triangle between titanomagnetite, PSD magnetite and SD magnetite.

SARM/SIRM (squareness) versus IRM hardness for B94/1

The whole of core B94/1 shows low SARM/SIRM (Figure 6.10). Section three of B94/1 has the highest SARM/SIRM, and it seems to decrease down the core. The upper core material plots near the mixing line between titanomagnetite and viscous magnetite.

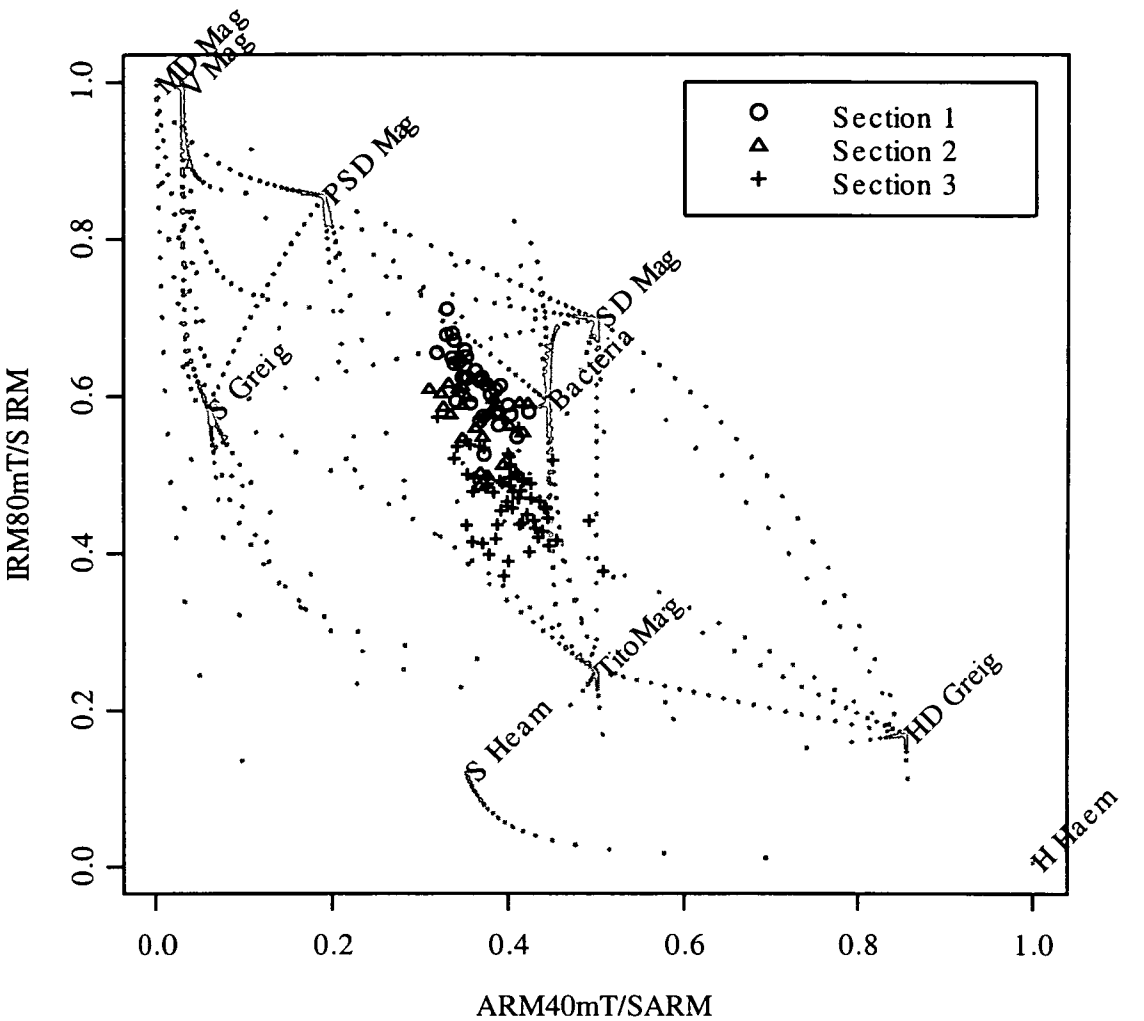

Figure 6.9. Biplot of the IRM hardness, increasing downwards against ARM hardness increasing to the right. The core material has been separated into the three sections used to describe the magnetic properties of the core. Also plotted are mineral magnetic end-members for reference, and points on the mixing curves between these end-members. For a further explanation see Chapter 2.8.

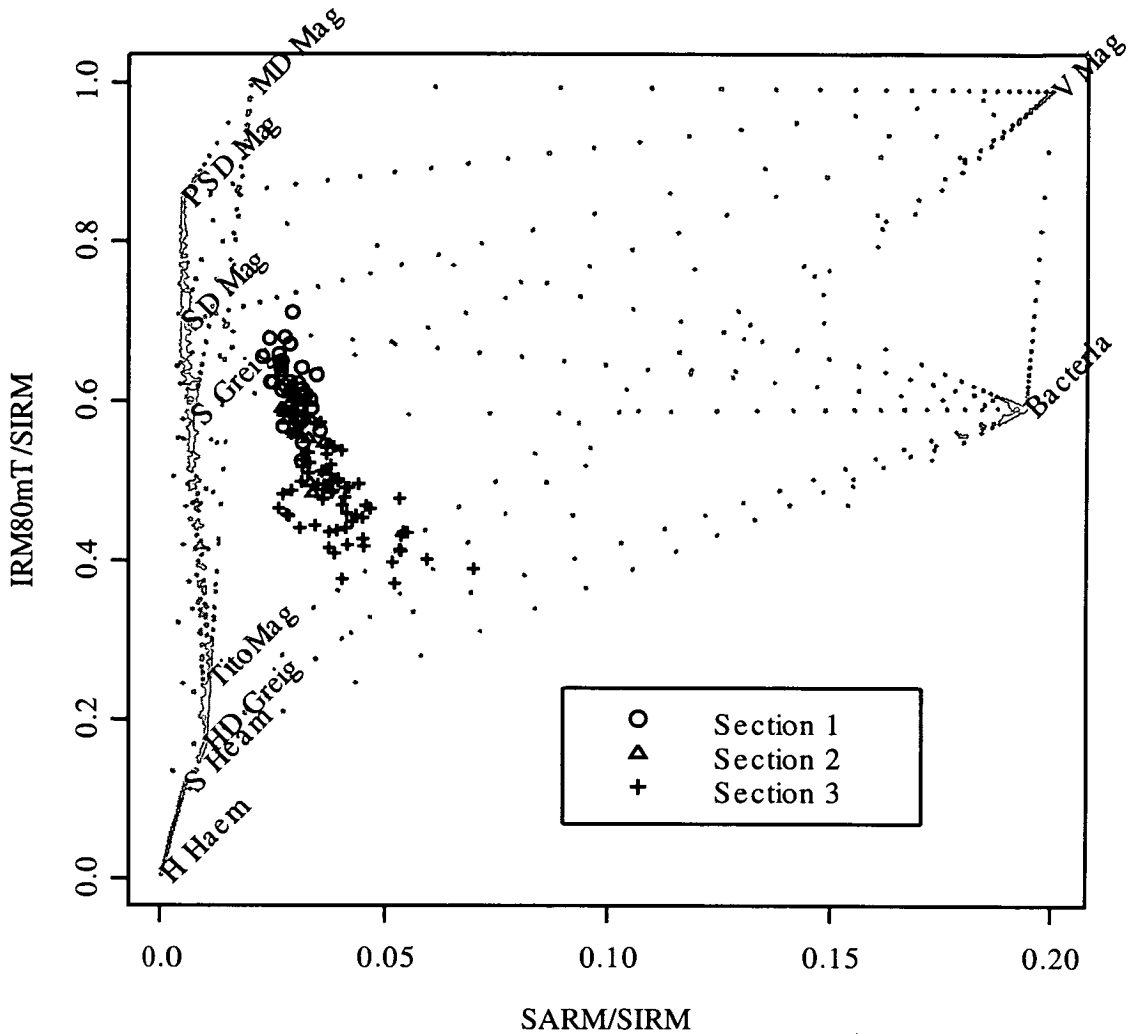

Figure 6.10. Biplot of the IRM hardness, increasing downwards against SARM/SIRM squareness increasing to the right. The core material has been separated into the three sections that were used to describe the magnetic properties of core B94/1. Also plotted are mineral magnetic end-members for reference, and points on the mixing curves between these end-members. For a further explanation see Chapter 2.8.

ARM versus IRM hardness for B94/3

In the biplot of ARM against IRM hardness for B94/3 (Figure 6.11), we see similar hardness properties to those of the B94/1 the core material. Once again, the upper sections, section three and four, are harder in both ARM and IRM properties than the lower two sections. Section four of the B94/3 core is the hardest section. The lower core and upper core materials are concentrated in two separate clusters, with relatively few samples plotting between them. As in Figure 6.9 the material from B94/3 also falls in a mixing triangle between titanomagnetite, PSD magnetite and SD magnetite.

SARM/SIRM (squareness) versus IRM hardness for B94/3

The SARM/SIRM against IRM hardness biplot for core B94/3 (Figure 6.12) is similar to the same biplot for B94/1 (Figure 6.10). The upper core material, sections one and two, show higher SARM/SIRM than the lower core material. Like the ARM against IRM hardness biplot for B94/3, two clusters are noticeable in the SARM/SIRM against IRM hardness biplot. These clusters separate the upper and lower core material.

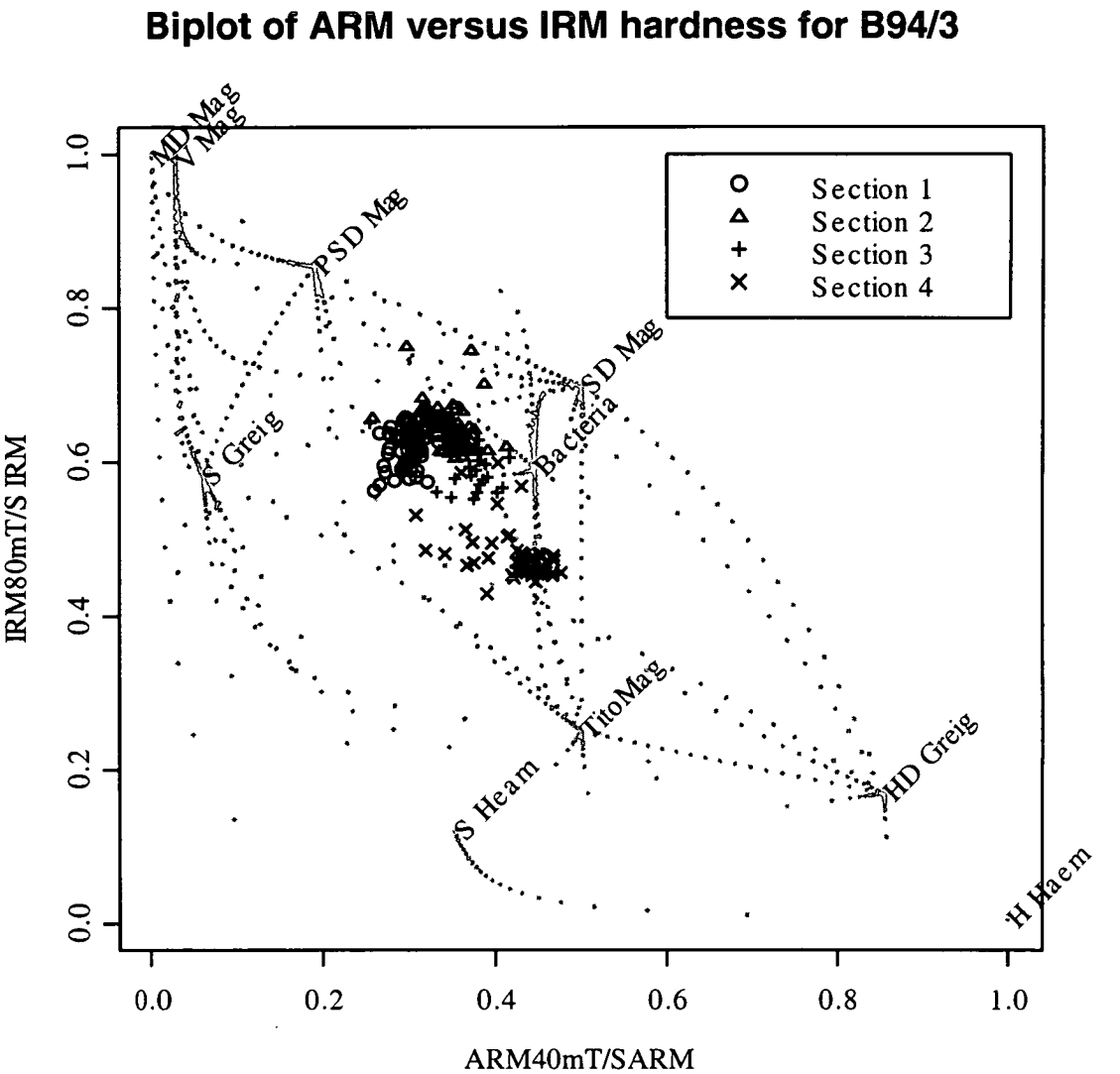

Figure 6.11. Biplot of the IRM hardness, increasing downwards against ARM hardness increasing to the right. The core material has been separated into four the four sections used to describe the magnetic properties of the core. Also plotted are mineral magnetic end-members for reference, and points on the mixing curves between these end-members. For a further explanation see Chapter 2.8.

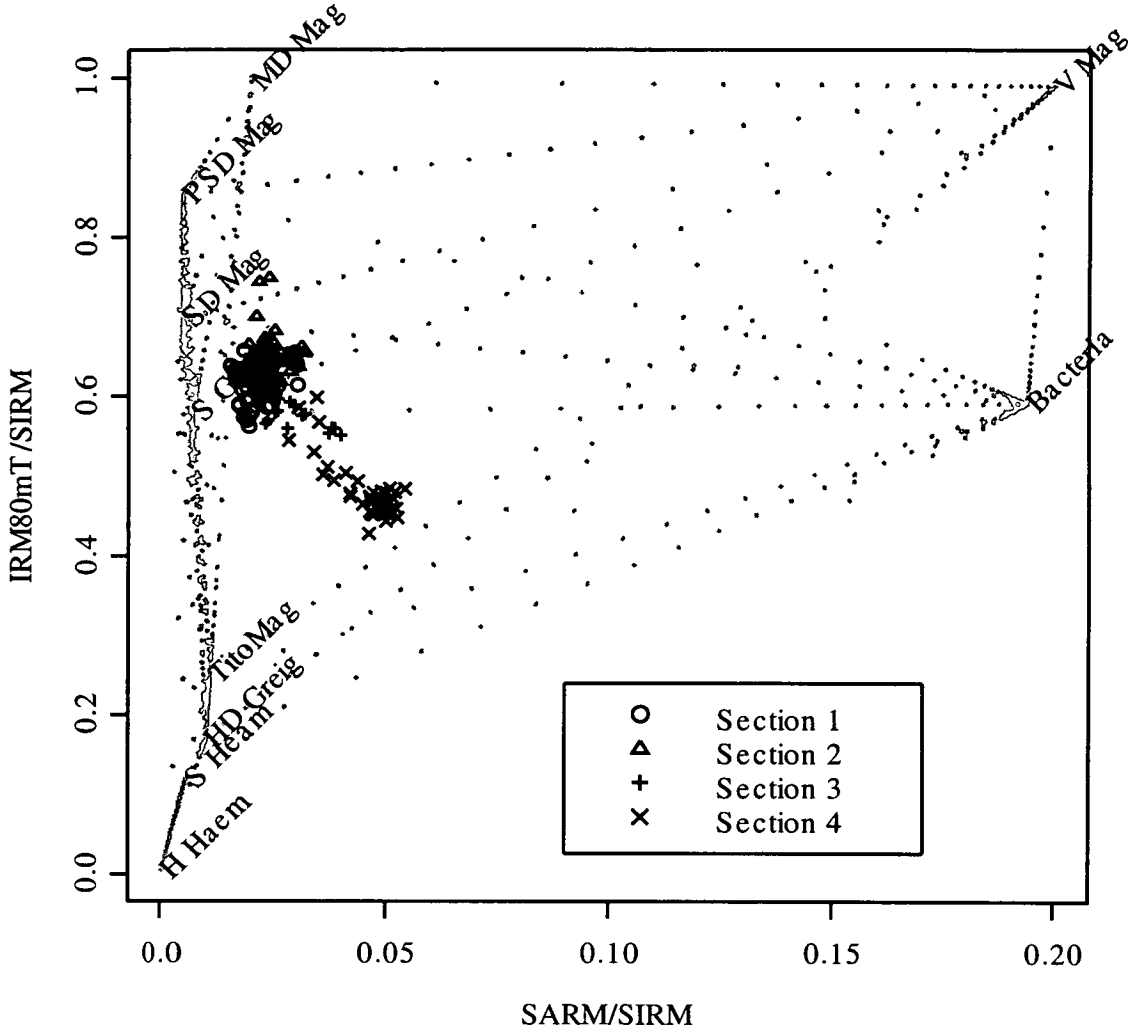

Figure 6.12. Biplot of the IRM hardness, increasing downwards against SARM/SIRM squareness increasing to the right. The core material has been separated into the four sections that were used to describe the magnetic properties of core B94/3. Also plotted are mineral magnetic end-members for reference, and points on the mixing curves between these end-members. For a further explanation see Chapter 2.8.

6.8.5 Babicora catchment samples

The magnetic properties of the twenty one catchment samples from the Babicora basin are best illustrated by biplots. Figure 6.13 and Figure 6.14 are two biplots of the magnetic properties of the catchment materials, Figure 6.13 shows ARM hardness against IRM hardness and Figure 6.14 shows squareness against IRM hardness.

ARM versus IRM hardness biplot for Babicora catchment samples

In Figure 6.13, there is a good separation of the different end-member types. The enhanced topsoil material plots near the viscous magnetite region, on or near the mixing line between viscous magnetite and pseudo single domain magnetite. The topsoil material plots in the harder region between pseudo single domain magnetite

and titanomagnetite. The subsoil group show harder ARM properties than the topsoils. Three of the four bedrock end-members plot close together, showing harder IRM properties than either topsoil or subsoil but with similar ARM hardness. One bedrock sample plots further to the right of this diagram, indicating harder ARM properties than the other three bedrocks. The wind-blown dust samples plot to the left of the bedrock samples, showing harder IRM and softer ARM properties than the bedrock samples.

IRM hardness against squareness biplot for Babicora catchment samples

In the IRM hardness against squareness biplot (Figure 6.14), we see less distinction between the catchment classifications than was apparent in the ARM hardness against IRM hardness biplot (Figure 6.13). The enhanced topsoil material again plots towards the viscous magnetite region of the biplot. Topsoil and subsoil materials show similar SARM/SIRM properties, only being slightly distinguishable by their IRM hardness, with the topsoils tending to be slightly softer than the subsoils. The bedrock and wind-blown dust samples plot below the subsoil material indicating greater IRM hardness. The wind-blown dust material shows a slightly higher SARM/SIRM ratio than the bedrock material.

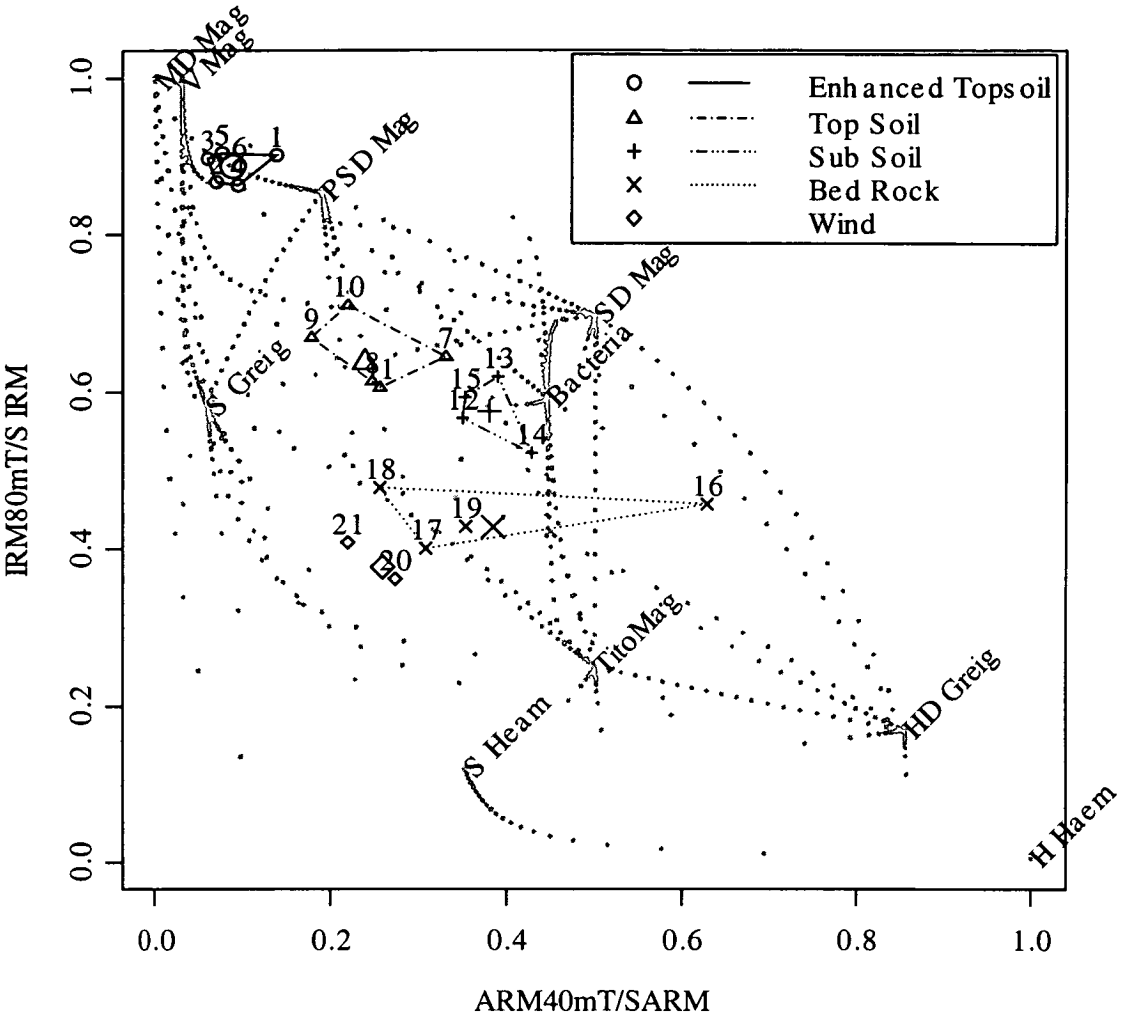

Figure 6.13. Biplot of the IRM hardness, increasing downwards against ARM hardness increasing to the right. The catchment material has been separated into five catchment material classifications. Namely enhanced topsoil, topsoil, subsoil, bedrock and wind-blown dust. Bounding boxes have been drawn around these catchment classifications. Large symbols show the locations of the mean of each classification type. Also plotted are mineral magnetic end-members for reference, and points on the mixing curves between these end-members. For a further explanation see Chapter 2.8.

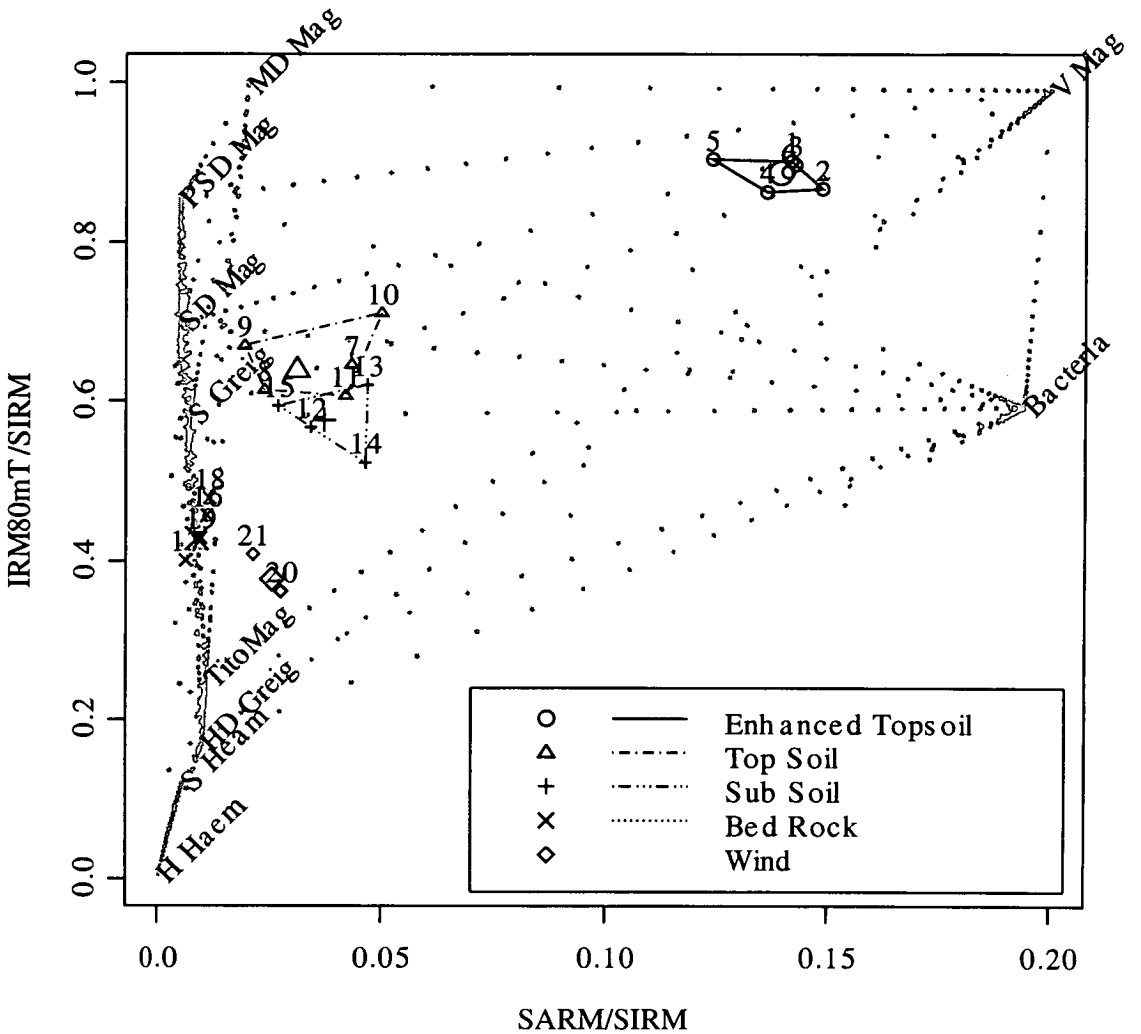

Figure 6.14. Biplot of the IRM hardness, increasing downwards against SARM/SIRM squareness increasing to the right. The catchment material has been separated into five catchment material classifications. Namely Enhanced topsoil, topsoil, subsoil, bedrock and wind-blown dust. Bounding boxes have been drawn around these catchment classifications. Large symbols show the locations of the mean of each classification type. Also plotted are mineral magnetic end-members for reference, and points on the mixing curves between these end-members. For a further explanation see Chapter 2.8.

6.8.6 Catchment sample sieving

Nine of the catchment samples that were collected from Lake Babicora were sieved to identify the dominant size fraction of the magnetic remanence carrying material within them. The nine samples were sieved and centrifuged to split them into five grain-size categories: >500μm, >63μm, >10μm, >2μm and <2μm. The resulting material was then subjected to the same eighteen magnetic measurements as the original sample (Chapter 2.4). Note that unlike the Pátzcuaro ultrasonic treatment was not used to disagregate the samples before sieving. Comparisons of the magnetic properties of the original material compared to the sum of the magnetic properties of the sieved sub-samples are shown in Figure 6.15. The mass specific SIRM contributions of different size fractions for different soil types are given in Figure 6.16, and the mass contribution of each size fraction to the bulk sample is shown in Figure 6.17. Also in Figure 6.17 are the results from two lake sediment samples. Unfortunately the magnetic properties of these samples were not measured, so they could not be included in Figures 6.15 or 6.16.

6.8.7 Comparison between the magnetic properties of unsieved and sieved soils from Babicora

The sum of the magnetic properties of the sieved materials from Babicora's catchment is generally similar to the magnetic properties of the bulk material pre sieving (Figure 6.15). This is not the case for topsoil 8 however, I believed that there was an error during the measurement of both ARM and IRM properties of the sieved material from this sample. Due to the problems with the magnetic measurements of the sieved material from topsoil 8, it was not included in the mass specific SIRM contribution data. One thing of note in Figure 6.15 is that the remanence properties of the topsoil material are generally stronger than the subsoil material. Also note that unlike the soil material from Pátzcuaro, no systematic loss of ARM is apparent in the Babicora catchment size splits. This may be the result of not using ultrasonic treatment to disagregate the soil samples.

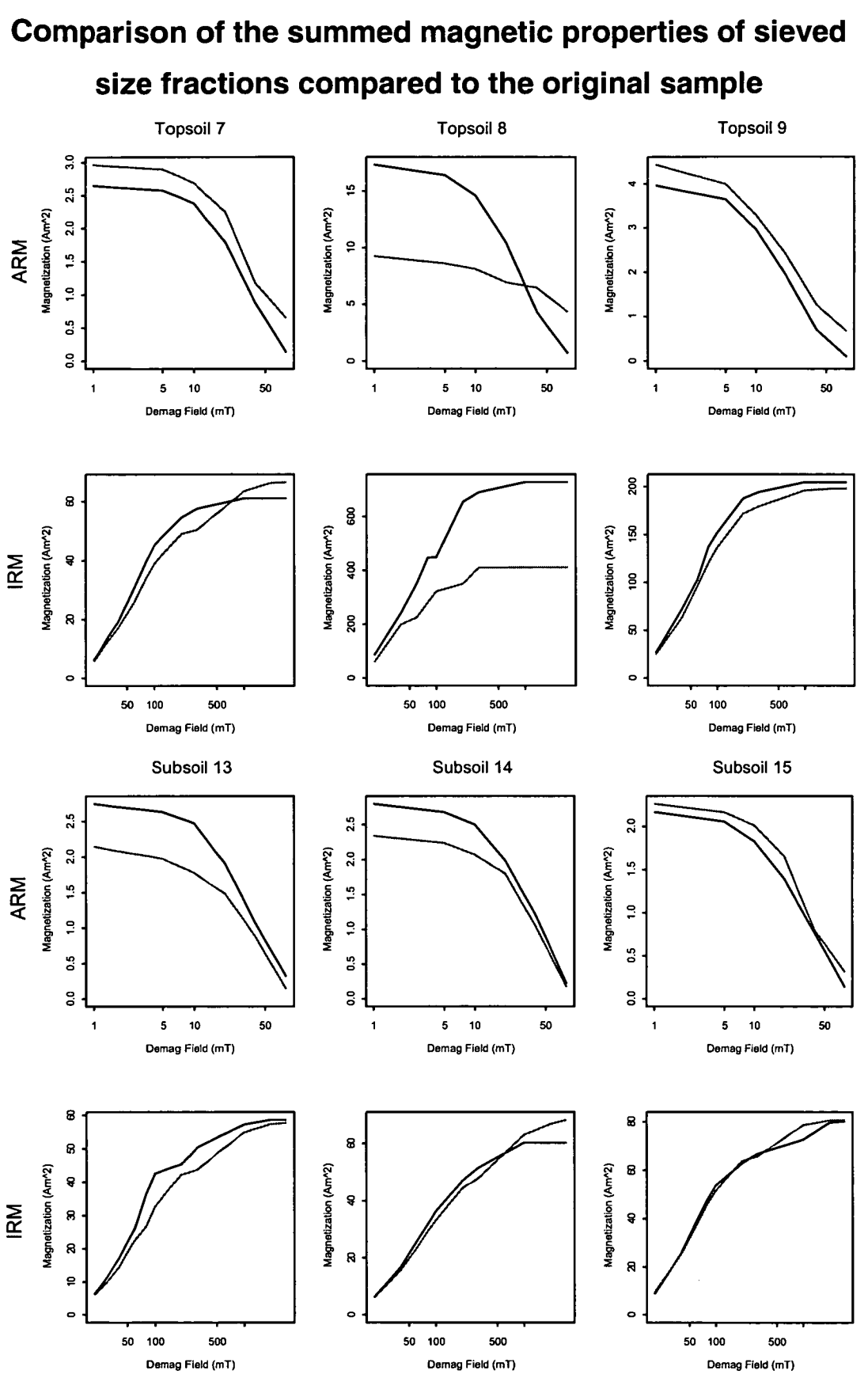

Figure 6.15. The magnetic properties of the sieved samples summed, are plotted in grey, the original sample is plotted in black. Two sets of samples are shown in each case the top row shows ARM demagnetisation and the bottom row shows IRM magnetisation.

6.8.8 Mass specific SIRM contributions for Babicora topsoil and subsoil size fractions

From Figure 6.16 we can see that the coarse sand fraction (>500μm) in the Babicora subsoil material has the highest SIRM per gram of all the size splits. The subsoil material displays a reduction in SIRM intensity with decreasing size. The topsoil material for Babicora also shows relatively strong SIRM properties in the coarse sand size fraction (>500μm), but it is the coarse silt fraction (>10μm) that has the highest SIRM intensity in the topsoils. The prominence of the magnetic properties of the coarse sand fraction may have negative implications for magnetic unmixing if sediment sorting has preferentially removed this material.

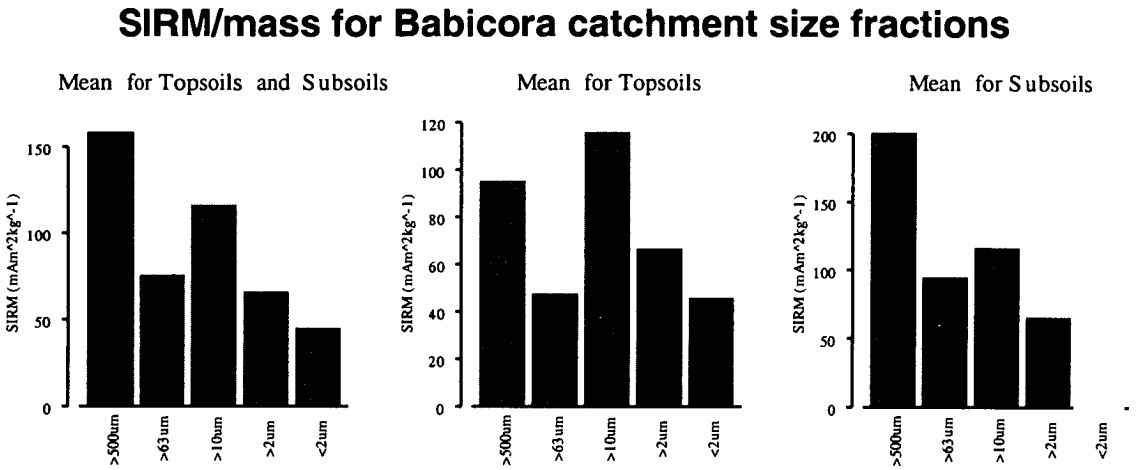

Figure 6.16. Mean SIRM divided by sample mass of size fractions from sieved topsoils and subsoils from the Babicora catchment

6.8.9 Particle size composition for Babicora

Figure 6.17 shows the particle size composition of three topsoils three subsoils and two sediment horizons from the Babicora catchment. Note that the subsoil material, particularly for subsoils 14 and 16, contains far more >500μm material than the topsoils. The core material is generally finer grained than the soil material, although a wide range of size fractions are present, particularly when considering that both of the horizons represented here are described as clay material in the core stratigraphy.

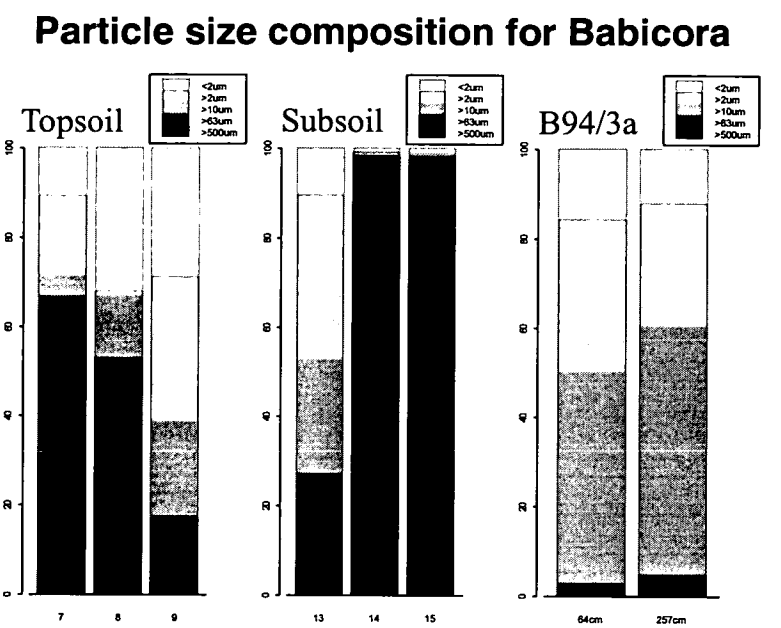

Figure 6.17. Particle size composition for six soils and two lake sediment horizons (B94/3a from 64 and 247 cm depth).

6.9 Magnetic unmixing of Babicora

Four unmixing models have been generated for each of the Babicora cores. Each model uses a different set of end-members to unmix the magnetic properties of the core that is being modelled. Bacterial magnetosomes were not included in any of these models, a test model was run with bacterial magnetosomes together with the end-members used in model 4 (described below). This test model did not include the bacteria end-member, as higher skill was always be achieved without it. Each model can be defined in terms of the end-members used to unmix the magnetic properties of the sediments. Because core B94/3 has dating constraints and has had previous work carried out on it (Metcalfe *et al.*, in press), it has been chosen as the test core for the modelling routines. The results for the modelling of B94/1 can be found in Appendix B, although the final model has been included at the end of this section for comparison. The four model types that have been applied to the cores are:

1. All catchment material.
2. Mean magnetic properties of each catchment end-member
3. Most extreme catchment end-member of each catchment type
4. Set of extreme catchment end-members

In order to decide which end-members to use in the 3rd and 4th models, a principal component analysis (PCA) was carried out on magnetic measurements of the catchment materials. The results of the PCA are represented in Figure 6.18. The plot of the 1st PCA component against the 2nd PCA component provides the largest distinction between the five end-member types. From this diagram the choice of which end-members to use in the 3rd (most extreme catchment end-members) and 4th (set of most extreme catchment end-members) end-member unmixing models was made. The samples chosen for the 3rd unmixing model were enhanced topsoil 3, topsoil 8, subsoil 13, and bedrock 19. For the 4th model four end-members were added to the selection for the 3rd model, namely enhanced topsoil 1, topsoil 9 subsoil 13, and bedrock 16.

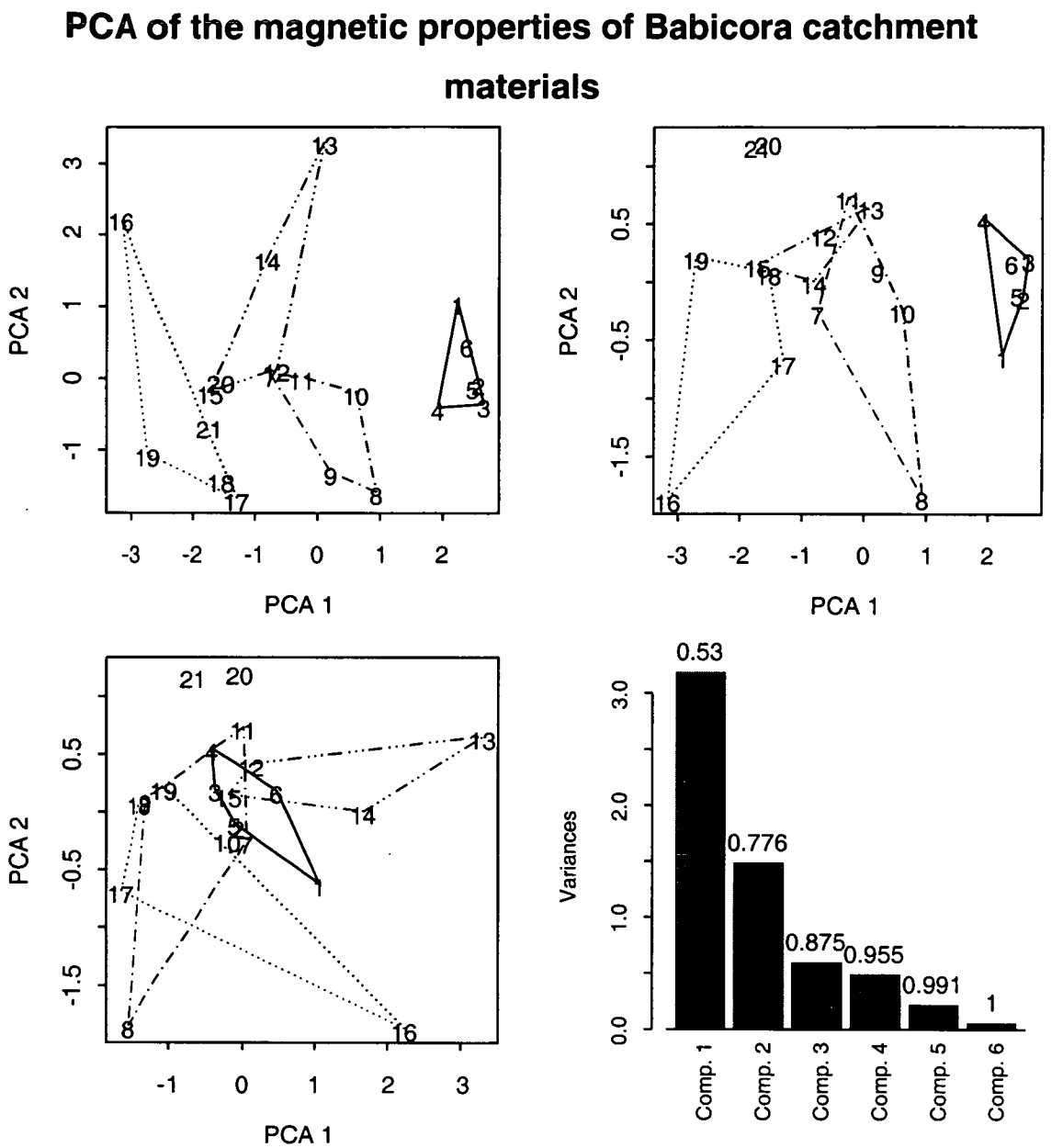

Figure 6.18. Plots of 1st, 2nd and 3rd PCA components of the magnetic properties of the Babicora catchment samples. Numbers 1-6 are enhanced topsoils, 7-11 are topsoils, 12-15 are subsoils, 16-19 are bedrock and 20 and 21 are wind-blown dust samples. Convex hulls have been plotted around each catchment type, except wind-blown dust. Barplot indicates the sum of the variance in the data that is accounted for by the inclusion of all the components up to the component indicated.

6.9.1 Results of unmixing models for B94/3a

Each of the unmixing models for core B94/3a is described below. In each case, the core has been separated into the same four subsections that were used to describe the magnetic properties of that core (Section 6.8.2). However, because core B94/3b is not included in the following models the first of these sections is truncated. The magnetic unmixing results are given in terms of the percentage of the core's mass that, at each sample horizon, is accounted for by a given magnetic end-member. Also plotted on Figure's 6.19, 6.20, 6.21, and 6.22 are the skill of the unmixing models.

All of the unmixing models for cores B94/3b and B94/1 are included for reference in Appendix B.

6.9.2 Model one B94/3a (All catchment material)

Model one for B94/3a (Figure 6.19) is a spiky model: the end-members selected to represent the magnetic properties of the core vary rapidly between core horizons. The class of catchment material that best fits the magnetic data varies on a horizon-to-horizon basis. This sharp switching between horizons is indicative of badly defined end-members. Note also the amount of the core's mass that is represented by a given end-member type can be as much as 300%. The effect of concentration of the magnetic material in a sediment horizon (Figure 6.15) could account for a slight over-estimation of the mass of the core; however, the degree of over-estimation apparent here is of concern.

Bedrock and topsoil dominate section one of model one for B94/3a (Figure 6.19). In section two of the model bedrock presence drops away to a few spikes at the top and bottom of the section. The magnetic properties of section two are mostly modelled with topsoil and subsoil. The topsoil presence in section two peaks at 277cm then falls off towards the top of the section. The presence of subsoil in this model generally increases towards the top of section two. Section three of model one is similar to section two in that the magnetic properties of the core are modelled predominantly with topsoil and subsoil. However, in section three there is also a larger presence of bedrock material. In section four of model one for B94/3a the topsoil and bedrock material fall to nothing within the first 40cm, the rest of the core is modelled entirely with subsoil material. The skill level for B94/3a is high, consistently over 0.9.

6.9.3 Model two B94/3a (Mean magnetic properties of each catchment type)

Model two for B94/3a (Figure 6.20) is far less variable than model one, (Figure 6.19) for the same core. However, there is an inverse relationship between the presence of the subsoil and bedrock end-member types and the topsoil end-member. Note also in this mean end-member model, the modelled mass of the core does not exceed 100% of the core's mass for any given end-member. This means that in this model the problems with overestimation of the cores mass by the unmixing have been avoided.

Section one of model two for B94/3a (Figure 6.20) is entirely modelled with topsoil and bedrock material. In section two, the topsoil end-member is always present, whereas the bedrock end-member comes and goes, with generally higher concentration in the lower and upper parts of the section. Section three of model two has two troughs in the topsoil end-member concentration at 160cm and 150cm depth. These troughs seem to be associated with subsoil peaks. The bedrock end-member is present at the bottom of section three and at one peak toward the top of the section but otherwise is absent. Section four of model two is similar to section four of model one in that it is almost entirely modelled with subsoil type material. The concentration of the subsoil material is higher at the top and bottom of section four. The skill for model two of B94/3a (Figure 6.20) is generally high except for in section four where it drops to an average of 0.82.

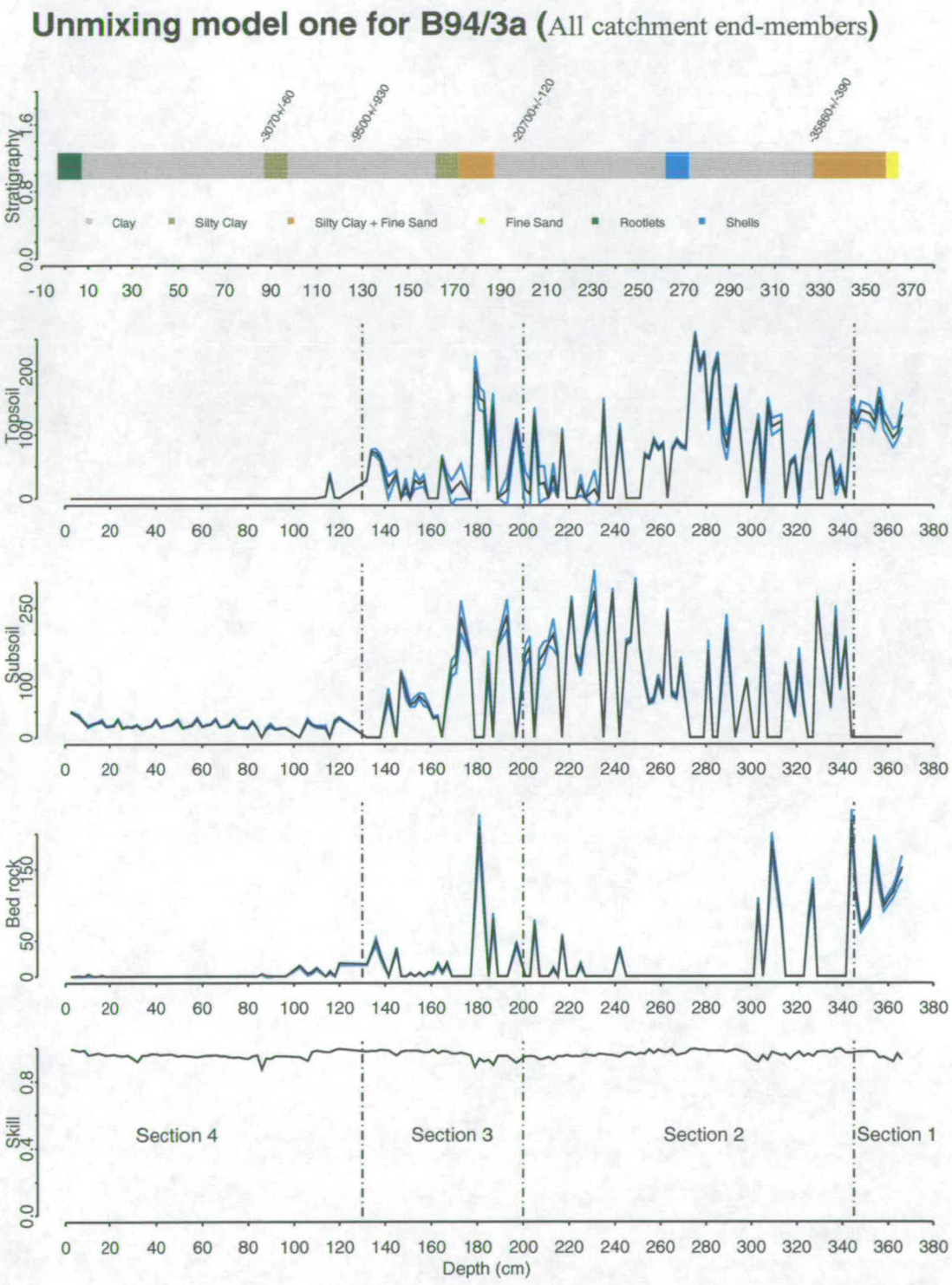

Figure 6.19. Magnetic unmixing model one (all Babicora catchment end-members) for B94/3a. Plots show the percentage of the core's mass explained by unmixing end-members against depth. Also plotted are the stratigraphy and radio carbon dates on the core. Vertical broken lines denote boundaries between core sections.

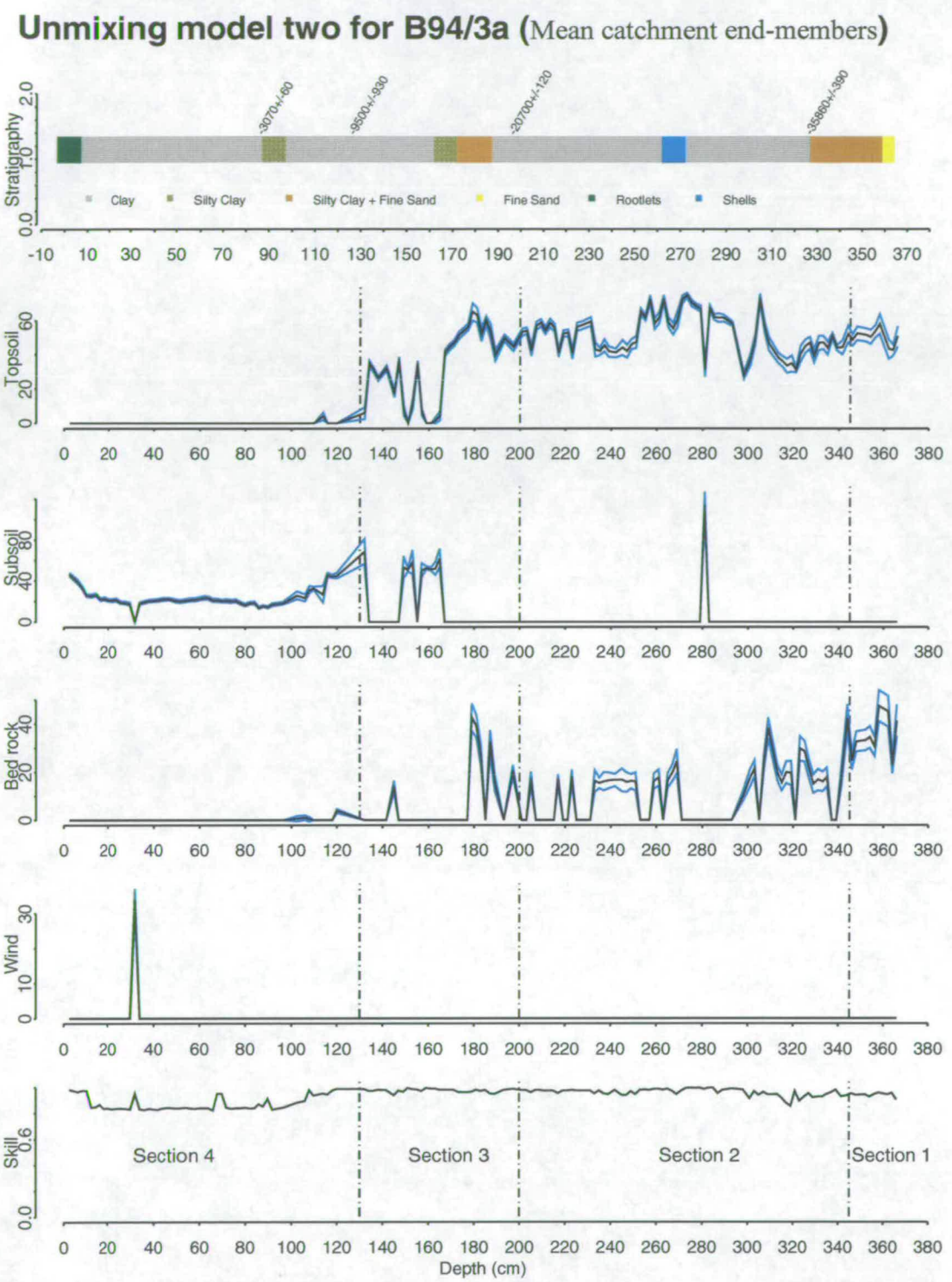

Figure 6.20. Magnetic unmixing model two (mean magnetic properties of each catchment end-member type) for B94/3a. Plots show the percentage of the core's mass explained by unmixing end-members against depth. Also plotted are the stratigraphy and radio carbon dates on the core. Vertical broken lines denote boundaries between core sections.

6.9.4 Model three for B94/3a (Most extreme catchment material)

The topsoil and subsoil end-member types of model three for B94/3a (Figure 6.21), show a strong resemblance to those in model two. However bedrock material is almost absent in this model.

Section one of model three for B94/3a, (Figure 6.21) is dominated by the topsoil end-member type. However there is a presence of subsoil material, but the unmixing inversion errors associated with subsoil are large. Section two of model three is mostly modelled with topsoil material. Subsoil material is at the bottom of section two, and for a prolonged horizon between 300cm and 275cm. In section three there is a drop in the concentration of topsoil type material. Between 170cm and 150cm in section three this unmixing model has included topsoil material. Section four is again dominated by subsoil material. The skill level for model three for B94/3a, (Figure 6.21), are generally high being consistently above 0.9.

6.9.5 Model four B94/3a (Set of extreme catchment materials)

The fourth model for B94/3a (Figure 6.22) uses two samples from each end-member type to unmixing the magnetic properties of the core. In the model that results from these unmixing end-members, an immediate similarity to model three and four is apparent.

Section one of model four for B94/3a (Figure 6.22) is predominantly modelled with topsoil and subsoil, though there is one peak of bedrock material at the bottom of the section. Like model three for the same section, there is a large degree of error in the subsoil end-member for section one. Section two of model four is dominated by topsoil material, although subsoil and bedrock are present in sporadic peaks, particularly in the bottom half of this section. Section three of the fourth unmixing model on B94/3a shows a gradual decline in the concentration of the topsoil end-member and a sudden appearance and continued presence in the subsoil end-member. The presence of the subsoil material lasts throughout section four. The skill of model four is again high, only falling below 0.9 once.

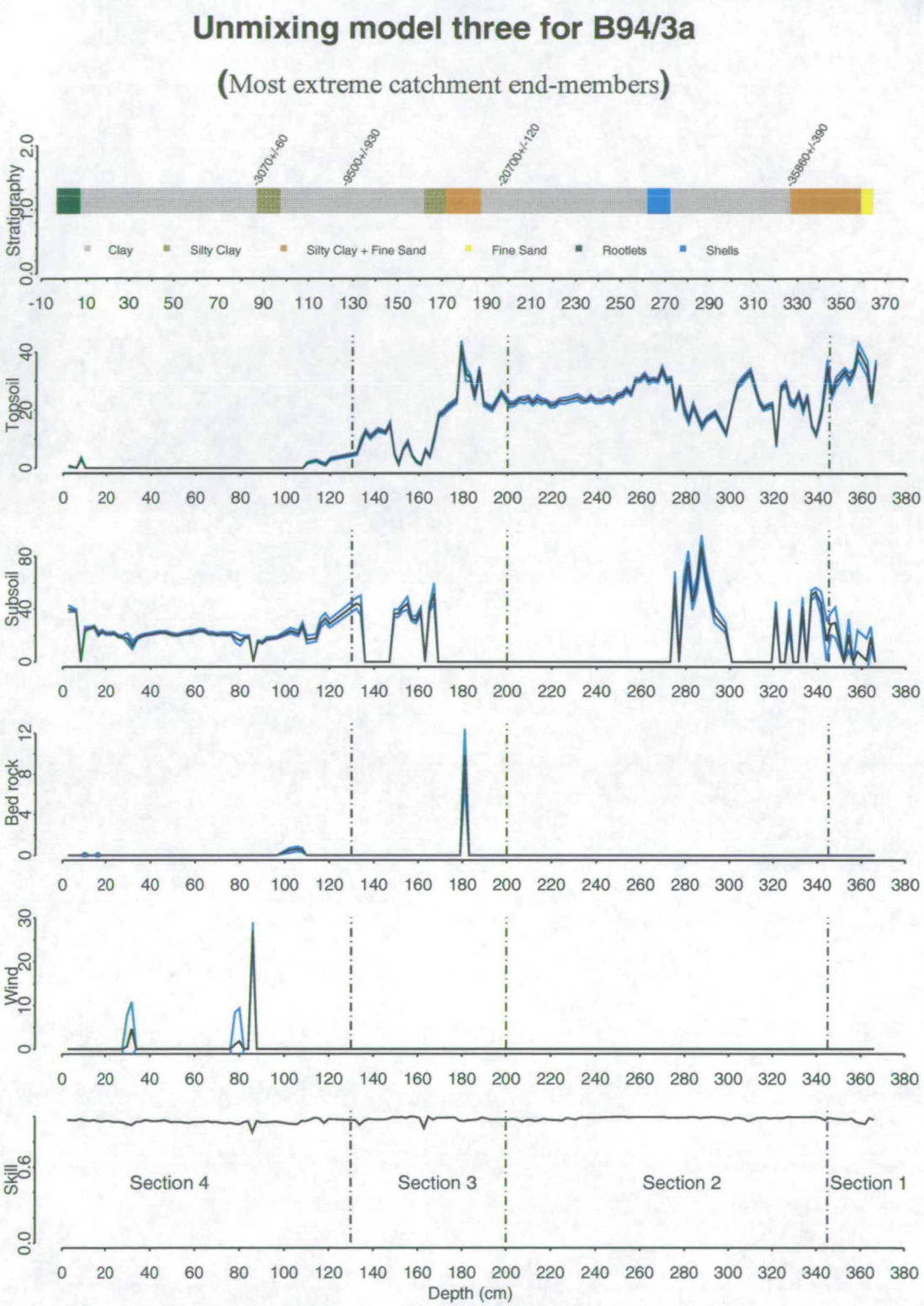

Figure 6.21. Magnetic unmixing model three (most extreme of each catchment end-member type) for B94/3a.. Plots show the percentage of the core's mass explained by unmixing end-members against depth. Also plotted are the stratigraphy and radio carbon dates on the core. Vertical broken lines denote boundaries between core sections.

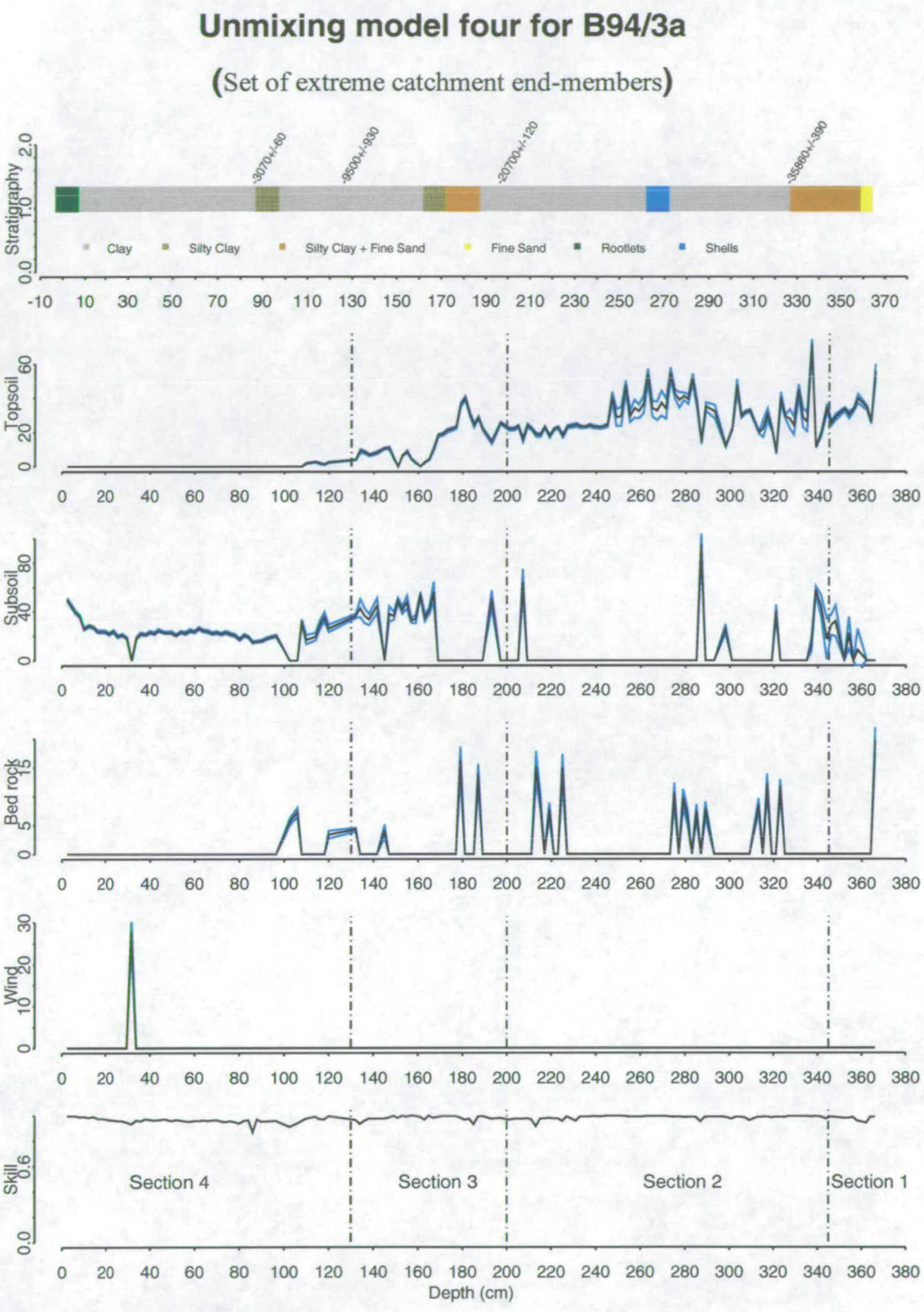

Figure 6.22. Magnetic unmixing model four (set of extremes of each catchment end-member type) for B94/3a. Plots show the percentage of the core's mass explained by unmixing end-members against depth. Also plotted are the stratigraphy and radio carbon dates on the core. Vertical broken lines denote boundaries between core sections.

6.9.6 Summary of models one to four on cores B94/3a, B94/3b and B94/1

Table 6.1 contains the mean skill and correlation coefficients between end-members for the four models made on each of the three Babicora cores. Negative correlation coefficients may indicate a model that switches between end-member types because it could not differentiate them.

From Table 6.1 the 4th (set of extreme catchment end-members) models, were chosen to unmix each of the cores. These models were chosen because they consistently display the highest skill and generally have positive or low negative correlation coefficients between end-member types. The fourth model for B94/3a does have a large negative correlation coefficient between topsoil and subsoil. However, I believed this is due to the change from topsoil to subsoil domination at the top of the core and not to swapping between poorly defined end-members.

Summary of unmixing models on each of the Babicora cores

Core and Model	Mean skill	Correlation between topsoil and subsoil	Correlation between topsoil and bedrock	Correlation between subsoil and bedrock
B94/1 model 1	0.966	-0.561	0.253	-0.319
B94/1 model 2	0.959	-0.560	-0.163	-0.252
B94/1 model 3	0.961	-0.160	-0.255	0.142
B94/1 model 4	0.975	-0.315	-0.143	-0.221
B94/3a model 1	0.960	-0.356	0.560	-0.345
B94/3a model 2	0.931	-0.718	0.482	-0.404
B94/3a model 3	0.972	-0.503	0.133	-0.066
B94/3a model 4	0.973	-0.596	0.262	-0.269
B94/3b model 1	0.970	-0.659	0.223	-0.308
B94/3b model 2	0.902	-0.625	-0.099	0.313
B94/3b model 3	0.964	-0.601	-0.201	-0.161
B94/3b model 4	0.964	-0.670	-0.305	0.366

Table 6.1 The mean skill of, and correlation coefficients between the end-member types of the four models for each of the three cores from Babicora.

6.9.7 Model four for Core B94/3b (Set of extreme catchment materials)

The model four unmixing results for B94/3b are shown in Figure 6.24. The core has been separated into two sections with the section boundary in the same place as it was for describing the magnetic properties of the B94/3 composite core Figure 6.7.

Section one of model four for B94/3b (Figure 6.24) is modelled almost entirely with the topsoil and subsoil end-members. The concentration of the topsoil end-member in section one increases from the bottom of the section towards the top. The lower part of section one has higher concentrations of subsoil material than the top. The errors on the subsoil material concentration for model four on core B94/3b are generally high. In section two of model four on core B94/3b there is a decrease in the concentrations of topsoil material and an increase in subsoil material. The skill level for this model is not as high as the skill for the same end-member models made on either of the other two cores, but still averages at 0.964, and is consistently well above 0.8.

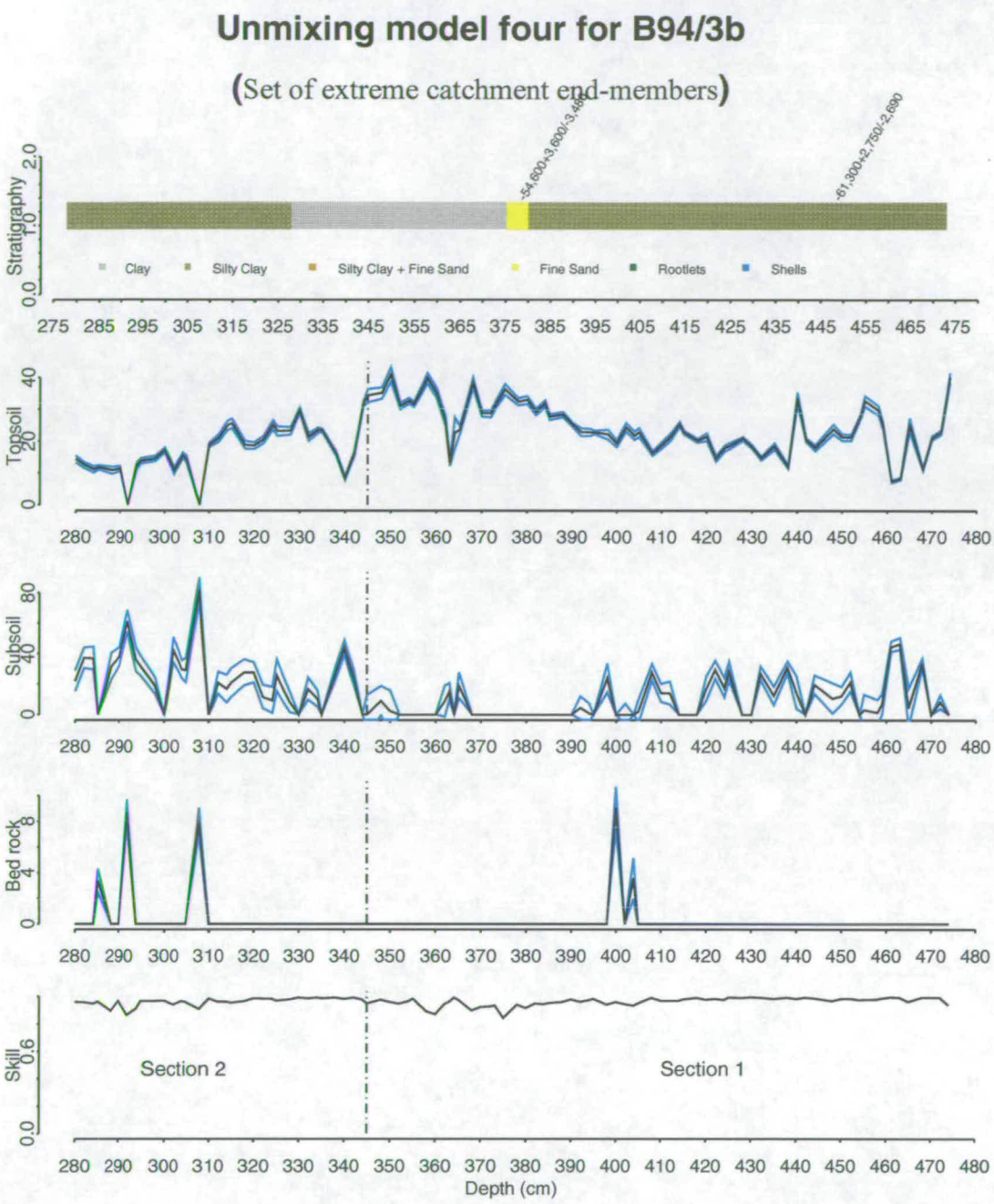

Figure 6.23. Magnetic unmixing model four (set of extremes of each catchment end-member type) for B94/3a. Plots show the percentage of the core's mass explained by unmixing end-members against depth. Also plotted are the stratigraphy and U series dates on the core. Vertical broken lines denote boundaries between core sections.

6.9.8 Combining the B94/3a and B94/3b models

The models for B94/3a and B94/3b are plotted in Figure 6.25 side by side, with the 75cm depth correction applied to B94/3b. Topsoil concentration is similar in both models around the line separating section one and section two. Although some features of the subsoil curve also match, the similarity is less obvious. The bedrock material is even less well matched between the two models. A composite model has been generated for the B94/3 core (Figure 6.25) by splicing the two models at 345cm this is the boundary between the first and second section of the core.

6.9.9 Model four for core B94/1 (Set of extreme catchment materials)

The fourth model for B94/1 is shown in Figure 6.23. This model is dominated by topsoil and subsoil, but also includes sporadic occurrences of bedrock and wind-blown dust. Model four for B94/1 has been split into the same three sections used to describe the magnetic properties of the core.

Section one of model four for B94/1 has high concentrations of topsoil and subsoil material. The topsoil concentration falls towards the top of section one. The second section of model four on B94/1 is again dominated by topsoil and subsoil type end-members. However, section two has lower concentrations of topsoil than section one and the subsoil material concentration seems less variable from horizon to horizon. In section three, there is a dramatic drop in topsoil material, and a slight increase in subsoil material. Wind-blown dust and bedrock derived material also sporadically appear in section three. The skill level for this model is high, averaging at 0.975, but drops towards the top of section three to around 0.9.

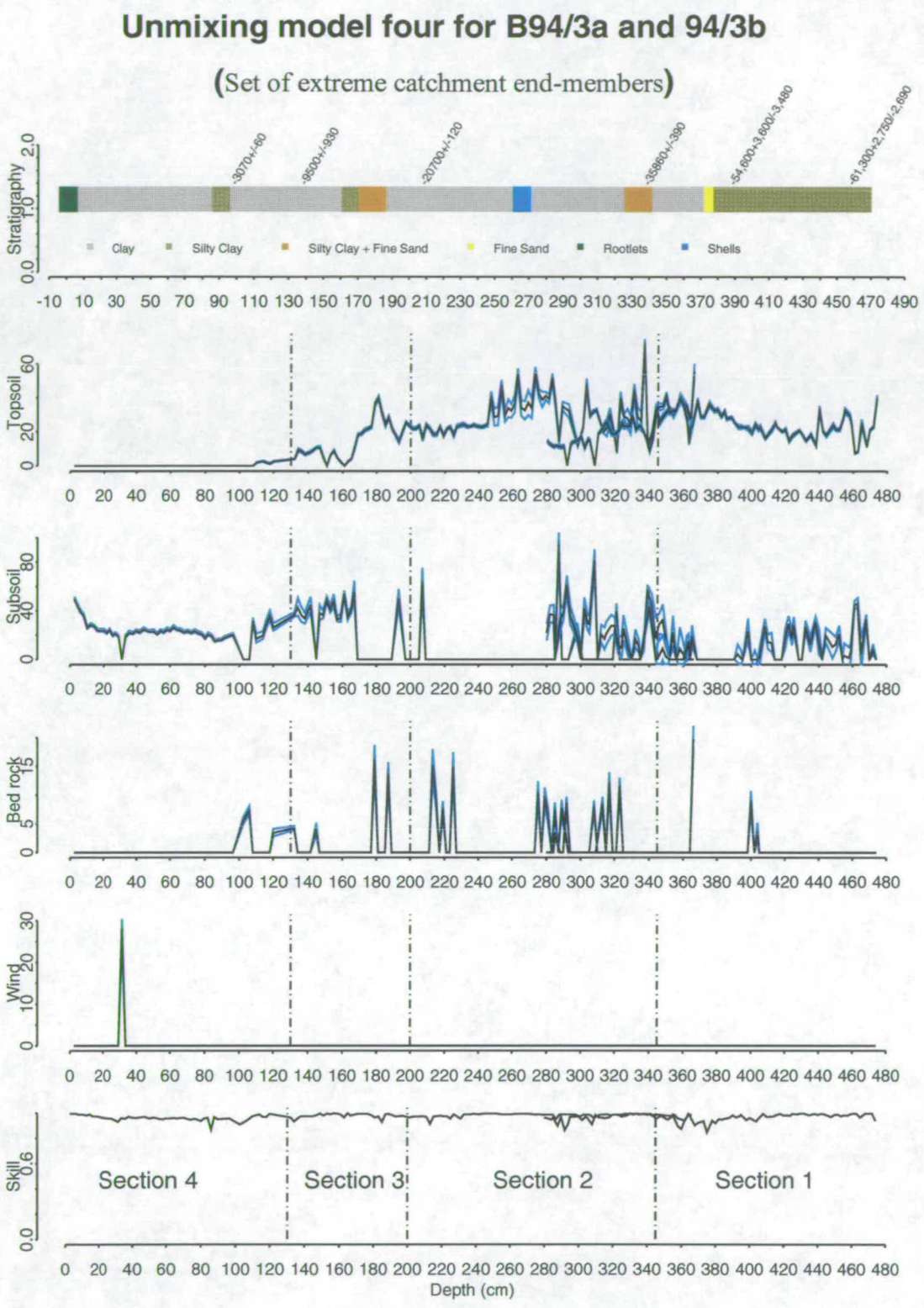

Figure 6.24. Magnetic unmixing model four (set of extremes of each catchment end-member type) for B94/3a and B94/3b plotted together. Plots show the percentage of the core's mass explained by unmixing end-members against depth. Also plotted are the stratigraphy and radio carbon and U series dates on the core. Vertical broken lines denote boundaries between core sections.

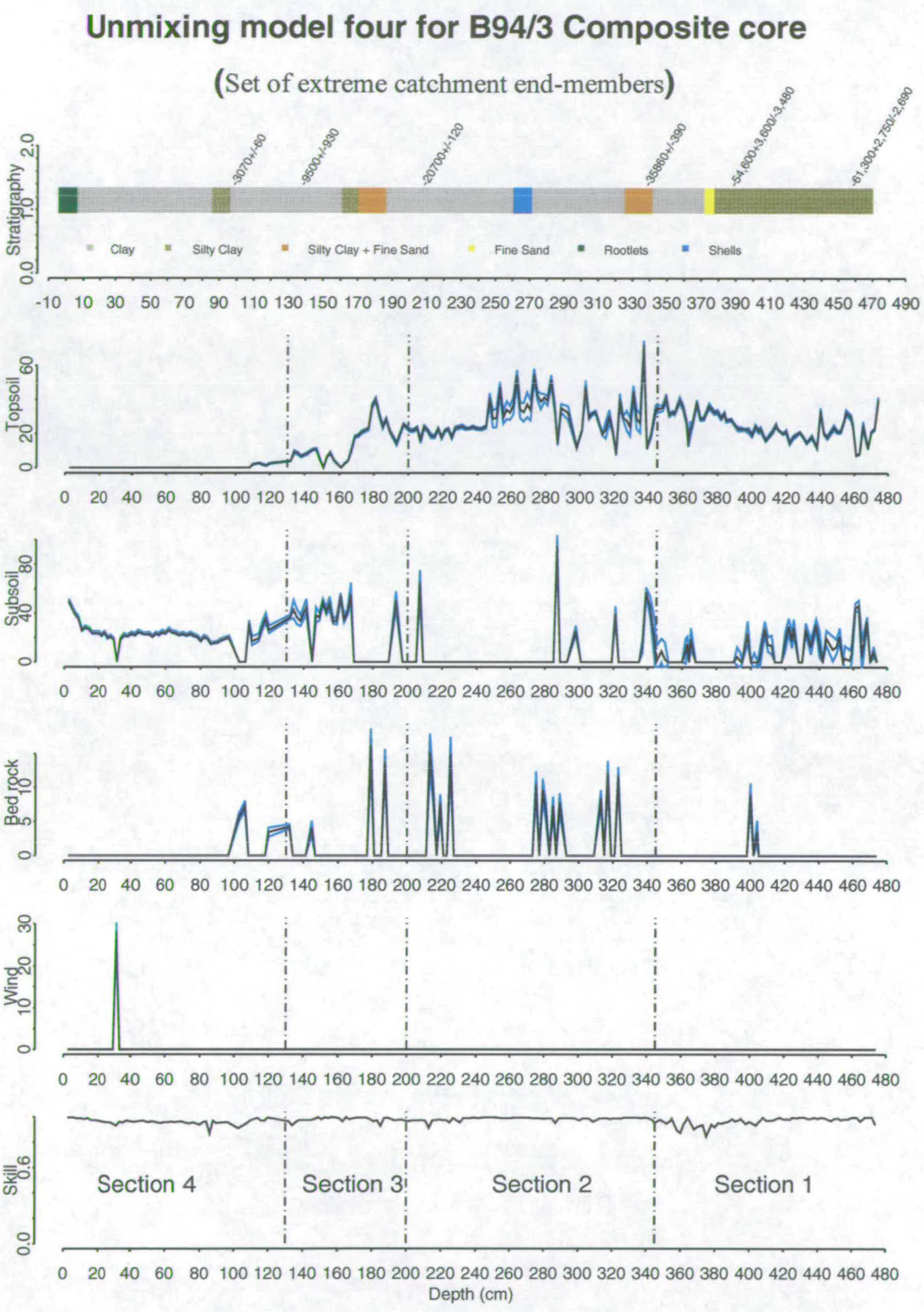

Figure 6.25.. Magnetic unmixing model four (set of extremes of each catchment end-member type) for B94/3, made by splicing models four for B94/3a and B94/3b at 345cm. Plots show the percentage of the core's mass explained by unmixing end-members against depth. Also plotted are the stratigraphy and radio carbon dates on the core. Vertical broken lines denote boundaries between core sections.

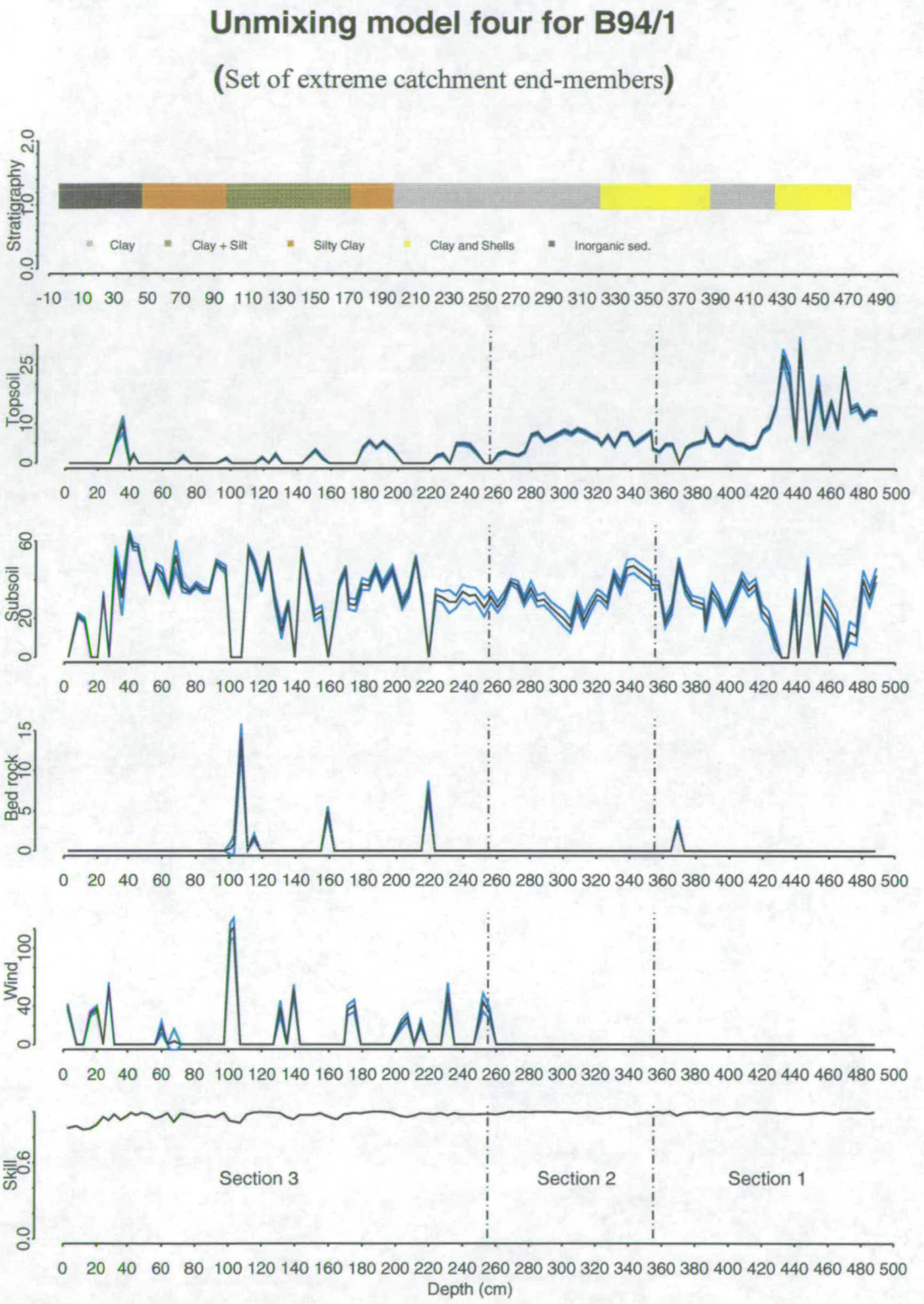

Figure 6.26. Magnetic unmixing model four (set of extremes of each catchment end-member type) for B94/1. Plots show the percentage of the core's mass explained by unmixing end-members against depth. Also plotted are the stratigraphy and radio carbon dates on the core. Vertical broken lines denote boundaries between core sections.

6.9.10 Summations of end-members

By adding together the contributions of end-members in the unmixing models, a better insight of erosional processes in the Babicora catchment can be gained. In Figure 6.27 and Figure 6.28 the contributions of the subsoil and bed-rock end-members have been summed to produce a "deep erosion" plot and the subsoil, topsoil and bed-rock have been summed to produce an "all erosion" plot.

Summations of end-members from model four for B94/1

In the summation of end-members plot for model four on B94/1 (Figure 6.27) topsoil erosion accounts for at most 30% of the mass of the core. For the majority of the model, above section one, the topsoil erosion figure is less than 10% of the cores mass. The deep erosion signal never exceeds 60% of the mass of the core, and averages less than 30%. Similarly the all erosion plot only exceeds 60% of the cores mass at one horizon near the top of section three. The mean mass of B94/1 accounted for by unmixing model four is just under 35%. The wind-blown dust end-member for model four on B94/1 shows very high concentrations, with one horizon accounting for over 100% of the mass of the core.

Summations of end-members from model four for B94/3

The summation of end-members plot for model four on core B94/3 (Figure 6.28) has a greater input of topsoil material than the same model for core B94/1. The topsoil end-member for sections one, two and three of B94/3 is always present and consistently accounts for over 20% of the cores mass. The mean input of topsoil material for model four for B94/3 is 18.7% of the core's mass. The deep erosion signature for model four on B94/3 shows only sporadic inputs of the deep erosion end-members until the middle of section two. Deep erosion increases dramatically, from the middle of section two, accounting for between 20% and 50% of the cores mass. The mean deep erosion signature for model four on B94/3 is 14%, but the mean Figure for the upper core, above 170cm, is 23%. The total erosion signature for B94/3 is generally well below 60%, with the highest erosion seen in sections two and three.

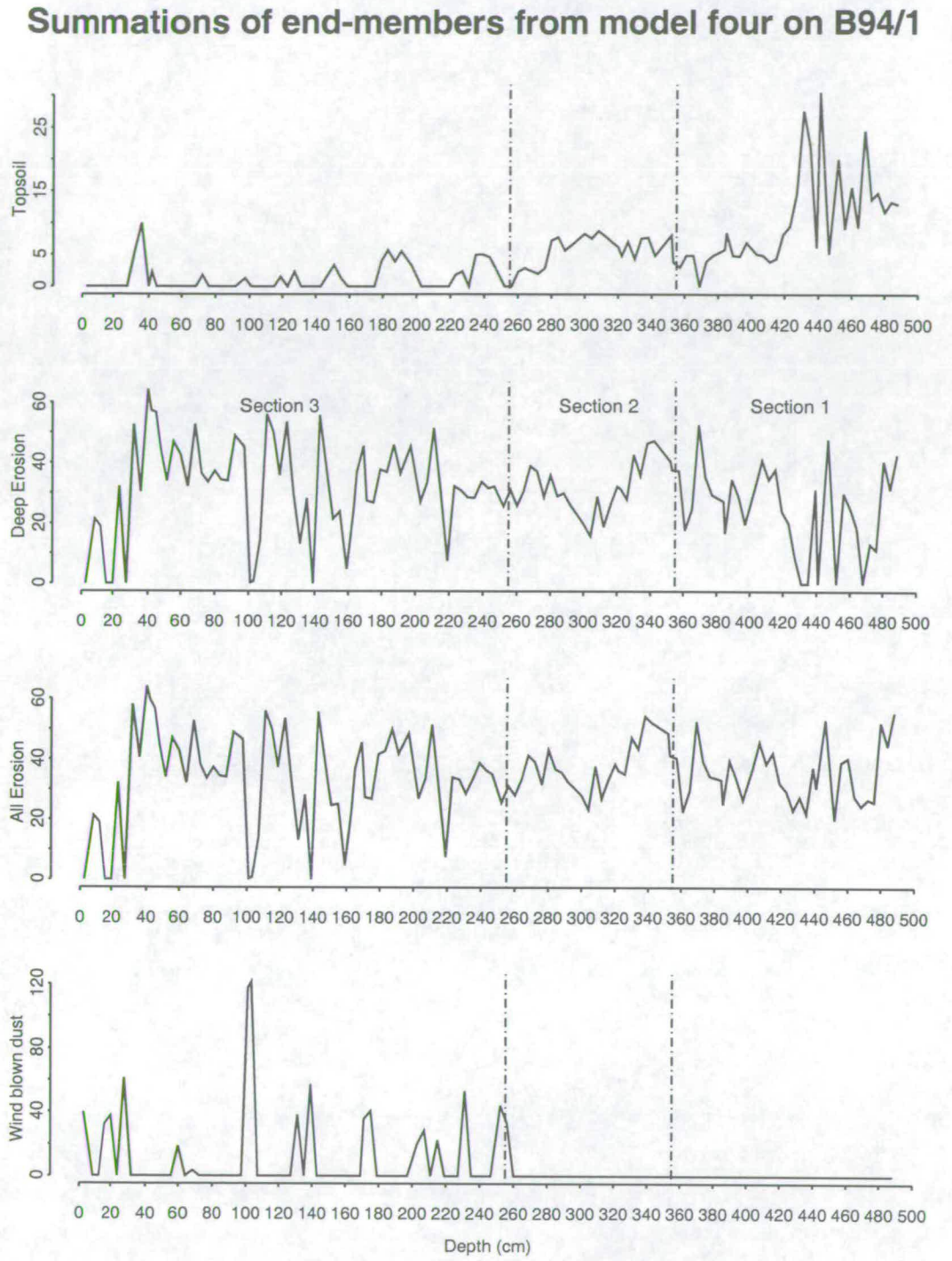

Figure 6.27. Summation of elements from unmixing model four (set of extreme catchment end-members) for B94/1. Shown are the contributions of topsoil material, deep erosion, (given by adding subsoil and bedrock end-members), all erosion, (from adding the contributions of topsoil subsoil and bedrock end-members) and the contribution of wind-blown dust. All summations are given in terms of the percentage of the core's mass accounted for by the given element.

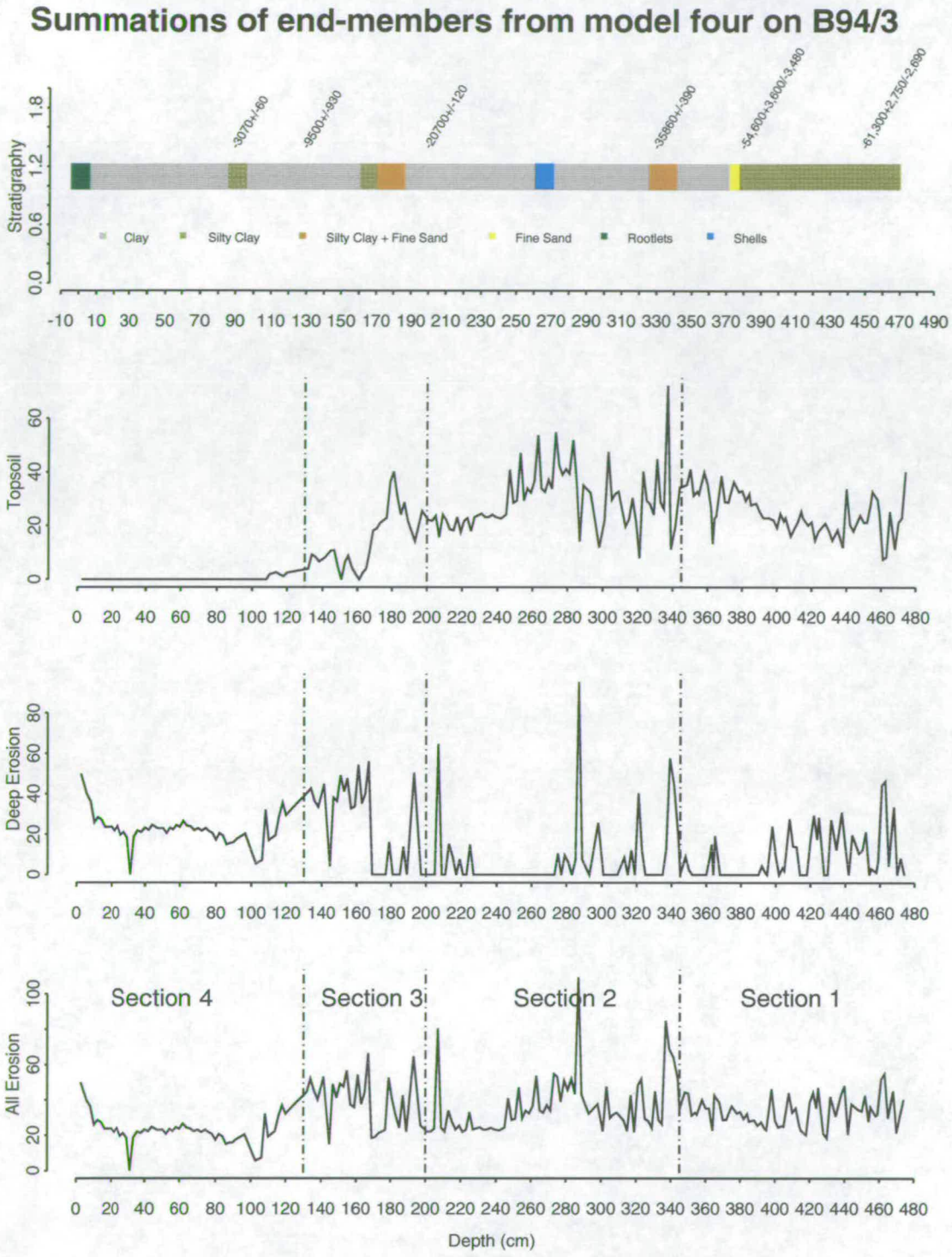

Figure 6.28. Summation of elements from unmixing model four (set of extreme catchment end-members) for B94/3. Shown are the contributions of topsoil material, deep erosion, (given by adding subsoil and bedrock end-members), and all erosion, (from adding the contributions of topsoil subsoil and bedrock end-members). All summations are given in terms of the percentage of the core's mass accounted for by the given element.

6.10 Interpretation of magnetic unmixing

Because core B94/3 has some dating control, it will be the more significant core in the interpretation of the magnetic unmixing models. For this reason I interpret the unmixing model on B94/3 before the model for B94/1. The unmixing models on B94/3 and B94/1 are described in the same sections that were used for describing their magnetic properties. Unfortunately because only one of the cores used in this study was dated, inferences on the state of the entire catchment are made from the study of a single core.

6.10.1 Interpretation of unmixing model four on B94/3

Figure 6.29 is a schematic diagram of the interpretation of the magnetic unmixing model for B94/3 described below. In the interpretation of the unmixing model of B94/3 all dates given, unless explicitly stated, are approximations which have been derived from the available radio carbon and U series dates on the core by assuming a constant rate of deposition between dates.

Section one

Section one of model four for B94/3 (Figure 6.26), 65,000 – 43,000yr B.P., starts with high levels of topsoil erosion in the catchment and sporadic layers of subsoil erosion. The subsoil erosion tapers off at around 390cm, just below a U series date of 54,600+3,600/-3,480yr B.P.. This period, from the bottom of the core to 390cm seems to be quite a variable time in the catchment, some deep erosion is taking place (Figure 6.26), but this input is not constant. The deep erosion may be due to gullying during high energy storm events. Metcalfe *et al.*, (in press) describe the catchment during this period of deposition as a high-energy environment, reporting large numbers of broken and crumpled pollen grains.

From 440cm up to the top of section one there is a steady increase in the topsoil erosion component in the unmixing model. The increasing topsoil erosion may indicate that rainfall in the catchment was becoming less seasonal and less intense. A reduction in the intensity of rainfall, and a climate change to less seasonal rainfall conditions could allow more topsoil material to be produced in the catchment by increasing vegetation cover. However, because the topsoil material is being delivered to the core site, there must still be some degree of instability in the catchment. The period of increasing topsoil erosion in the model is briefly interrupted at 363cm, which corresponds to approximately 48,000yr B.P.. This point of reduced topsoil erosion may correspond with a lake shallowing period indicated in the diatom record that occurred around 50,000yr B.P. (Metcalfe *et al.*, in press).

Section two

During the second section of model four on B94/3 (43,000yr B.P. – 21,000^{14}Cyr B.P.) (Figure 6.26), the magnetic properties of the core sediment are almost entirely modelled with topsoil material. From the bottom of the section (345cm) to 285cm depth (43,000yr B.P. – 31,000^{14}C yr B.P.) the topsoil end-member is highly variable, ranging from over 60% to under 10% of the core mass. During this period there are occasional horizons of subsoil and bedrock end-members. This part of the model (345cm to 285cm depth) is indicative of a high energy catchment, with deep erosion, and is similar to the material at the bottom of the core up to 390cm. Sporadic large

inputs of topsoil may be associated with storm events. Metcalfe *et al.* (in press) interpret the diatom and pollen data from much of this period as indicating lower lake levels. The chemical data for this period also indicate a high-energy environment (Metcalfe *et al.*, in press). Low lake levels, as indicated by the diatom data, would result from a lower effective humidity. A combination of low effective humidity, deep erosion and variable topsoil erosion suggests that the rainfall during this period (43,000yr B.P. – 31,000^{14}C yr B.P.) was highly seasonal.

Above 285cm there is a marked increase in the topsoil end-member concentration, which then decreases between 260cm and 240cm (28,000 to 26,000^{14}C yr B.P.) before stabilising towards the top of the section (200cm). No deep erosion is seen between 273cm and 215cm, (29,000 and 24,500^{14}C yr B.P.). Conversely to the lower part of section two, the upper part of section two seems to record a period of catchment stability. The decreasing concentration of the topsoil end-member between approximately 28,000 and 26,000^{14}C yr B.P. may indicate a change to less seasonal rainfall. The deep erosion after 24,500^{14}C yr B.P., indicates another period of catchment instability, possibly caused by reduced or more seasonal rainfall limiting vegetation cover resulting in gullying (Chapter 3.5.1). If the higher erosion was caused by a reduction in rainfall reducing vegetation cover, we could expect the rainfall to be lower than 800mm a year (Figure 3.11). Diatom and pollen data indicate that much of section two of the core is associated with a deep freshwater lake. However, diatom evidence suggests that after 29,000^{14}C yr B.P. the lake was shallower than it was previously.

Section three

In section three of model four (approximately 21,000 – 10,000^{14}C yr B.P.) (Figure 6.26), for B94/3 there is a dramatic shift from a topsoil-dominated model to a subsoil-dominated model. From the bottom of section three (200cm) there is a rapid increase in the topsoil end-member concentration up to a peak of around 30% of the core's mass at 180cm, (approximately 18,000^{14}C yr B.P.). This rise in the topsoil end-member concentration is followed by an equally rapid fall, which lasts until 160cm (approximately 15,000^{14}C yr B.P.), at which point topsoil erosion falls to zero for the first time in this model. The initial increase in the topsoil end-member concentration (200cm - 180cm) occurs at the same time as bedrock end-member inclusion in the unmixing model. Just above 160cm (approximately 15,000^{14}C yr B.P.) prolonged subsoil end-member inclusion is established. The initial large rise in the topsoil end-member concentration at the same time as bedrock erosion in the catchment indicates a period of high catchment instability between 21,000 and 18,000^{14}C yr B.P. This instability is also reported in the geochemistry for this part of the core (Metcalfe *et al.*, in press). The reduction of the topsoil end-member concentration between 180cm and 160cm (18,000 - 15,000^{14}C yr B.P.) coinciding with a switch to subsoil erosion indicates a change in erosional processes. Rather than shallow topsoil erosion, most of the material delivered to the core site is coming from deeper in the soil profile. This suggests that the deep erosional structures which are now prolific in the Babicora catchment (Figure 3.12) may have been formed at this time. Deep erosional features are likely to occur if vegetation cover is reduced (Chapter 3.5.1). The subsoil seen in the unmixing model (Figure 6.26) is most likely an indication that climate had changed in a manner that was not beneficial to the plant life in the Babicora basin. It may be that this change was an increase in the seasonality of precipitation, and a change to conditions that are prevalent at present.

Between 160cm and 150cm there is a small peak of topsoil erosion, which then falls to zero again at 150cm (13,000^{14}C yr B.P.). Another small topsoil erosion peak occurs at 145cm (12,000^{14}C yr B.P.) before a slow decline to zero at a depth of 110cm. Neither of these topsoil peaks account for more than 15% of the cores mass. Metcalfe *et al.*,(in press) report a shallowing of the lake in the diatom record around 12,700^{14}C yr B.P. (15,000 cal yr B.P.) followed by an increase in lake level. The reduction in rainfall seen by Metcalfe *et al.*, (in press) may explain the loss of topsoil material in the model at 13,000^{14}C yr B.P. as being the result of a reduction in precipitation. However Urrutia-Fucugauchi *et al.*, (1997) and Ortega-Ramirez *et al.*, (1998) both report high lake levels between 16,000yr B.P. and 11,000 yr B.P. in the south of the lake, although the high lake levels they report are relative to the lower lake levels later in the sequence.

Section four

Section four of model four for B94/3 (10,000^{14}C yr B.P. to present) (Figure 6.26) is dominated by the subsoil unmixing end-member. There is some topsoil erosion in the upper part of section four, which stops at 110cm (7,500^{14}C yr B.P.). Subsoil concentration falls after 150cm (the point where it first appears in section two), until just below 100cm, where it falls to zero and is replaced by bedrock type erosion. The subsoil end-member then re-emerges with a near constant concentration almost to the top of the core, where the concentration increases for the last 20cm. The initial reduction in the topsoil end-member concentration between 130cm and 105cm, (10,000 – 7,500^{14}C yr B.P.) may be due to a reduction in precipitation between these points. Urrutia-Fucugauchi *et al.*, (1997) and Ortega-Ramirez *et al.*, (1998) both see a progressive reduction of precipitation from 11,000^{14}C yr B.P., and Metcalfe *et al.*, (1997) report increasing concentrations of $CaCO_3$, associated with lake shallowing. There is very little change in the model between 95cm and 20cm, with a near constant presence of subsoil material. This region of the core seems to represent similar conditions to those that presently exist in Babicora: low rainfall, falling seasonally and creating deep erosional channels. The increase in subsoil erosion towards the top of the core may indicate that human activities in the catchment at present are accelerating erosion. The wet period that is reported in Urrutia-Fucugauchi *et al.*, (1997) and Metcalfe *et al.*, (1997) as occurring between 6,500 and 2,700 yr B.P. is not seen in the magnetic unmixing model.

Summary of the unmixing model four on B94/3 compared with previous studies

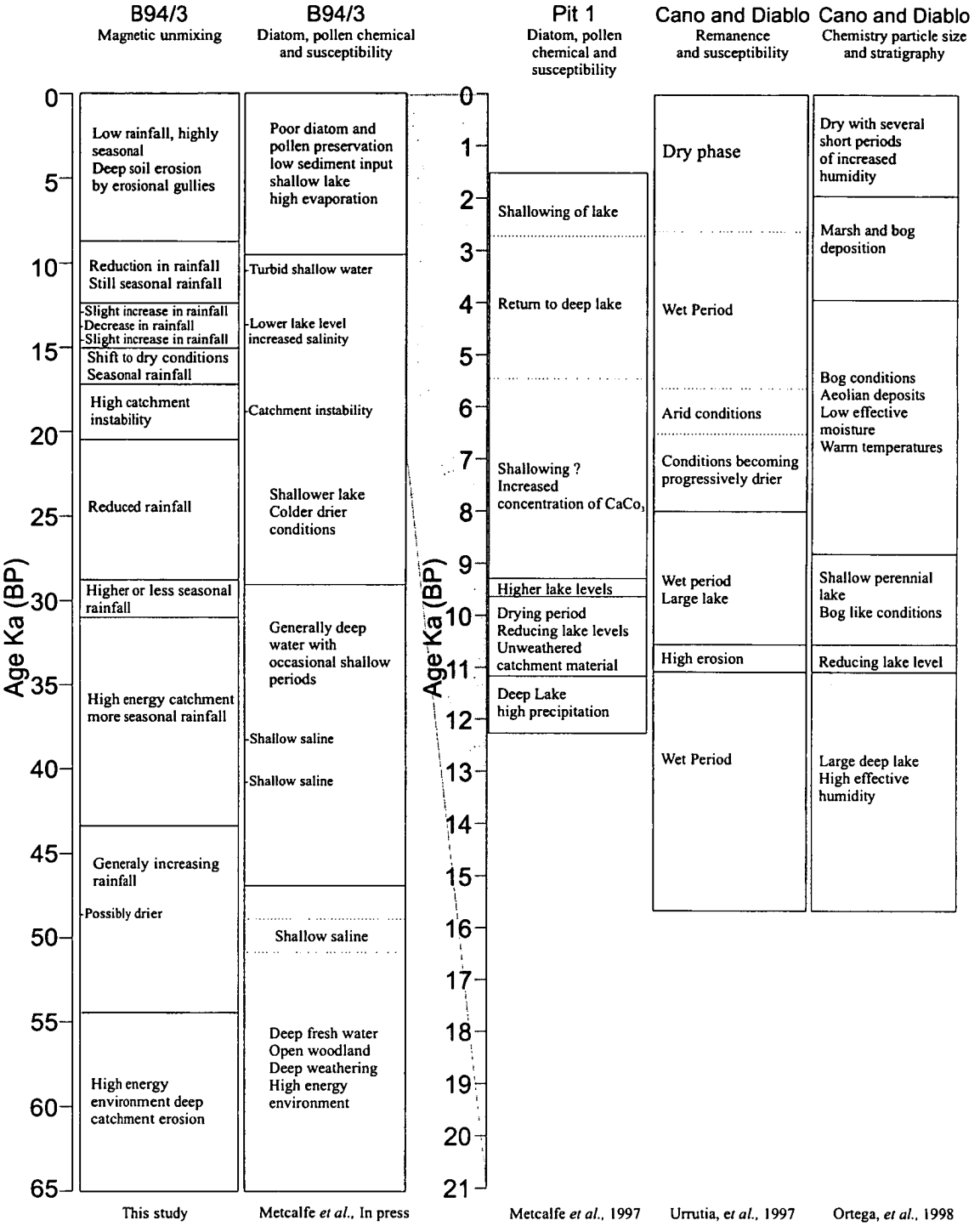

Figure 6.29. Comparison between a summary of the magnetic unmixing model on B94/3 and other studies carried out on cores from Lake Babicora. Dotted lines indicate uncertainty in dates. Note different time scale for B94/3 and the other three studies.

6.10.2 Interpretation of unmixing model four on B94/1

Unfortunately no dates are available for the material from B94/1, which makes the interpretation of the core somewhat difficult. However, a link between the diatom flora in B94/3 and B94/1 Figure 6.3, Section 6.4 suggests that B94/1 covers over 36,000 years of sedimentation. However the link between the diatoms in cores B94/1 and B94/3 is not conclusive, so no attempt is made to date specific horizons in B94/1.

Section one

Section one of model four on B94/1 (Figure 6.24) starts with several peaks in the topsoil end-member concentration. These peaks include the highest values of the topsoil end-member seen in this model. Alternating with the peaks in the topsoil end-member are peaks in subsoil. The alternating peaks and troughs in the topsoil and subsoil end-members continue up to 430cm when subsoil becomes dominant. This behaviour seems to indicate that the modelling procedure may have had difficulties in distinguishing between topsoil and subsoil in section one. However the high levels of topsoil erosion coupled with subsoil erosion indicates a high-energy environment at the bottom of B94/1. The deposition system then changes at 420cm to a more balanced system where subsoil dominates the signal. Indicating that there is sustained deep soil erosion taking place in the catchment, but that topsoil formation and erosion is still taking place albeit at a lower rate. The reduced levels of topsoil above 420cm, could be due to a reduction of rainfall in the catchment. The increased concentration of subsoil material above 420cm suggests that deeper erosion is taking place in the catchment, perhaps as a result of more seasonal rainfall leading to erosional gullies.

Section two

The second section of the model for B94/1 (Figure 6.24) is less variable than section one. Topsoil erosion increases slightly, from the level seen at the top of section one, then stays stable for most of section two before dropping to a couple of percent of the core's mass at 275cm. Subsoil erosion in section two starts high, troughs at around 300cm, before rising again at the top of the section. The increase in the concentration of the topsoil end-member in section two suggests higher rainfall, or less seasonal rainfall, promoting topsoil formation and reducing the relative input of subsoil material. If the zone between the bottom of the section and 275cm represents higher, or less seasonal rainfall, then the reduction of topsoil and increase in subsoil erosion at the top of section two indicates a return to lower more seasonal rainfall that was seen at the top of section one.

Section three

For the majority of section three (Figure 6.24), there is very little topsoil material in the model. However, in section three are the highest concentrations of subsoil erosion in the model as well as frequent occurrences of wind-blown dust and occasional occurrences of bedrock material. The high levels of subsoil and the occurrences of bedrock material indicate deep weathering taking place in the catchment. The wind-blown dust inputs may indicate low rainfall, leading to desiccation and a reduction in floral cover allowing wind erosion. However the occasional occurrences of the topsoil end-member, at 240, 190, 150 and 35cm

suggest wetter periods, where topsoil development occurs, and deep erosion is reduced by plant growth.

If the match between cores B94/1 and B94/3 is to be accepted, this would imply that B94/1 covers a period roughly equivalent to sections two, three and four from core B94/3. Accepting this correlation it appears that prolonged subsoil erosion starts far earlier in the centre of the Babicora basin than the North and the centre of the basin sees considerably lower topsoil input than the North. This implies that the variation of soil erosion is large across Babicora basin during the time represented by the sediments in these cores.

The interpretation of core B94/1 is in many ways similar to that of the upper two sections of B94/3. However, if the B94/1 core only spans the same time period as the upper two sections of B94/3 then the sedimentation rate for the B94/1 core would have to be on average 2.6 times as high as that for the B94/3 core. This seems unlikely as the Pit 1 site, further south in the basin, has a sedimentation rate only 10% greater than B94/3. In conclusion, the only way to fully understand the implications of the unmixing model on B94/1 would be to have one or more radio carbon dates on the core. Dating would resolve the issue of either a great difference in sediment history, or a very different sedimentation rate between cores B94/1 and B94/3.

6.12 Discussion

The magnetic unmixing of core B94/3 has provided a quantitative model of the erosion history of the Babicora catchment. Comparing the interpretation of this magnetic unmixing model with previous work carried out on the sediments from Lake Babicora shows that many of the features previously seen in diatom, stratigraphic, pollen, chemical, particle size and magnetic analysis are also apparent in the magnetic unmixing models. However, there are some differences between the findings of previous studies and this work.

Of the four palaeolimnological investigations of Lake Babicora only one (Metcalfe *et al.*, in press) analyses sediments that were deposited before 21,000yr B.P.. Metcalfe *et al.'s*, (in press) study of B94/3 indicates that Babicora has witnessed a large degree of climate variability over the last 65,000 years. The most distinct change in the nature of Lake Babicora reported by Metcalfe *et al.*, (in press) occurred at approximately 29,000yr B.P.. At this time the lake depth reduces as the climate becomes drier and colder. All three of the other palaeolimnological studies investigated (Metcalfe *et al.*, 1997; Urrutia-Fucugauchi *et al.*, 1997; and Ortega-Ramirez *et al.*, 1998) report a further reduction of lake level at approximately 11,000yr B.P.. A period of increased lake level is reported by Metcalfe *et al.*, (1997), Urrutia-Fucugauchi *et al.*, (1997), and Ortega-Ramirez *et al.*, (1998), though the timing of this period varies between the three studies. Metcalfe *et al.*, (1997) date the onset of higher lake levels at 5,400yr B.P. whereas Urrutia-Fucugauchi *et al.*, (1997) and Ortega-Ramirez *et al.*, (1998) date this at 5,600 and 4,000yr B.P. respectively. There is also a discrepancy in the dating of the end of this higher lake level period. Ortega-Ramirez *et al.*, (1998) and Urrutia-Fucugauchi *et al.*, (1997) report a

reestablishment of drier conditions at 2,800 yr B.P., whereas Metcalfe *et al.*, (1998) date the reduction of lake level at 2,000 yr B.P..

The reduction in lake level reported by Metcalfe *et al.*, (in press) at 29,000^{14}C yr B.P. occurs at a time as a cessation of subsoil erosion and a gradual reduction in topsoil erosion in the unmixing model of B94/3 between. One of the most dramatic features of the unmixing model of B94/3 is a rapid increase in topsoil erosion between 21,000 and 18,000^{14}C yr B.P., followed by an equally rapid reduction of topsoil erosion until a horizon with no topsoil content occurs at 15,000^{14}C yr B.P.. The unmixing model switches to a subsoil-dominated model at this point. The high topsoil erosion period coincides with a section of core B94/3 that Metcalfe *et al.*, (in press) associate with high catchment instability. The further reduction of lake level seen in the previous studies at 11,000 yr B.P. coincides with reductions in both topsoil and subsoil end-members in the magnetic unmixing model. The high lake level period reported by Metcalfe *et al.*, (1997), Urrutia-Fucugauchi *et al.*, (1997) and Ortega-Ramirez *et al.*, (1998), as occurring at some time between 5,600 and 2,000yr B.P. is not apparent in the unmixing model.

The differences between the magnetic unmixing model and the previous studies carried out by Metcalfe *et al.*, (1997), Urrutia-Fucugauchi *et al.*, (1997), and Ortega-Ramirez *et al.*, (1998) may be due to the location of the sources of the sediments used in the studies. B94/3 comes from the North of Babicora, close to the present lake, where as the other three studies use materials from the South of the basin. The separation of the core sites could also explain the difficulties with matching the unmixing models carried out on the undated core (B94/1) and B94/3. However, the change between topsoil and subsoil erosion at 15,000^{14}C yr B.P. in the unmixing model for B94/3 indicates a change in the Babicora catchment that has not been identified by any other study. It is possible that the magnetic unmixing has identified an important period in the history of Lake Babicora that is not apparent in other studies. However, mistakes in the unmixing model through inappropriate or missing end-members, although unlikely due to the high skill level of the model, cannot be ruled out.

6.11 Conclusions

1. High-resolution magnetic measurements of B94/3a and B94/3b have been used to identify a 75cm overlap between the two cores. Other techniques have proved unable to correlate the two core sections.
2. The unmixing routines run on B94/1 and B94/3 have been able to distinguish between the input of material derived from topsoil, subsoil, bedrock and, in the case of B94/1, wind-blown dust.
3. The identification of these materials within the sediment core B94/3 gives insight into the erosion patterns within the Babicora catchment for the last 65,000 years.
4. Interpretation of the unmixing model has allowed the identification of processes that have affected the Babicora catchment.
5. Reductions in lake level that were identified in the magnetic unmixing model for B94/3 as occurring at 29,000yr B.P. and 11,000yr B.P. are also apparent in previous studies of Lake Babicora.
6. The unmixing model of B94/3 identifies a dramatic change in erosion source from topsoil to subsoil at 15,000^{14}C yr B.P.. This change has not been identified by any of the previous studies of Lake Babicora.
7. Differences between the unmixing models for B94/1 and B94/3 indicate either a large difference in sedimentation rate or sediment source between the centre and North of Babicora.

Chapter 7

The magnetic properties of Mexican soils

In this chapter I investigate the relationship between the magnetic properties of soils and rainfall. This is accomplished by comparing the magnetic properties of soil profiles sampled in Mexico to the precipitation at the soil sample site. Mexico was chosen as the site for soil collection due to the large rainfall gradients present there. I have developed 270 models relating soil magnetics to rainfall. From this set of initial models, the three that display the best skill are selected and interpreted.

7.1 Introduction

Previous work on the magnetic properties of Chinese loess and world soils has led to a proposed relationship between magnetic susceptibility and annual precipitation; namely that the higher the precipitation a soil is subject to the more enhanced its magnetic susceptibility in the upper part of its profile (Chapter 3.4) (Maher *et al.*, 1994). The aim of this chapter is to look at the effect of rainfall on the magnetic properties of a wide range of soils from Mexico. I collected 89 soil profiles from across pronounced rainfall gradients in Mexico. The 89 soil profiles sampled provided 431 soil sub-samples, representing annual precipitation ranging from less than 300mm to more than 4500mm. Distinguishing topsoil from subsoil in many cases is not straightforward. Three different selection processes were used to discriminate topsoil from subsoil material in the soil profiles. Using the measured magnetic properties of the identified topsoils and subsoils together with precipitation data for Mexico, models of the relationship between rainfall and soil magnetics have been generated. These models were tested for skill and fit. The models generated only took magnetic data and rainfall into account. No specific attempt to remove other soil forming factors (parent material, climate (other than precipitation), vegetation (not related to rainfall), time or topography) (Chapter 3.4) was made. Despite this, statistically significant relationships between rainfall and magnetics have been found.

7.2 Field work

Two field seasons were spent in Mexico collecting soils from across pronounced rainfall gradients. The first field season, Spring 1999, was spent in the dry-to-arid north west of Mexico, sampling soils in the Sierra Madre Occidental mountain range, in the Sonoran and Chiuahuan deserts and in Baja California. The second field

season, Spring 2000, was spent in the humid-to-tropical central west of Mexico, sampling soils from the Valley of Mexico, over the Sierra Madre Oriental and across the Veracruz coastal area, as far as Tuxtla. The locations of the soil sample sites are plotted on a precipitation map of Mexico in Figure 7.1a and on soil and geology maps in Figure 7.1b. The soil map (Figure 7.1b) indicates that a wide range of soil types have been sampled, and the geology map indicates that the soils had formed in a diverse range of geological settings. Many of the soils in this study will have inherited strongly magnetic materials from their parent substrates. This study in common with Maher and Thompson (1999) does not discount soils that were:

8. Burnt (burning enhances a soils susceptibility);
9. Poorly drained (iron reduction in waterlogged soils counters fine magnetite production);
10. Acidic (acidic soils are unfavourable for magnetite precipitation (Taylor *et al.*, 1987));
11. Eroded soils (these may have lost their enhanced upper layer);
12. Soils containing strongly magnetic materials from tephra falls or atmospheric pollutants;
13. Soils inheriting strongly magnetic minerals from parent substrates;
14. Soils on slowly weathering or iron-deficient parent substrates.

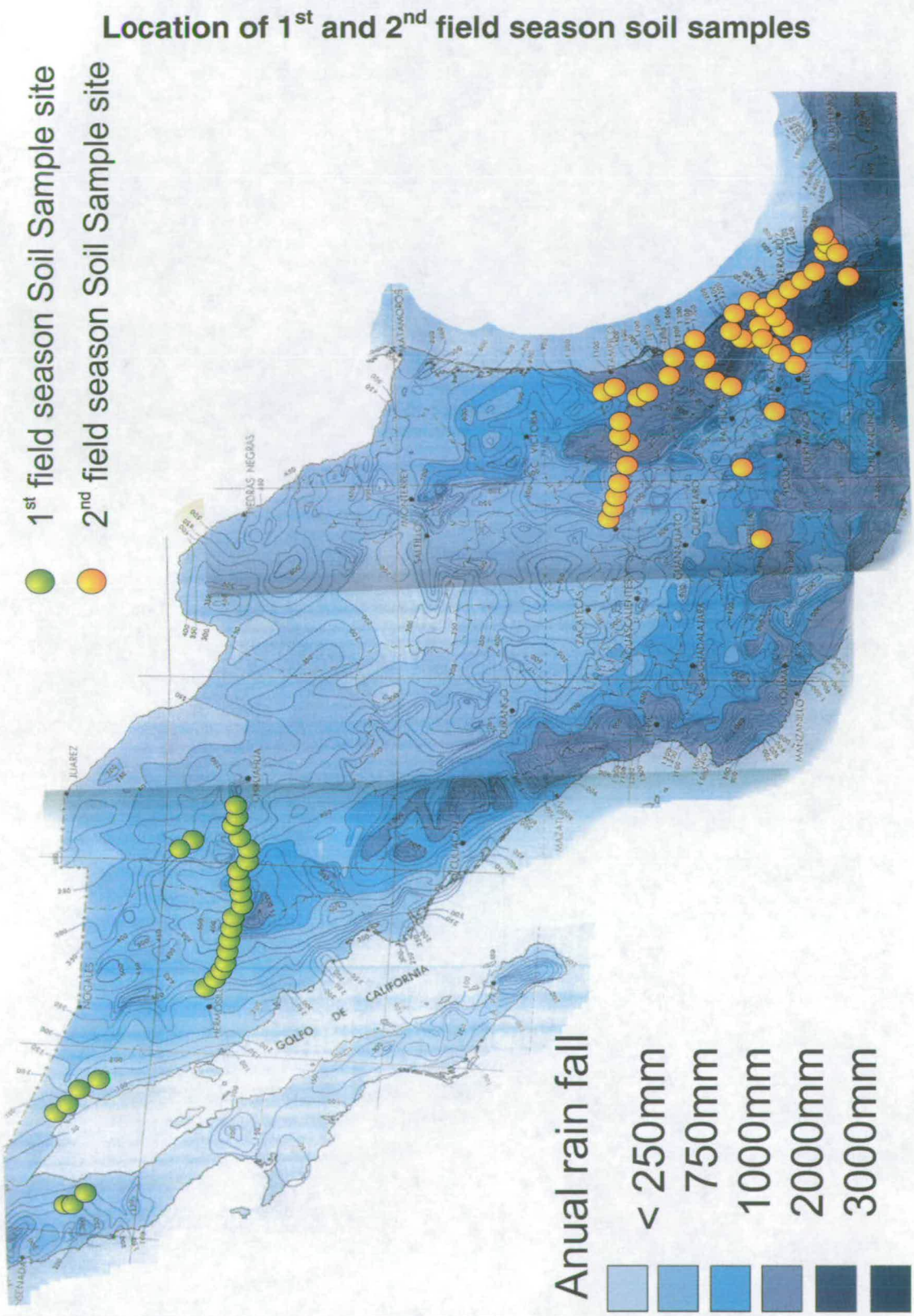

Figure 7.1a. A map of the annual precipitation in Mexico with soil ample sites from the 1st and 2nd field season visits to Mexico (1st field season in green, 2nd field season in orange).

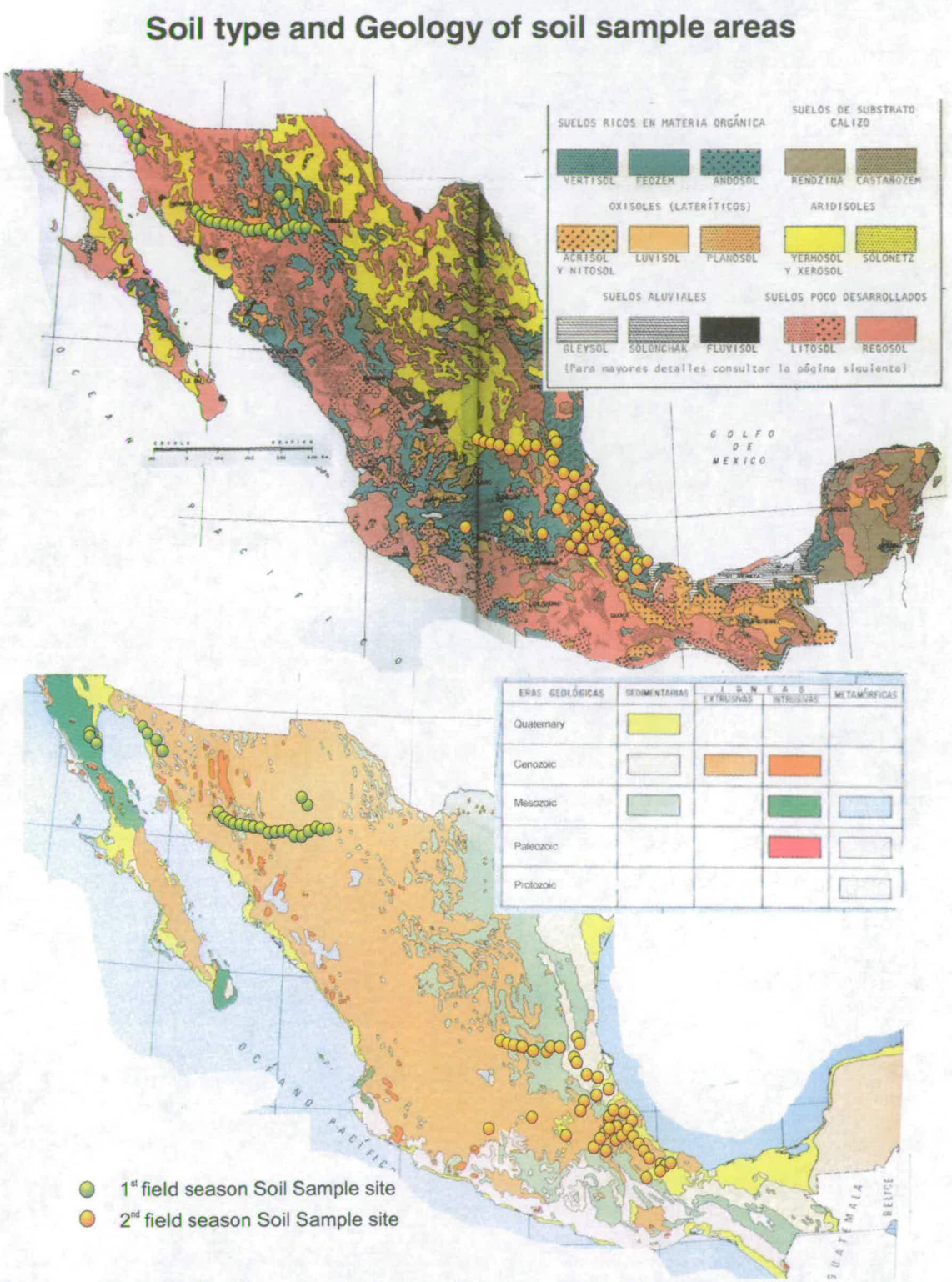

Figure 7.1b. Maps of the soil type (top) and Geology (bottom) on Mexico with soil ample sites from the 1st and 2nd field season visits to Mexico (1st field season in green, 2nd field season in orange).

Most of the soil samples in this study came from road cuttings. To avoid exposed soil material that may have been contaminated by exhaust fumes and industrial activities, the exposed surface of the soil profile was removed using a trowel or geological hammer, and samples were taken from as deep within the profile as possible. Typically four samples were taken at each site with a 15cm vertical spacing. Additionally, samples were taken to encompass material from each major colour and

texture horizon within the profile. For all but seven of the sampled soils a photograph was taken (Figure 7.4) and a GPS location was noted. Once back in the laboratory, the soils were sieved to remove material greater than 5mm, then packed in 2cm diameter plastic cylinders before being subjected to 18 magnetic measurements. The measurements made were the standard measurements used throughout this study (Chapter 2.4) consisting of 2 susceptibility measures (high and low frequency), followed by ARM magnetisation (99mT ac field with 0.1 mT dc field) then ARM demagnetisations (at 5, 10, 20, 40, and 80mT) and finally ten IRM magnetisations (at increasing fields of 20, 40, 60, 80, 100, 200, 300, 1000, 2000, and 3000 mT). After these magnetic measurements, the soils were dried and weighed.

7.3 Climate data

Two types of meteorological stations exist within Mexico: there are over 1,800 "estaciones climatológicas", which measure temperature and precipitation; and around 100 "observatorios meteorológicas", which make more detailed climate observations, including cloud cover, evaporation, air pressure, and wind speed and direction. As well as these long term climate stations there are a large number of temporary stations and studies, which have added data to the Mexican climate data-set. A location map of all of the Mexican climate stations is provided (Figure 7.2). Note that, as usual, the highest concentrations of meteorological stations are to be found near the major population centres in the central belt (Figure 7.2),. There are fewer climate stations in the northern part of Mexico, especially in the north west, near the Sonoran desert.

Few summaries of the climatological data sets from Mexican meteorological stations are available. For instance Figure 7.1a is a precipitation map that was compiled by the Dirección Geografía y Meteorología using data for the period 1931 – 1970. This map (Figure 7.1) and others like it, were used to plan the field work. Detailed precipitation data were extracted from a database of the climate data for all the climate stations in Mexico. The climate database used, "Extractor Rapido de Informacion Climatica" or ERIC, covers the period from 1960 to 1990. However, for many climate stations large sections of data this period are not present, and there were also day-to-day gaps in the climate record for some stations. For instance, some stations do not have readings for weekends or one particular month of each year. Such gaps and hiatuses in climate records are not uncommon. In order to collate annual precipitation data for the areas of Mexico where soils were sampled, it was necessary to extract useful data from the incomplete climate data in ERIC. For each station, a monthly mean precipitation was calculated for each month of each year of available data. A month's mean precipitation was only accepted if fewer than four days data were missing. In the north of Mexico, where climate stations were sparse, a yearly precipitation average for a station was only made if more than five examples of each month were available. In the south of Mexico, where data are much more abundant, an annual average precipitation was only calculated for stations with ten or more examples of each month's mean precipitation. Mean annual precipitation was worked out in this manner for the climate stations surrounding the soil sampling sites (Figure 7.2). Figure 7.2 shows the positions of the climate stations (black dots) used to calculate precipitation at soil sample locations. Figure 7.3 shows a map of the precipitation in the soil sampling regions of Mexico based upon the precipitation data

extracted from ERIC. Precipitation was estimated at each of the soil sites by using a 2D linear interpolation between climate stations. This assumption is not ideal, especially in mountainous regions. However, as the mean distance between a soil sample site and the nearest climate station was only 6km in the north of Mexico and 4km in the south, this assumption was considered acceptable. Fifteen soil sample sites were outside of the climate data extracted from ERIC. For these sites an annual precipitation value was derived from the precipitation map (Figure 7.1).

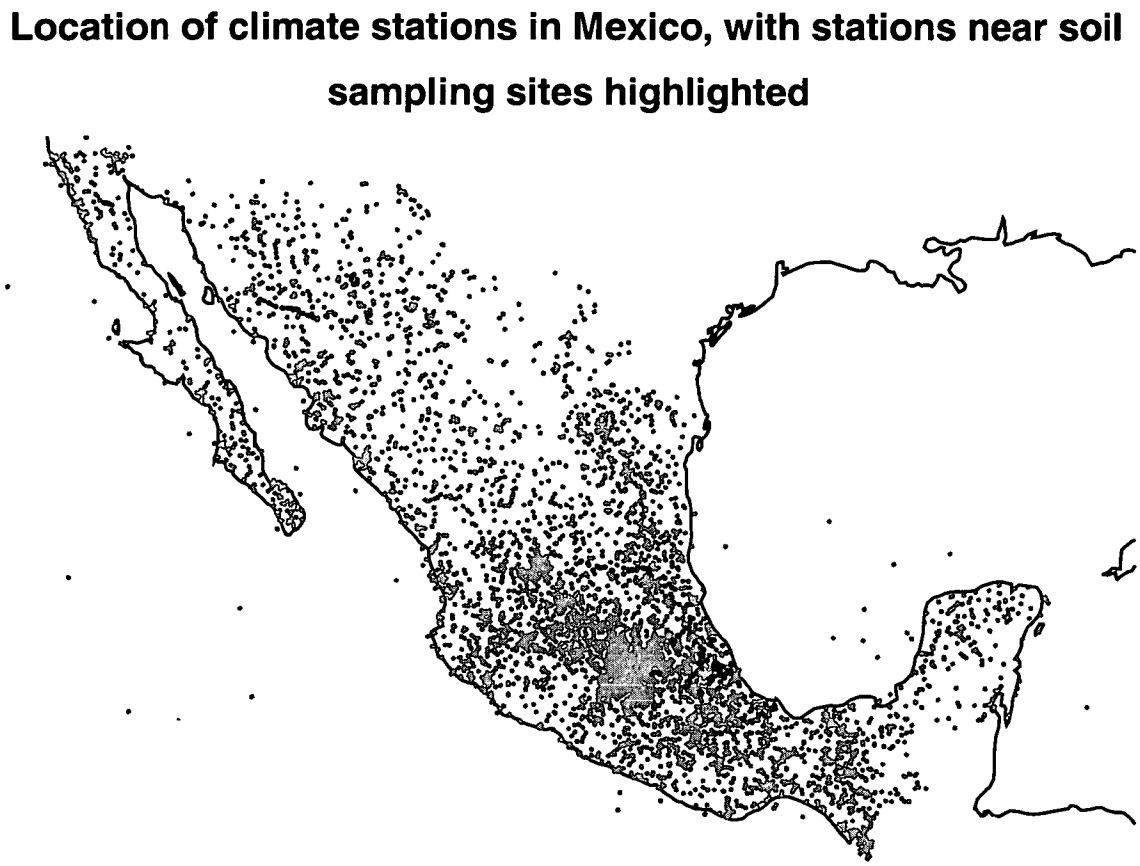

Figure 7.2. Locations of climate stations in ERIC, (grey dots). Black dots represent locations of climate stations used to estimate rainfall at soil sampling sites.

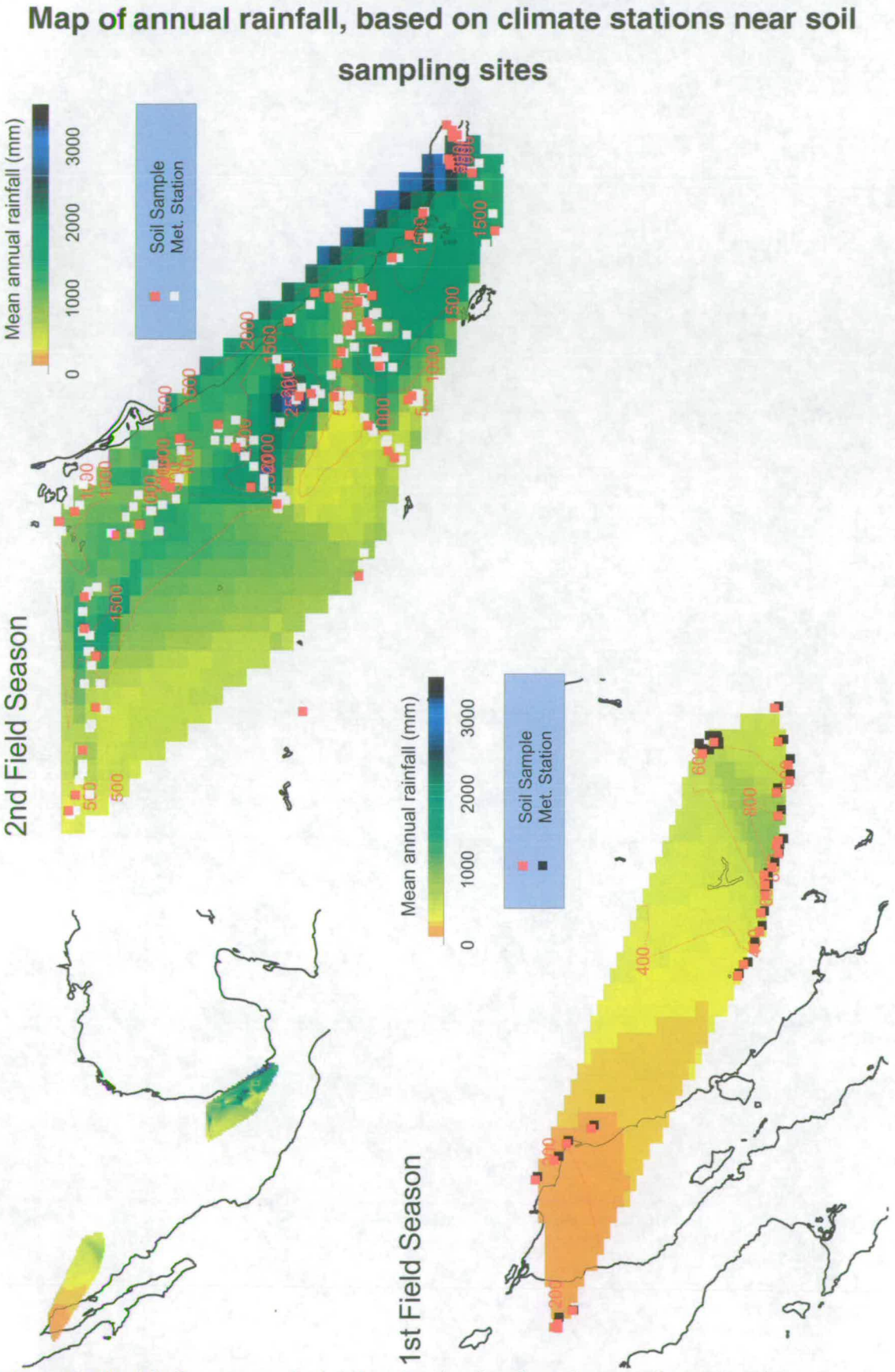

Figure 7.3. Model of mean annual rainfall made using data from close to soil sampling sites. Sampling sites and meteorological stations used in the generation of this model are also shown.

7.4 Topsoil and subsoil selection procedures

In order to compare the magnetic properties of topsoils and subsoils to mean annual rainfall, these horizons had to be identified within the soil profiles collected. Three different procedures were used to select topsoil and subsoil horizons within the 89 soil profiles. The three selection procedures were based on,

1. Field notes and photographs of the soil profiles,
2. Magnetic susceptibility data,
3. SARM/SIRM ratio.

7.4.1 Procedure one

The first procedure used field notes taken at the time of the soil sampling together with photographs of the soil profiles, to try to identify distinct upper and lower soil horizons. Topsoils were generally taken as materials with higher organic content and darker coloration than the material below in the soil profile. Material that predominantly consisted of leaf litter and twigs was not included in the topsoil classification. For thin soil profiles it was occasionally necessary to use a bedrock sample as the lower soil material. Procedure one was successful for 73 soil samples. For thirteen of the 89 soils collected it was impossible to distinguish clear topsoil and subsoil horizons using field data and photographs. Figs 7.4A and 7.4B show photographs of soil profiles from Mexico.

Photographs of two soil profiles

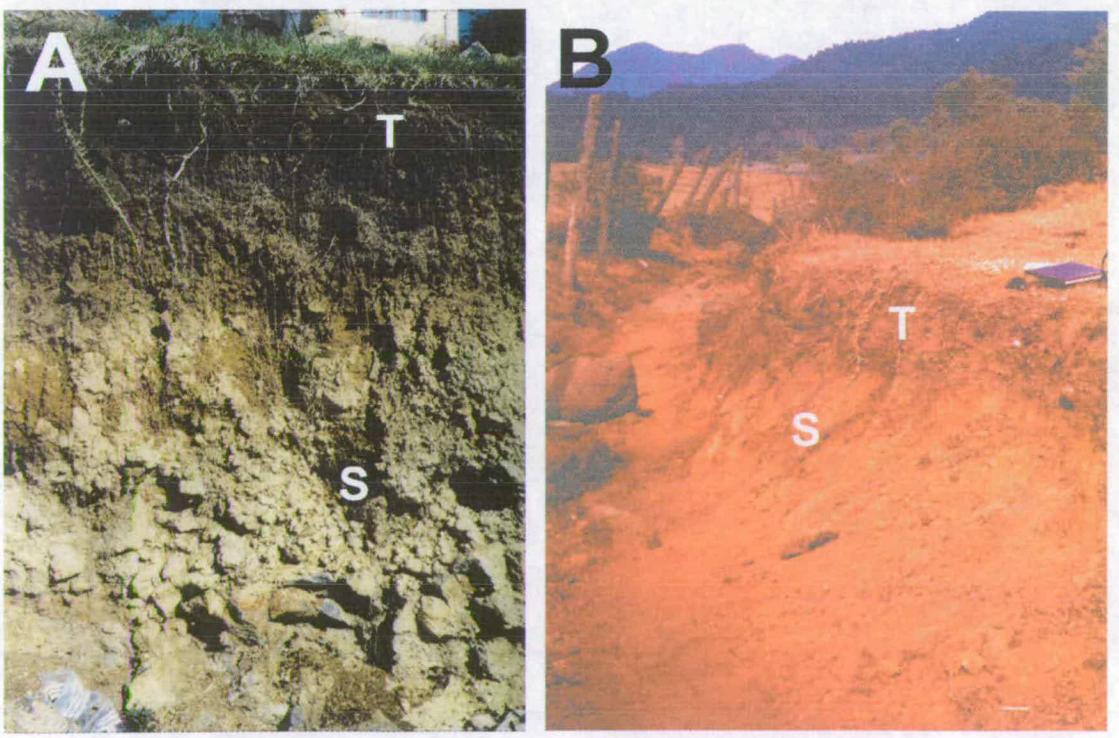

Figure 7.4. Photographs of two soil profiles, topsoils (T) and subsoil (S) marked. Profile A, comes from the lowlands near Jalapa in the south west of Mexico ($19^0$35' N, $97^0$00' W), the annual rainfall for this soil site is 980mm yr^{-1}. Profile B comes from the central highlands of Mexico ($19^0$32'N, $101^0$23' W) and has an annual rainfall of 1300mm yr^{-1} (some colour distortion has occurred during the processing of this picture). Topsoil and subsoil classification have been made by colour in A and by texture and the presence of roots in B.

The other two procedures for selecting soil horizons that represent topsoil and subsoil materials use magnetic data from the soil profiles. The first of the magnetic selection procedures uses the magnetic susceptibility of the soil profile. High magnetic susceptibility at the top of the soil profile was used to identify topsoil material and lower susceptibility lower in the soil profile to identify subsoil. Most of the soil profiles collected did not show classic LeBorgne susceptibility enhancement, where the susceptibility rises through the soil profile to a peak at the surface. For this reason each soil profile was classified by the following 5 criteria. Examples of the following classifications are shown graphically in Figure 7.5.

7.4.2 Procedure two

Soil enhancement classification

1. Classic LeBorgne susceptibility enhancement: increasing susceptibility up to the highest sample in the profile. Topsoil = top sample, subsoil = bottom sample.
2. Classic LeBorgne susceptibility enhancement, except for a fall in susceptibility at the top of the profile. Topsoil = uppermost sample before susceptibility drop, subsoil = bottom sample.
3. Susceptibility starts high, at the bottom of the profile, drops then rises again at the top of the profile. Topsoil = top sample, subsoil = sample with the lowest susceptibility before susceptibility rise.
4. At the bottom of the profile susceptibility is high, it falls to a trough and then rises again higher in the profile, before falling again at the surface. Topsoil = uppermost sample before susceptibility drop, subsoil = sample with the lowest susceptibility before susceptibility rise.
5. No discernible susceptibly enhancement is seen in the profile. Topsoil = NA, subsoil = NA.

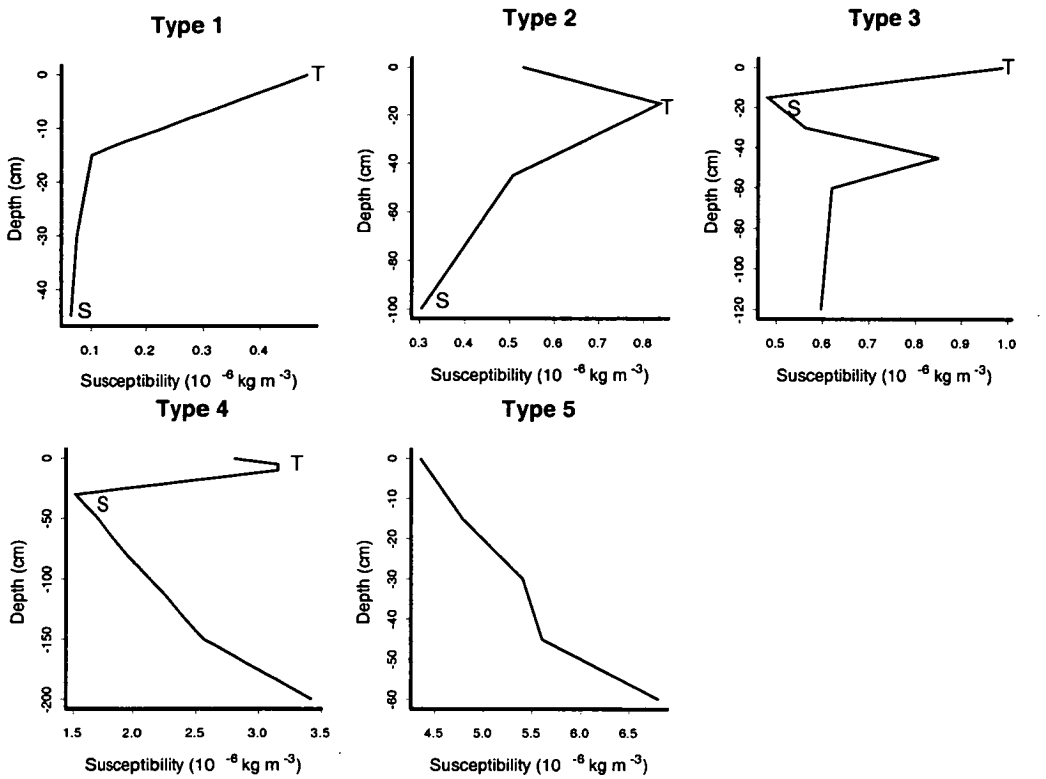

Figure 7.5. Examples of the five soil susceptibility enhancement classifications with topsoil (T) and subsoil (S) samples marked. The soil samples illustrated are type 1 = SB6, type 2 = SA5, type 3 = SU1, type 4 = SF6 and type 5 = ST3.

7.4.3 Procedure three

The second magnetic measurement procedure for identifying samples to represent topsoil and subsoil material used the SARM/SIRM ratio. This ratio was used as it is sensitive to the presence of fine grained magnetite, on the SP-SD grain-size boundary. Material on the SP-SD grain-size boundary is thought to be responsible for the magnetic enhancement of soils (Maher, 1998). The same soil enhancement classifications used to identify topsoil and subsoil with the susceptibility curve were applied to the SARM/SIRM curve of each profile. Table 7.1, is a summary of the classification of topsoil and subsoil material using the magnetic susceptibility and SARM/SIRM methods.

Summary of susceptibility and SARM/SIRM classifications of soil profiles

Enhancement classification	Susceptibility procedure	SARM/SIRM procedure
Type 1	23	14
Type 2	22	26
Type 3	22	16
Type 4	7	10
Type 5 (no topsoil or subsoil identified)	15	23

Table 7.1. Summary of the susceptibility and SARM/SIRM classifications of soil profiles, showing the number of soils out of 89 classified as type 1 to 5 by susceptibility and SARM/SIRM enhancement (procedure 2 and 3).

7.5 Magnetic results from the soil profiles

Biplots showing the remanence ratios were plotted for the topsoils and subsoils selected by each of the three selection procedures, (Figs 7.6, 7.7, 7.8, 7.9, 7.10, and 7.11). These biplots show the difference between the magnetic properties of the topsoil and subsoil materials selected by three different selection procedures. In each case the first biplot shows ARM hardness against IRM hardness, and the second biplot shows SARM/SIRM ratio against IRM hardness. A circle represents the position of the topsoil material in each biplot. A line connects each of the topsoils to its corresponding subsoil. Also plotted on these biplots are the mean properties of the selected topsoils (black square) and subsoils (black triangle)

For the ARM and IRM hardness plot for topsoils and subsoils chosen using procedure one (field notes and profile photographs) (Figure 7.6), a wide range of magnetic hardness can be observed. However, none of the topsoil samples have an ARM_{40}/SARM ratio above 0.4, and there is only one topsoil with IRM_{80}/SIRM lower than 0.3. The general trend in Figure 7.6 is that the samples selected to represent topsoils are softer than those chosen to represent subsoils, in both ARM and IRM properties.

No strong trend is noticed in the squareness biplot for the topsoils and subsoils chosen using procedure one (field notes and profile photographs) (Figure 7.7). The difference in SARM/SIRM ratio between topsoils and subsoils for these samples shows no noticeable trend. There is very little difference between the mean magnetic properties of the topsoils and subsoils represented in Figs 7.6 and 7.7

Biplot showing ARM hardness against IRM hardness for topsoils and subsoils chosen using field notes and photographs

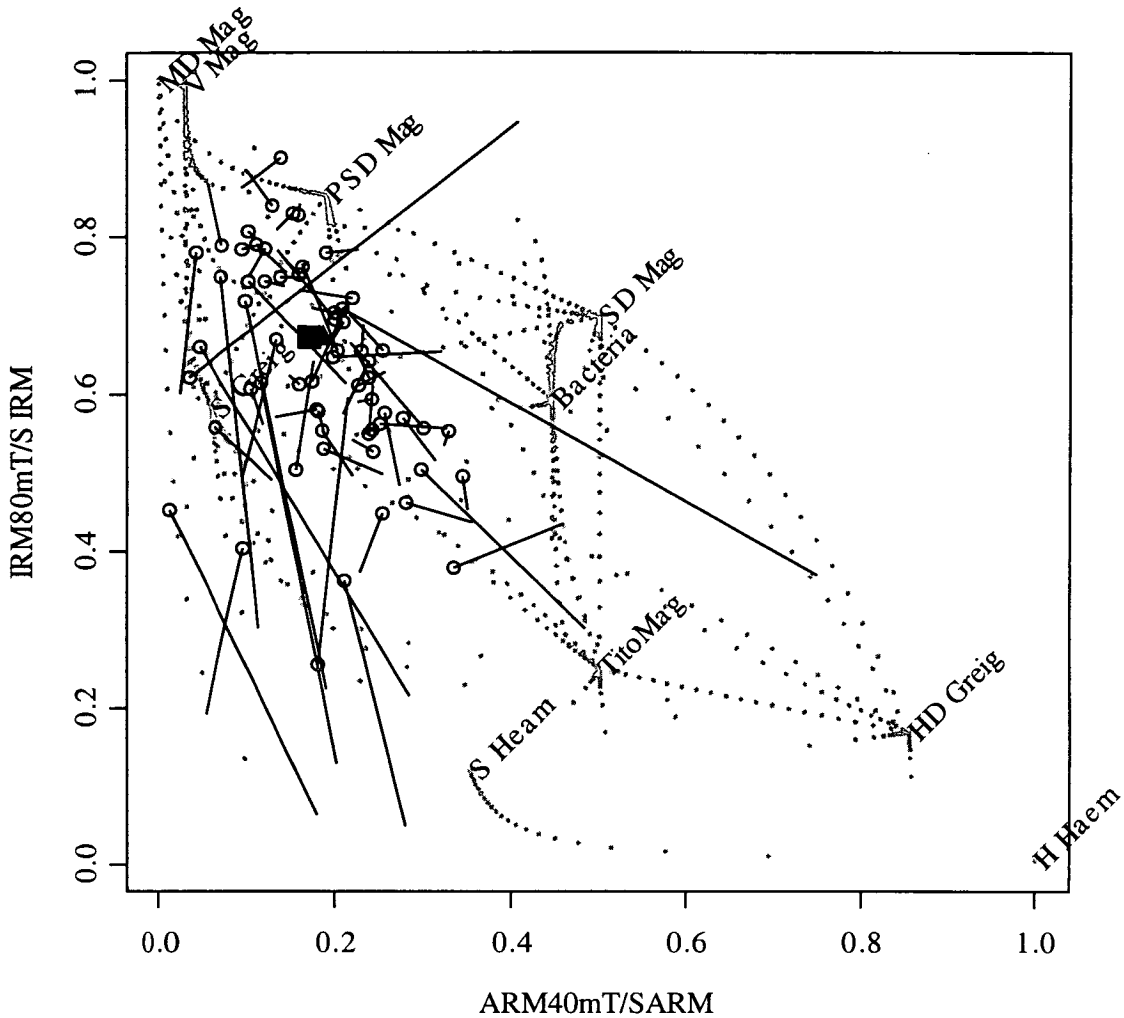

Figure 7.6. Biplot of ARM hardness (increasing to the right), and IRM hardness (increasing downwards). Topsoils (circles) and subsoils (end of line connected to each circle), chosen from Mexican soil profiles, using field notes and photographs of soil profiles. The mean magnetic properties of the topsoils are plotted as a black square, and the mean magnetic properties of the subsoils as a black triangle. Also plotted are mineral magnetic end-members for reference, and points on the mixing curves between these end-members. For a further explanation see Chapter 2.8.

Biplot showing squareness (SARM/SIRM) against IRM hardness for topsoils and subsoils chosen using field notes and photographs

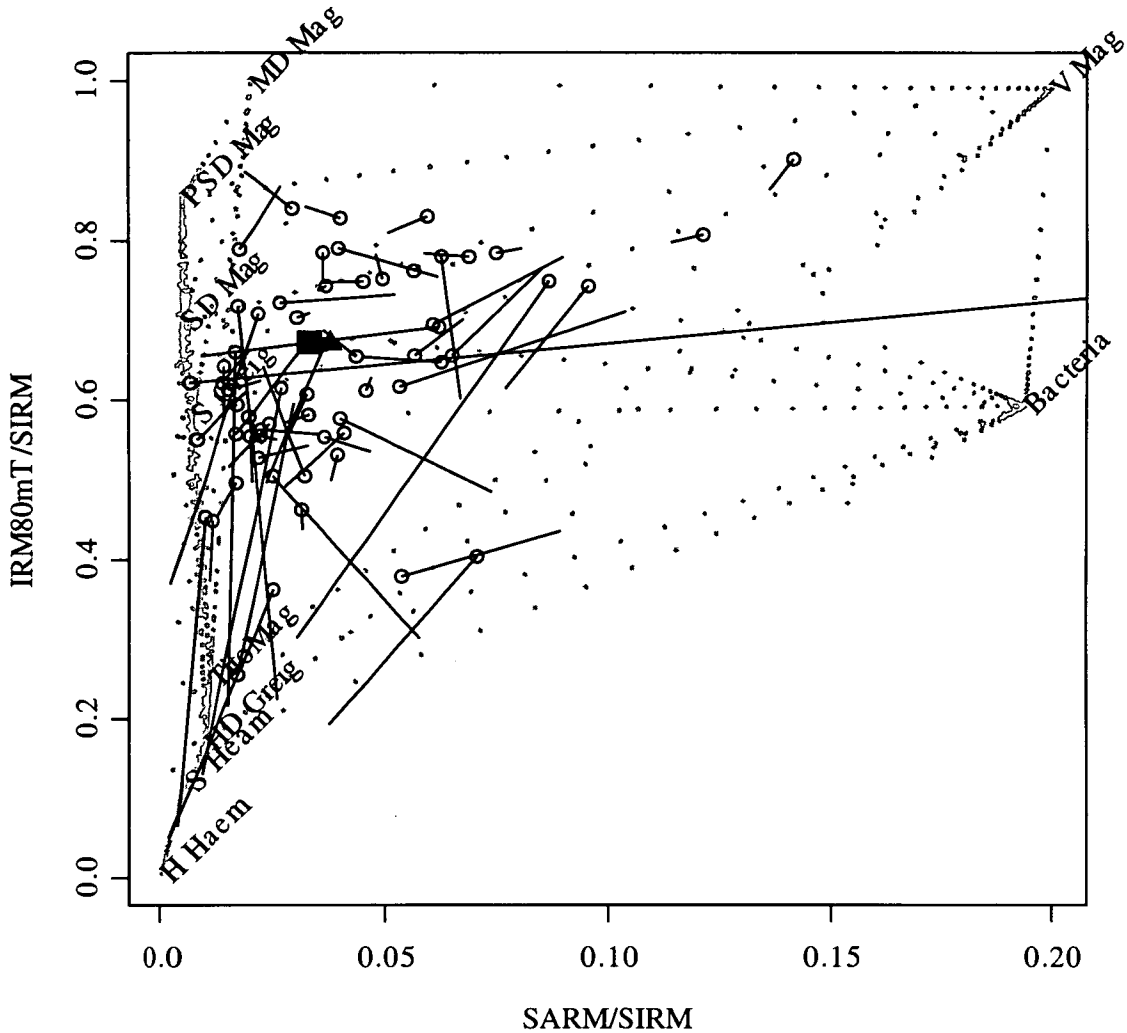

Figure 7.7. Biplot of the squareness (increasing to the right), and IRM hardness (increasing downwards). Topsoils (circles) and subsoils (end of line connected to each circle), chosen from Mexican soil profiles, using field notes and photographs of soil profiles. The mean magnetic properties of the topsoils are plotted as a black square, and the mean magnetic properties of the subsoils as a black triangle. Also plotted are mineral magnetic end-members for reference, and points on the mixing curves between these end-members. For a further explanation see Chapter 2.8.

The ARM against IRM hardness plot for samples chosen using procedure two (soil profile susceptibility) (Figure 7.8) shows a similar trend to that seen in the sample plot for the topsoils and subsoils selected using procedure one (field notes and photographs) (Figure 7.6). The topsoils tend to show softer ARM and IRM properties than their subsoil partners do. Like the topsoils identified with procedure one (field notes and photographs), those selected with procedure two(soil profile susceptibility) do not have an ARM_{40}/SARM higher than 0.4 or a $SIRM_{80}$/SIRM lower than 0.3. Again, like the procedure one (field notes and photographs) selected topsoils and subsoils, there is no significant trend in the SARM/SIRM ratio between topsoils and subsoils selected using procedure two (susceptibility profile) (Figure 7.9).

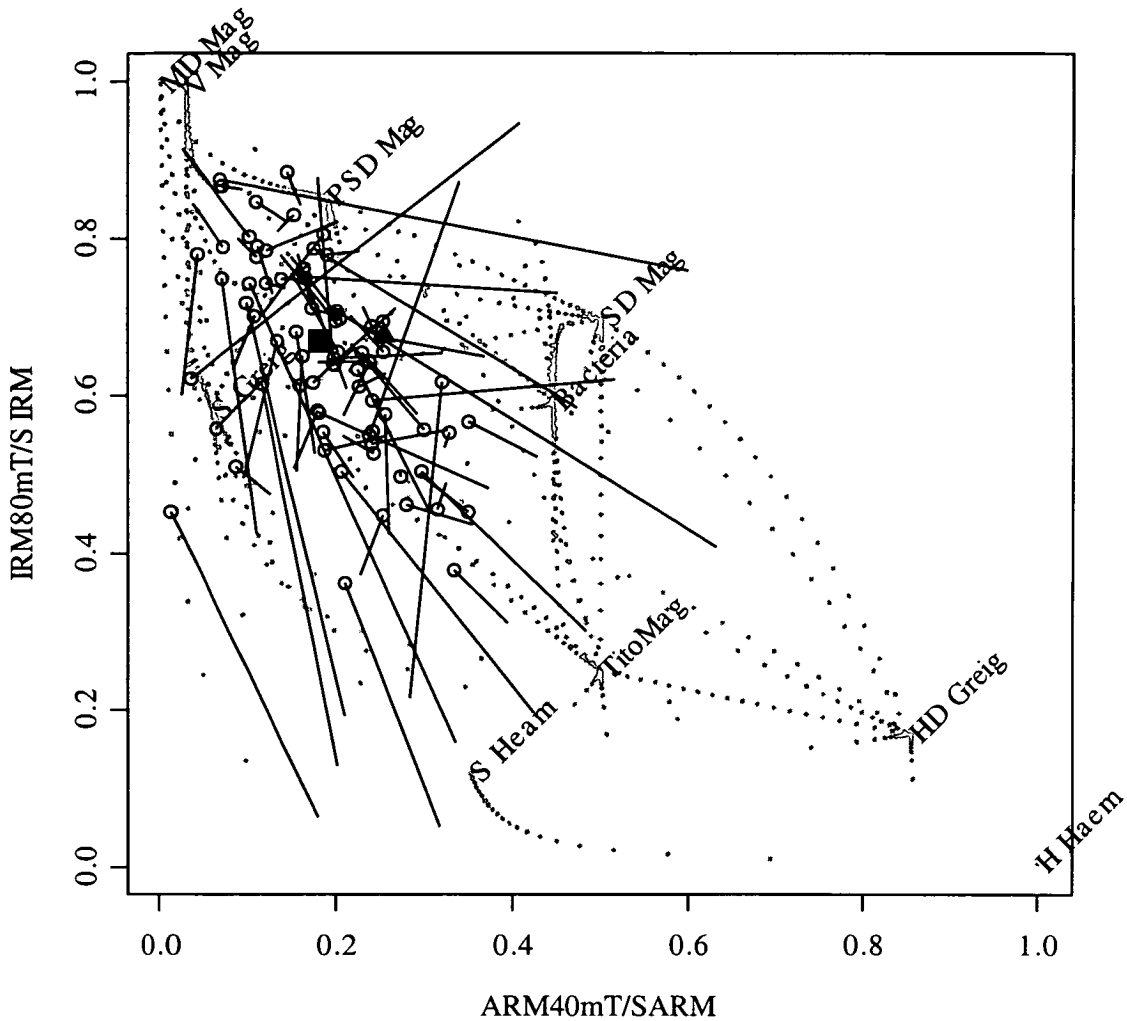

Figure 7.8. Biplot of the ARM hardness (increasing to the right), and IRM hardness (increasing downwards). Topsoils (circles) and subsoils (end of line connected to each circle), chosen from Mexican soil profiles, using the magnetic susceptibility profile. The mean magnetic properties of the topsoils are plotted as a black square, and the mean magnetic properties of the subsoils as a black triangle. Also plotted are mineral magnetic end-members for reference, and points on the mixing curves between these end-members. For a further explanation see Chapter 2.8.

Biplot showing squareness (SARM/SIRM) against IRM hardness for topsoils and subsoils chosen using magnetic susceptibility

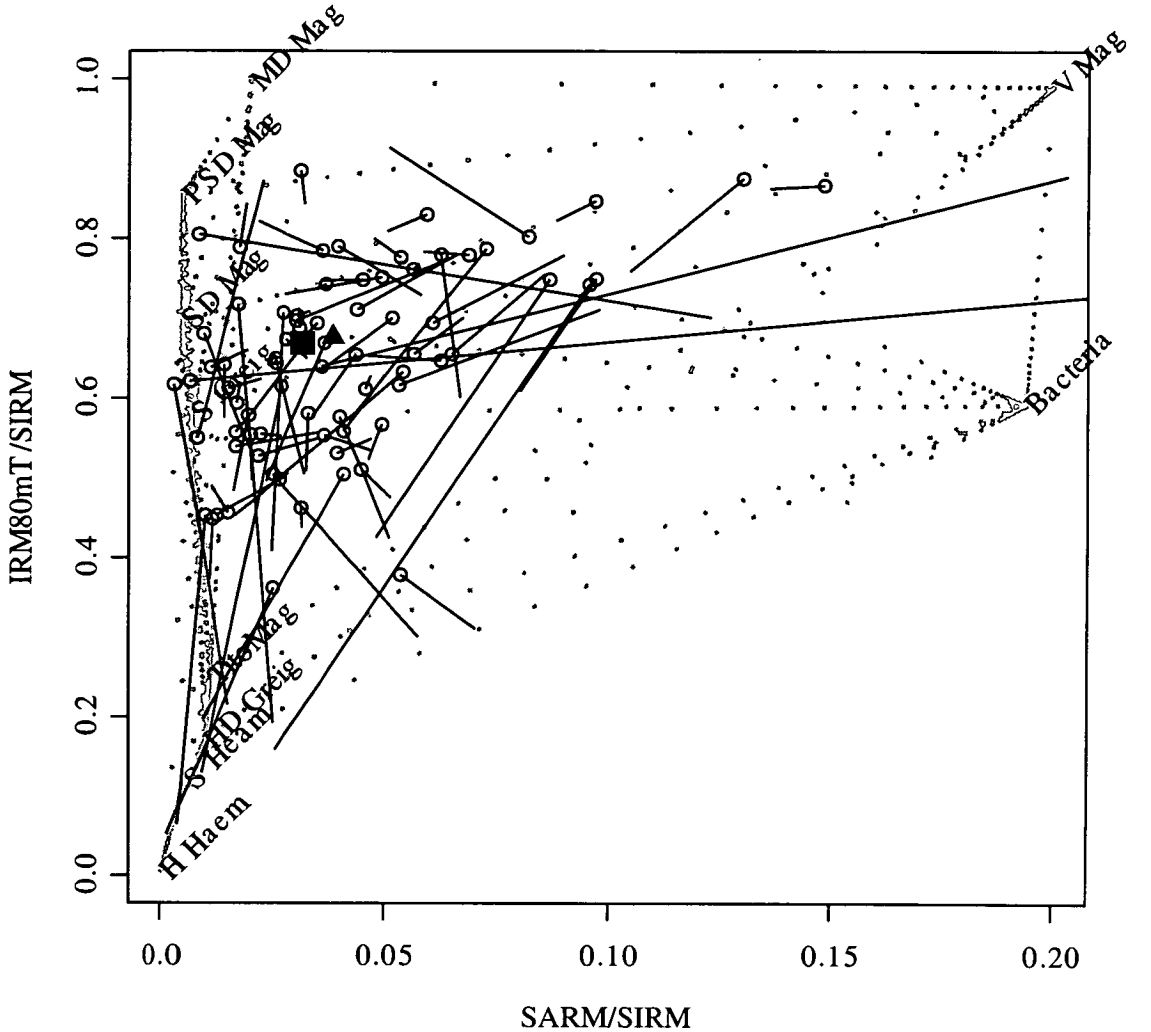

Figure 7.9. Biplot of the squareness (increasing to the right), and IRM hardness (increasing downwards). Topsoils (circles) and subsoils (end of line connected to each circle), chosen from Mexican soil profiles, using the magnetic susceptibility profile. The mean magnetic properties of the topsoils are plotted as a black square, and the mean magnetic properties of the subsoils as a black triangle. Also plotted are mineral magnetic end-members for reference, and points on the mixing curves between these end-members. For a further explanation see Chapter 2.8.

The ARM against IRM biplot for the topsoil and subsoil horizons selected using procedure three (SARM/SIRM profile) (Figure 7.10) has similar characteristics to the other two procedures of topsoil and subsoil selection: the topsoils are generally softer in both ARM and IRM properties than their subsoil counterparts. The squareness biplot of the ARM profile selected topsoil and subsoil material (Figure 7.11) obviously shows topsoils always having higher SARM/SIRM than their counterpart subsoils (this was the selection criterion for these topsoil and subsoil materials). The topsoils and subsoils selected using procedure three (SARM/SIRM profiles) show the greatest difference in mean magnetic properties on both the ARM against IRM hardness biplot and the ARM_{40}/SARM against IRM hardness biplot. The mean

magnetic properties of procedure three (SARM/SIRM profile) selected topsoils are softer and higher in ARM_{40}/SARM than the mean magnetic properties of subsoils selected by the same procedure (Figure 7.10).

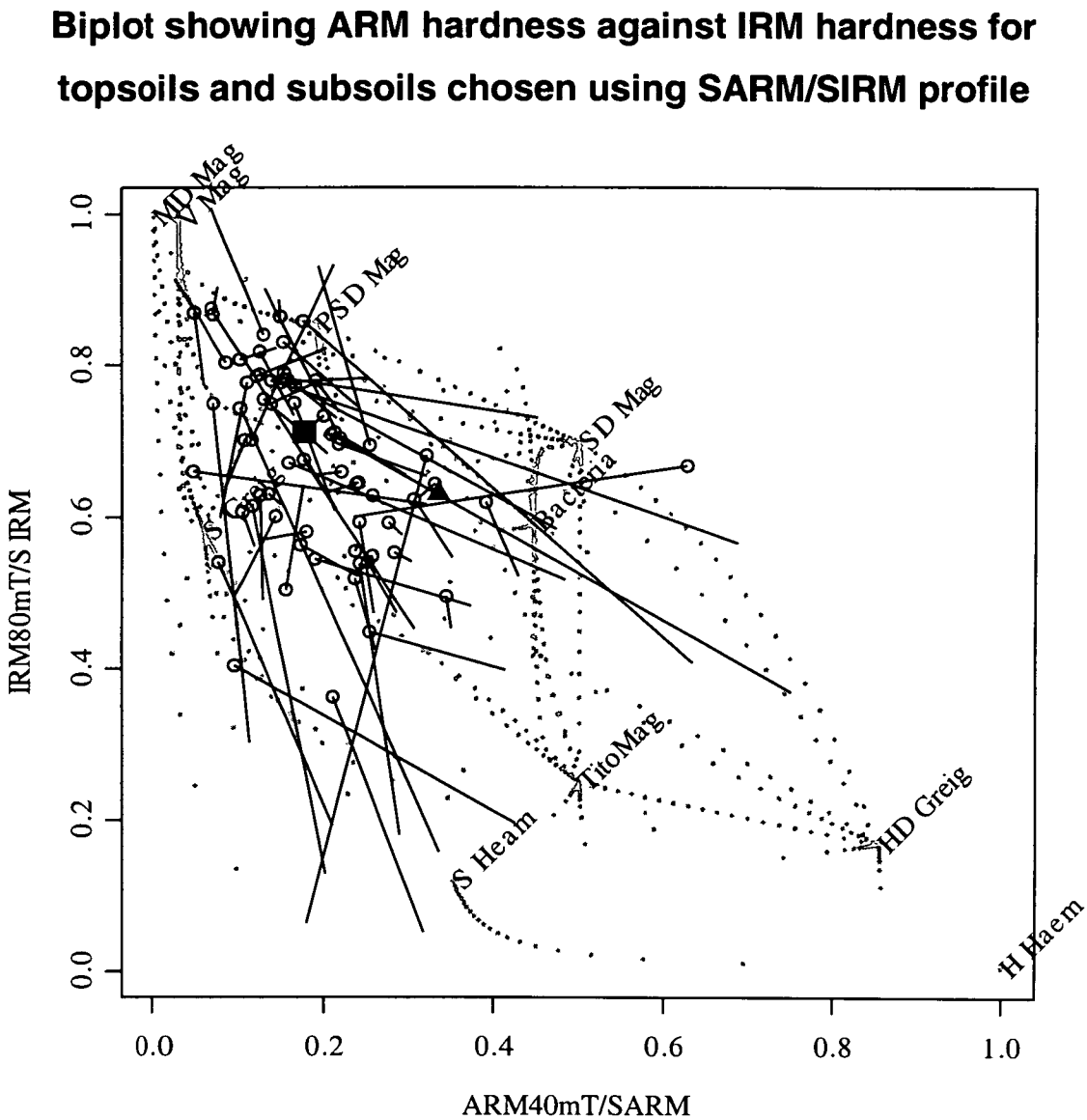

Figure 7.10. Biplot of the ARM hardness (increasing to the right), and IRM hardness (increasing downwards). Topsoils (circles) and subsoils (end of line connected to each circle), chosen from Mexican soil profiles, using the SARM/SIRM profile. The mean magnetic properties of the topsoils are plotted as a black square, and the mean magnetic properties of the subsoils as a black triangle. Also plotted are mineral magnetic end-members for reference, and points on the mixing curves between these end-members. For a further explanation see Chapter 2.8.

Biplot showing squareness (SARM/SIRM) against IRM hardness for topsoils and subsoils chosen using SARM/SIRM profile

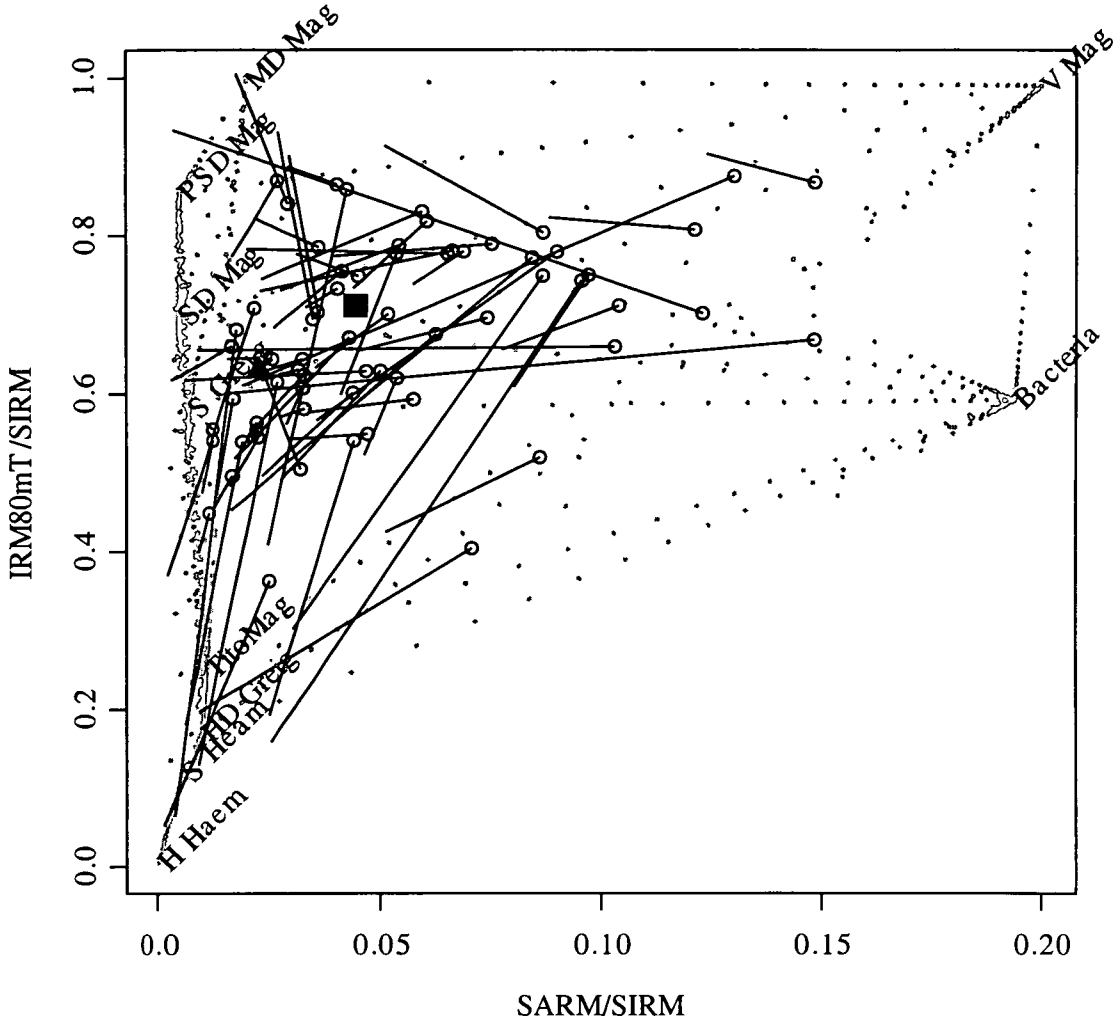

Figure 7.11. Biplot of the squareness (increasing to the right), and IRM hardness (increasing downwards). Topsoils (circles) and subsoils (end of line connected to each circle), chosen from Mexican soil profiles, using the SARM/SIRM profile. The mean magnetic properties of topsoils are plotted as a black square, and the mean magnetic properties of the subsoils as a black triangle. Also plotted are mineral magnetic end-members for reference, and points on the mixing curves between these end-members. For a further explanation see Chapter 2.8.

Table 7.2, is a summary of the information shown in the previous six biplots. For the topsoils and subsoils selected by procedures one and two just under 60% of the topsoils show softer ARM properties than their subsoil partner. Similarly just fewer than 60% of the procedure one and two subsoils show softer IRM properties than their topsoil partners. No clear relationship is seen between the SARM/SIRM ratio for topsoils and subsoils selected using procedure one (photographs and field notes). The topsoils and subsoils selected using procedure three (SARM/SIRM profile) show a more consistent ARM and IRM softening between subsoil and topsoil.

Summary of magnetic differences between topsoils and subsoils selected using three different techniques

	Procedure one (photo and field note selected soils)	Procedure two (susceptibility selected soils)	Procedure three (SARM/SIRM selected soils)
Reduction in ARM hardness	59%	59.5%	74.2%
Reduction in IRM hardness	59%	59.5%	80.3%
Increase in SIRM/SARM	49.2%	44.6%	100%

Table 7.2. Shows the percentage of soils which showed reduction in ARM hardness, IRM hardness and increase in SARM/SIRM ratio between their subsoil and topsoil samples, for the three different procedures of selecting topsoils and subsoils.

7.6 Comparing soil magnetics and rainfall data

In the next stage of the investigation of a link between soil magnetic properties and rainfall in Mexico I have compared the magnetic properties of soils with the rainfall at the soil collection site. Plots of selected magnetic properties of topsoil and subsoil samples chosen by each of the three soil selection procedures have been generated (Figs 7.12, 7.13 and 7.14). The barcharts are ordered with increasing rainfall downwards, each bar represents a given magnetic property of one soil site. The magnetic parameters plotted are the susceptibility of the topsoil and subsoil, the SARM of the topsoil, the ARM_{40}/SARM of the topsoil and the susceptibility and SARM/SIRM difference between the topsoil and subsoil samples. Table 7.3 shows the r^2 between each of the displayed magnetic measurements (Figure 7.12, 7.13 and 7.14) and the rainfall at each of the sites. There is little correlation between rainfall and these six basic magnetic measurements and ratios. However, low correlation would be expected as a single magnetic parameter or ratio of parameters is unlikely to be able to account for the variability in the soil data set given that soil forming factors have not been taken into account (Section 7.1 and 7.2).

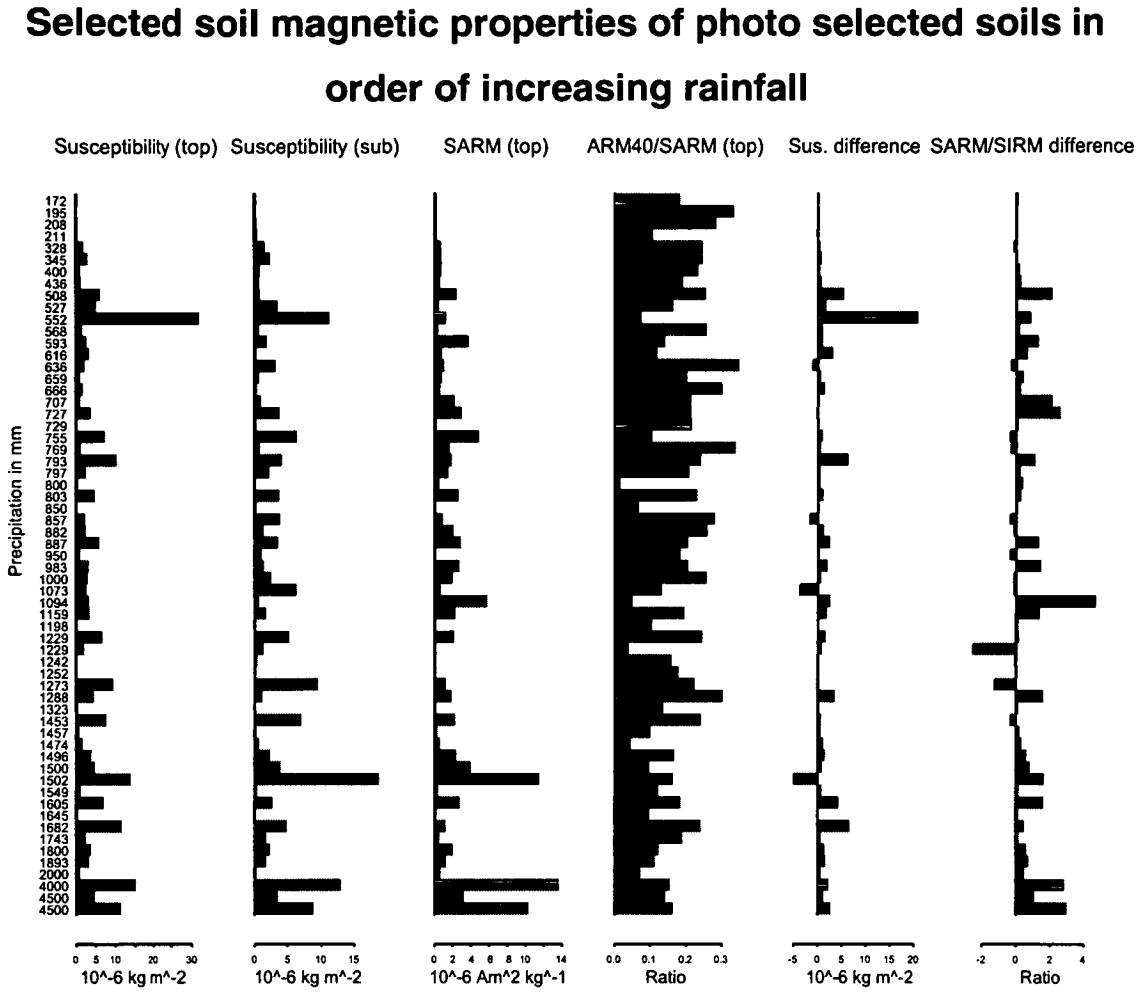

Figure 7.12. Magnetic parameters of top and subsoils selected using photographs and field notes, plotted as bars in order of increasing rainfall, numbers on left are annual rainfall at that soil site in mm. From left to right the barcharts show, topsoil susceptibility, subsoil susceptibility, topsoil SARM, topsoil ARM_{40}/SARM, topsoil minus subsoil susceptibility, and topsoil minus subsoil SARM/SIRM.

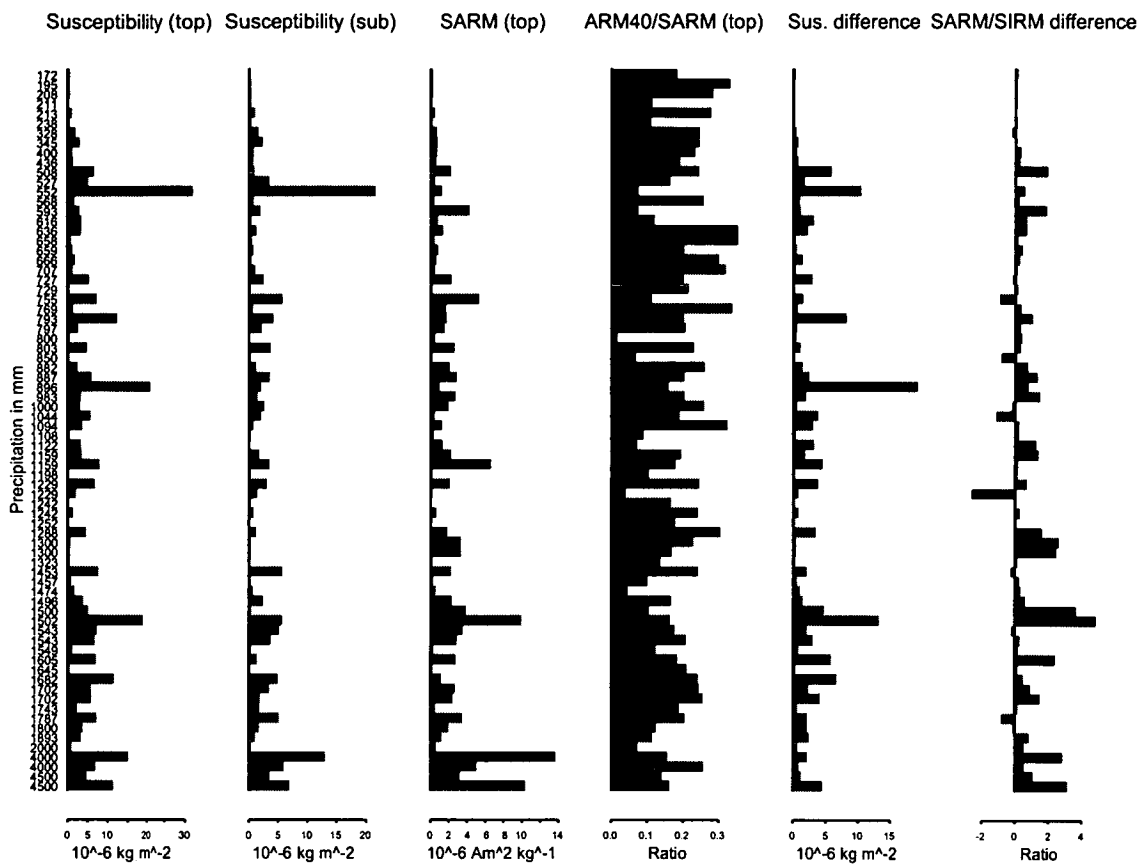

Figure 7.13. Magnetic parameters of top and subsoils selected using the susceptibility profile, plotted as bars in order of increasing rainfall, numbers on left are annual rainfall at that soil site in mm. From left to right the barcharts show, topsoil susceptibility, subsoil susceptibility, topsoil SARM, topsoil ARM_{40}/SARM, topsoil minus subsoil susceptibility, and topsoil minus subsoil SARM/SIRM.

Selected soil magnetic properties of SARM/SIRM selected soils in order of increasing rainfall

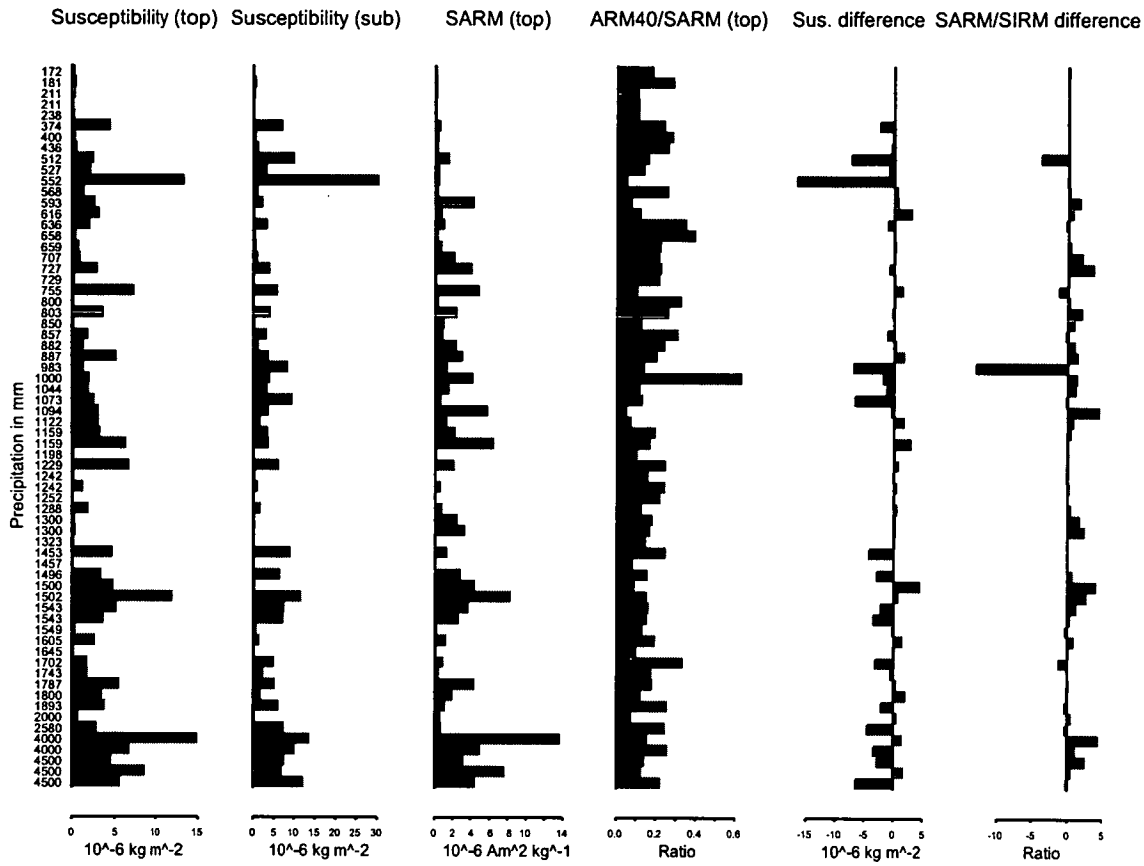

Figure 7.14. Magnetic parameters of top and subsoils selected using the SARM/SIRM profile, plotted as bars in order of increasing rainfall, numbers on left are annual rainfall at that soil site in mm. From left to right the barcharts show, topsoil susceptibility, subsoil susceptibility, topsoil SARM, topsoil ARM_{40}/SARM, topsoil minus subsoil susceptibility, and topsoil minus subsoil SARM/SIRM.

r^2 between selected magnetic parameters and soil site rainfall

	Susceptibility (top)	Susceptibility (sub)	SARM (top)	ARM_{40}/SARM (top)	Susceptibility difference	SARM/SIRM difference
Photo selected	0.074	0.144	0.333	0.072	0.011	0.336
Susceptibility selected	0.062	0.119	0.371	0.027	0.010	0.117
SARM/SIRM selected	0.211	0.118	0.291	0.005	0.006	0.029

Table 7.3. r^2 between the mean annual rainfall at each soil site and topsoil susceptibility, subsoil susceptibility, topsoil SARM, topsoil ARM_{40}/SARM, topsoil susceptibility – subsoil susceptibility, topsoil SARM/SIRM – subsoil SARM/SIRM.

7.7 Generation of soil magnetics, precipitation models

Regression models relating annual rainfall to soil magnetics have been generated. It is hoped that these multi-component magnetics to rainfall relationships will account

for more of the variability in the soil magnetics data than single soil magnetic parameters (Figures 7.12 - 7.14). Separate models were generated for each of the three topsoil and subsoil horizon selection procedures, and in turn, for each of three different rainfall functions, rainfall; logged rainfall and square rooted rainfall. Hence nine different model types were investigated (light grey boxes in Figure 7.15). The fifteen magnetic measurements and ratios listed in Table 7.4. from both the topsoils and subsoils were used to were used as potential covariates when fitting the linear models.

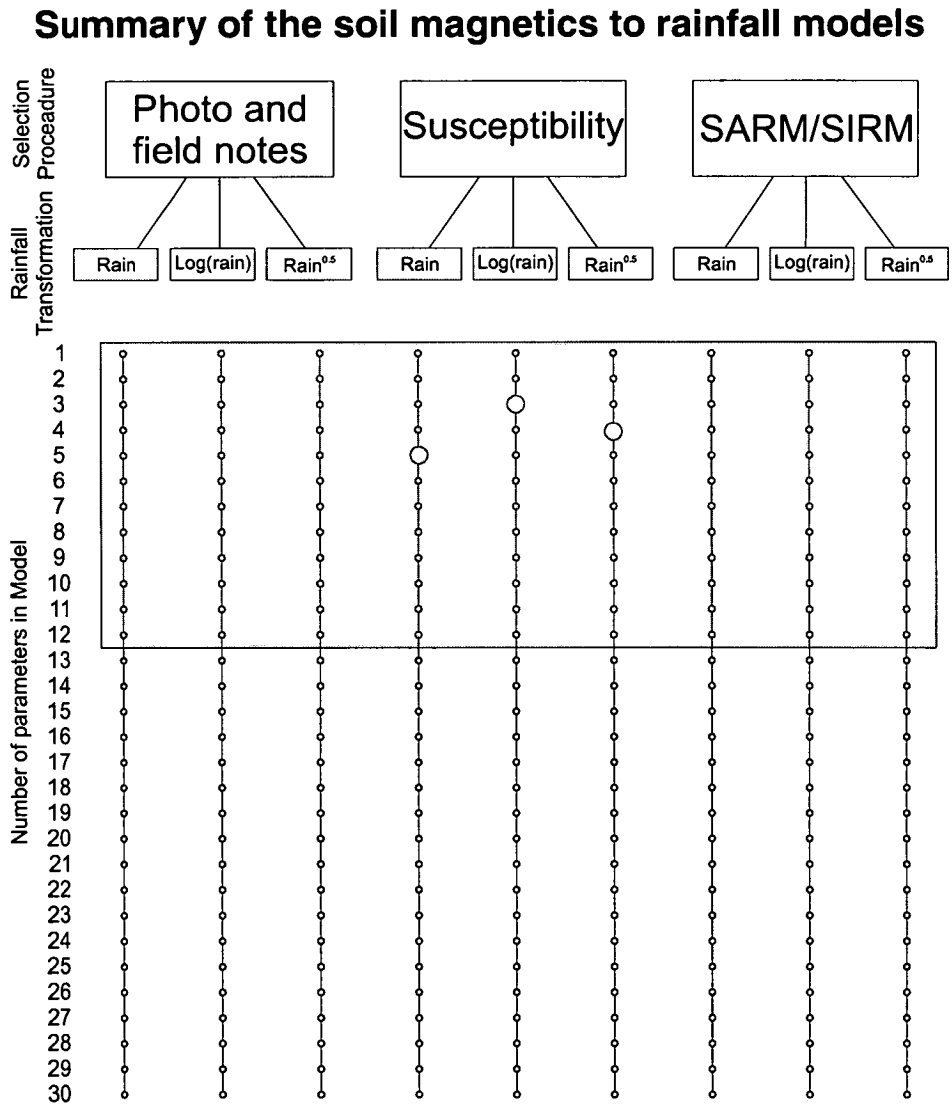

Figure 7.15. Summary of the 270 different soil magnetics to rainfall models generated. Models are shown as grey dots, large dots show the models with highest skill, and the large dark grey box indicates models shown in Figure 7.16.

The aim of the modelling was to construct the simplest linear models possible that explained a reasonable proportion of the variance. As a first step, thirty preliminary models were generated for each of the nine model types. The preliminary models consisted of linear combinations of from one to thirty of the magnetic parameters. The preliminary models were selected because they had the highest R^2 possible for that number of magnetic parameters. For example, the top right model in fig 7.15 is:

$$\sqrt{rain} = 28.096 + 2.223 * SARM^{top}$$

Equation 7.1

$SARM^{top}$ was selected as the single parameter exhibiting the highest correlation with rainfall using topsoils and subsoils selected by procedure one (photograph and field notes). In total 270 different models were generated at this stage of the selection procedure. All 270 models are represented graphically in Figure 7.15, where each model type is shown as a light grey box and each model as a dot. For all of these 270 models three selection parameters were calculated to assist in further selection namely i) correlation between the model and rainfall, ii) correlation between rainfall and predictions of rainfall made by the "leave one out" cross validation method (Chapter 4.3.3), and iii) skill (Equation 4.8). Graphs of these three selection parameters plotted against the number of parameters allowed (or levels) for the first twelve levels are shown in Figure 7.16. Simple, but parsimonious, models which account for a high proportion of the climatic variation stand out most clearly in Figure 7.16 as peaks in the traces of skill (black line).

Topsoil and subsoil magnetic parameters selected for modelling of rainfall

Measurement	Description
Susceptibility	Magnetic content.
Frequency dependent susceptibility	Detects material on the SD – super paramagnetic boundary.
SARM	All ARM remanence material.
ARM_{10}	ARM remanence material with very soft component removed.
ARM_{40}	ARM remanence material with soft component removed.
ARM_{80}	Hard ARM remanence material.
ARM_{40}/SARM	Ratio of Hard ARM to full ARM.
SARM/SIRM	Ratio of ARM remanence acquisition to saturation IRM acquisition, good for identifying magnetic interactions.
IRM_{40}	Soft IRM component.
IRM_{100}	Soft and medium IRM component.
IRM_{300}	All but hardest IRM component.
SIRM	Full IRM.
IRM_{40}/SIRM	Ratio of soft IRM to full IRM.
IRM_{100}/SIRM	Ratio of soft and medium IRM to full IRM.
IRM_{300}/SIRM	Ration of all but hardest IRM to full IRM.

Table 7.4. Magnetic measurements and ratios of magnetic measurements selected for linear modelling between soil magnetics and rainfall. Each measurement was included for each topsoil and subsoil.

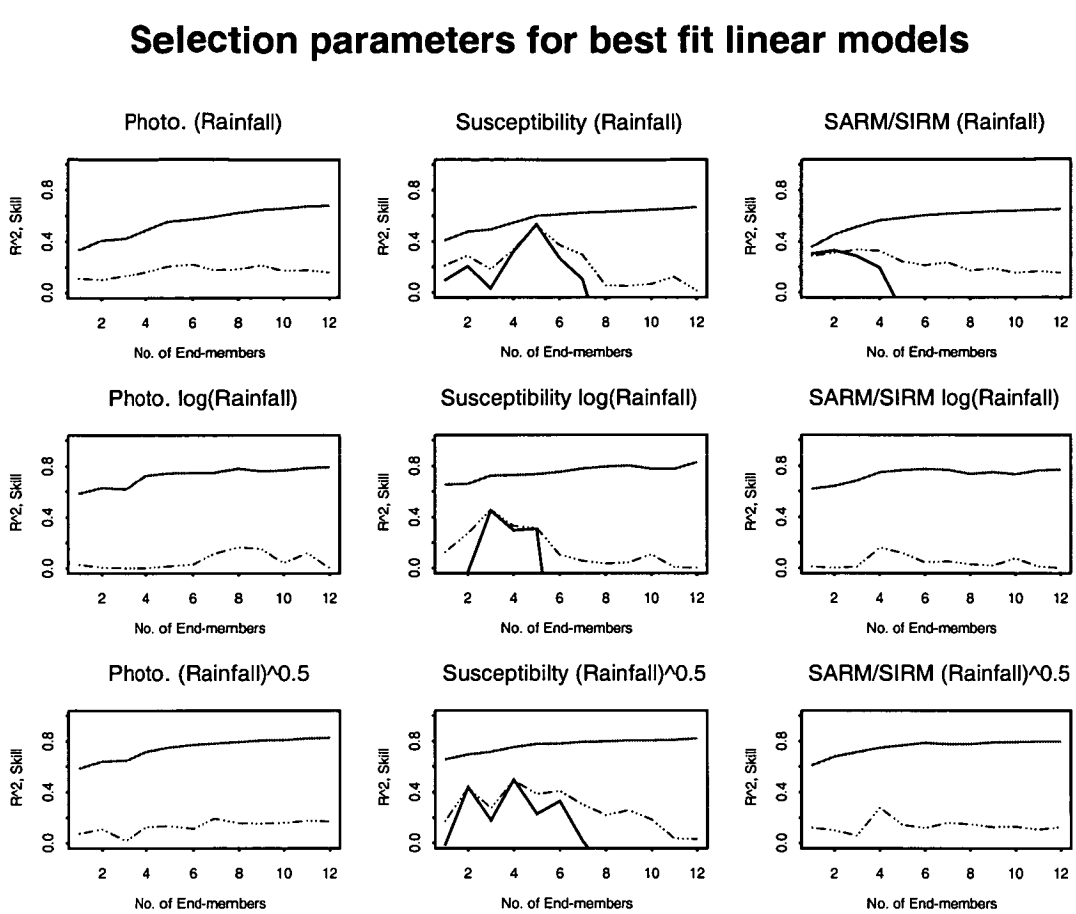

Figure 7.16. Summary of linear models between the three rainfall measurements (annual rainfall, logged rainfall and square rooted rainfall) on rows, and magnetic measurements on soils selected by the three topsoil and subsoil selection methods (on columns). Each plot shows the R^2 (grey line) skill (black line) and R^2 of predicted rainfall using the "leave one out" method (broken line), for the highest R^2 linear models for between one and twelve end-members.

Table 7.5 summarises the R^2, R^2 between rainfall and "leave one out" predictions of rainfall as well as the skill level for the three best models. Each of the highest skill models use topsoils and subsoils selected using the magnetic susceptibility of the soil profile. Also presented in Table 7.5 is the p value for each of these models. The p value gives the probability that a correlation at least as good as that seen in the observed model could occur in random data. Here the p values are all extremely low indicating that the models are reliable.

Best skill models for soil magnetics to rainfall, logged rainfall and square rooted rainfall

Model type	Number of magnetic parameters	p value	R^2	R^2 (Predicted rainfall to rainfall)	Skill
Rainfall	5	$2.33*10^{-12}$	0.599	0.524	0.533
$(Rainfall)^{0.5}$	4	$4.791*10^{-10}$	0.753	0.490	0.490
Log(Rainfall)	3	$4.379*10^{-8}$	0.73	0.456	0.451

Table 7.5. Summary of the number of magnetic parameters, p value, R^2 correlation coefficient, R^2 between rainfall and predicted rainfall (using "leave one out" model) and skill, for the best model relating magnetic parameters to rainfall, logged rainfall and square rooted rainfall, for each soil sampling site.

7.8 Results of soil magnetics, precipitation models

Table 7.6 shows which of the topsoil and subsoil magnetic parameters were used to generate each of the rainfall, logged rainfall and square rooted rainfall models for each of the three methods of topsoil and subsoil selection. Note that there is a great degree of similarity between all the different models with topsoil ARM_{40} and ARM_{40}/SARM in most of the models. IRM parameters are selected less often than ARM parameters, and always for subsoils. Susceptibility is not chosen at all. The models for method one (susceptibility profile) and three (photographs and field notes) of topsoil and subsoil selection chose mostly topsoil magnetic properties. The models for method two (SARM/SIRM ratio) of topsoil and subsoil selection method chose mostly subsoil magnetic properties. Because the linear models relating soil magnetics to rainfall, logged rainfall and square rooted rainfall, were dominated by ARM parameters, further models that included more ARM parameters, at the expense of some IRM parameters were generated. However, it was found that these models had lower skill than those generated with the existing selection of magnetic parameters.

Summary table for of magnetic parameters used in the 1, 2 and 3 component rainfall models

		Rainfall									Log (Rainfall)									Rainfall$^{0.5}$								
Soil selection method		Photo			Sus.			Ratio			Photo			Sus.			Ratio			Photo			Sus.			Ratio		
Number of parameters		3	4	5	3	4	**5**	3	4	5	3	4	5	**3**	4	5	3	4	5	3	4	5	3	**4**	5	3	4	5
Susceptibility	Top																											
	Sub																											
F.D. susceptibility	Top								+				+				+		+									+
	Sub																											
SARM	Top		+	+					+									+	+				-				+	+
	Sub							+	+	+								+	+							+	+	+
ARM_{10}	Top		-								-			-	-	-												
	Sub				-	-	-	-	-	-								-	-					-	-	-	-	-
ARM_{40}	Top	+		-	+	+	+				+	+	+	+	+	+				+	+	+	+	+	+			
	Sub																	+	+								+	+
ARM_{80}	Top	-																										
	Sub		+					+	+	+										+						+		
ARM_{40}/SARM	Top	-			-	-	-				-	-	-	-	-					-	-	-	-	-	-			
	Sub		-																									
SARM/SIRM	Top															-												
	Sub																											
IRM_{40}	Top									+																		
	Sub			-								-	-								-	-						
IRM_{100}	Top																											
	Sub			+		+	+					+	+								+	+						
IRM_{300}	Top														+													
	Sub																							+	+			
SIRM	Top																											
	Sub			-			-															-			-			
IRM_{40}/SIRM	Top																											
	Sub																+											
IRM_{100}/SIRM	Top																											
	Sub																-											
IRM_{300}/SIRM	Top															+												
	Sub															-												

Table 7.6. Summary table of magnetic parameters included in each of the linear models relating magnetic properties of soils to rainfall, logged rainfall and square rooted rainfall. Positive coefficient indicated by + negative coefficient by -. Best models indicated with bold writing in second row. Photo = models selected with photographs and field notes, sus. = models selected with susceptibility profiles, ratio = models selected with SARM/SIRM ratio.

Plots of actual rainfall against modelled and predicted rainfall for the highest skill models are represented in Figure 7.17. As would be expected the plots of predicted rainfall against actual rainfall, display a lower fit than the plots of modelled rainfall against actual rainfall. There is a gap between rainfalls of 2000mm yr^{-1} and 3500mm yr^{-1}, as susceptibility enhancement was not identified in any of the few soil samples collected in this rainfall range.

Modelled and predicted mean annual rainfall plotted against actual rainfall, for the highest skill models

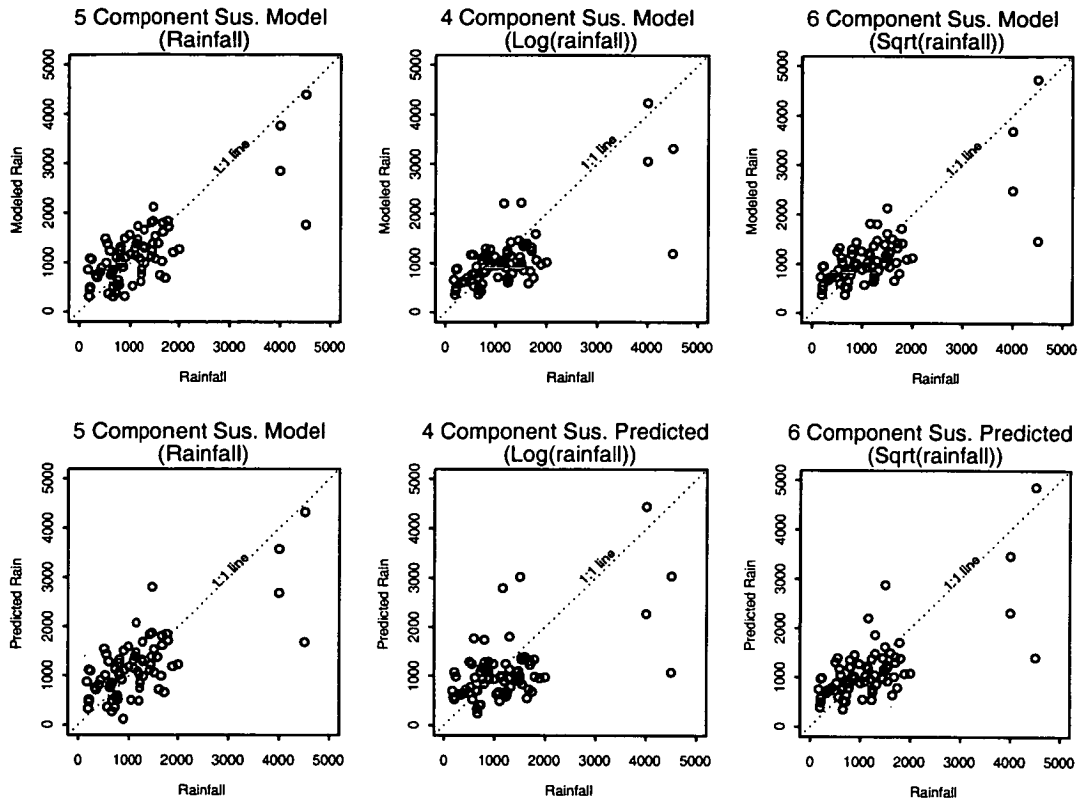

Figure 7.17. Plots of the modelled rainfall and predicted rainfall (using the "leave one out" method) against the actual rainfall at each soil site. The three models represented are for mean annual rainfall, log (mean annual rainfall) and square root (mean annual rainfall). Broken line lies on the 1:1 relationship.

The highest skill models for relating susceptibility-selected topsoil and subsoil magnetic properties to mean annual rainfall, logged mean annual rainfall and square rooted mean annual rainfall are given in Equations 7.2, 7.3 and 7.4.

Model 1, best skill model relating magnetic properties of susceptibility-selected topsoils and subsoils to mean annual rainfall

$$\text{Rainfall} = 1472.9 + 1932 * ARM_{10}^{top} - 3630 * ARM_{40}^{top} / SARM^{top} - 304 * ARM_{10}^{sub} + 106.4 * IRM_{300}^{sub} - 98 * SIRM^{sub}$$

Equation 7.2

Model 2, best skill model relating magnetic properties of susceptibility-selected topsoils and subsoils to logged mean annual rainfall

$$Log(\text{Rainfall}) = 7.261 - 0.310 * ARM_{10}^{top} + 2.665 * ARM_{40}^{top} - 4.354 * ARM_{40}^{top} / SARM^{top}$$

Equation 7.3

Model 3, best skill model relating magnetic properties of susceptibility-selected topsoils and subsoils to square rooted mean annual rainfall

$$\sqrt{\text{Rainfall}} = 33.6 + 24.26 * ARM_{40}^{top} - 55.5 * ARM_{40}^{top} / SARM^{top} - 3.98 * ARM_{10}^{sub} + 0.093 * IRM_{300}^{sub}$$

Equation 7.4

7.8.1 Overview of the best three models

The first thing to notice about the best three models (Equations 7.2, 7.3 and 7.4) relating rainfall to soil magnetic properties, is their similarity. There are only six different soil magnetic parameters represented in all three models, out of a possible choice of thirty soil magnetic parameters. There is also good consistency between models. Specifically, where a model contains a parameter that is present in another model the sign of the multiplier is the same in all but one case (Table 7.7).

Summary of best skill magnetic parameter to rainfall models

	Constant	ARM_{10}^{top}	ARM_{40}^{top}	ARM_{40}^{top}/ $SARM^{top}$	ARM_{10}^{sub}	IRM_{300}^{sub}	$SIRM^{sub}$
Rainfall	1472.9	1932		-3630	-304	106.4	-98
Log(rainfall)	7.26	-0.310	2.665	-4.35			
$(Rainfall)^{0.5}$	36.6		24.26	-55.5	-3.98	0.093	

Table 7.7. Coefficients for the best skill models that relate the magnetic parameters of topsoil and subsoil materials chosen using the susceptibility method, to rainfall. Negative coefficients are grey.

The barplots, Figs 7.18, 7.19 and 7.20, show summaries of the model components, for each of the best three models, applied to the susceptibility-selected topsoils and subsoils. The plots of models one and three (Figs 7.18 and 7.20) indicate that the subsoil magnetic components generally make a negative rainfall contribution to the overall model. The topsoil components of model one (Figure 7.18) generally make a positive rainfall contribution. However the topsoil components of models two and three (Figs 7.19 and 7.20) generally make a negative rainfall contribution.

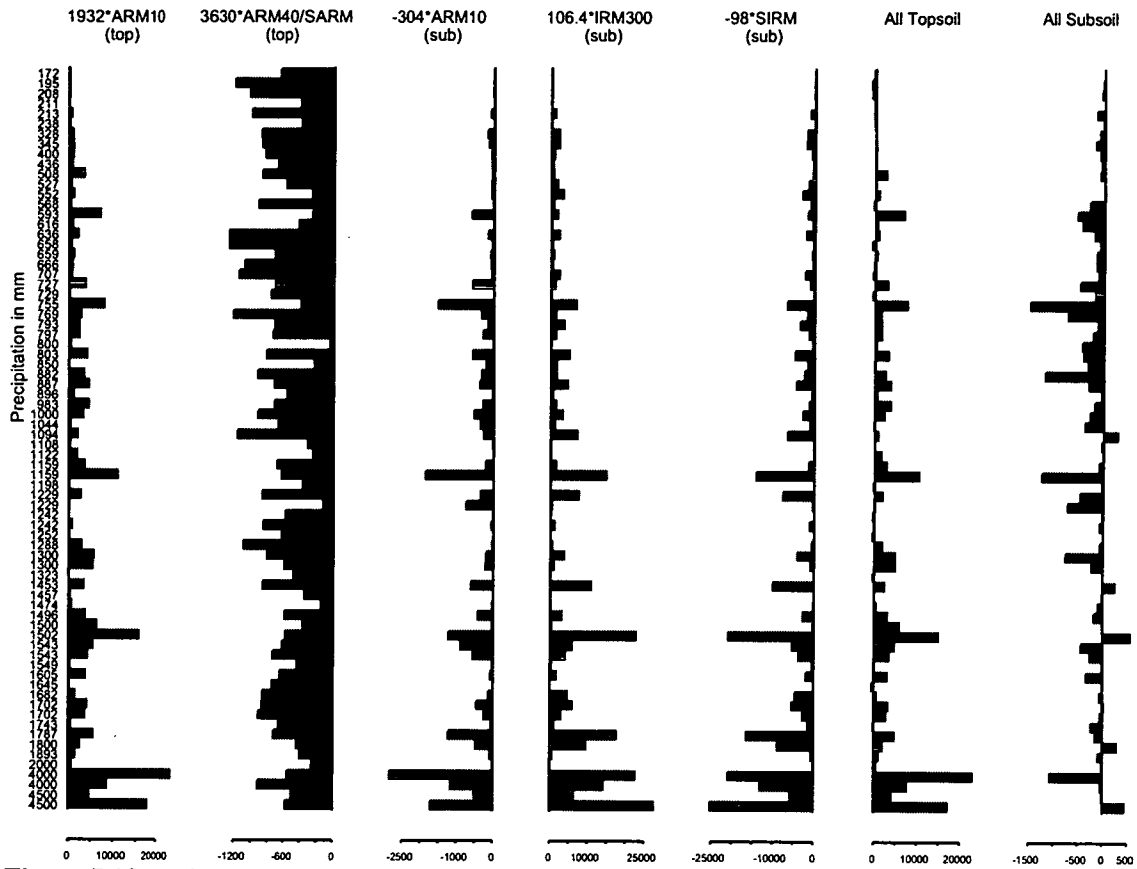

Figure 7.18. Multiplication of relevant soil magnetic parameters by model 1 (Equation 7.2) linear model coefficients. Also plotted are the result of summing all topsoil and all subsoil components. Bars in order of increasing rainfall downwards, numbers on left are annual rainfall at that soil site in mm.

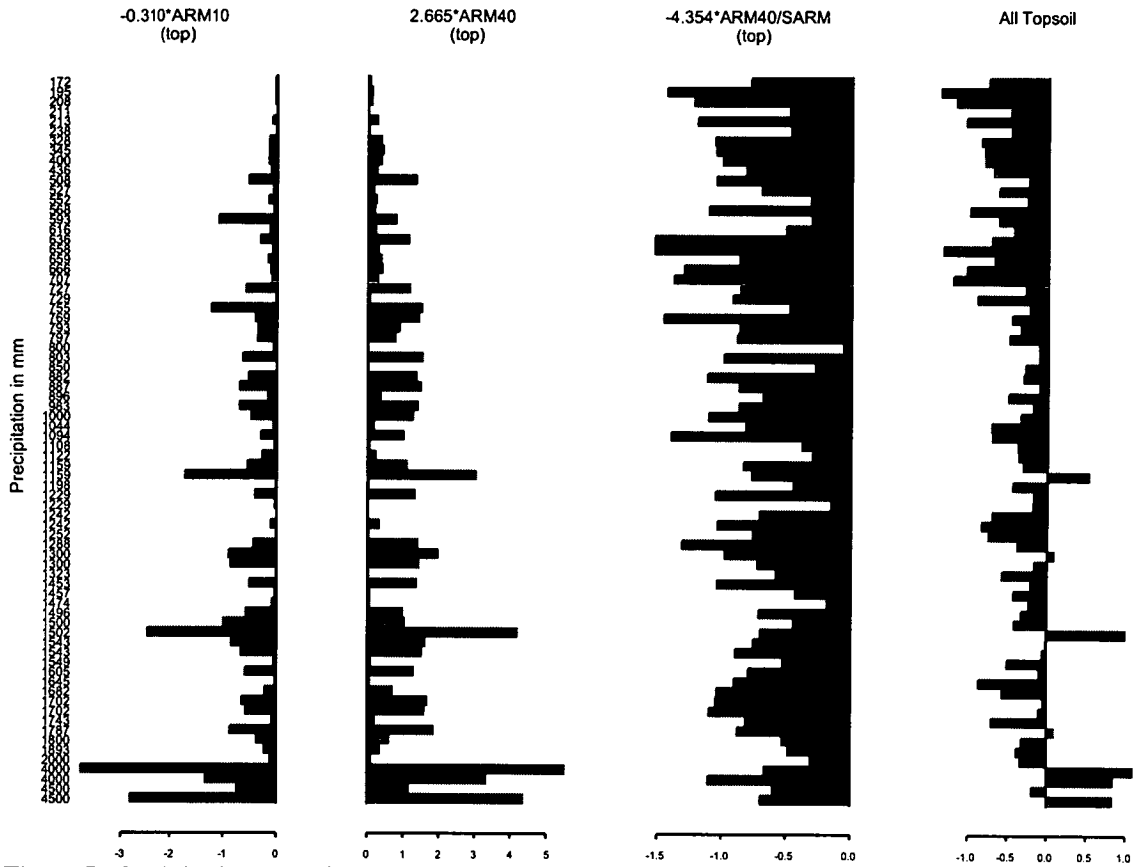

Figure 7.19. Multiplication of relevant soil magnetic parameters by model 2 (Equation 7.3) linear model coefficients. Also plotted are the result of summing all topsoil components. Bars in order of increasing rainfall downwards, numbers on left are annual rainfall at that soil site in mm.

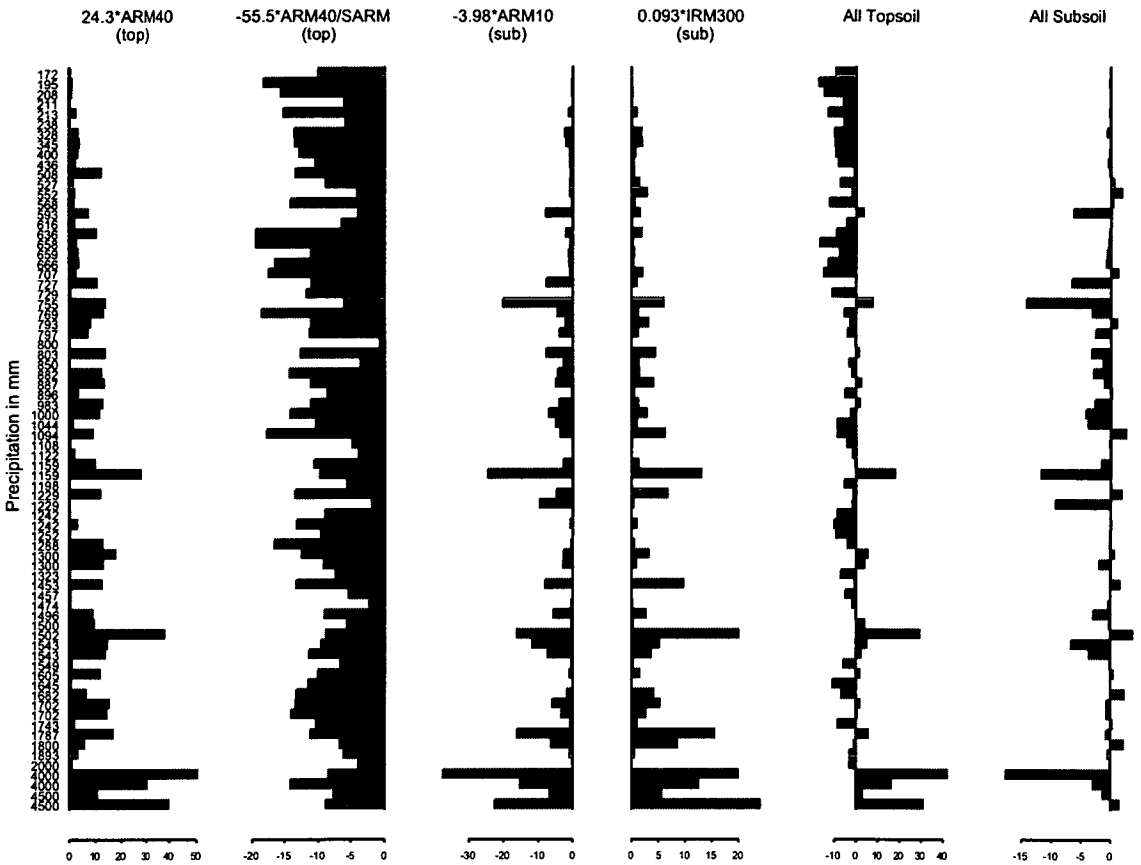

Figure 7.20. Multiplication of relevant soil magnetic parameters by model 3 (Equation 7.4) linear model coefficients. Also plotted are the result of summing all topsoil and all subsoil components. Bars in order of increasing rainfall downwards, numbers on left are annual rainfall at that soil site in mm.

7.9 Interpretation of the soil magnetics to rainfall models

The $ARM_{40}^{top}/SARM^{top}$ ratio is present in all three of the highest skill models and its coefficient is always negative. This means that soils collected in high rainfall regions tend to have low $ARM_{40}^{top}/SARM^{top}$ ratios, indicating that they contain material that is easily demagnetised by an ARM_{40} field. A common characteristic in models one and two (Equations 7.2 and 7.3) is a positive coefficient for ARM_{10}^{top}, indicating that soils which experience high rainfall exhibit high ARM magnetisation. The models' selection of ARM_{10}^{top} instead of $SARM^{top}$ suggests that the softest ARM component is not important in the characterisation of high rainfall soils. The ARM_{10}^{sub} parameter appears in models one and three (Equations 7.2 and 7.4). Unlike the coefficients for ARM_{10}^{top} in models one and two (Equations 7.2 and 7.3), the coefficients for ARM_{10}^{sub} in models one and three are negative. The negative coefficient for ARM_{10}^{sub} allows the models to remove subsoil magnetics, equalising the magnetic properties of soils developing on highly magnetic materials and those developing on less magnetic materials. The subsoil parameter IRM_{300}^{sub} also occurs in models one and three. In both cases its coefficient is positive. However, in Figure 7.18 and 7.20 the overall contribution of the subsoil magnetic components, for models one and three, is negative. None of the models use the susceptibility parameter for either

topsoil or subsoil material. Perhaps this is because the ARM_{10}^{top} parameter provides a more reliable indication of topsoil enhancement, as it does not include the effects of paramagnetic and diamagnetic material, or the softest ARM component.

The magnetic properties of several magnetic minerals, and magnetotactic bacteria have been multiplied by the coefficients of the best three models, (Equations 7.2, 7.3 and 7.4) and then summed. This has been done in order to investigate how rainfall might effect the magnetic mineralogy of the soils in this study. The result of multiplying the magnetic properties of magnetic minerals and magnetotactic bacteria by the topsoil and subsoil coefficients of the best three models can be seen in Figure 7.21, 7.22 and 7.23. In the case of model two, which only has topsoil coefficients, these are plotted on their own. The conversion of the magnetic minerals by the three models' coefficients indicates whether different magnetic materials in topsoils and subsoils are associated with high or low rainfall for the soils in this study. However care must be taken when interpreting these diagrams, as the models contain constant term as well as the magnetic parameter coefficients. Also, models two and three relate magnetic parameters to the log and square root of mean annual rainfall respectively. The constant term in all three models and model two and three's relationship to non-linear rainfall, means that the interpretation of the position of the minerals in Figure 7.21 7.22 and 7.23, should be carried out in relative and not absolute terms.

In both models one and three, the magnetic minerals, MD magnetite, PSD magnetite, soft haematite and hard haematite plot near the zero on the subsoil axis. These minerals plotting near the zero on the subsoil axis indicates that their presence in the subsoil is not a rainfall indicator. In model one and model three, SD magnetite plots in the positive part of the subsoil axis, and bacteria and viscous magnetite in the negative part of the subsoil axis. To understand the association of bacteria and viscous magnetite in subsoils to lower rainfall, it is necessary to look at the effect of these two materials when multiplied by the topsoil coefficients. In model one, bacteria and viscous magnetite are the only materials in the positive section of the topsoil axis, in model three, bacteria is the only material in the positive topsoil axis, and viscous magnetite is close to the zero line. The combination of a material that plots in the positive or near zero topsoil axis and the negative subsoil axis, indicates that high rainfall will either increase the topsoil, or decrease the subsoil concentration of these materials. Figure 7.21 and 7.23 indicate that soils which experience high rainfall will have more material which is similar to viscous magnetite or magnetotactic bacteria in their topsoil than in their subsoil. Interestingly, SD magnetite shows the opposite relationship in both models one and three. SD magnetite in models one and three is in the positive section of the subsoil axis and the negative section of the topsoil axis, suggesting that high rainfall will deplete single domain magnetite in the topsoil.

Model two uses no subsoil parameters, this makes the interpretation of Figure 7.22 more straightforward. Bacteria and MD magnetite are the only materials which plot in the positive section of the graph, although viscous magnetite only just falls in the negative section. SD magnetite, titanomagnetite and soft and hard haematite all fall in the high negative section of the plot. The positions of the minerals in Figure 7.22 indicate that soils in the study set that are associated with high rainfall have magnetic properties similar to bacterial magnetosomes, MD magnetite and viscous magnetite.

Soils with magnetic properties similar to soft or hard haematite, SD magnetite and titanomagnetite were associated with lower rainfall. A possible explanation for this finding would be the transformation of haematite, SD magnetite and titanomagnetite materials into bacterial magnetite, viscous magnetite or MD magnetite in wet conditions.

7.9.1 Soil magnetics climo-functions

Looking at Figure 7.17 and Table 7.7, we see that there appears to be a relationship between rainfall and soil magnetics for the soils collected in Mexico. However, the predictive capabilities and skill of the models linking soil magnetics to rainfall are not very good. None of the models developed have a skill over 0.6 and the predicted rainfall (Figure 7.17) in many cases is in error by over 500mm. It is not recommended that any of the soil magnetic to rainfall models that have been developed using these Mexican soils should be used as climo-functions.

Multiplication of magnetic minerals by model one topsoil and subsoil magnetic parameter coefficients

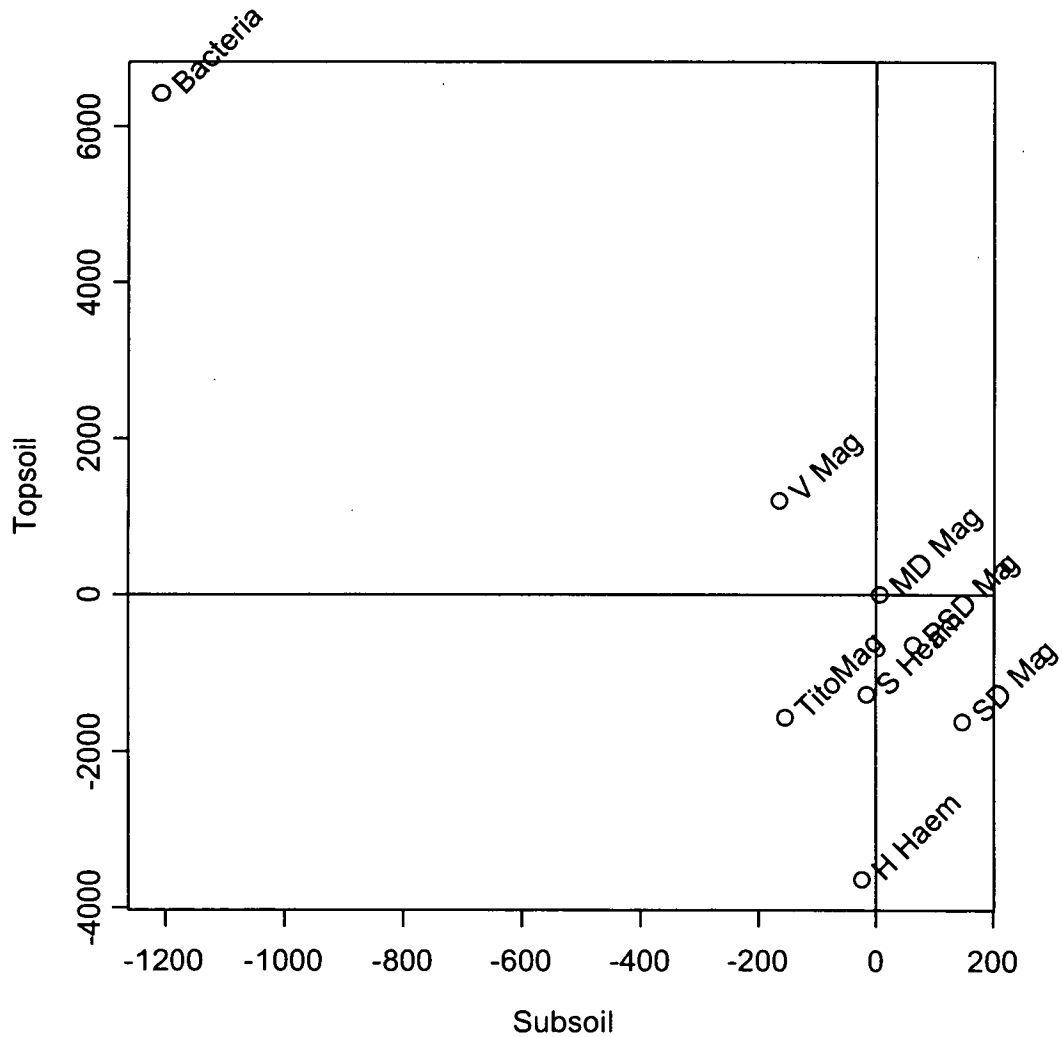

Figure 7.21. Biplot of magnetic minerals magnetic parameters multiplied by model one (Equation 7.2) subsoil (horizontal) and topsoil (vertical) parameter coefficients, then summed.

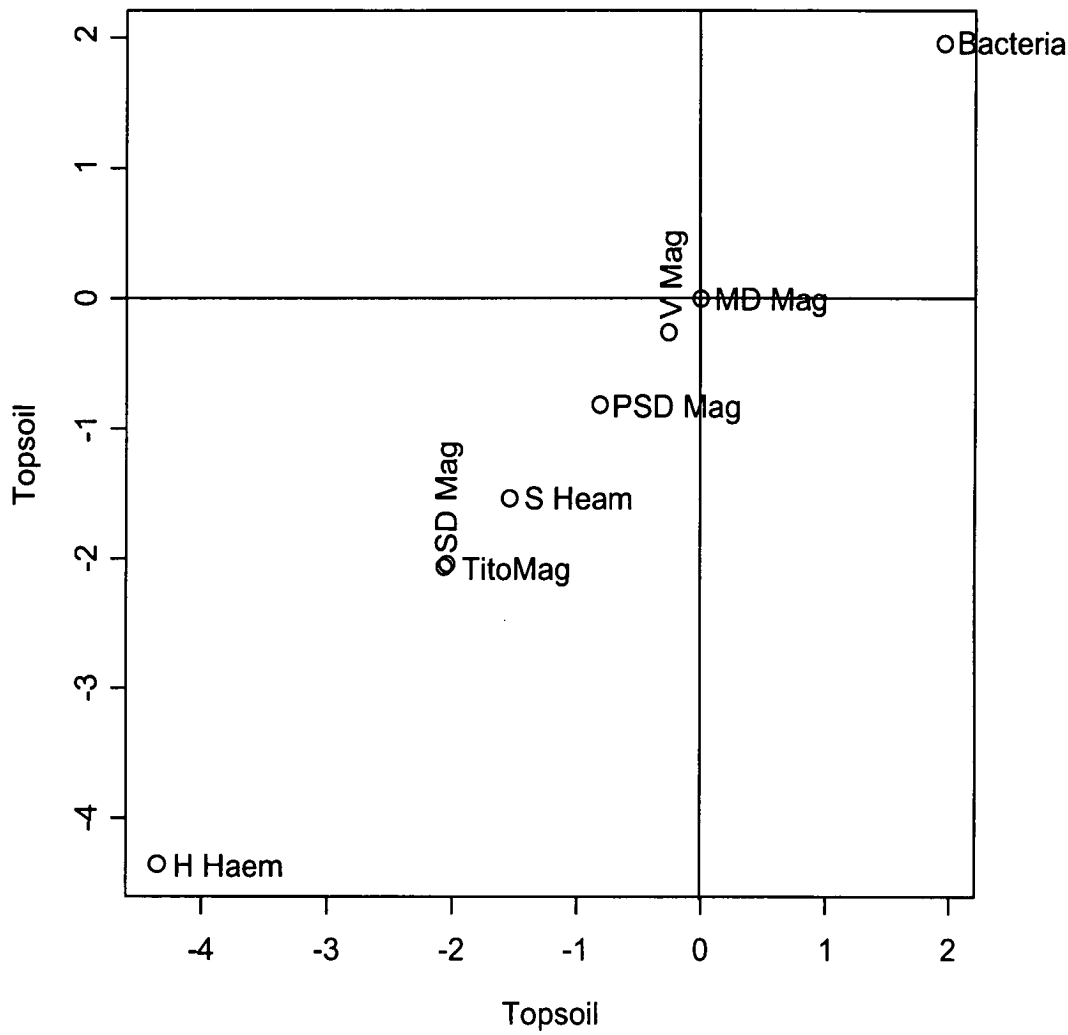

Figure 7.22. Biplot of magnetic minerals magnetic parameters multiplied by model two (Equation 7.3) topsoil (horizontal and vertical) parameter coefficients, then summed.

Multiplication of magnetic minerals by model three topsoil and subsoil magnetic parameter coefficients

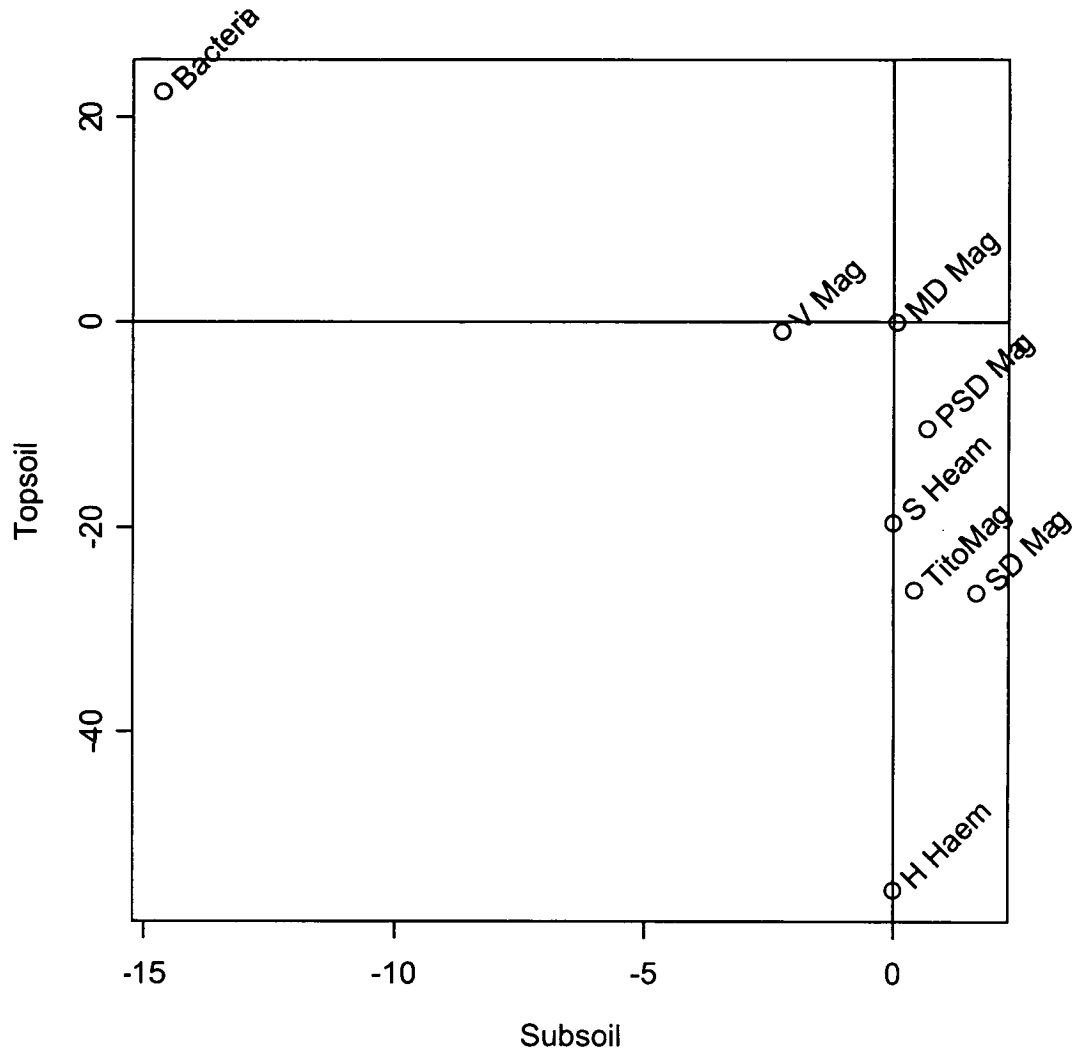

Figure 7.23. Biplot of magnetic minerals magnetic parameters multiplied by model three (Equation 7.4) subsoil (horizontal) and topsoil (vertical) parameter coefficients, then summed.

7.10 Discussion

Previous studies have indicated a link between a soil's magnetic enhancement and the annual rainfall that it receives (Maher *et al.,* 1994). This relationship, when applied to the magnetic properties of loess and palaeosol deposits in China, gives access to a long palaeoclimate record (Maher *et al.,* 1994; Maher and Thompson, 1999). A rainfall-susceptibility relationship has also been found in soils from the Northern Hemisphere Temperate Zone (Maher and Thompson, 1995). However, for these soils, only the magnetic susceptibility was measured, and only one soil in the sample set received more than 1,500mm of rainfall per year.

Eighty-nine soil profiles from Mexico, which received an annual rainfall of between 300 and 4,500mm, have provided the raw material for this investigation into the

relationship between soil magnetics and rainfall. For each sample from each soil profile, eighteen remanance and susceptibility measurements have been made. This constitutes the largest soil remanence data set from a single country to have been investigated for a link between soil magnetic properties and rainfall.

The results of the modelling work that has been carried out on the Mexican soil profile data set show that a statistically significant relationship exists between the magnetic properties of the soils in the data set and rainfall. This is despite the fact that no specific account was made of soil forming factors other than rainfall (Chapter 3.4 and Chapter 7.1). The fact that significant relationships between soil magnetics and rainfall are found in the highly varied set of soils in this study, even without discounting "undesirable soils" (Chapter 3.4.3 and Chapter 7.2), indicates that soil magnetics are strongly related to rainfall.

Susceptibility enhancement is the best method of distinguishing between topsoil and subsoil material when investigating the relationship between soil-magnetics and rainfall. Of the different soil magnetic measurements, ARM properties were found to be the most sensitive to rainfall. An indication of the effects of high rainfall on the magnetic mineral assemblage of soils has been discovered by multiplying the magnetic properties of magnetic minerals and magnetotactic bacteria magnetosomes by the topsoil and subsoil coefficients of the highest skill models. Similar to the findings of previous workers (Maher, 1998; Maher and Thompson, 1999), it was found that topsoils in high rainfall regions show an enhancement of materials with magnetic properties similar to viscous magnetite and magnetotactic bacteria magnetosomes. However, the action of magnetotactic bacteria in soils is not suggested as a cause of the difference between the magnetic properties of soils from high rainfall and low rainfall regions. Both Maher and Thompson (1995) and Dearing *et al.*, (2001) have found that the concentrations of magnetotactic bacteria in soils are too low to explain a soil-magnetics to rainfall relationship. Instead, the evidence here is in agreement with (Maher, 1998; Maher and Thompson, 1999) who suggest that weakly magnetic iron oxides are transformed into fine-grained magnetite when subjected to high rainfall.

Unfortunately, none of the models generated in this study has a sufficient skill or predictive capability to act as a climo-function. If a climo function is to be sought greater care should be taken over the choices of soils, in regard to the soil forming factors described by Jenny (1941) (Chapter 3.4) and the undesirable soils for susceptibility enhancement as listed by Maher and Thompson (1999) (Chapter 3.4.3).

7.11 Conclusions

1. Susceptibility enhancement was found to be the best method of selecting topsoils and subsoils for the analysis of a relationship between soil magnetic properties and rainfall.
2. A statistically significant relationship exists between the magnetic properties of soils collected from across steep rainfall gradients in Mexico, and the mean annual rainfall at those locations.
3. The ARM properties of soils show the strongest dependence on rainfall, especially ARM_{10} and ARM_{40}/SARM of the topsoil.
4. Neither susceptibility nor frequency dependent susceptibility were selected by any of the high skill models to relate soil magnetics to rainfall in Mexico.
5. In this study it was found that high rainfall increased the abundance of materials with magnetic properties similar to viscous magnetite and magnetotactic bacteria magnetosomes.

Chapter 8

Conclusions

At the end of each of the previous chapters I have given a summary of results and findings for that chapter. In this chapter I shall bring together these findings and look at their relevance in a wider context.

8.1 Unmixing

I have developed a new unmixing technique that facilitates quantitative interpretation of environmental magnetic measurements made on sediment sequences. This technique converts magnetic measurements, through the use of the non-negative least squares method, into concentrations of magnetic end-members. By using end-members collected from within a lake's catchment, it is possible to identify the most likely source of lake core material. Unmixing the magnetic properties of lake sediments in terms of catchment end-members gives a better understanding of the environment in which the sediment was deposited.

The use of non-negative least squares means that the non-convergence and local minima problems of the established SIMPLEX technique can be avoided. A parsimonious stepwise end-member selection routine allows a wider variety of catchment material end-members to be included in the unmixing model without fear of over-fitting. I have also generated two different tests that can be run upon unmixing models. The first of these tests gives an estimation of the error on the end-members of the unmixing model, by looking at the stability of the inversion matrix. The second test gives a measure of the unmixing model's skill. The skill measure defines the predictive capability of the unmixing model, and through its use the validity of the unmixing model can be tested.

Tests of the unmixing model, using synthesised measurements of five different mixtures of six catchment end-members, have been carried out. The results of these tests have shown that the new unmixing technique can successfully unmix two component magnetic mixtures. Unmixing is possible even when the magnetic properties of the individual magnetic end-members are very similar.

The non-negative least squares unmixing technique provides a fast method of turning magnetic data from lake sediment cores into a record of sediment source history. This unmixing method is unique because it not only avoids the local minima problems encountered by previous techniques, but also gives error bounds on the

concentration of source types, plus a measure of the model's skill. I suggest that this method could be routinely used with lake sediment cores to identify interesting core horizons, which could then be studied further with more time consuming techniques.

8.2 Application of magnetic unmixing

The application of the new unmixing technique to cores taken from two highland lakes in Mexico, uniquely allows the quantitative modelling of lake sediment sources through time. The identification of soil erosion, and the differentiation between topsoil and subsoil erosion in the magnetic unmixing models, gives an indication of both the quantity and seasonality of rainfall in a lakes catchment. This in turn gives a strong indication of the environment at the time of sediment deposition.

The interpretations of the unmixing models generated for Lake Pátzcuaro and Lake Babicora are in broad agreement with the previous studies of the lake sediments. For Lake Pátzcuaro in the Southern Mexican plateau, two successive drops in lake level at 10,000 and 5,000 ^{14}C yr B.P. coincide with reductions in the amount of soil erosion in the lake catchment. Three periods of high core susceptibility that occur after 3,500 ^{14}C yr B.P. are attributed by the model to topsoil and subsoil influx. It had been suggested by O'Hara *et al.*, (1993) that these high susceptibility periods in Lake Pátzcuaro's sediments were related to soil erosion caused by farming. The results of the magnetic unmixing strengthen this hypothesis. O'Hara *et al.*, (1993) also report that the second period of high erosion, which lasted from 2,530 until 1,190 ^{14}C yr B.P., was more severe than the period of high erosion before or after it. This is, again, supported by the magnetic unmixing model, which indicates a large volume of subsoil and bedrock erosion in the Pátzcuaro catchment at this time.

The unmixing models produced for Lake Babicora in the Northern Mexican plateau have also identified erosion patterns that are consistent with the results of previous palaeolimnological studies. Two lake level reductions, at 29,000 and 11,000 ^{14}C yr B.P., coincide with reductions in the concentrations of topsoil and subsoil erosion in the unmixing model. However, a previously reported increase in lake level at around 5,000yr B.P. is not seen in the unmixing model. One feature that is apparent in the unmixing model that is not apparent in any of the previous work on Lake Babicora, is a dramatic shift from topsoil erosion to subsoil erosion at 15,000 ^{14}C yr B.P. I believe that the change from topsoil to subsoil erosion at this time was caused by a switch to more seasonal rainfall causing large, erosional gullies.

8.3 The magnetic properties of Mexican soils

Previous work looking at the relationship between annual rainfall and the magnetic properties of soils has been mostly limited to soil receiving less than 1,500mm of precipitation a year. The majority of these studies concentrate on the magnetic susceptibility of the soils in question (Maher *et al.*, 1994; Han *et al.*, 1996; Maher and Thompson, 1995; Maher and Thompson, 1999). This study is the first to investigate a link between the magnetic remanence properties of soil profiles and rainfall, for soils receiving an annual precipitation of between 300 and 4,500mm.

Multiple component linear models relating annual rainfall to the magnetic properties of topsoils and subsoils selected by one of three procedures were produced. The highest skill models were selected in order to ensure that over-fitting of the precipitation data by the large amount of magnetics data did not occur. The three highest skill models all used a selection procedure that chose topsoils and subsoils on the basis of the susceptibility of the soil profile. These highest skill models showed that a highly significant relationship exists between soil-magnetics and rainfall in the soils from this data set in spite of the fact that the relationship developed did not account for any soil forming factors other than annual rainfall.

During the model selection process it was noticed that the ARM properties of soils, and especially topsoils, were selected more often than the IRM properties. Further investigation of the best skill models relating soil-magnetics to rainfall showed that the soils that received higher rainfall tended to exhibit magnetic properties similar to fine grained magnetite and magnetotactic bacteria magnetosomes. However, both Maher and Thompson (1995) and Dearing *et al.*, (2001) have shown that magnetotactic bacteria are an unlikely cause for the magnetic enhancement of soils that receive high rainfall.

8.4 Further Work

It is difficult to find an independent test of the unmixing model. One possible method would be to create physical mixtures of catchment material and then attempt to unmix them using magnetic measurements. However, unmixing physical catchment mixtures would not prove that the unmixing procedure works for lake sediments. Alternatively, it may be possible to test magnetic unmixing if a lake could be found that had sediments whose sources could be identified by other means i.e. chemistry or sediment colour. A more qualitative test of the unmixing procedure could be achieved by multiple magnetic extraction experiments, on both catchment and sediment samples. Extraction, coupled with X-ray diffraction and optical and transmission electron microscope analysis, may give a further insight into the similarity between the remanence-carrying material in the lake sediments and in the lake catchment.

Further work needs to be carried out to discover what effects sediment sorting and winnowing has on the magnetic unmixing models. All the models developed here used bulk magnetic properties of catchment samples. Perhaps unmixing in terms of the magnetic properties of various size fraction splits of catchment material could improve the applicability of magnetic unmixing. Also more systematic sampling of lake catchment material could be helpful in the characterisation of soil magnetic properties when unmixing.

The work that has been carried out on the set of soils I collected in Mexico strengthens the case for a link between the magnetic properties of soils and rainfall. To further investigate this relationship it would be advantageous to remove as many of the other factors of soil formation from the sample set as possible. An ideal soil sample set for investigating the relationship between soil magnetics and rainfall would consist of soils of the same age on the same parent material but with varying rainfall. It would seem that loess plateaus may be the ideal place to identify, and gain

a better understanding of the relationship between soil magnetics and climate. I would certainly suggest that ARM parameters, and ARM ratios should be measured in any future studies, as these magnetic properties of a soil seem to be the most sensitive to rainfall.

References

Abdul-Razzaq, W., and Gautam, M., 2001. Discovery of magnetite in exhausted material from a diesel engine. *Applied Physics Letters*, **78**, 218-219.

Bazylinski, D.A., Garret-Reed, A.J., and Frankel, R.B., 1994. Electron microscopic studies of magnetosomes in magnetotactic bacteria. *Microscopic Research Technology,* **27**, 389-401.

Blakemore, R.P., 1975. Magnetotactic bacteria. *Science*, **190**, 377-379.

Bloemendal, J., and Barton, C.E., 1985. Correlation between rayleigh loops and frequency-dependant and quadrature susceptibility: Application to magnetic granulometry of rocks. *Journal of Geophysical Research,* **90**, 8789-8792.

Bradbury. J.P., 1989. Late Quaternary lacustrine paleoenvironments in the Cuenca de Mexico. *Quaternary Science Reviews*, **8**, 75-100.

Bradbury. J.P., 2000. Limnologic history of lago de Pátzcuaro, Michoacán, Mexico for the past 48,000 years: impacts of climate and man. *Palaeogeography, Palaeoclimatology, Palaeoecology*, **163**, 69-95.

Bridges, E.M., 1997. World soils (third edition). Cambridge University Press.

Bridgwater, N.D., Heaton, T.H.E. and O'Hara, S.L., 1999. A late Holocene palaeolimnological record from central Mexico, based on floral and stable-isotope analysis of ostrocod shells. *Journal of Palaeolimnology*, **22 (4)**, 283-297.

Canfield, D.E., and Berner, R.A., 1986. Dissolution and pyritization of magnetite in anoxic marine sediments. *Geochemica et Cosmochimica*, **51**, 645-659.

Chacón, A.T., 1993. Lake Pátzcuaro, Mexico: Watershed and water quality deterioration in a tropical high-altitude Latin American lake. *Lake and Reservoir Management,* **8**, 37-47.

Chacón, A.T. and Iribe, E.M., 1997. Climatic trends, water balance and Lake Pátzcuaro, a tropical high altitude lake. *Quaternary International*, **43/44**, 43-51.

Chacón, A.T., Ross, L.G., Beveridge, M.C.M., and Watson, A.I., 1992. The application of SPOT multispectral imagery for the assessment of water quality Lake Pátzcuaro, Mexico. *International Journal of Remote Sensing*, **13**, 587-603.

Cook, E.R., Meko, D.M., Stahle, D.W., and Cleaveland, M.K., 1999. Drought reconstructions for the continental United States. *American Meteorological Society*, **12**, 1145-1162.

Crozier, W.D., 1960. Black, magnetic spherules in sediments. *Journal of Geophysical Research*, **9**, 2971-2977.

Dankers, P., 1981. Relationship between median destructive field and remanent coercive forces for dispersed natural magnetite, titanomagnetite and hematite. *Geophysical Society of the Royal Astronomical Society,* **64**, 447-461.

Day, R., Fuller, M., and Schmidt, V.A., 1977. Hysteresis properties of titanomagnetites: grain-size and compositional dependence. *Physics of the Earth and Planetary Interiors.* **13**, 260-267.

Dearing J.A. and Flower, R.J., 1982. The magnetic susceptibility of sedimenting material trapped in Lough Neagh, Northern Ireland, and its erosional significance. *Limnology and Oceanography*, **27**, 969-975.

Dearing, J.A., Hannam, J.A., Anderson, A.S. and Wellington, E.M.H., 2001. Magnetic, geochemical and DNA properties of highly magnetic soils in England. *Geophysics Journal International*, **144**, 183-196.

Dearing, J.A., Hay, K.L. Baban, S.J.M., Huddleston, A.S., Wellington, E.M.H., and Loveland, P.J., 1996 Magnetic susceptibility of soil: an evaluation of conflicting theories using a national data set. *Geophysics Journal International*, **127**, 728-734.

Dekkers, M.J., 1988. Some rockmagnetic parameters for natural Goethite, Pyrrhotite and fine-grained Haematite. Utrecht: Geologica Ultraiectina.

Eriksson, M.G., and Sandgren, P., 1999. Mineral magnetic analysis of sediment cores recording recent soil erosion history in central Tanzania. *Palaeogeography, Palaeoclimatology, Palaeoecology*, **152**, 365-383.

Fassbinder, J.W.E., Stanjek, H., and Vali, H., 1990. Occurrence of bacterial magnetite in soil. *Nature*, **343**, 161-163.

Fine, P., Singer, M.J. and Verosub, K.L., 1992. Use of magnetic-susceptibility measurements in assessing soil uniformity in chronosequence studies. *Soil Science Society of America Journal*, **56**, 1195-1199.

Folkoff, M.E., 1987. Climatic control of soil acidity in the B horizon of United States soils. *Physical Geography*, **8**, 82-97.

Han, J., Lu, H., Wu, N., and Gou, Z., 1996. Magnetic susceptibility of modern soils in China and climate conditions. *Studia Geophysica et Geodetica,* **40**, 262-275.

Hastenrath, S., 1976. Variations in low-altitude circulation and extreme climatic events in the tropical Americas. *Journal of Atmospheric Science,* **33**, 202-215.

Heller, F. and Liu, H., 1982. Magnetostratographic dating of the loess deposits in China. *Nature*, **300**, 431-433.

Heller, F. and Liu, H., 1984. Magnetism of Chinese loess deposits. *Geophysics Journal of the Royal Astronomical Society*, **77**, 125-141.

Heller, F. and Liu, H., 1986. Palaeoclimatic and sedimentary history from magnetic susceptibility of loess in China. *Geophysics Research Letters*, **13**, 1169-1172.

Heller, F., Liu, X., Wu, T.S., and Xu, T.C., 1991. Magnetic susceptibility of loess in China. *Earth and Planetary Science Letters*, **103**, 301-310.

Hesse, P.P., 1994. Evidence for bacterial palaeoecological origin of mineral magnetic cycles in oxic and sub-oxic Tasman Sea sediments. *Marine Geology,* **117**, 1-17.

Hounslow, M.W., and Cox, J., (In press). Magnetic characteristics of Fe-Oxide inclusions in sediment silicate particles, *Geophysical Research Letters.*

Hounslow M.W. and Maher, B.A., 1996. Quantitative magnetic extraction and analysis of carriers of magnetisation in sediments. *Geophysics Journal International*, **124**, 57-74.

Hovan, S.A., and Rea, D.K., 1991. Post-Eocene record of eolian deposition at sites 752, 754 and 756, eastern Indian Ocean. *Proceedings of the Ocean Drilling Program, Scientific Results*, **121**, 219-227.

Hovan, S.A., Rea, D.K. and Pisias, N.G., 1991. Late Pleistocene continental climate and ocean variability recorded in northwest Pacific sediments. *Paleoceanography*, **6**, 349-370.

Hovan, S.A., Rea, D.K., Pisias, N.G. and Shackleton, J., 1989. A direct link between the China loess and marine $\delta^{18}O$ records: aeolian flux to the north Pacific. *Nature*, **340**, 296-298.

Hudson, N.W., 1981. Soil conservation, Batsford. London.

Hunt, C.P., Banerjee, S.K., Han, J., Solheid, S., Oches, E., Sun, W. and Liu T., 1995. Rock magnetic proxies of climate change in the loess-palaeosol sequences of the western loess plateau of China. *Geophysics Journal International*, **123**, 232-244.

Jauregui, O.E. and Klaus, D., 1976; Some aspects of climate fluctuations in Mexico in relation to drought. *Geofisicia International*, **16**, 45-61.

Jenny, H., 1941. Factors of soil formation. New York: McGraw-Hill.

Johnson D.E., 1998 Applied Multivariate Methods for Data Analysts. Duxbury Press.

Jones, B.F., and Bowser, C.J., 1978. The mineralogy and related chemistry of lake sediments. In Lerma, A. (ed), Lakes: Chemistry, Geology, Physics, New York: Springer-Verlag, 179-200.

Kapicka, A., Petrovsky, E., Ustjak, S., and Machackova., 1999. Proxy mapping of fly-ash pollution of soils around a coal-burning power plant: a case study in the Czech Republic. *Journal of Geochemical Exploration*, **66**, 291-297.

Karlin, R., and Levi, S., 1983. Diagenesis of magnetic minerals in recent haemiplegic sediments. *Nature*, **303**, 327-330.

Kletescha, G. and Banerjee, S.K., 1995. Magnetic stratigraphy of Chinese Loess as a record of natural fires. *Geophysical Reasearch Letters.*, **22**, 1341-1343.

Kneller, E.F. and Luborsky, F.E., 1963. Particle size dependence of coercivity and remanence of single-domain particles. *Journal of Applied Physics*, **34**, 656-658.

Konhauser, K.O., 1998. Diversity of bacterial iron minerlization. *Earth Science Reviews,* **43**, 91-121.

Kukla. G.J., Heller, F., Liu, X.M., Xu, T.C., Liu, T.S., and An, Z.S., 1988. Pleistocene climates dated by magnetic susceptibility, *Geology.* **16**, 811-814.

Kutzbach, J.E. and Street-Perrott, F.A., 1985. Milankovitch forcing of fluctuations in the level of tropical lakes from 18 to 0kyr BP. *Nature*, **317**, 130-134.

Lawson, C.L., and Hanson, R.J., 1995. Solving Least Squares Problems. Society for Industrial and Applied Mathematics, Philadelphia.

Leborgne, E, 1955. Abnormal magnetic susceptibility of top soil. *Annales de Geophysique,* **11,** 399-419.

Lees J.A., 1997. Mineral magnetic properties of mixtures of environmental and synthetic materials: linear additivity and interaction effects. *Geophysical Journal International*, **131**, 335-346.

Lees J.A., 1999. Evaluating magnetic parameters for use in source identification, classification and modelling of natural and environmental materials. In, Walden, J., Oldfield, F., and Smith. (eds) Environmental Magnetism: a practical guide. Technical Guide, No. 6. Quaternary Research Association, London.

Leslie, B.W., Lund, S.P., and Hammond, D.E., 1990. Rock magnetic evidence for the dissolution and authigenic growth of magnetic minerals within anoxic marine sediments of the Californian continental borderland. *Journal of Geophysical Research*, **95**, 4437-4452.

Liverman, D., 1993. The regional impact of global warming in Mexico: uncertainty, vulnerability and response. In Schmandt, J. and Clarkson (eds), The Regions and Global Warming, Oxford University Press.

Lovley, D.R., Stolz, J.F., Nord, G.L. and Phillips, E.J.P., 1987. Anaerobic production of magnetite by a dissimilatory iron-reducing micro-organism. *Nature*, **330**, 252-254.

Lu, H., Liu, T., Gu, Z., Liu, B., Zhou, L., Han, J., and Wu, N., 2000. Effect of burning C3 and C4 plants on the magnetic susceptibility signal of soils. *Geophysical Research Letters*, **27**, 2013-2016.

Liu, X.M., Rolph, T., Bloemendale, J., Shaw, J. and Liu, T.S., 1994. Remanence characteristics of different magnetic grain-size categories at Xifeng in the loess plateau of China. *Quaternary Research*, **42**, 162-165.

Maher, B.A., 1988. Magnetic properties of some synthetic sub-micron magnetites. *Geophysical Journal,* **94**, 83-96.

Maher, B.A., 1998. Magnetic properties of modern soils and Quaternary loessic paleosols: paleoclimatic implications. *Palaeogeography Palaeoclimatology Paleoecology*, **137**, 25-54.

Maher, B.A. and Hounslow, M.W., 1999. Magnetic records of aeolian dust, Indian ocean. In B.A. and Thompson, R. (eds.) Quaternary climates environments and magnetism, Maher, Cambridge University Press.

Maher, B.A., and Thompson, R., 1991. Mineral magnetic record of the Chinese loess and paleosols. *Geology*, **19**, 3-6.

Maher, B.A., and Thompson, R., 1992. Paleoclimatic significance of the mineral magnetic record of the Chinese loess and paleosols. *Quaternary Research*, **37**, 155-170.

Maher, B.A. and Thompson, R., 1995. Paleorainfall reconstructions from pedogenic magnetic susceptibility variations in the Chinese loess and paleosols, *Quaternary Research*, **44**, 383-391.

Maher, B.A., and Thompson, R., 1999. Magnetism and palaeoclimate in the Chinese loess. In Maher, B.A., and Thompson, R. (eds) Quaternary climates, environments and magnetism. Cambridge University Press.

Maher, B.A., Thompson, R., and Hounslow, M.W., 1999. Introduction to: Maher, B.A., and Thompson, R (eds) Quaternary climates, environments and magnetism. Cambridge University Press.

Maher, B.A., Thompson, R. and Zhou, L.P., 1994. Spatial and temporal reconstructions of changes in the Asian palaeomonsoon: A new mineral magnetic approach. *Earth and Planetary Science Letters*, **125**, 462-471.

McElhinny, M.W., and McFadden, P.L. 2000. Palaeomagnetism continents and Oceans. *International Geophysics Series*, **73.**

Meju, M. A., 1994., Geophysical Data Analysis: Understanding Inverse Problem Theory and Practice. Society of Exploration Geophysicists.

Metcalfe, S.E. (Pers. Comm.) Department of Geography, University of Edinburgh, Edinburgh.

Metcalfe, S.E., Bimpson, A., Courtice, A.J. O'Hara, S.L. and Taylor, D.M., 1997. Climate change at the monsoon/Westerly boundary in Northern Mexico. *Journal of Paleolimnology,* **17**, 155-171.

Metcalfe, S.E., Say, A., Black, S., McCulloch, R., and O'Hara, S.L., In press. Wet conditions during the last glacial in the Chihuahuan desert, Alta Babicora basin, Mexico. *Quaternary Research.*

Metcalfe, S., Street-Perrott, F.A., Perrott, R.A. and Harkness, D.D., 1991. Palaeolimnology of the Upper Lerma Basin, central Mexico: A record of climatic change and anthropogenic disturbances since 11,600 Yrs BP. *Journal of Paleolimnology*, **5**, 197-218.

Mosiño Alemáne P.A. and Garcia, E., 1974. The climate of Mexico. In Bryson R.A. and Hare, F.K. (eds) Climates of North America, Elsevier world survey of climatology 11.

Moskowitz B.M., Frankel, R.B., and Bazylinski, D.A., 1993. Rock magnetic criteria for the detection of biogenic magnetite. *Earth and Planetary Science Letters*, **120**, 283-300.

Mullins, C.E., 1977. Magnetic susceptibility of the soil and its significance in soil science- A review, *Journal of Soil Science*, **120**, 671-674.

Nagata, T., 1961. Rock Magnetism. Maruzen Company LTD.

Nedler, J.A. and Mead, R., 1965. A simplex method for function minimisation. *Computer Journal*, **7**, 308-313.

O'Hara, S.L., 1991. Historical evidence of fluctuations in the level of Lake Pátzcuaro, Michoacán, México over the last 600 years. *The Geographical Journal*, **159**(1), 51-62.

O'Hara S.L., and Metcalfe, S.E., 1997. The climate of Mexico since the Aztec period. *Quaternary International*, **43/44**, 25-31.

O'Hara, S.L., Metcalfe, S.E., and Street-Perrott, F.A., 1994. On the arid margin: The relationship between climate, humans and the environment. A review of evidence from the highlands of central Mexico. *Chemosphere*, **29**, 965-981.

O'Hara. S.L., Street-Perrott, F.A., and Burt, T.P., 1993. Accelerated soil erosion around a Mexican highland lake caused by prehispanic agriculture. *Nature*, **362**, 48-51.

Oldfield, F., 1991. Environmental magnetism - a personal perspective. *Quaternary Science Reviews*, **10**, 73-85.
Oldfield, F., 1999. Environmental magnetism; the range of applications. In Walden, J. Oldfield, F. and Smith, J.P. (eds.) Environmental magnetism: a practical guide. Technical Guide, No. 6. Quaternary Research Association, London.

Oldfield, F., 1999. The rock magnetic identification of magnetic mineral and magnetic grain size assemblages. In Walden, J. Oldfield, F. and Smith, J.P. (eds.)

Environmental magnetism: a practical guide. Technical Guide, No. 6. Quaternary Research Association, London.

Oldfield, F., Thompson, R., and Dickson, D.P.E., 1981. Artificial enhancement of stream bedload: a hydrological application of superparamagnetism. *Physics Earth Planetary interior,* **26**, 107-124.

Ortega-Guerrero, B., Thompson, R., and Urrutia-Fucugauchi, J., 2000. Magnetic properties of lake sediments from Lake Chalco, central Mexico, and their palaeoenvironmental implications. *Journal of Quaternary Science*, **15**, 127-140.

Ortega-Ramirez, J., Valiente-Banuet, A., Urrutia-Fucugauchi, J., Montera-Gutierrez C.A., and Alvarado-Valdez, G., 1998. Paleoclimatic changes during the late Pleistocene – Holocene in Laguna Babicora, near the Chihuahuan desert, Mexico. *Canadian Journal of Earth Science*, **35**, 1168-1179.

Parker, S.P., 1994. Dictionary of Geology and Mineralogy. McGraw-Hill.

Peck, J.A., and King, J.W., 1996. Magnetofossils in the sediment of Lake Baikal, Siberia. *Earth and Planetary Science Letters,* **140**, 159-172.

Petersen, N., Von Dobeneck, T., and Vali, H., 1986. Fossil bacterial magnetite in deep sea sediments from the south Atlantic. *Nature*, **320**, 611-615.

Ramsey, F.L. and Schafer, D.W., 1997. The Statistical sleuth. Duxbury Press.

Pye, K., 1989. Processes of fine particle formation, dust source regions, and climatic changes. In Leinen, M. and Sarnthein, M. (eds.), Paleoclimatology and Paleometerology: Modern and past patterns of Global Atmospheric Transport. Kluwer Academic Publishing, 3-30.

Rea, D.K., 1994. The paloeclimatic record provided by eolian deposition in the deep sea: the geologic history of wind. *Review of Geophysics.,* **32**, 159-195.

Reading, H.G. and Levell, B.K., 1996. Controls on the sedimentary rock record. In by Reading, H.G. (eds) Sedimentary Environments: Processes, Facies and Stratigraphy. Blackwell Science.

Roberts, A.P., Reynolds, R.L., Verosub, K.L., and Adam, D.P., 1996. Environmental magnetic implications of greigite (Fe_3S_4) formation in a 3 m.y. lake sediment record from Butte Valley, northern California. *Geophysical Research Letters*, **23**, 2859-2862.

Robles-Gil, P., 1994. Mexican diversity of flora. CEMEX.

Rosas, I., Mazari, M. Saavedra, J. and Baez, A.P., 1985. Benthic organisms as indicators of water quality in Lake Pátzcuaro, Mexico. *Water, Air and Soil Pollution*, **25**, 401-414.

Ryan, B.F., and Joiner, B.L., 1994. Minitab Handbook third edition. Duxbury Press.

Sagnotti, L., Florindo, F., Verosub, K.L. Wilson, G.S., and Roberts, A.P., 1998. Environmental magnetic record of Antarctic palaeoclimate from Eocene/Oligocene glaciomarine sediments, Victoria Land Basin. *Geophysics Journal International*, **134**, 653-662.

Selley, R.C., 2000. Applied sedimentology. Academic Press.

Singer, M.J. and Fine, P., 1989. Pedogenic factors affecting magnetic susceptibility of northern California soils. *Soil Science Society of America Journal*, **53**, 1119-1127.

Singer, M.J. Fine, P. Verosub, K.L. and Chadwick, O.A., 1992. Time dependence of magnetic susceptibility of soil chronosequences on the California coast. *Quaternary Research*, **37**, 323-332.

Sly, P.G., 1978. Sedimentary processes in lakes. In Lerma, A (eds) Lakes: Chemistry, Geology, Physics. New York: Springer-Verlag. 65-89.

Snowball, I.F and, Thompson, R., 1988. The occourence of greigite in sediments from Loch Lomond. *Jopurnal of Quaternary Science*, **3**, 121-125.

Stacey, F.D., 1992. Physics of the Earth. Brookfield Press.

Stuiver, M and Reimer, P.J., 1994. *Radiocarbon*, **35**, 215-230.

Tauxe, L., 1993. Sedimentary records of relative paleointensity of the geomagnetic field. *Reviews of Geophysics*, **31**, 319-354.

Tauxe, L., 1998. Palaeomagnetic Principles and Practice. Kluwer Academic Publishers

Taylor, R.M., Maher, B.A. and Self, P.G., 1987. Magnetite in soils: I. The synthesis of single-domain and superparamagnetic magnetite. *Clay Minerals*, **22**, 411-422.

Terrett, N.L. 2000. Late Pleistocene - Holocene climatic variability at Lake Pátzcuaro, Mexico: An interpretation of events through diatom analysis. Unpublished Masters of Research thesis.

Thompson, R., 1986. Modelling magnetisation data using SIMPLEX. *Physics of the Earth and Planetary Interiors*, **42**, 113-127.

Thompson R., Battarbee, R.W. O'Sullivan, P.E. and Oldfield, F., 1975. Magnetic susceptibility of lake sediments, *Limnology and Oceanography*, **20**, 687-698.

Thompson R., Bloemendal, J., Dearing, J.A., Oldfield, F., Rummery, T.A., Stober, J.C., and Turner, G.M., 1980. Environmental applications of magnetic measurements, *Science*, **207**, 481-486

Thompson, R., and Maher, B.A., 1994. Spatial and temporal reconstructions of changes in the Asian palaeomonsoon: A new mineral magnetic approach. *Earth and Planetary Science Letters*, **125**, 461-471.

Thompson, R. and Maher, B.A., 1995. Age models, sediment fluxes and palaeoclimatic reconstructions for the Chinese loess and palaeosol sequences. *Journal of Geophysics International*, **123**, 611-622.

Thompson, R., and Oldfield, F., 1986. Environmental Magnetism. London: Allen and Unwin.

Urrutia-Fucugauchi, J., Ortega-Ramirez, J., and Cruz-Gatica, R., 1997. Rock magnetic study of late Pleistocene-Holocene sediments from the Babicora lacustrine basin, Chihuahua, northern Mexico. *Geofisica International*, **36**, 77-86.

Vali, H. and Kirschvink, J.L., 1989. Magnetofossil dissolution in a palaeomagnetically unstable deep-sea sediment. *Nature,* **339**, 203-206.

Verosub, K.L., and Roberts, A.P., 1995. Environmental magnetism: past, present and future. *Journal of Geophysical Research*, **100**, 2175 - 2192.

Walden, J., Slattery, M.C., and Burt, T.P., 1997. Use of mineral magnetic measurements to fingerprint suspended sediment sources: approaches and techniques for data analysis. *Journal of Hydrology*, **202**, 353-372.

Watts, W.A. and Bradbury, J.P., 1982. Paleoecological studies at Lake Pátzcuaro on the west-central Mexican Plateau and at Chalco in the Basin of Mexico. *Quaternary Research*, **17**, 56-70.

White, R.E., 1997. Principles and Practice of Soil Science. Blackwell Science, London.

Yu, L., and Oldfield, F., 1989. A multivariate mixing model for identifying sediment source from magnetic measurements. *Quaternary Research*, **32**, 168-181.

Zhou, L.P., Oldfield, F., Wintle, A.G., Robinson, S.G., and Wang, J.T., 1990. Partly pedogenic origin of magnetic variations in Chinese loess. *Nature*, **346**, 737-739.

Appendix A

Unmixing tests

This appendix contains three unmixing tests not included in the chapter on unmixing (Chapter 4.6).

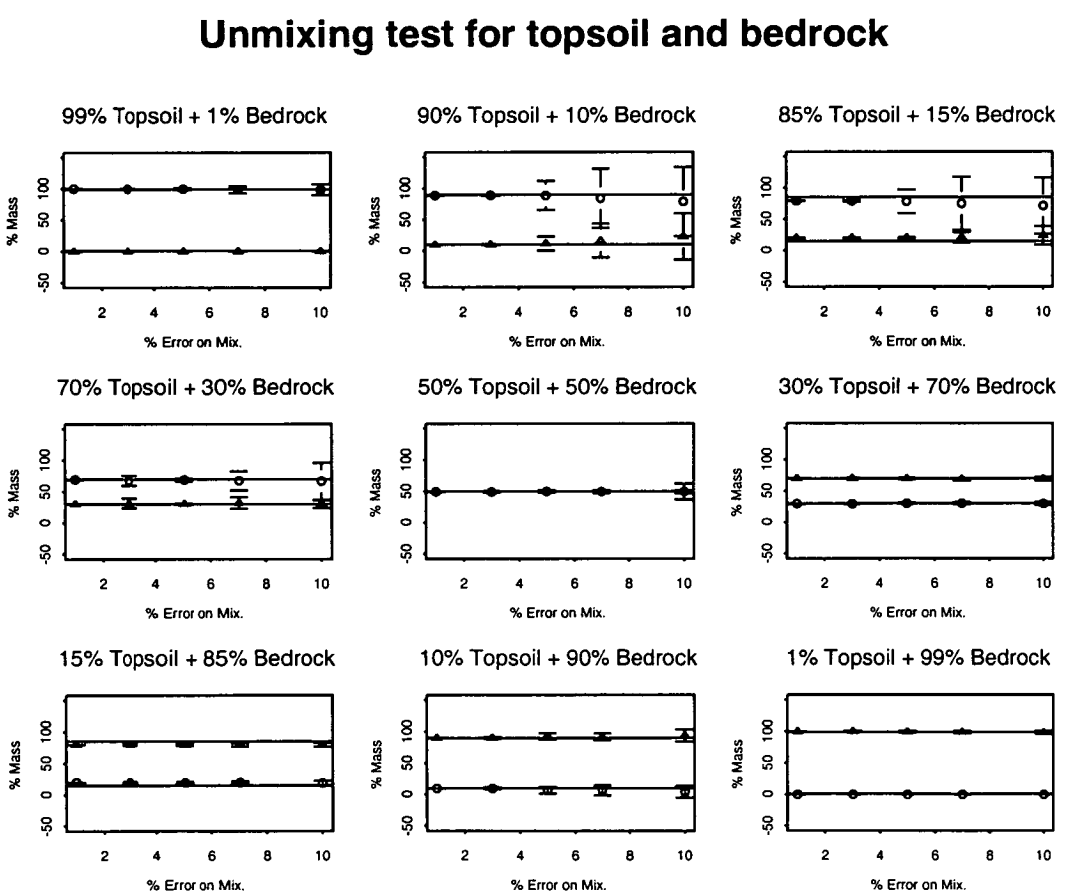

Figure A.1. Unmixing test results for nine different concentrations of topsoil and bedrock. On each plot five different percentage error tests are plotted along the horizontal axis and the modelled percentage mass of both end-members on the vertical axis (triangle for topsoil, circle for bedrock). Horizontal lines show the actual mixture that was being unmixed. Symbols show mean result of fifty different unmixing experiments, error bars show standard deviations.

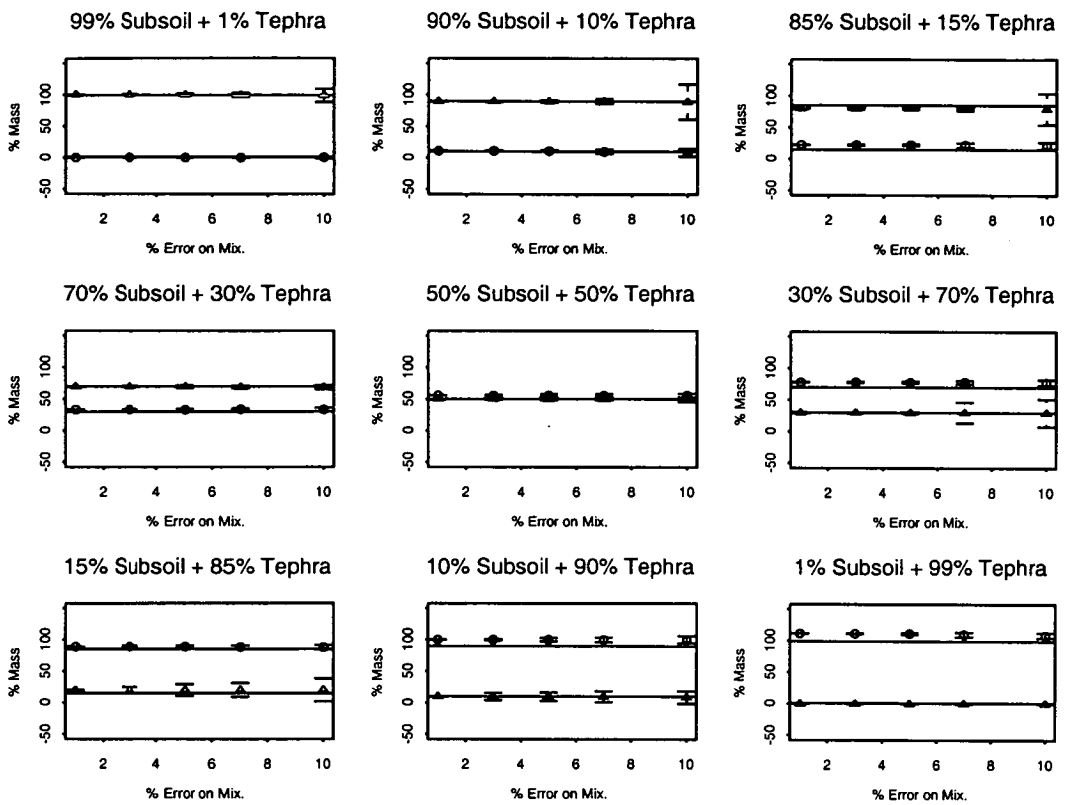

Figure A.2. Unmixing test results for nine different concentrations of subsoil and tephra. On each plot five different percentage error tests are plotted along the horizontal axis and the modelled percentage mass of both end-members on the vertical axis (triangle for subsoil, circle for tephra). Horizontal lines show the actual mixture that was being unmixed. Symbols show mean result of fifty different unmixing experiments, error bars show standard deviations.

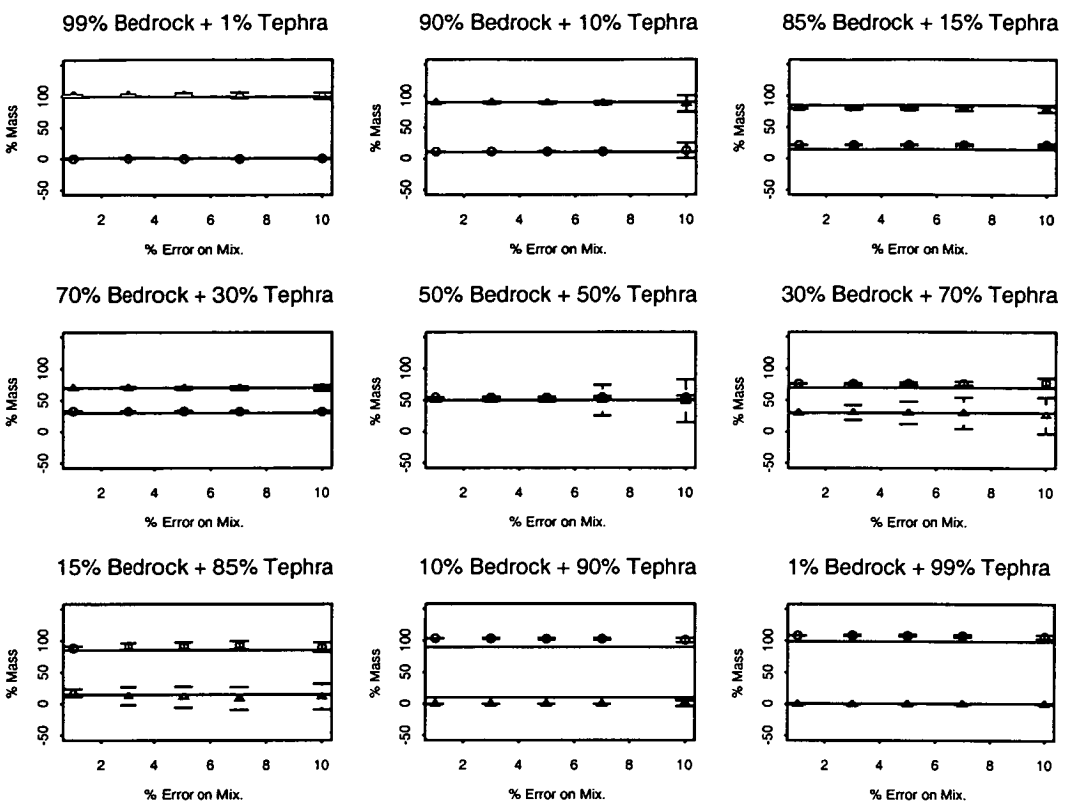

Figure A.3. Unmixing test results for nine different concentrations of bedrock and tephra. On each plot five different percentage error tests are plotted along the horizontal axis and the modelled percentage mass of both end-members on the vertical axis (triangle for bedrock, circle for tephra). Horizontal lines show the actual mixture that was being unmixed. Symbols show mean result of fifty different unmixing experiments, error bars show standard deviations.

Appendix B

Unmixing models for cores KD, B94/1 and B94/1

This appendix contains the unmixing models for core KD from lake Pátzcuaro and cores B94/1 and B94/3b from lake Babicora. For core KD there are three unmixing models:

1. Mean end-member properties,
2. most extreme end-member properties,
3. bounding end-member samples.

These models relate to the equivalent models for core C4 found in Chapter 5.7.

For both core B94/1 and B94/3 there are also three unmixing models:

1. All catchment material,
2. mean end-member properties,
3. most extreme end-member properties.

These models relate to the equivalent models on core B94/1a, found in chapter 6.9.

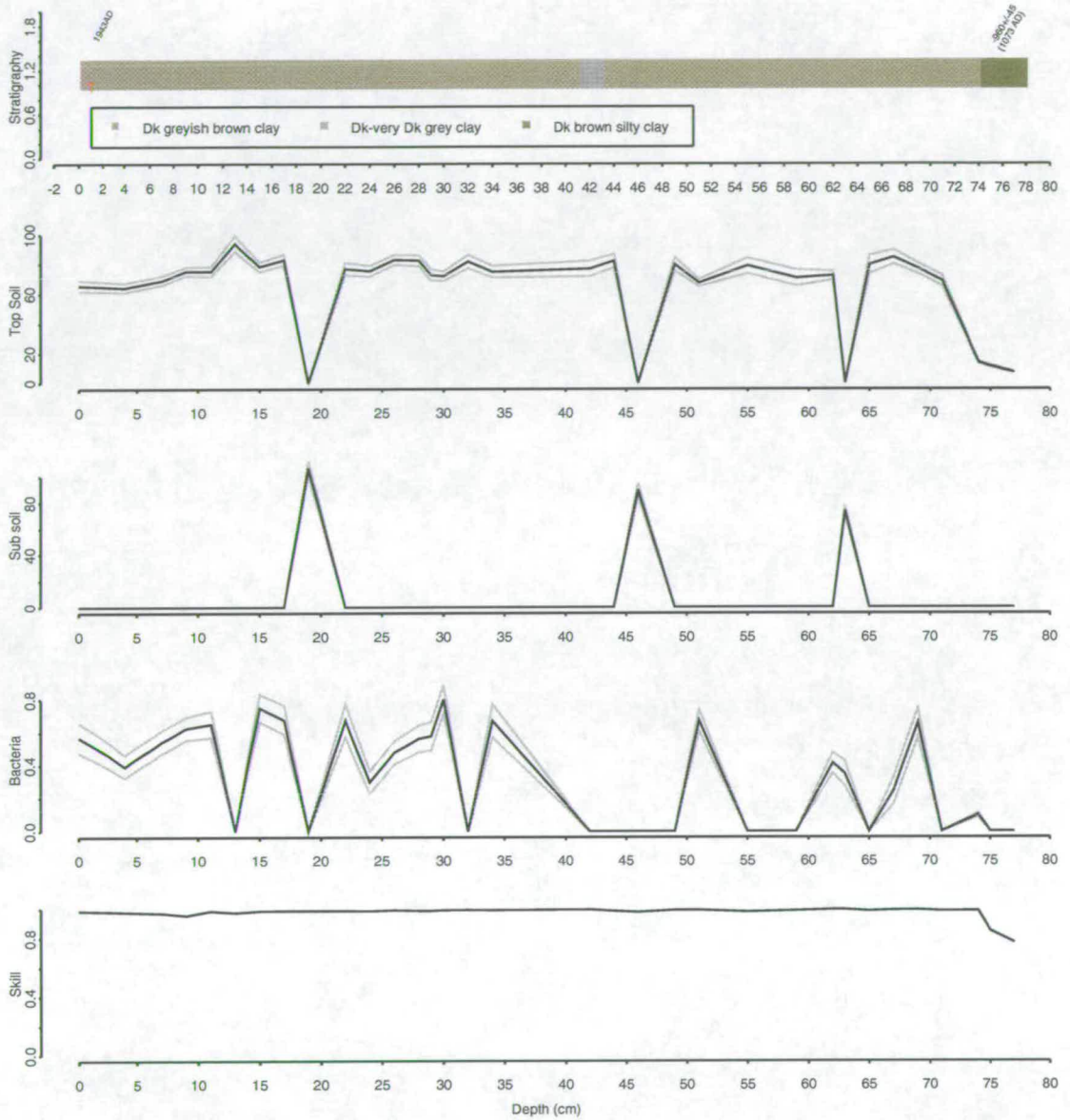

Figure B.1. Magnetic unmixing model two for core KD, with percentage of the cores mass explained by each end-member type against depth in cm. The grey lines show the extent of the errors from the stability of the inversion matrix. Also plotted is the skill of the model, the stratigraphy, and tephra layers (T).

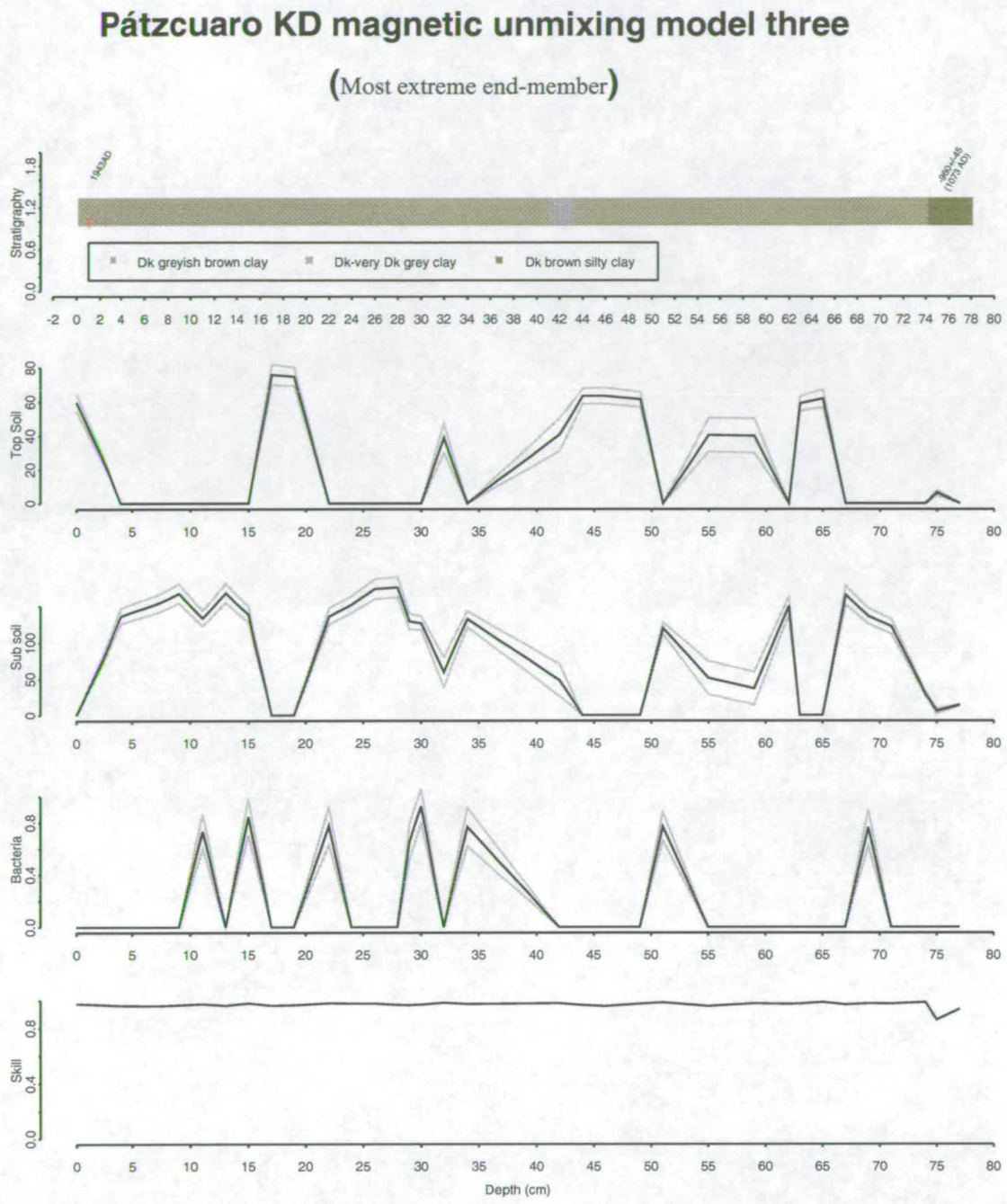

Figure B.2. Magnetic unmixing model three for core KD, with percentage of the cores mass explained by each end-member type against depth in cm. The grey lines show the extent of the errors from the stability of the inversion matrix. Also plotted is the skill of the model, the stratigraphy, and tephra layers (T).

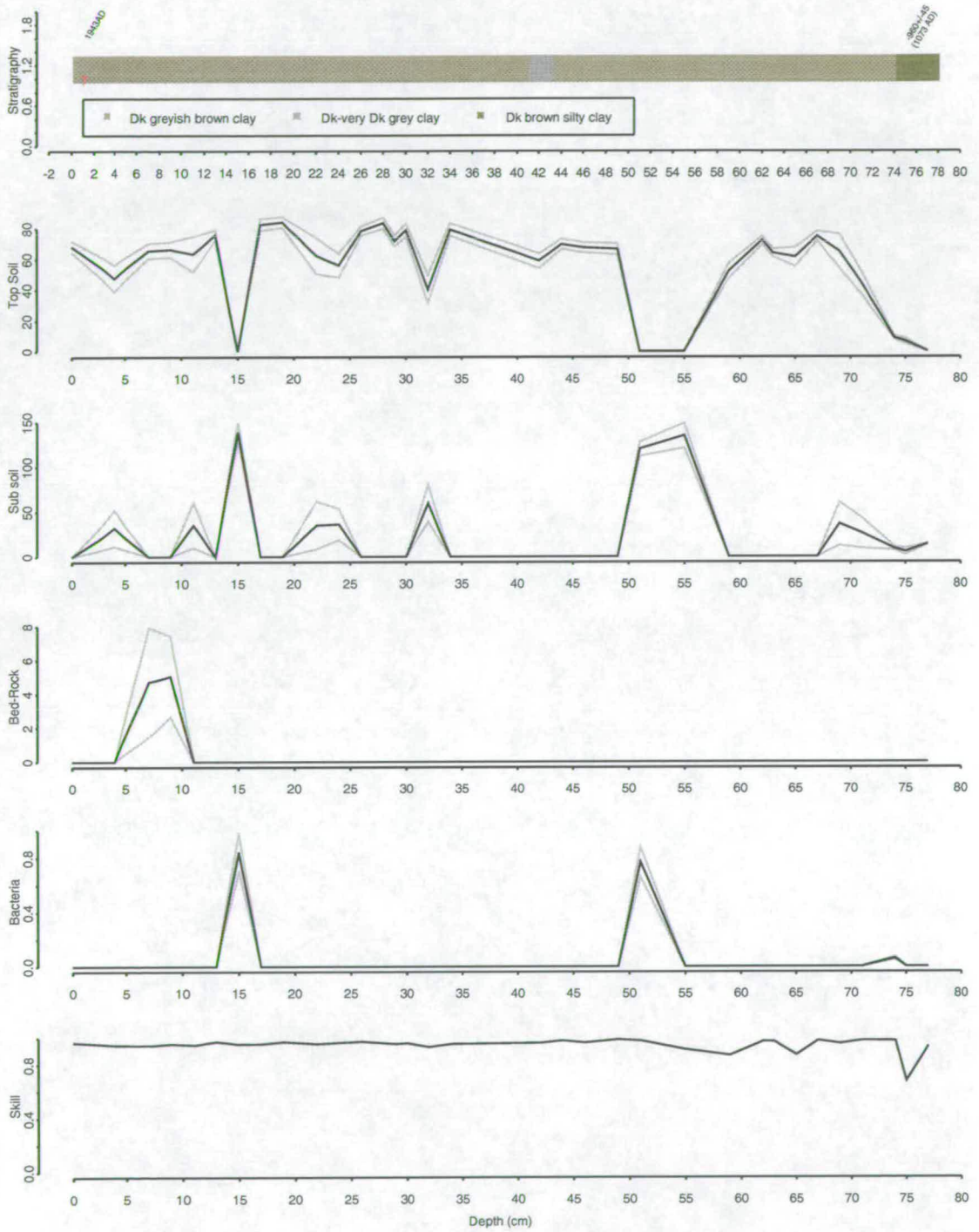

Figure B.3. Magnetic unmixing model four for core KD, with percentage of the cores mass explained by each end-member type against depth in cm. The grey lines show the extent of the errors from the stability of the inversion matrix. Also plotted is the skill of the model, the stratigraphy, and tephra layers (T).

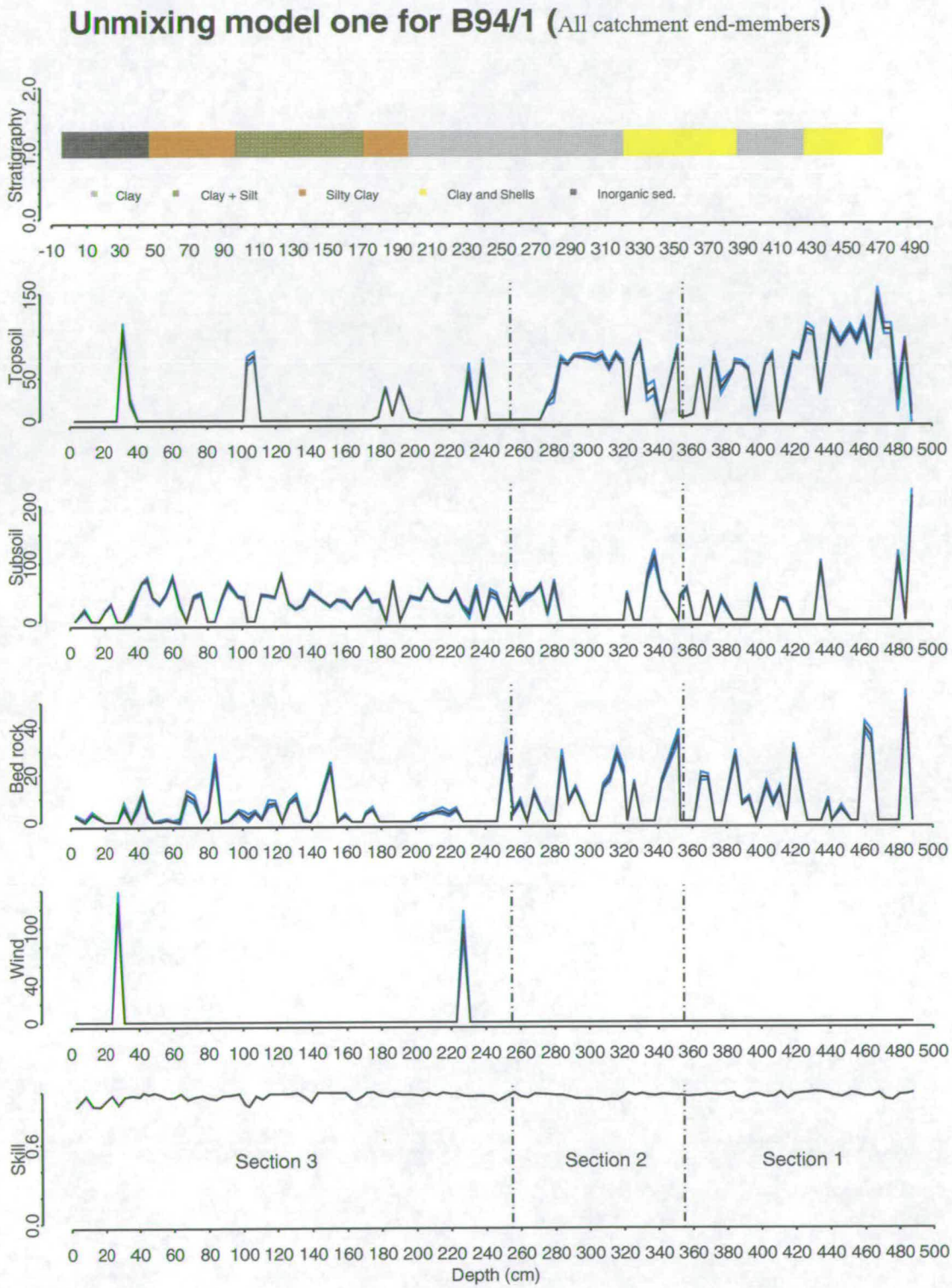

Figure B.4. Magnetic unmixing model one (all Babicora catchment end-members) for B94/1. Plots show the percentage of the cores mass explained by unmixing end-members against depth. Also plotted is the stratigraphy the core. Vertical broken lines denote boundaries between core sections.

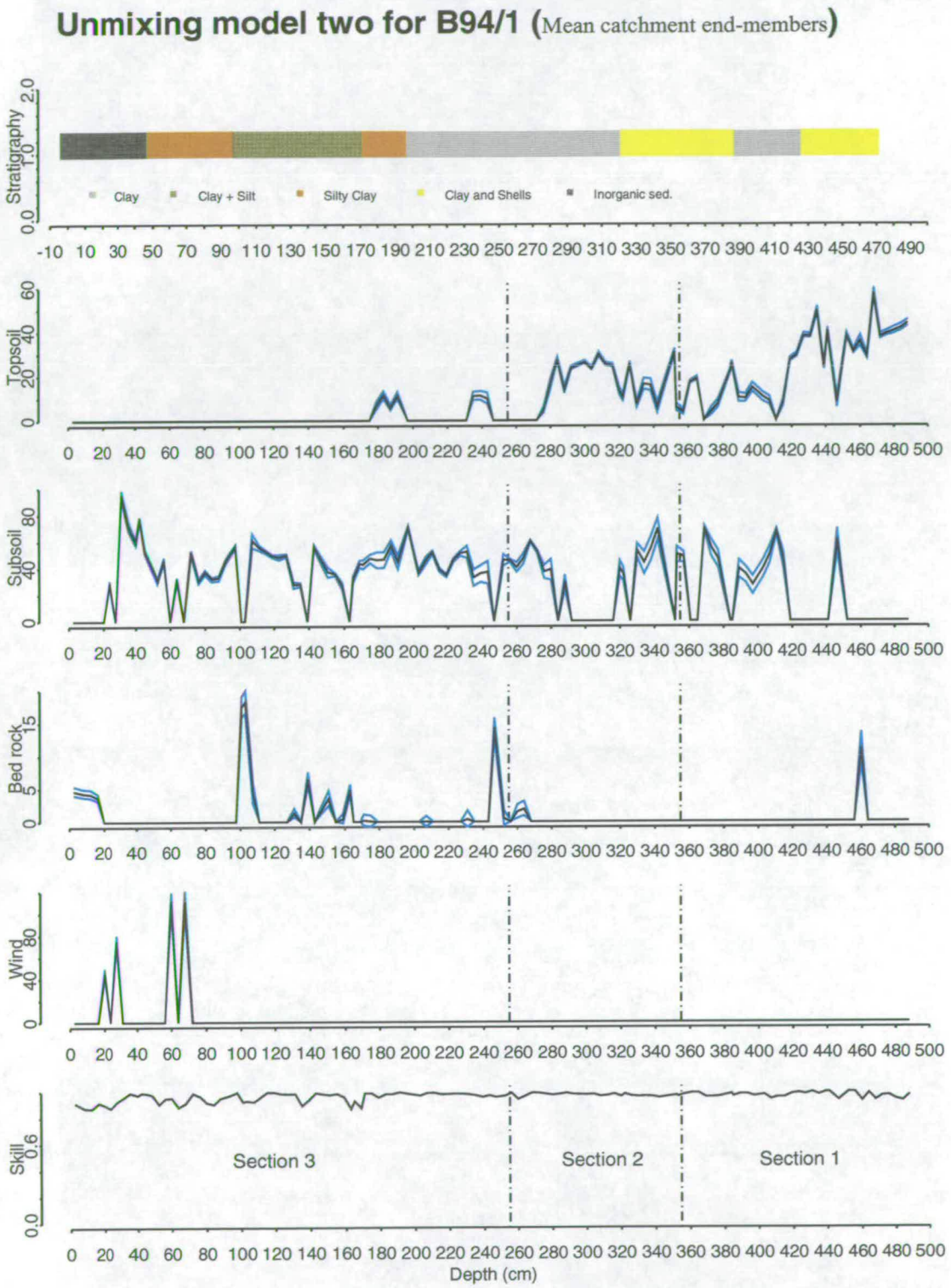

Figure B.5. Magnetic unmixing model two (mean magnetic properties of each catchment end-member type) for B94/1. Plots show the percentage of the cores mass explained by unmixing end-members against depth. Also plotted is the stratigraphy. Vertical broken lines denote boundaries between core sections.

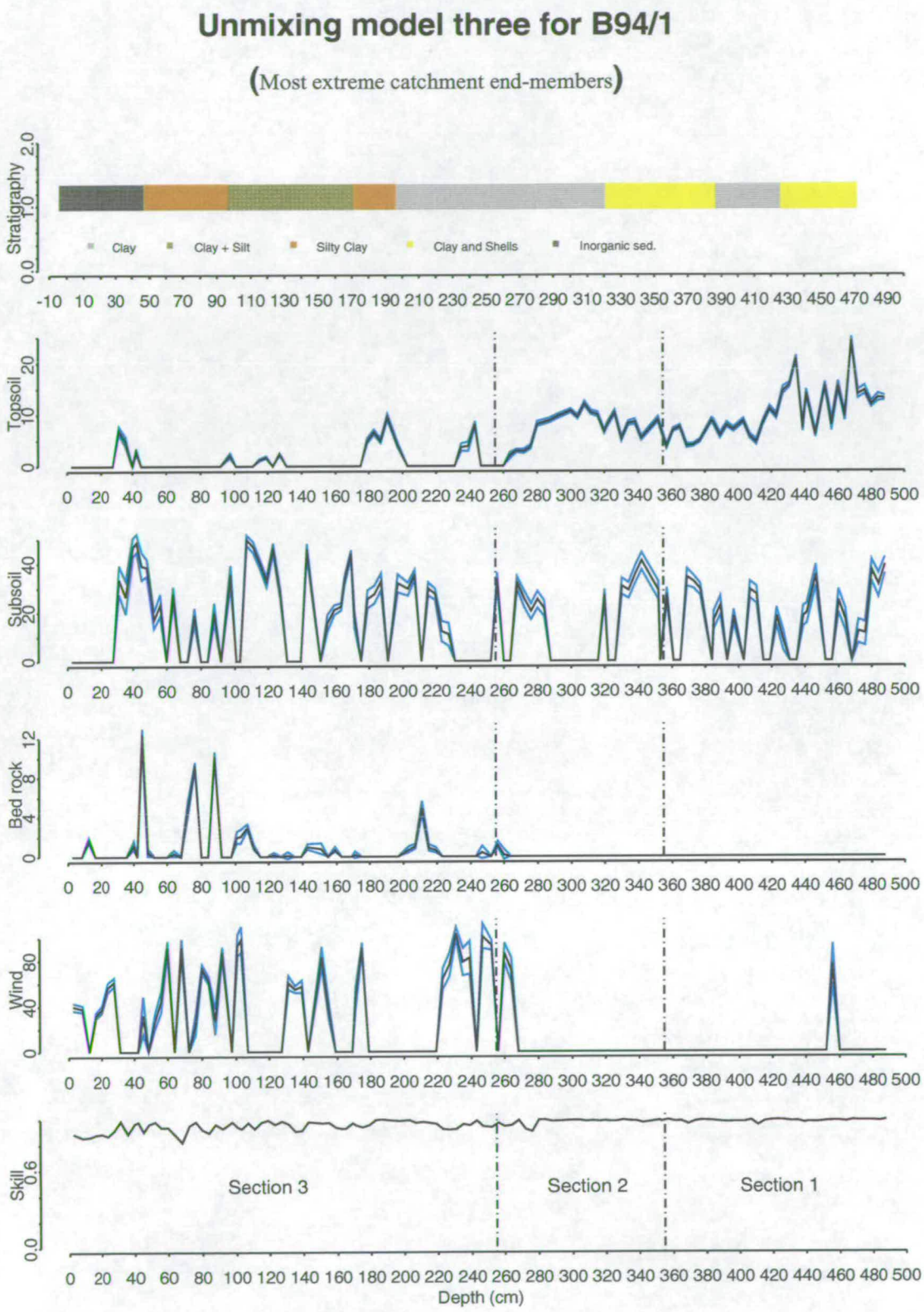

Figure B.6. Magnetic unmixing model three (most extreme of each catchment end-member type) for B94/1. Plots show the percentage of the cores mass explained by unmixing end-members against depth. Also plotted is the stratigraphy of the core. Vertical broken lines denote boundaries between core sections.

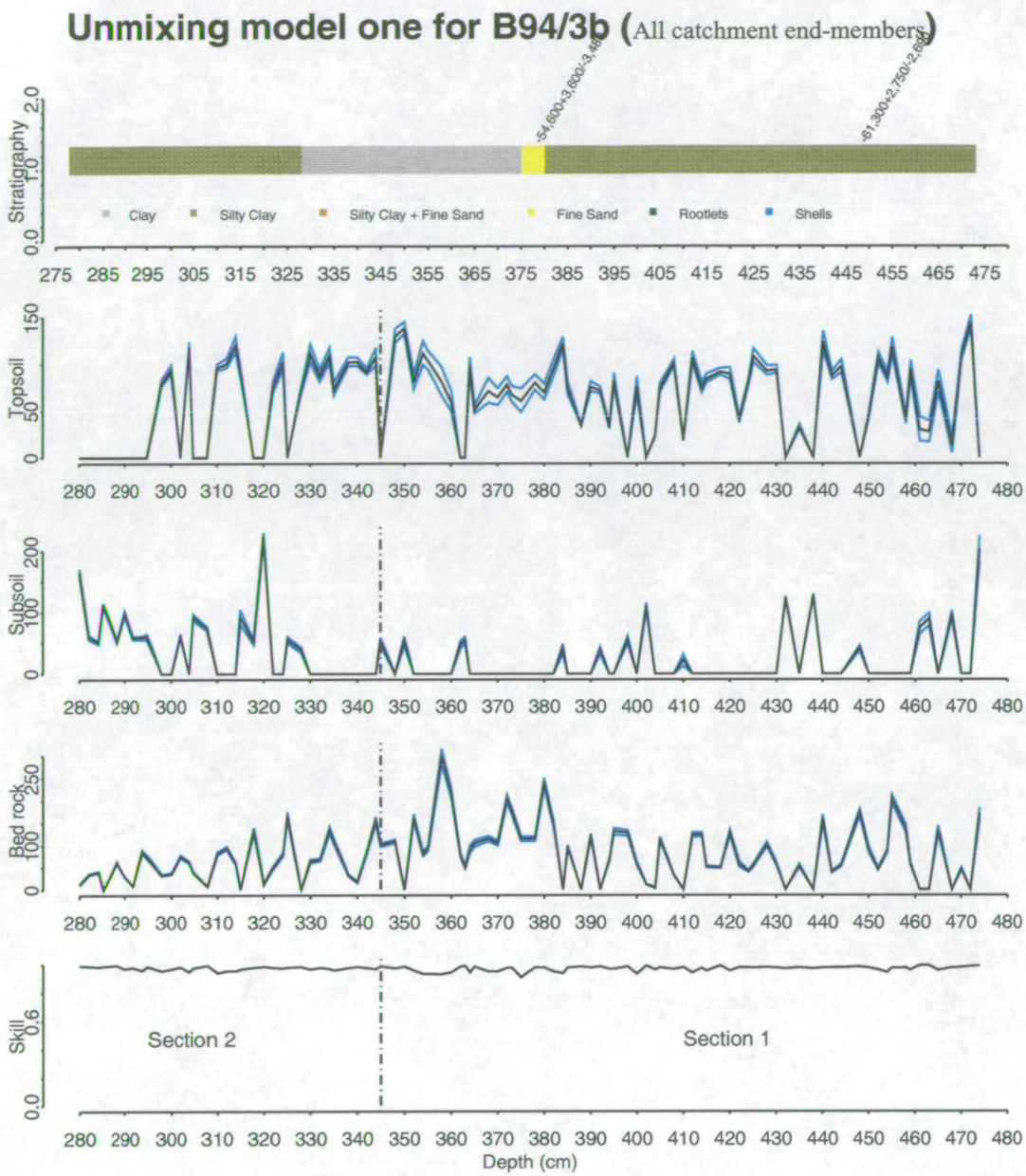

Figure B.7. Magnetic unmixing model one (all Babicora catchment end-members) for B94/3b. Plots show the percentage of the cores mass explained by unmixing end-members against depth. Also plotted is the stratigraphy the core. Vertical broken lines denote boundaries between core sections.

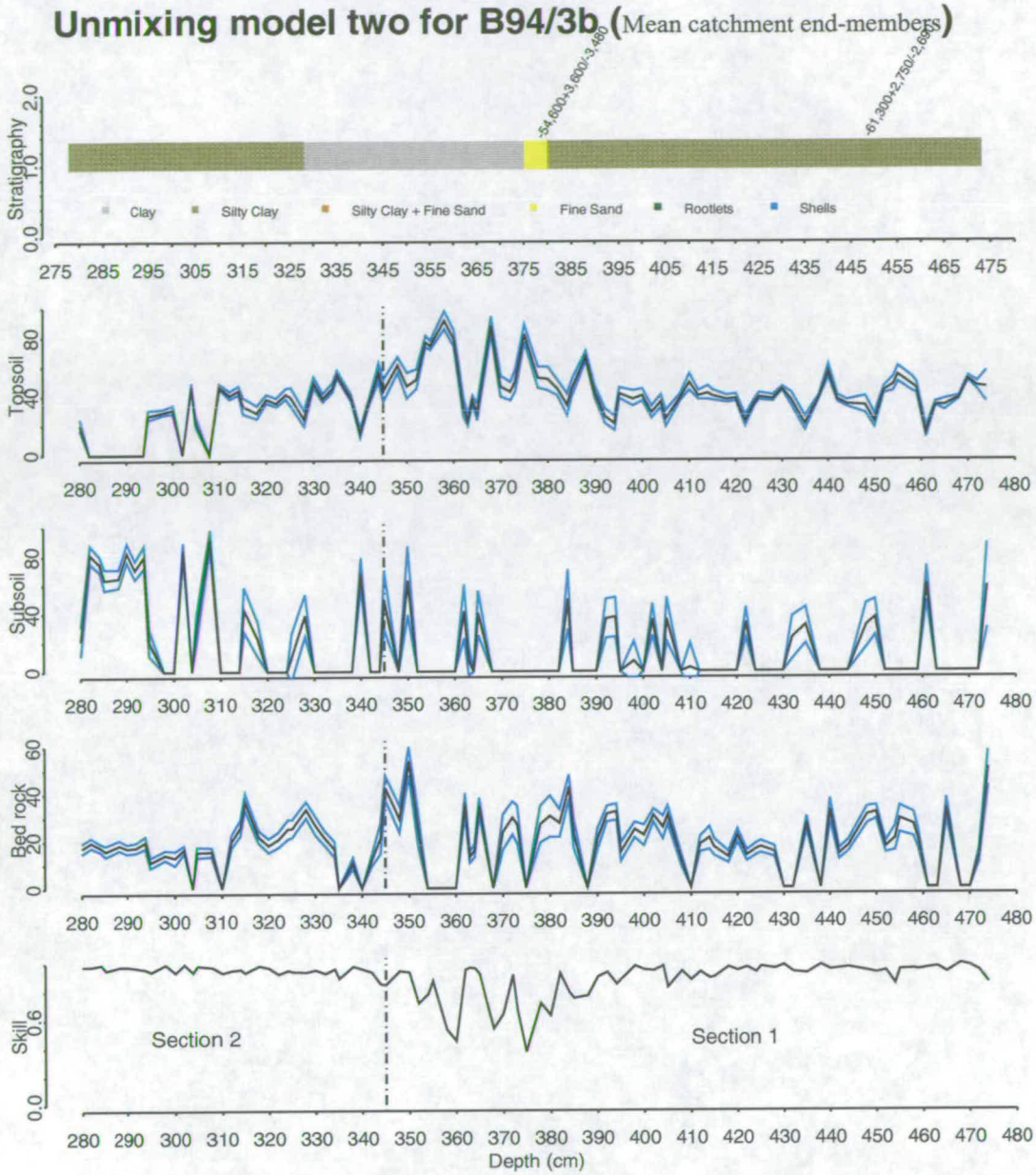

Figure B.8. Magnetic unmixing model two (mean magnetic properties of each catchment end-member type) for B94/3b. Plots show the percentage of the cores mass explained by unmixing end-members against depth. Also plotted is the stratigraphy. Vertical broken lines denote boundaries between core sections.

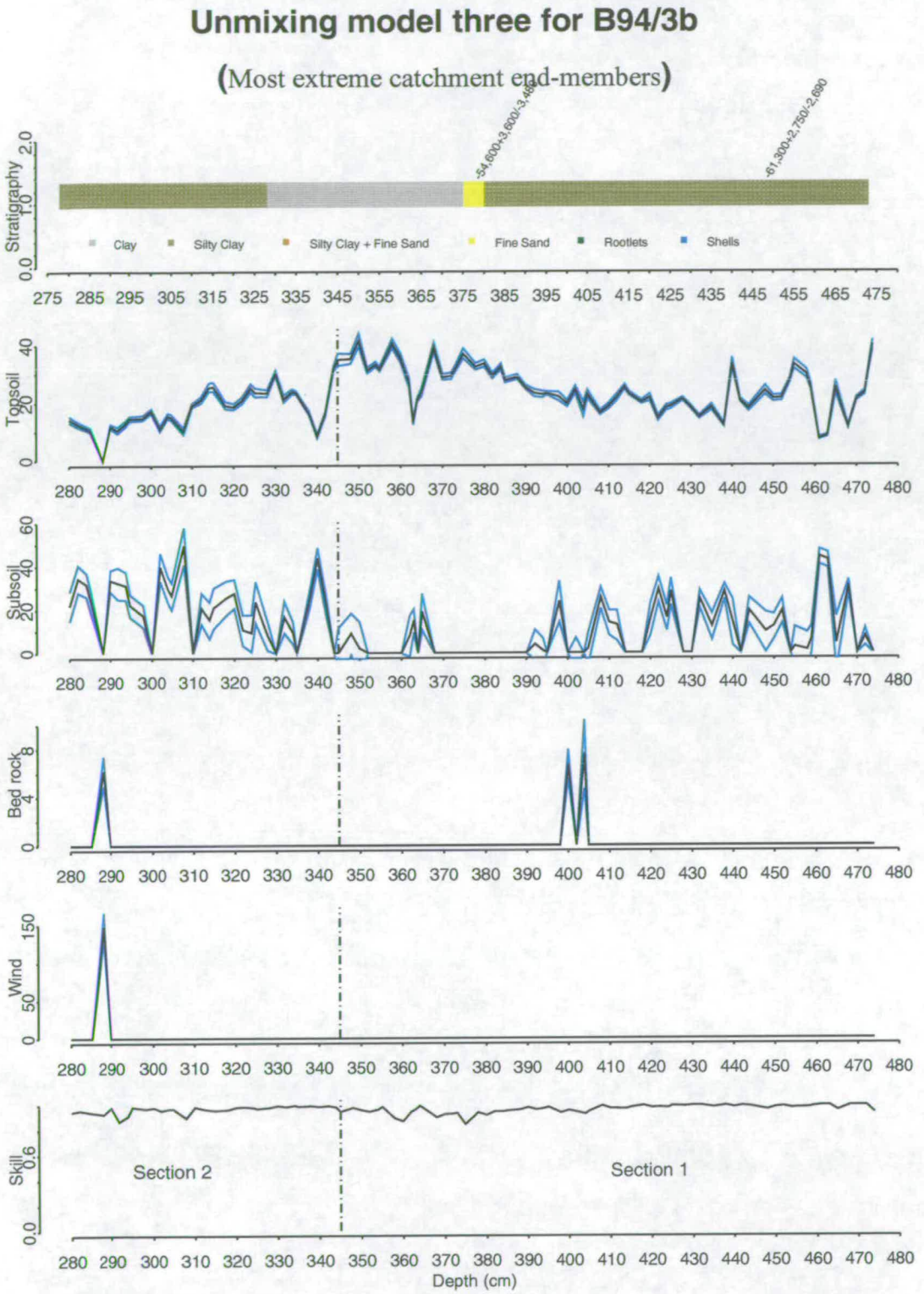

Figure B.9. Magnetic unmixing model three (most extreme of each catchment end-member type) for B94/3b. Plots show the percentage of the cores mass explained by unmixing end-members against depth. Also plotted is the stratigraphy of the core. Vertical broken lines denote boundaries between core sections.

Appendix C

Splus unmixing routines

This Appendix contains two of the Splus routines used to unmix the magnetic properties of sediment cores in terms of catchment end members. Step 2 is the F-testing non-negative least squares part of the unmixing routine. Errata is used to estimate the errors on the unmixing model, using the stability of the inversion matrix. Skillcore52 is a leave five out prediction method, which when used in conjunction with core skill generates a skill measure for the unmixing model.

Unmixing

ftestinc *is an f-testing Subroutine, which takes in the effective number of parameters (*`ep`*) the number of end-members in the present model (*`nn`*) and the residuals for the new model (*`newmod`*) and the old model (*`oldmod`*). It returns 1 if there is a significant improvement (at the 95% level) in the new model as compared to the old model, and returns 0 if not.*

```
ftestinc_function(ep,nn,newmod,oldmod){
fref_c(161.4,18.5,10.13,7.71,6.61,5.99,5.59,5.32,5.12,4.96,4.48,
4.75,4.67,4.60,4.54,4.49,4.45,4.41,4.38,4.35,4.32,4.3,4.28)
ftst_((oldmod-newmod)*ep-nn)/oldmod
#print(c("Required",fref[ep-nn],"Actual",ftst))
 if(ftst>fref[ep-nn]){
 return(1)}

 else{
 return(0)}
}
```

step 2 *is the main body of the unmixing work, it takes in the data for the core to be unmixed (*`core`*) which should be arranged as a matrix, with core horizons as rows and magnetic measurements as columns.* `Endmem`*, is a matrix of end-members each end-member fits on a row, and each measurement as a column. The effective number of parameters is held in* `ep` *and the norm value should always be given as 1. The output of the unmixing is given as a matrix that contains the quantity of each end-member included at each horizon of the model. The output comes as a matrix, with a row for each core sample, and a column for each unmixing end-member.*

```
step2_function(core, endmem, ep, norm){
#declare variables
      index <- 1:nrow(endmem)
```

```
      output <- matrix(0, ncol = nrow(endmem) + 1, nrow =
nrow(core))
      for(i in 1:nrow(core)) {
#find the 1st end-member using an R-test
            rtest <- cor(core[i,  ], t(endmem))
            rbest <- index[rtest == max(rtest)]
            included <- rbest     #make the 1st model
            curentmod <- nnls.fit(endmem[included,  ], core[i,
],
                  weights = 1/core[i,  ])
            semtempmod <- curentmod
#two indexs, outind limits the nuber of samples left out
#and gg tests for inprovment.
            gg <- 1
            outind <- 0
            while(gg != 0) {
                  gg <- 0
                  leftout <- index[ - included]
                  outyes <- 0
                  newendind <- 0
      #Loop to add end members and test systematically
                  for(j in 1:length(leftout)) {
                        modend <- rbind(endmem[included,  ],
                          endmem[leftout[j],  ])
                        tempmod <- nnls.fit(t(modend), core[i,
                          ], weights = 1/core[i,  ])
      #test if new model is better than old
                        if(sum((tempmod$resid)^2) < sum((
                          semtempmod$resid)^2)) {
                          semtempmod <- tempmod
                          if(ftestinc(ep, length(included), sum(
                            (tempmod$resid)^2), sum((curentmod$
                            resid)^2)) > 0) {
                            gg <- 1
                            newendind <- j
      #The index of the new end-member
                          }
                        }
                  }
                  if(gg == 1) {
                        curentmod <- semtempmod
                        included <- c(included, leftout[
                          newendind])
                        print(c(i, "Up One", included))
                  }
#New bit that removes end-members if more than 3 in model
                  if(length(included) > 2) {
                        outind <- outind + 1
                        for(k in 1:outind) {
                          modend <- (endmem[included[ - k],  ])
                          tempmod <- nnls.fit(t(modend), core[i,
                            ], weights = 1/core[i,  ])
                          if(k == 1) {
                        goalpost <- (sum(tempmod$resid)^2 + 100
                          }
                          if((sum(tempmod$resid)^2) < goalpost &&
                            ftestinc(ep, length(included) - 1,
                            sum((curentmod$resid)^2), sum((
```

```
                        tempmod$resid)^2)) == 0) {
                        goalpost <- (sum(tempmod$resid)^2)
                        semtempmod <- tempmod
                        outind <- j
    #The index of the member to be removed
                        outyes <- 1
                      }
                    }
                }
                if(outyes == 1) {
                    curentmod <- semtempmod
                    included <- included[ - outind]
                    print(c(i, "Down One", included))
                }
#stop the looping if all end-members are included
                if(length(included) == nrow(endmem)) {
                    gg <- 0
                }
            }
            output[i, c(included)] <- curentmod$coef
            output[i, (nrow(endmem) + 1)] <- 10
    }
    return(output)
}
```

Error and skill analysis

errata *takes the output of step2 (*`model`*) and compares it with the original core data (*`core`*) and the unmixing end-members (*`endmembers`*) in order to generate a matrix of predicted errors for the unmixing model. The output is given as a matrix with the same number of rows as the core, and the same number of columns as the number of unmixing end-members.*

```
errata
function(core, endmembers, model)
{
#line to take off the last data point of the model
    model <- model[, - ncol(model)]  #define useful terms for
 later
    index <- 1:nrow(endmembers)
    output <- matrix(0, ncol = ncol(model), nrow =
nrow(model))
    for(i in 1:nrow(core)) {
        inmod <- index[model[i,  ] != 0]
        if(length(inmod) > 1) {
            p <- lm(core[i,  ] ~ -1 + t(endmembers[c(inmod),
                ]), weights = (1/core[i,  ])^2)
        }
        else {
            p <- lm(core[i,  ] ~ -1 + endmembers[c(inmod),
                ], weights = (1/core[i,  ])^2)
        }
        output[i, c(inmod)] <- summary(p)$coef[, 2]
        print(i)
    }
```

```
      return(output)
}
```

skillcore52 *is a function which makes "leave one out" predictions for an unmixing model. The function takes in the magnetics data measured on the core (*core*), the end-member data measured on the catchment samples (*samps*), and the effective number of parameters for the unmixing model (*ep*). The function returns the leave five out predictions of the magnetic measurements made on the core. The output is given in terms of a matrix, with a row for each core horizon and a column for each magnetic measurement.*

```
skillcore52_function(core, samps, ep){
      nmes <- ncol(core)
      lcore <- nrow(core)
      nsamp <- nrow(samps)
      output <- matrix(nrow = lcore, ncol = nmes)
      for(i in 1:nmes) {
            remo <- c((i - 2), (i - 1), i, (i + 1), (i + 2))
            if(i == 1) {
                  remo <- c(1, 2, 3)
            }
            if(i == 2) {
                  remo <- c(1, 2, 3, 4)
            }
            if(i == 17) {
                  remo <- c(15, 16, 17, 18)
            }
            if(i == 18) {
                  remo <- c(16, 17, 18)
            }
            xcore <- core[,  - c(remo)]
            xsamps <- samps[,  - c(remo)]
            mod <- step2(xcore, xsamps, ep, 1)
            remod <- remix(mod[,  - (ncol(mod))], samps)
            output[, i] <- remod[, i]
            print(output)
      }
      return(output)
}
```

*coreskill takes in the leave five out predictions made by skill core (*ski*) and the original magnetic measurements made on a core (*core*), and returns the skill of the core.*

```
coreskill_function(ski, core)
{
      output <- vector(length = nrow(ski))
      for(i in 1:nrow(ski)) {
            output[i] <- skill(ski[i,  ], core[i,  ])
            print(i)
      }
      return(output)
}
```